ACTINIDE-AMINOPOLYCARBOXYLATE COMPLEXATION THERMODYNAMICS: AMERICIUM, BERKELIUM, CALIFORNIUM, AND EINSTEINIUM

by

Matthew Urban

A thesis submitted to the Faculty and the Board of Trustees of the Colorado School of Mines in partial fulfillment of the requirements for the degree of Master of Science (Nuclear Engineering).

Golden, Colorado

Date _____

Signed: _____

Matthew Urban

Signed: _____

Dr. Jenifer C. Shafer

Thesis Advisor

Signed: _____

Dr. Mark Deinert

Committee Member

Golden, Colorado

Date _____

Signed: _____

Dr. Mark Jensen

Program Director

Nuclear Science and Engineering Department

ABSTRACT

Previous experiments revealed evidence for modestly selective interactions, encouraged by orbital degeneracy driven covalency, between berkelium and curium using the aromatic aminopolycarboxylate dipicolinic acid. To further probe the ability for the heaviest available actinides to participate in orbital degeneracy driven covalent interactions, solvent extraction competition investigations were completed with the late actinides americium, berkelium, californium, and einsteinium. These studies were completed with aliphatic aminopolycarboxylates (nitrilotriacetic acid, 2-hydroxyethyl ethylenediaminetriacetic acid, trans-1,2-cyclohexanediaminetetraacetic acid, and diethylenetriaminepentaacetic acid). The stability constants and thermodynamic parameters derived from these studies may provide some indication of covalency in heavy actinide-aliphatic amine complexation chemistry. The stability constants derived for all metal-ligand complexes in this study were compared to lanthanide stability constants of the same aminopolycarboxylates (APCs) in linear free energy relationships to address, in part, whether a difference in selectivity exists between the late actinides and their lanthanide counterparts. Californium and einsteinium displayed a 2% difference in selectivity from europium and gadolinium, respectively, in absolute terms. Little evidence was obtained that shows intra-actinide selectivity between the aliphatic amines and the trivalent actinides.

TABLE OF CONTENTS

LIST OF FIGURES

LIST OF TABLES

LIST OF SYMBOLS

Stability constant……..β

Standard deviation……σ

ACKNOWLEDGEMENTS

I would like to thank Dr. Jenifer Shafer and the Colorado School of Mines Nuclear Science and Engineering program for accepting me into the masters of science program, the United States Army for allowing me to take the time to study and complete this thesis, and most importantly, my wife, Savanna, for supporting me throughout this research.

CHAPTER 1

INTRODUCTION

1.1 Executive Summary

Recent investigations into crystal structures of the trivalent actinides berkelium and californium and dipicolinic acid suggest covalent interactions between the aromatic amine and the metal ion (Albrecht-Schmitt, 2015, 2016). This result is surprising, in that the trivalent actinides were thought to only form ionic bonds. Few investigations were performed with the late trivalent actinides due to availability until now.

Solvent extractions were performed with bis-2-ethylhexyl phosphoric acid competing with several different aminopolycarboxylates (APCs) at different temperatures to find stability constants and thermodynamic parameters of the actinides-APC complexes. Stability constants and thermodynamic parameters were obtained between americium, berkelium, californium, and einsteinium and the aliphatic APCs nitrilotriacetic acid (NTA), 2-hydroxyethyl ethylenediaminetriacetic acid (HEDTA), trans-1,2-cyclohexanediaminetetraacetic acid (CDTA), and diethylenetriaminepentaacetic acid (DTPA). No significant trends were observed, but 1:2 metal-ligand complexes were formed between NTA and californium or einsteinium, which was not observed between the other actinides. These results were compared to lanthanides with similar ionic radii as the studied actinides, and californium and einsteinium both displayed a 2% selectivity increase when compared to the baseline americium-neodymium linear free energy relationship, in absolute terms. However, all linear free energy relationships were statistically identical to the control system Am-Nd. No trends in selectivity were observed, therefore the aliphatic amines can be said to not show any significant orbital degeneracy driven covalent

interactions with the late actinides. Studies into the aromatic amines and the late actinides may show more covalent interactions.

1.2 Motivation

Recent work has suggested significant covalent interactions in californium compounds with borates and aromatic amino-polycarboxylates, but it is not obvious how the suggested covalency in in these systems will impact complexation thermodynamics or if covalent interactions are available for the neighboring heavy actinides. Since differences in complexation thermodynamics between metals drive separations, understanding how bonding energetics change for actinides through the series would aid in the design of better separation schemes for californium-252 production, the advanced fuel cycle, and, potentially, decontamination and remediation of nuclear accidents involving mixed-oxide (MOX) fuel.

1.3 Thesis Organization

This thesis is divided into 7 chapters. Chapter 1 contains the executive summary and motivation of work. Chapter 2 contains the background overview, literature review, and hypothesis of the work. Chapter 3 contains the procedures used in the work. Chapter 4 contains the results, and chapter 5 discusses those results. Chapter 6 concludes the work with a summary of findings and uses for the work conducted. Chapter 7 contains future work suggestions to further enhance our understanding of the actinide series and its rich chemistry.

Appendix A contains individual Van't Hoff plots of the extraction and competition studies, and tables containing all stability constants of the metal-ligand reactions found during the experiments. Appendix B contains acid dissociation constants of the APCs used in this study, and comparison stability constants. Appendix C contains an example calculation used to

determine stability constants of actinide-APCs. Appendix D contains the raw data collected through experimental work, and fit plots of the data.

CHAPTER 2

BACKGROUND

2.1 The Nuclear Fuel Cycle

Nuclear power constitutes roughly 20% of the world's 15 terrawatt electrical power production (Tsoulfanidis, 2013). The percentage of nuclear power that comprises a given countries energy portfolio varies from 1.5% in Iran to 80% in France (IAEA, 2016). All countries utilize a uranium-based fuel cycle, depicted in Figure 2.1 (Tsoulfanidis, 2013).

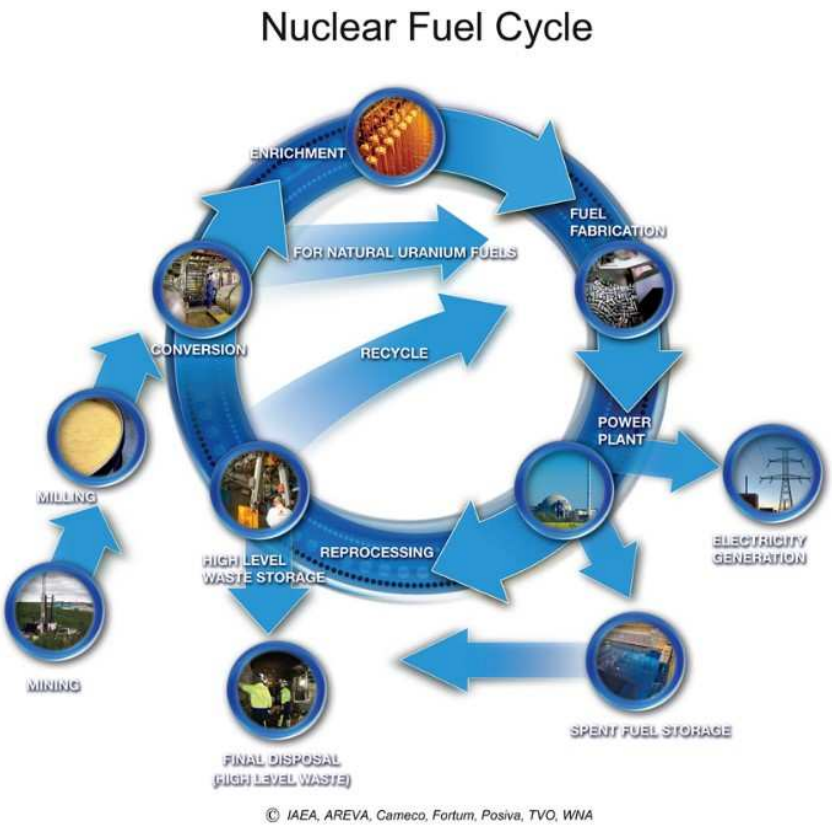

Figure 2.1: The Nuclear Fuel Cycle (IAEA, 2016)

In this type of fuel cycle, the buildup of transuranics (neptunium, plutonium, americium, and curium) generates a potential long-term waste management issue since many of the uranium, plutonium and neptunium isotopes produced via neutron capture and beta decay during power production have half-lives between several thousand years to millions of years. An example of

transuranic production is provided in equation 1, where uranium-238 captures a thermal neutron and through a series of beta decays, transmutes into plutonium-239.

$$^{238}\mathrm{U} + {}^{1}_{0}\mathrm{n} \rightarrow {}^{239}\mathrm{U} \overset{\beta-}{\rightarrow} {}^{239}\mathrm{Np} \overset{\beta-}{\rightarrow} {}^{239}\mathrm{Pu} \quad (1)$$

Open, partially open or closed fuel cycles are possible options to manage used nuclear fuel (Tsoulfanidis, 2013). In an open fuel cycle, used nuclear fuel is recovered from a reactor and eventually buried in a geologic repository where the fuel cannot interact with the surface environment or groundwater movement for thousands to millions of years (Tsoulfanidis, 2013). In a partially open fuel cycle, plutonium present in used nuclear fuel is selectively recovered from uranium, other transuranics (neptunium, americium and curium), and fission products and fabricated into mixed-oxide (MOX) fuel (Tsoulfanidis, 2013). The composition of MOX fuel is nominally 95% depleted uranium and 5% plutonium-239 (Tsoulfanidis, 2013). Fully closing the fuel cycle includes recovering Pu, Np, Am and Cm for their transmutation to shorter lived isotopes in fast neutron spectrum reactors.

Currently, sufficient uranium geological reserves and sufficient amounts of mined uranium preclude closing or partially closing the fuel cycle in the United States. Because of these, and other political issues, the United States is operating under an open fuel cycle model. Open fuel cycles are inefficient regarding fuel utilization and engender long term waste management issues. These long term waste management issues correspond to increased risk that radioactive material stored in permanent geological containment may leak from the intended barrier. Further, the United States does not have a working permanent repository for storing used nuclear fuel since the Yucca Mountain site was closed in 2009 (Zhang, 2016). Consequently, used fuel currently sits in storage pools and dry casks at nuclear power plant sites, creating a risk of release from accidental or malicious actions. Since the closure of Yucca

Mountain, interest in a partially closed or fully closed nuclear fuel cycle has increased to manage used nuclear material from reactors.

Partially open fuel cycles provide the benefit of recycling plutonium produced during initial power production from uranium-based nuclear fuel. This is potentially attractive since only five percent of the available energy is recovered in an open fuel cycle (Tsoulfanidis, 2013). More energy can be produced by recovering plutonium generated in the reactor for production of MOX fuel. Additionally, the heavier plutonium isotopes produced (^{240}Pu, ^{241}Pu and ^{242}Pu) during irradiation of MOX fuel are less attractive for weaponization since they have different half-lives than plutonium-239, potentially larger neutron capture cross sections, and spontaneous fission decays of the nuclides that complicate weapons production.

Several nations have already implemented a partially closed fuel cycle, including France and Japan (Tsoulfanidis, 2013). These nations reprocess used nuclear fuel using the Plutonium-Uranium Redox EXtraction (PUREX) process, a solvent extraction scheme developed to separate plutonium and uranium from used nuclear fuel for weapons development, illustrated generally in equation 2.

$$MX_n + \overline{pS} \rightarrow \overline{MX_nS_p} \qquad (2)$$

The metal salt MX_n reacts with the solvating extractant $\overline{pS}$ to pull the metal salt into the organic phase (Rousseau, 1987). In the PUREX process specifically, plutonium and uranium are extracted from used nuclear fuel by extraction with tri-butyl phosphate dissolved in kerosene. Plutonium is selectively recovered from uranium in the organic phase by reducing plutonium to the less extractable trivalent state. Uranium is recovered from the organic phase by contacting with a dilute nitric acid aqueous phase. This is the most mature separation scheme currently in

use on an industrial scale. The PUREX process leaves behind fission products and minor actinide waste, with the minor actinides generating the majority of radiation after a few hundred years.

Another separation process created as an adjunct to PUREX is the Actinide-Lanthanide Separation Process, or ALSEP. This process takes trivalent lanthanide and actinide rich raffinate from the PUREX process, and attempts to separate the americium and curium from the lanthanide fission products by solvent extraction (Brown et al., 2016). The organic phase consists of a neutral diglycolamide such as N,N,N',N'-tetra(2-ethylhexyl)diglycolamide (T2EHDGA) and an acidic phosphorus based extractant such as 2-ethylhexylphosphonic acid (HDEHP), or mono-2-ethylhexyl ester acid (HEH[EHP]) in a hydrocarbon diluent. The aqueous phase consists of a soft donor complexant such as DTPA or HEDTA in slightly acidic media that strips the actinides out of the organic phase while leaving the lanthanides bound to the extractant in the organic phase.

Californium production requires separation of the heavy actinides from lanthanide fission products and target material. Purification schemes at Oak Ridge and Savannah River use the "Cleanex" and TRialkyl Amine Extraction (TRAMEX) processes to purify the Californium-252 isotope after irradiation (Osbourne-Lee & Alexander, 1995). TRAMEX solvent extraction separates the Americium, Curium, and Californium in the target from fission products using an HDEHP anion exchange extraction and keeping the fission products in the aqueous phase using 11 to 12 M lithium chloride. The "Cleanex" process is used to remove impurities from the target material using an HDEHP extraction, oxidation of molybdenum to the +4 state, and stripping of the transplutonium elements from the organic to the aqueous state. These two processes are batch processes, and require large amounts of lithium chloride that can corrode the structural materials of the tanks involved (King et al., 1980).

Scenarios exist where it may be advantageous to implement a closed fuel cycle, such as countries wishing to be self-sustaining, concerns over long term waste storage, far future colonies on outer planets, and eventual depletion of uranium mining resources. In a closed nuclear fuel cycle, used fuel is reprocessed into new fuel, waste fission products are disposed of in geologic storage or used, and elements such as neptunium, plutonium, and americium are used as fuel and transmuted in fast neutron spectrum reactors (Tsoulfanidis, 2013). While transmutation of transuranics is a goal, an increase in heavy actinide production could exist relative to what occurs in an open or partially open fuel cycle. Depending on the design of a given reactor and fuel, modest amounts of the trivalent actinides americium, curium, berkelium, californium, and einsteinium could be generated, as seen in equations 3, 4, and 5, and Figure 2.2.

$$^{239}\mathrm{Pu} \xrightarrow{2(n,\gamma)} {}^{241}\mathrm{Pu} \xrightarrow{\beta-} {}^{241}\mathrm{Am} \xrightarrow{(n,\gamma)} {}^{242}\mathrm{Am} \xrightarrow{\beta-} {}^{242}\mathrm{Cm} \quad (3)$$

$$^{239}\mathrm{Pu} \xrightarrow{4(n,\gamma)} {}^{243}\mathrm{Pu} \xrightarrow{\beta-} {}^{243}\mathrm{Am} \xrightarrow{(n,\gamma)} {}^{244}\mathrm{Am} \xrightarrow{\beta-} {}^{244}\mathrm{Cm} \xrightarrow{5(n,\gamma)} {}^{249}\mathrm{Cm} \xrightarrow{\beta-} {}^{249}\mathrm{Bk} \xrightarrow{\beta-} {}^{249}\mathrm{Cf} \quad (4)$$

$$^{249}\mathrm{Cf} \xrightarrow{4(n,\gamma)} {}^{253}\mathrm{Cf} \xrightarrow{\beta-} {}^{253}\mathrm{Es} \quad (5)$$

The chemistry of these elements, particularly berkelium, californium, and einsteinium, are poorly understood. Since understanding the fundamental chemistry of the elements created in nuclear fuel encourages better understanding and management of the fuel cycle as a whole, interest exists in developing a more robust understanding of the heavy actinide chemistry.

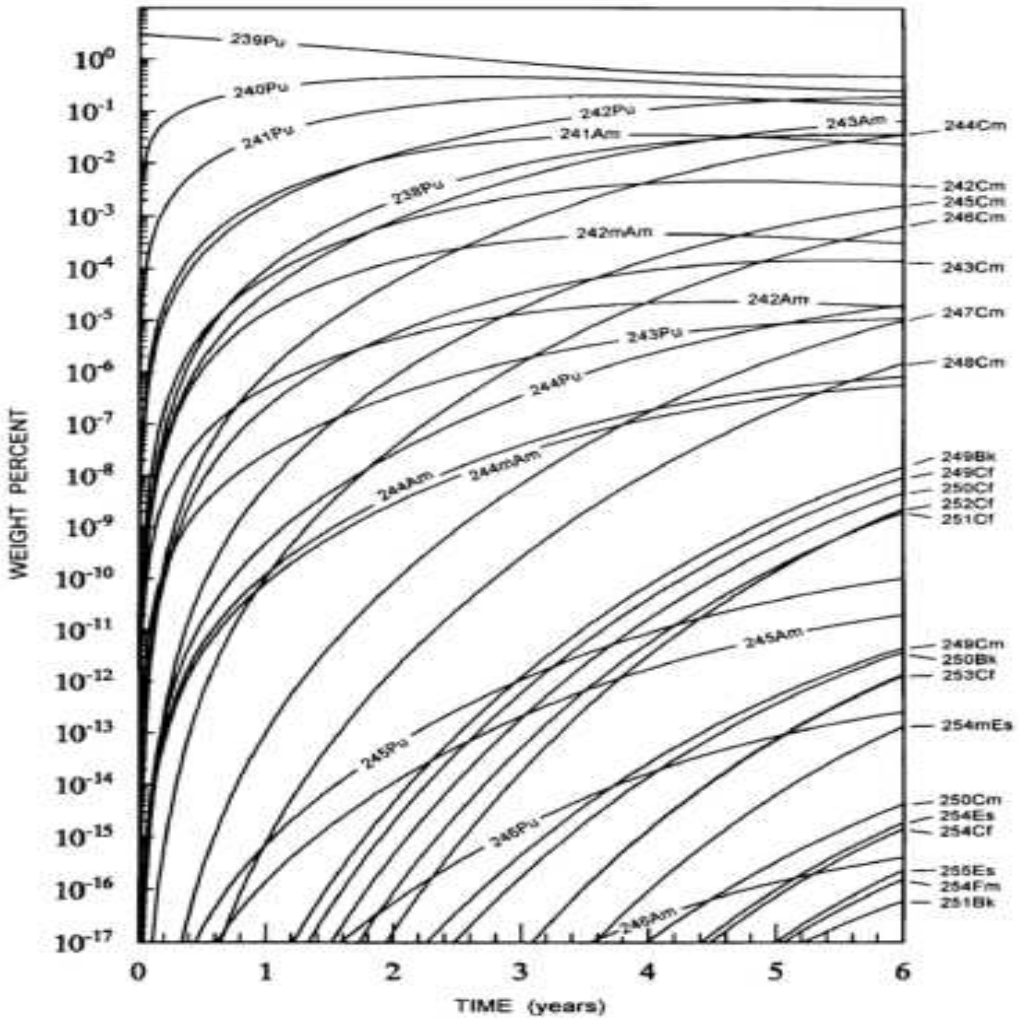

Figure 2.2: Weight percent of transuranic isotopes produced in MOX fuel as a function of time in a thermal spectrum reactor. As fuel is recycled continuously, production of these isotopes increases. These trace isotopes may cause problems in controlling a thermal reactor as many are either neutron absorbers or decay via spontaneous fission, releasing neutrons and affecting the neutron economy of the reactor (Choppin et al., 2001).

2.2 Overview of actinide covalency

Lanthanides are almost always found in the trivalent oxidation state, with severe conditions required to push them into different oxidation states. Early actinides can be found in many different oxidation states, but the trans-plutonium actinides (Am, Cm, Bk, Cf, Es) are almost always found in the trivalent state (again, requiring significant effort to remove them

from the trivalent state). Lanthanides appear in used nuclear fuel as fission products, and trivalent actinides appear in the same fuel as activation and decay products. If efficient transmutation of the actinides in fast neutron spectrum reactors is sought, a selective group separation of the actinides from the lanthanide fission products is necessary due to neutron absorption by the lanthanide fission products. Separations of lanthanides and trans-plutonium actinides have proven difficult, since their oxidation states cannot be readily manipulated, ionic radii of the trivalent actinides are similar to those of the lanthanides, and their chemistry is comparable and largely ionic. Frequently, the perceived ability for the actinides to interact preferentially with soft donors (nitrogen, sulfur) is used to generate a separation between the trivalent actinides and the lanthanides. The selective interaction of actinides with soft-donor ligands is thought to stem from a limited ability for actinides to participate in covalent interactions or overlap of f-orbitals (Braley, 2013), but studies using the heavier trivalent actinides are limited.

Suggestions of covalent behavior in the trivalent Actinides stem from Glenn Seaborg's work with americium and curium in the 1940s and 1950s, as he attempted to separate lanthanide fission products from americium and curium. He and Kenneth Street Jr. found that, after loading trivalent *f*-elements using 0.1 M hydrochloric acid on a DOWEX-50 resin column, americium and curium separated from the lanthanides more easily when eluting with highly concentrated hydrochloric acid than expected (Seaborg & Street, 1950). Seaborg and Street concluded the trivalent actinides formed weak covalent coordination complexes with chloride ions due to the difference in stability of the 4*f* and 5*f* orbitals, resulting in the 5*f* orbital electrons more easily affected by external influences (Seaborg et al., 1954). The trivalent 5*f* actinides are more spatially extended with respect to the 6d orbitals than the lanthanide 4*f* orbitals with respect to

the 5*d* orbitals. Seaborg and Street then suggested that the 5f orbitals can therefore participate in hybridized covalent bonding while the lanthanide 4*f* orbital, which is more deeply shielded than the 5*f* orbital, cannot (Seaborg & Street, 1950).

It has been proposed that actinides have a greater tendency to form covalent bonds since they bond more strongly to certain ligands than their electronic lanthanide analogues. Since the minor actinides and lanthanides have similar ionic radii (Braley, 2013), it has been proposed that the 5*f* orbital protrudes out further and is the reason for the increased covalent interaction of the actinides. The experimental evidence for the reason behind the covalent interactions is lacking, however, and other suggestions include the *s* orbitals as the cause of increased covalency in the actinides (Choppin, 2002), or the mixing of the 5*f* and 6*d* orbitals (Neidig et al, 2013).

Since this early work with the trivalent actinides and lanthanides, more experiments were completed throughout the 1950s and 1960s using soft-donor ligands in solvent extraction and ion exchange separations. Often, these researchers only assessed the stability constants for the given experiments and not the enthalpic or entropic contributions giving rise to these overriding stability constants. Further, experiments were conducted with vastly different ionic strengths, temperatures, and methods.

Throughout the latter half of the 20th century, researchers continued to study the trivalent actinides and their solution chemistry. Gregory Choppin studied the actinides and their solution chemistry most thoroughly, describing how the actinides interact in solution as hard acids and rarely interact with soft donors in the aqueous phase except for nitrogen bearing ligands, with oxygen donors such as aminopolycarboxylates (Choppin, 1982). Choppin concluded the enthalpic binding contribution potentially arising from nitrogen interactions with trivalent actinides and lanthanide were comparable (Choppin, 1982). Therefore, an enthalpic 'covalency

signature' for actinide interactions with aminopolycarboxylates was not observable (Choppin, 1982). There may be reasons to believe this study should be reassessed (*vide infra)*.

Table 1 shows the enthalpy values previously gathered from Gregory Choppin through calorimetry and solvent extraction studies (Braley, 2013).

Table 2.1: Change in Enthalpy Values for Trivalent Actinide-NTA Complex Formation at 0.5 M Ionic Strength and 25°C [kJ/mol]. Parenthetical values indicate error amounts. (Braley, 2013)

APC	Am^{3+}		Cm^{3+}		Cf^{3+}	Es^{3+}
	Calorimetry	Solvent Extraction	Calorimetry	Solvent Extraction	Solvent Extraction	Solvent Extraction
IDA	-4(1)	-18(1)		-14(1)		
NTA	-13(1)	-9(1)	-11(2)	-3(2)	0.8(2)	1.8(2)
EDTA	-24(1)	-32(1)	-29(1)	-29(2)		
CDTA	-10(1)		-10(2)			
TMDTA	-13(1)	-13(1)				
DTPA	-40(1)	-16(2)	-14(2)			

The data in this table indicate poor agreement between enthalpic studies, due possibly to errors in interlab investigations and variance in differing techniques that propagate through the study. For certain systems, Choppin assessed the residual enthalpy of complexation, or the enthalpy arising just from nitrogen complexation from an APC with a given actinide. This was done by assuming the enthalpy arising from acetate-actinide interactions was a reasonable model for the oxygen-metal interactions that occur during metal-APC binding (Choppin & Schneider, 1970).

This assumption and data treatment have some inherent limitations. The acetate enthalpies were from data measured in 2.0 M ionic strength media, whereas the actinide-APC complexation enthalpies were completed in 6.60 M, 0.5 M, and 0.1 M acid media. It must be noted that there are serious errors associated in the 6.60 M data analysis, and therefore, no results from this study were used. Additionally, only the enthalpy for the 1:1 acetate-metal complex was

used to correct for multiple metal-oxygen interactions in the metal-APC complex. Presumably the metal-oxygen interactions would become less exothermic as subsequent oxygens are added to the metal complex. Finally, actinide-lanthanide comparisons were done between metal ions that had significantly different ionic radii and, consequently, charge density and reactivity. More fair comparisons could be completed by correcting these limitations.

2.3 Recent findings

More recent studies have concluded that these trivalent actinides do exhibit covalent bonding behavior, but now the degree and type of covalency is the question. Neidig, Clark, and Martin studied the types and degrees of covalency in the actinides and concluded that actinides may form covalent bonds by orbital overlap or near degeneracy (Neidig et al., 2013). The early actinides, with their rich redox chemistry and multiple valence states, show orbital overlap of the 5*f* and 6d orbitals, contributing to stronger covalent interactions (Neidig et al., 2013). The trivalent actinides, however, exhibit metal-ligand bonding through "virtual 6*d* orbital interactions with filled ligand lone pairs" (Neidig et al., 2013). There is also a much larger than expected 5*f* orbital mixing into occupied metal-ligand bonding orbitals. This does not necessarily indicate a buildup of charge at the midpoint of the bond, but may indicate a near degeneracy. Also, a change from the 2*p* orbital of oxygen to the 3*p* orbital of soft donor ligands may contribute to the covalency of the bond (Neidig et al., 2013).

Borate and dipicolinic acid (DPA) systems have shown unexpected covalent interactions with trivalent californium (Albrecht-Schmitt, 2014), (Albrecht-Schmitt, 2015). The californium borate study found that californium was the only actinide borate to display substantial electronic property changes. These findings were used to suggest that a possible "break" in the actinide series may occur at californium. Since borates have a highly electron rich environment and have

minimal potential applications for used nuclear fuel separations, the same group then studied the californium dipicolinate system. Dipicolonic acid is an aminopolycarboxylate ligand that has acidic acid dissociation constants, an electron rich environment due to the aromatic ring attached to the amine group, and demonstrated selectivity for trivalent actinides over trivalent lanthanides. This second report confirmed a difference between the californium systems relative to the borate and dipicolinate systems containing curium. The Albrecht-Schmitt research group postulates that variation in chemical behavior starting at californium stems from the relative ease at which the californium ion can be reduced to the divalent state. Since the divalent state becomes more favorable with increasing actinide atomic number, this effect should become more pronounced with einsteinium, mendelevium, nobelium, and lawrencium. Figure 3 shows the absorption spectra of curium dipicolinate and californium dipicolinate (Albrecht-Schmitt, 2015).

While the broadened spectroscopic transitions and suppressed magnetic moments observed for californium are suggestive of actinide covalency, it is not obvious how covalency would impact the complexation thermodynamics. Examination of elements beyond curium might present differences in thermodynamic properties at californium and support Albrecht-Schmitt's hypothesis of a break in the series. Further, Choppin's actinide thermodynamics review compares thermodynamic data obtained by different methods at different laboratories under different conditions, and these values obtained are in poor agreement (Choppin et al., 2006). A single lab performing these characterizations would be better able to compare thermodynamic data, since conditions would be standardized throughout the series of experiments. Since the available data is ambiguous regarding potentially different trans-actinide thermodynamic data starting at californium, we must fully examine the complexation behavior of the late actinides

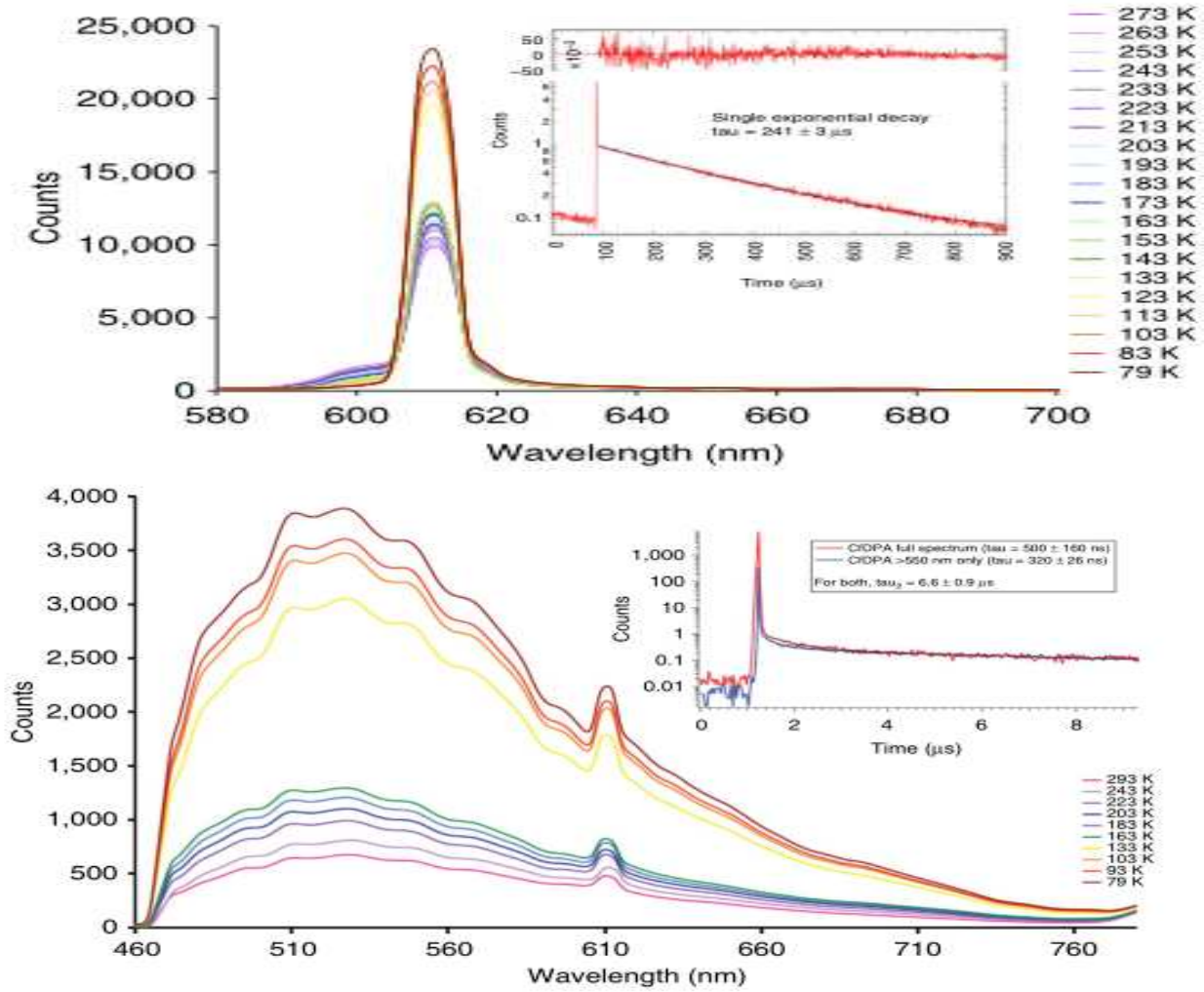

Figure 2.3: Photoluminescence spectra of curium dipicolinate (top) and californium dipicolinate (bottom). 420 nm visible light was used to excite the dipicolinate crystals, and while curium shows a slightly broadened peak relative to lanthanide dipicolinates, californium presents an unexpected broad peak, similar to d-block elements. (Albrecht-Schmitt, 2016)

and lanthanides to determine if there is a thermodynamic break in the behavior of the actinides at californium.

2.4 Hypothesis

If aliphatic amines are able to participate in significant covalent interactions with the heavier actinides, then significant differences should be observed in complexation thermodynamics for the heavier actinides relative to the lanthanides and earlier trivalent actinides.

2.5 Project Specific Reagents

This project used four different APCs to complex with the heavy actinides in the aqueous phase, and one organic extractant to complex with the heavy actinides in the organic phase. The aminopolycarboxylates nitrilotriacetic acid (NTA), 2-hydroxyethyl ethylenediaminetriacetic acid (HEDTA), trans-1,2-cyclohexanediaminetetraacetic acid (CDTA), and diethylenetriaminepentaacetic acid (DTPA) have previously been studied as complexing agents useful in separations between actinides and lanthanides, with HEDTA and DTPA used in industrial scale processes (Fuger, 1958).

2.5.1 Nitrilotriacetic acid (NTA)

NTA is a simple tetradentate aminopolycarboxylic acid consisting of one tertiary nitrogen center with three acetic acid groups attached. It is an industrial chemical widely used in detergents to control metal ions in water, enhancing detergent effectiveness (Gousetis & Opgenorth, 2000). While NTA is an intrinsically stable molecule, NTA breaks down readily in the environment, forming environmentally friendly molecules (Gousetis & Opgenorth, 2000). The neutral form of NTA is practically insoluble in water, but may be dissolved under basic conditions, as the metal salt is soluble in water. Complexation reactions with trivalent metals, including lanthanides and

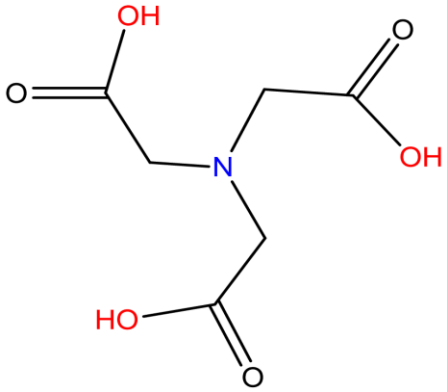

Figure 2.4: Nitrilotriacetic Acid Molecular Structure

actinides, have been reported to be very favorable (Choppin et al., 2006). NTA may form up to

four bonds with a trivalent metal. Table 2 lists the protonation constants, with the fully protonated constant omitted, as pH electrodes are usually limited to a pH of 2.

Table 2.2: Acid Dissociation Constants and Thermodynamic Information for NTA at Standard Conditions I = 0.5 M Ionic Strength and 25°C. (Choppin et al., 1977)

Protonated Ligand	pKa	ΔH° [KJ/mol]
H_1NTA	9.570	-24.2
H_2NTA	2.641	0
H_3NTA	1.569	0

2.5.2 2-Hydroxyethyl Ethylenediaminetriacetic acid (HEDTA)

HEDTA is a pentadentate diamine with two acetic acid groups bonded to one nitrogen and one acetic acid group and one alcohol group bonded to the other nitrogen. HEDTA is similar in structure to EDTA, a common chelating agent. However, the substitution of an alcohol group allows for better solubility than EDTA. As with NTA, HEDTA complexes with both lanthanides and actinides, where the three acetate groups complex to the metal center. The actinides are thought to form stronger complexes with HEDTA due to the influence of the diamine. Protonation

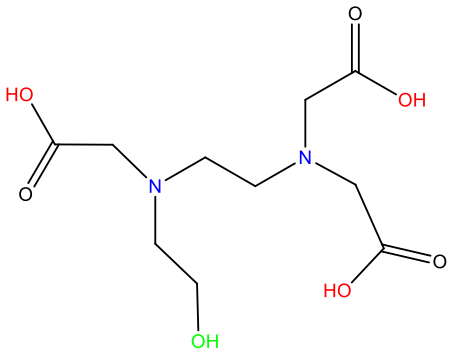

Figure 2.5: 2-Hydroxyethyl Ethylenediaminetriacetic Acid Molecular Structure

constants are listed in Table 3, with the fourth constant omitted.

Table 2.3: Acid Dissociation Constants and Thermodynamic Information for HEDTA at Standard Conditions I = 0.5 M Ionic Strength and 25°C. (Choppin, 1977)

Protonated Ligand	pKa	ΔH° [KJ/mol]
H_1HEDTA	9.79	-28
H_2HEDTA	5.40	-12(I = 0.1)
H_3HEDTA	2.71	4.6(I = 0.1)

2.5.3 Trans-1,2-cyclohexanediaminetetraacetic Acid (CDTA)

CDTA is a hexadentate APC ligand, with two amine groups attached to a cyclohexane ring and four carboxylic acid groups attached. The amine groups are attached to the cyclohexane

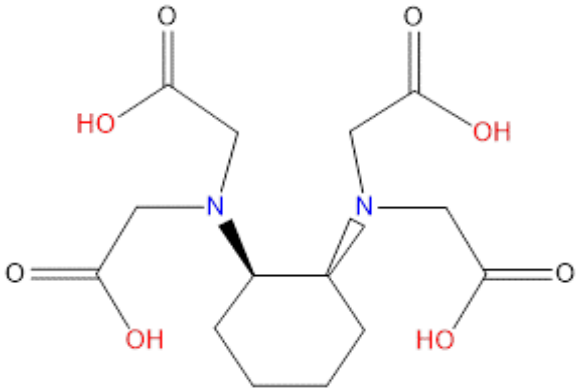

Figure 2.6: Trans-1,2-cyclohexanediaminetetraacetic acid molecular structure

ring in the trans conformation. Essentially, this molecule was designed off of the backbone of EDTA, only adding a cyclohexane ring to provide a more rigid structure. Therefore, the ligand only bonds to metal ions in one conformation. Protonation constants for CDTA are listed in Table 2.4.

Table 2.4: Acid Dissociation Constants and Thermodynamic Information for CDTA at Standard Conditions I = 0.5 M Ionic Strength and 25°C (Choppin et al. 1977)

Protonated Ligand	pKa	ΔH° [KJ/mol]
H_1CDTA	11.30	-38.8
H_2CDTA	6.51	-10.7
H_3CDTA	3.01	-1.4
H_4CDTA	2.38	-1.7
H_5CDTA	1.65	0

2.5.4 Diethylenetriaminepentaacetic acid (DTPA)

DTPA is a potentially octadentate ligand, with three amine groups and five carboxylic acid groups. This ligand can potentially form eight bonds with a metal ion. At pHs of 2.0 to 3.0, deprotonated DTPA competes with a protonated species to form metal complexes.

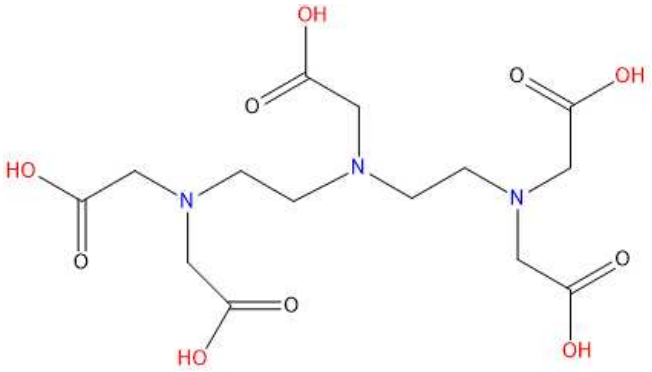

Figure 2.7: Diethylenetriaminepentaacetic acid molecular structure

DTPA was considered as a ligand to use in several reprocessing schemes to separate trivalent actinides from lanthanide fission products in used nuclear fuel. DTPA's protonation constants are listed in Table 2.5.

Table 2.5: Acid Dissociation Constants and Thermodynamic Information for DTPA at Standard Conditions I = 0.5 M Ionic Strength and 25°C (Choppin, 1977)

Protonated Ligand	pKa	ΔH° [KJ/mol]
H_1DTPA	9.90	-33
H_2DTPA	8.32	-17
H_3DTPA	4.10	-6.2
H_4DTPA	2.70	-1
H_5DTPA	2.10	2
H_6DTPA	1.60	0

2.5.5 HDEHP Organic Cation Exchange Extractant

HDEHP is a dialkylphosphoric acid, soluble in organic media but insoluble in water and even less soluble in acidic aqueous media. It is a di-ester of phosphoric acid and 2-ethylhexanol.

HDEHP has been investigated as a replacement for TBP in the PUREX process, and is used in laboratory scale actinide and lanthanide extractions. While TBP is a solvating extractant, HDEHP extracts using a cation exchange mechanism, where the hydrogen ion exchanges for the desired metal on the extractant.

HDEHP is a self-associating dimer acid (Marcus & Kertes, 1969). Figure 8 shows the dimer structure. For the trivalent metals, three HDEHP dimers are required to bind to the metal to

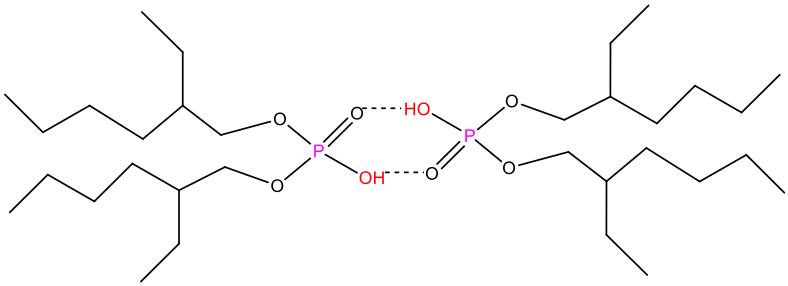

Figure 2.8: Bis-2-ethylhexyl Phosphoric Acid Dimer Structure

extract it into the organic phase. HDEHP is a strong complexant that can compete with APCs, and shows consistent behavior over a wide range of temperatures, concentrations acid concentrations, and is ideal for use in this study. Further, its extraction of trivalent metals is fast, minimizing extraction limitations.

CHAPTER 3

EXPERIMENTAL CONDITIONS OF COMPETITION STUDIES BETWEEN NTA, HEDTA, CDTA, AND DTPA AND HDEHP

For all extraction and distribution studies, common media and methods were used. A solvent extraction method consisting of HDEHP dissolved in n-dodecane contacted with aqueous 0.5 M Na/$HClO_4$ media was selected as the separation model due to the predictability of the system and the relative ease of use.

3.1 Chemicals

HDEHP was obtained from Sigma Aldrich at 97% purity and purified using the method described by Zhenshui, Ying, Wanwu, and Xun (Zhenshui et al., 1995). Purity of the HDEHP was verified at >99% by NMR. n-Dodecane was obtained from Sigma Aldrich at >99% purity and used without further purification. NTA was obtained from TCI chemicals and dissolved without further purification after comparison of recrystallized NTA with unpurified NTA yielded no significant differences in metal distribution between the two solutions. HEDTA was obtained from Alfa Aesar, CDTA was obtained from Combi-Blocks, and DTPA was obtained from Fluka Analytical at >99% purity. All APCs were used without further purification. $NaClO_4$ was obtained from Sigma Aldrich at >98% purity, recrystallized thrice, and dissolved in nitrogen degassed 18 MΩ water.

Radiotracer stock solutions of americium-241 nitrate were obtained from Dr. Gregory Choppin's laboratory through Dr. Thomas Albrecht-Schmitt and his research group. These stocks were diluted and dissolved in perchlorate media after heating and evaporation treatment to remove the nitrate ions. Radiotracer stock solutions of berkelium chloride were obtained from Oak Ridge National Laboratory. These stocks were directly dissolved in perchlorate media. A

radiotracer stock solution of californium-249 chloride was obtained from Thomas Albrecht-Schmitt's laboratory and was diluted directly without any treatment to remove chloride ions[1]. Radiotracer stock solutions of einsteinium-253 and einsteinium-254 where obtained from the Oak Ridge National Laboratory High Flux Reactor and Chemical Separations Division.

3.2 Potentiometry

All potentiometric measurements were conducted on all APC reagents used in the study using a Thermo Scientific Orion Ross 8103BNUWP pH probe and compared using solutions of known pcH (pH corrected from hydrogen ion activities) to obtain corrected hydrogen ion concentrations. Potentiometric measurements were also conducted on final APC solutions and blank $NaClO_4$ solutions to obtain pcHs used in data analysis. Hydrogen ion concentrations were also obtained using a Thermo Scientific Orion Ross 8103BNUWP pH probe of solutions containing no radiotracer and radiotracer to obtain differences in pcH after adding radiotracers, and hydrogen ion concentrations were corrected for radiotracer additions.

3.3 Extraction Studies

Extractions of actinides using selected HDEHP concentrations were performed to obtain K_{ex} values at different temperatures used throughout the distribution studies. HDEHP solutions were created in n-dodecane media either directly from purified HDEHP or diluted from a solution in n-dodecane containing high concentration HDEHP.

To pre-equilibrate these organic phases with sodium perchlorate ions, these HDEHP solutions were contacted with a blank (no radiotracer) aqueous phase of studied ionic strength

[1] It is of note that significant berkelium-249 contamination of the californium-249 stock was discovered after all experiments were conducted. It is unlikely that this contamination affected measurements, as counting statistics were gathered on a gamma counter, and Bk-249 has no appreciably gamma emission.

(0.5 M $NaClO_4$) and constant pcH of 2.5 at constant temperature in a 1:1 ratio of organic to aqueous solution. These solutions were first allowed to reach the studied temperature in a water bath or a Labnet Temperature Controlled Shaker water bath for 15 °C determinations for fifteen minutes, mixed for approximately ten seconds on a VWR Standard Vortex Mixer, returned to a water bath for ten minutes for phase separation, centrifuged in a Beckton Dickinson Clay Adams Compact II centrifuge for approximately ten seconds to fully separate the phases, then returned to the water bath for another ten minutes. After this process, the pre-equilibrated organic phase was taken and placed into 2 mL sample vials, split into 800 µL phases into each sample vial. Aqueous phases were placed into waste. HDEHP concentrations used in K_{ex} determinations are listed in Table 3.1. Note that the differences in HDEHP concentration are due to the increased extraction of the metal ions across the actinide series.

Table 3.1: HDEHP concentrations used in K_{ex} determinations, listed in molarity for ease of use.

Radiotracer	HDEHP Concentrations (mM)
Am-241	1, 2, 3, 5
Bk-249	0.5, 0.6, 0.7, 0.8, 0.9
Cf-249	0.1, 0.2, 0.3, 0.4, 0.5
Es-253/254	0.1, 0.2, 0.3, 0.4, 0.5

Radiotracer solutions consisting of a blank sodium perchlorate phase at constant pcH of 2.5 and constant ionic strength of either 0.1 M or 0.5 M were created by adding microliter amounts of prepared radiotracer. These aqueous phases were contacted with a 1:1 volume of n-dodecane and were pre-equilibrated in a similar manner to the HDEHP phases as described above. The radiotracer aqueous phase was split into three 800 µL samples and placed into the same 2 mL sample vials as the HDEHP solutions to create a 1:1 organic/aqueous experiment run in triplicate.

K_{ex} determination experiments were conducted by varying the HDEHP concentration and temperature, with each experiment conducted in triplicate. Each sample vial was placed on a Labnet International Accutherm temperature controlled shaker[2] for twenty minutes to allow the vials to reach the studied temperature. After twenty minutes, the shaker was started at 1500 rpm for a length of time described in Table 3.2.

Table 3.2: Radiotracer K_{ex} Determination Contact Times

Radiotracer	Temperature (°C)	Contact Time
Am-241	15, 25, 35, 45, 55	1 hr
Bk-249	15, 25, 35, 45, 55	1 hr
Cf-249	25, 35, 45, 55	30 min
Cf-249	15	45 min
Es-253/254	25, 35, 45, 55	30 min
Es-253/254	15	45 min

After the contact time is achieved, the vials were left at temperature for twenty minutes to allow bubbles to dissipate and phases to separate. Once separation is achieved, the vials were centrifuged in a Beckton Dickinson Clay Adams Compact II centrifuge for approximately ten seconds to fully achieve phase separation. The vials were then returned to the Labnet shaker for ten to fifteen minutes to settle at temperature before sampling.

After this contact process, each vial was removed from the shaker, and 600 µL of the organic phase was sampled directly with a 200 µL pipette three times into either a gamma counting tube (Cf-249), or 4 mL of Ecoscint liquid scintillation cocktail (Am-241, Bk-249, and Es-253/254). This process may increase sampling error, but reduced the amount of radiotracer solution required per experiment. The remaining organic phase was then pipetted out of the

[2] The Labnet temperature controlled shaker top directly from Labnet could not accommodate the 2 mL sample vials used in the study. Therefore, a custom aluminum block was created by a drill press and bolted onto the shaker, with vial spaces in a 7x5 configuration. Each temperature used was measured using a thermocouple inserted into a 2 mL sample vial filled with DI water and allowed to equilibrate. Each space in the block was measured and variations in any temperature were determined to be only 0.1 °C.

reaction vial with a plastic fine tip pipette. The aqueous phase was then sampled, 600 μL bubbling through the top of the solution to the bottom and dispensing the aqueous phase into a new gamma tube or liquid scintillation vial.

All samples were then counted on either a Cobra gamma counter for Cf-249, a Canberra Liquid Scintillation Counter for Am-241 and Bk-249, or a Hidex Liquid Scintillation Counter for Es-253/254.

3.4 APC Distribution Studies

APC distribution studies were conducted in a similar manner as the extraction studies, with a few adjustments. The aqueous phase contained the appropriate APC during pre-equilibration and extraction steps and only one HDEHP concentration was used for a given APC. An ionic strength of 0.5 M was maintained with NTA, HEDTA, CDTA, and DTPA throughout all experiments. All experiments were run in triplicate. Temperatures and contact times used are listed in Table 3.3. APC concentrations are listed in Table 3.4, and HDEHP concentrations are listed in Table 3.5.

Table 3.3: Radiotracer Temperatures, and Contact Times

Radiotracer	APC	Temperatures (°C)	Contact Times
Am-241	NTA, HEDTA	15, 25, 35, 45, 55	2 hr
Bk-249	NTA, HEDTA	15, 25, 35, 45, 55	2 hr
	CDTA, DTPA	25, 30, 35, 45, 55	2 hr
Cf-249	All	15, 25, 35, 45, 55	1 hr
Es-253/254	NTA, HEDTA, & CDTA	15, 25, 35, 45, 55	2.5 hr
	DTPA	25, 35, 45	

Table 3.4: APC Concentrations Used

Radiotracer	NTA (mM)	HEDTA (mM)	CDTA (mM)
Am-241	0.05, 0.075, 0.1, 0.2, 0.3, 0.4, 0.5, 1	0.01, 0.025, 0.05, 0.075, 0.1, 0.25, 0.35, 0.5	not studied
Bk-249	0.1, 0.25, 0.4, 0.5, 0.6, 0.75, 1, 1.1, 1.2, 1.5	0.05, 0.1, 0.3, 0.5, 0.7, 1, 2, 3, 4, 5	0.01, 0.03, 0.05, 0.1, 0.3, 0.5, 1
Cf-249	0.1, 0.5, 0.75, 1, 2, 3, 4, 5	0.1, 0.25, 0.5, 0.75, 1, 3, 5, 7	0.01, 0.03, 0.05, 0.07, 0.1, 0.5
Es-253/254	1, 2, 3, 4, 5	0.5, 0.75, 1, 3, 5, 7	0.03, 0.05, 0.07, 0.1, 0.2

Table 3.5: HDEHP concentrations used in APC competition studies

Radiotracer	Ligand Study	HDEHP Concentration (mM)
Am-241	NTA	5.0
	HEDTA	5.0
Bk-249	NTA	4.25
	HEDTA	5.0
	CDTA	20.0
	DTPA	20.0
Cf-249	NTA	1.365
	HEDTA	5.193
	CDTA	20.0
	DTPA	20.0
Es-253/254	NTA	1.365
	HEDTA	5.193
	CDTA	15.0
	DTPA	20.0

DTPA at pcHs studied is known to form two species, a protonated complex and unprotonated complex. Therefore, it was necessary to study DTPA concentrations at different pcHs to obtain thermodynamic parameters. DTPA pcH studies were conducted at 25°C, 35°C, 45°C, and 55°C to obtain thermodynamic information for Bk and Cf, and 25°C, 35°C, and 45°C for Es. Am-241 DTPA complexes were not studied. DTPA concentrations are listed in Table 3.6.

Table 3.6: DTPA pcH Concentration Conditions

Radiotracer	pcH 1.9 (mM)	pcH 2.1 (mM)	pcH 2.3 (mM)	pcH 2.5 (mM)
Bk-249	0.01, 0.05, 0.1, 0.3, 0.5	0.1, 0.5, 1, 2, 3, 4, 5	0.01, 0.05, 0.1, 0.3, 0.5	0.01, 0.05, 0.1, 0.3, 0.5
Cf-249	0.1, 0.3, 0.5, 0.7, 1	0.1, 0.3, 0.5, 0.7, 1	0.1, 0.3, 0.5, 0.7, 1	0.1, 0.3, 0.5, 0.7, 1
Es-253/254	0.1, 0.3, 0.5, 0.7, 1	0.1, 0.3, 0.5, 0.7, 1	0.1, 0.3, 0.5, 0.7, 1	

CHAPTER 4

RESULTS

4.1 Extraction Equilibria

The extraction of metals by the organic cation exchange molecule HDEHP is shown by the equation 6, where M is a trivalent metal ion.

$$M^{3+} + \overline{3HDEHP_2} \rightarrow \overline{M \cdot ((HDEHP)_2)_3} + 3H^+ \quad (6)$$

Equation 1 shows that one trivalent metal ion will complex with three HDEHP dimers. Each HDEHP dimer will exchange one hydrogen ion from the phosphoric acid into the aqueous phase. Therefore, the extraction constant of the reaction will be obtained by equation 7 (Heathman & Nash, 2012).

$$K_{ex} = \frac{\left[\overline{M \cdot ((HDEHP)_2)_3}\right][H^+]^3}{[M^{3+}]\left[\frac{\overline{HDEHP}}{2}\right]^3} \quad (7)$$

The concentration of trivalent metal bonded to the HDEHP in the numerator divided by the concentration of metal ion in the aqueous phase is known as the distribution of the metal, as shown in equation 8.

$$D_o = \frac{\left[\overline{M \cdot ((HDEHP)_2)_3}\right]}{[M^{3+}]} \quad (8)$$

The distribution ratio makes solving for the extraction constant using a non-linear least squares method easier, and allows easier understanding of extraction behavior with differing conditions, such as temperature variations and the presence of aminopolycarboxylates in the aqueous phase.

Thermodynamic parameters may be deduced from a Van't Hoff analysis. Inverse temperature in Kelvin is plotted against the natural logarithm of the extraction constants to obtain a line. The slope of the trend line is the negative change in enthalpy divided by the universal gas

constant, and the intercept is the change in entropy divided by the universal gas constant, illustrated in equation 9.

$$\ln K_{eq} = -\frac{\Delta H}{RT} + \frac{\Delta S}{R} \quad (9)$$

The Gibbs free energy may be obtained from the standard enthalpy and entropy changes or the stability constant at T = 25°C via equation 10a or 10b. All Gibbs free energy changes were calculated using equation 10b due to lower error propagation unless otherwise noted.

$$\Delta G° = \Delta H° - T\Delta S° \quad (10a)$$

$$\Delta G° = -RT\ln K \quad (10b)$$

All error calculations are displayed as 1σ in tables and plots.

4.1.1 Extraction Equilibria Results

All extraction equilibria were expected to present exothermic behavior, or an inverse relationship between temperature and extraction constants. Plots of the log values of the HDEHP dimer concentration (x-axis) versus the log of the distribution coefficients (y-axis) should have slopes of around 3, indicating a cubic power dependence of HDEHP dimer concentration on distribution coefficient.

Americium extraction trials, depicted in Figure 4.1, yielded unusual results for the temperature trial of 25°C. The slope of T = 25°C is 2.49, while all other lines yield slopes closer to 3. It is possible that T = 25°C phases became contaminated during the sampling process, yielding incorrect distribution coefficients at certain data points. Since other temperature data sets yield predicted relationships, the T = 25°C was removed from further consideration and K_{ex} values for this relationship were interpolated from thermodynamic results.

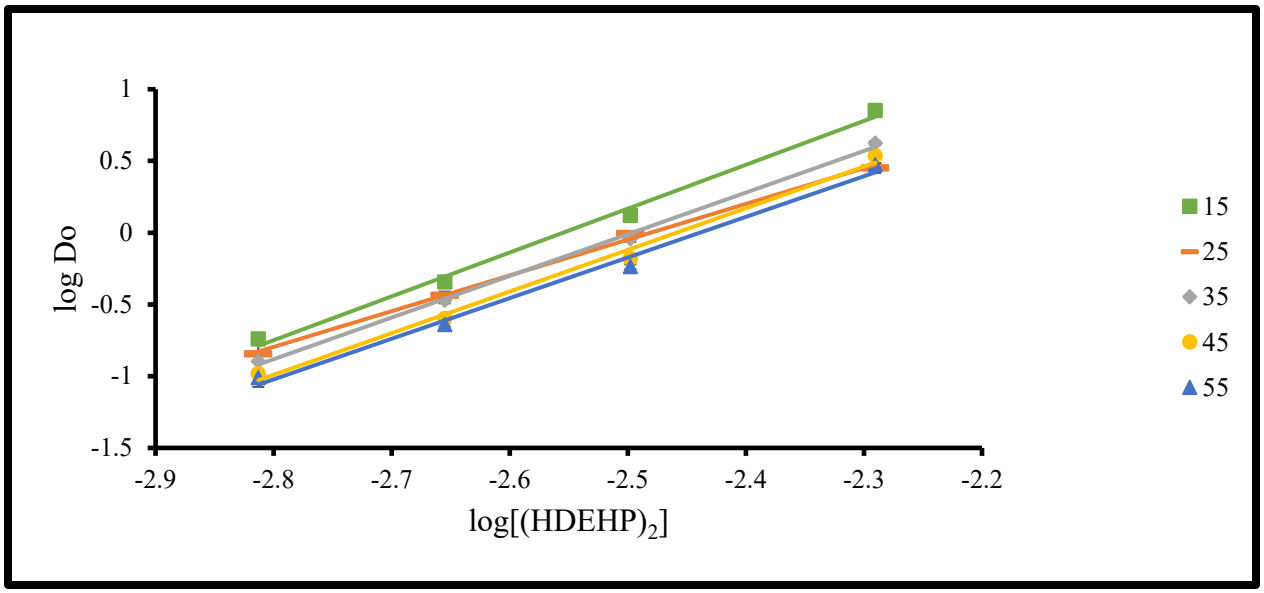

Figure 4.1: Results of americium equilibrium extraction trials, I = 0.5 M, pcH = 2.5, HDEHP in n-dodecane.

The distribution ratios, standard deviations, and HDEHP molal concentrations may be analyzed to determine the extraction coefficient for each temperature using a non-linear least-squares analysis tool like the QTIplot program. The program plots the non-linear data and uses equation 7 to determine the extraction constant based on the distribution ratios and HDEHP concentrations while assuming a constant hydrogen ion concentration. The results of this analysis are listed in Table 4.1.

Table 4.1: Americium HDEHP Extraction Constants I = 0.5 M. The T = 25°C data is extrapolated.

Temperature (°C)	K_{ex}	Error
15	86	4
25	69	5
35	61	2
45	51	1
55	41	2

Berkelium extraction constants were assessed in a similar method to americium, with the extraction lines shown in Figure 10. All temperature lines had a slope of 2.5 or greater except the T = 25°C data set.

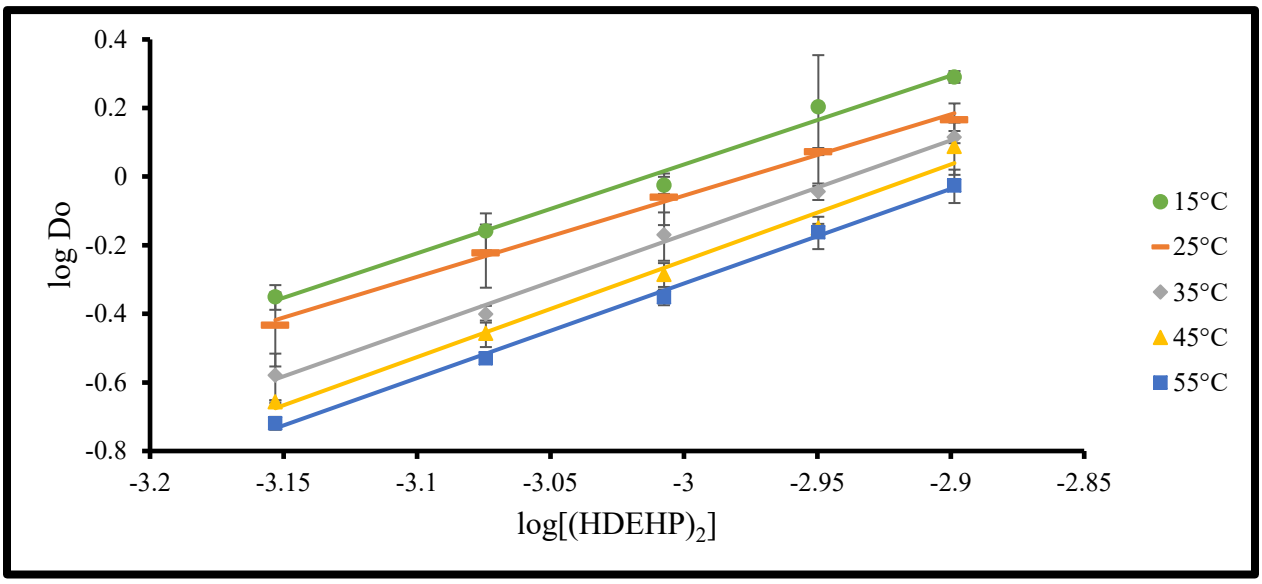

Figure 4.2: Results of berkelium equilibrium extraction trials, I = 0.5 M, pcH = 2.5.

The extraction constants for berkelium HDEHP are listed in Table 4.2. Under the same conditions as americium, berkelium extracts slightly more than americium, and has more temperature variability.

Table 4.2: Berkelium-HDEHP extraction constants, I = 0.5 M.

Temperature (°C)	K_{ex}	Error
15	103	4
25	76	5
35	59	1
45	44	2
55	33.8	0.6

Californium extracts into the organic phase much stronger than either americium or berkelium. Extraction experimental results are shown in Figure 4.3. However, results from the

non-linear least squares analysis (shown in Table 4.3) and the Van't Hoff analysis yield overly large extraction constants results.

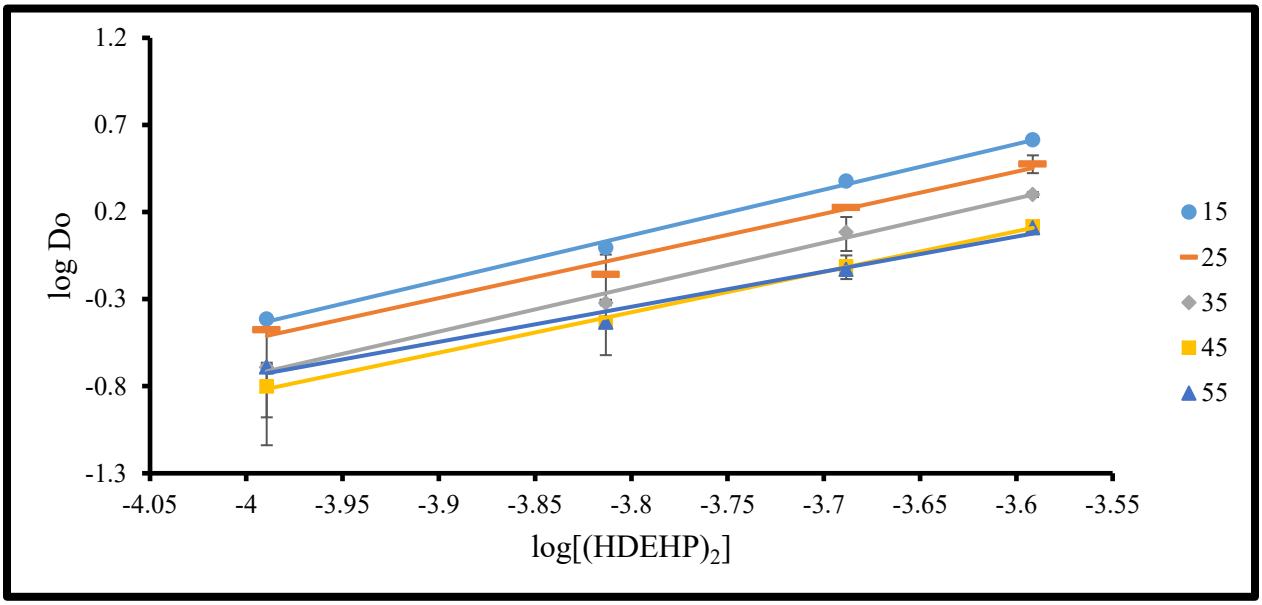

Figure 4.3: Results of californium equilibrium extraction trials, I = 0.5 M, pcH = 2.5.

Table 4.3: Californium HDEHP extraction constants, I = 0.5 M.

Temperature (°C)	K_{ex}	Error
15	72,000	6,000
25	47,000	1,300
35	31,000	2,300
45	23,000	800
55	32,000	7,400

Based on the three previous elements, einsteinium was expected to extract better than californium. Figure 4.4 shows the results of the einsteinium extraction experiments.

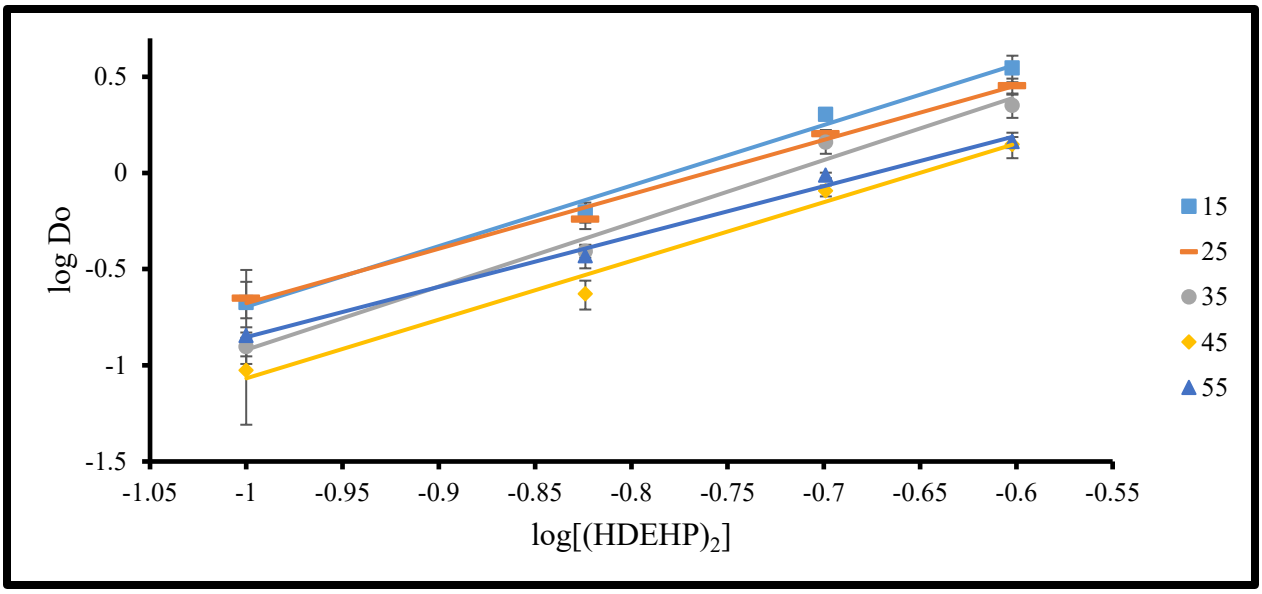

Figure 4.4: Results of einsteinium equilibrium extraction trials, I = 0.5 M, pcH = 2.5.

Either the T = 45°C set does not follow the pattern of decreasing extraction with increasing temperature, or the T = 55°C set, which crosses the T = 35°C line, is incorrect. It is more likely that the T = 35°C data set is incorrect due to large errors in the distribution values. Results of the non-linear least squares analysis are listed in Table 4.4.

Table 4.4: Einsteinium extraction constants

Temperature (°C)	K_{ex}	Error
15	5,700	270
25	5,300	280
35	3,800	320
45	2,400	170
55	3,300	320

4.1.2 Extraction equilibria thermodynamics

These extraction constants may be used to determine thermodynamic information related to the extraction of americium with HDEHP. A Van't Hoff analysis of actinide extraction

constants produces the plot depicted in Figure 4.5, with the trend line equation listed above the lines.

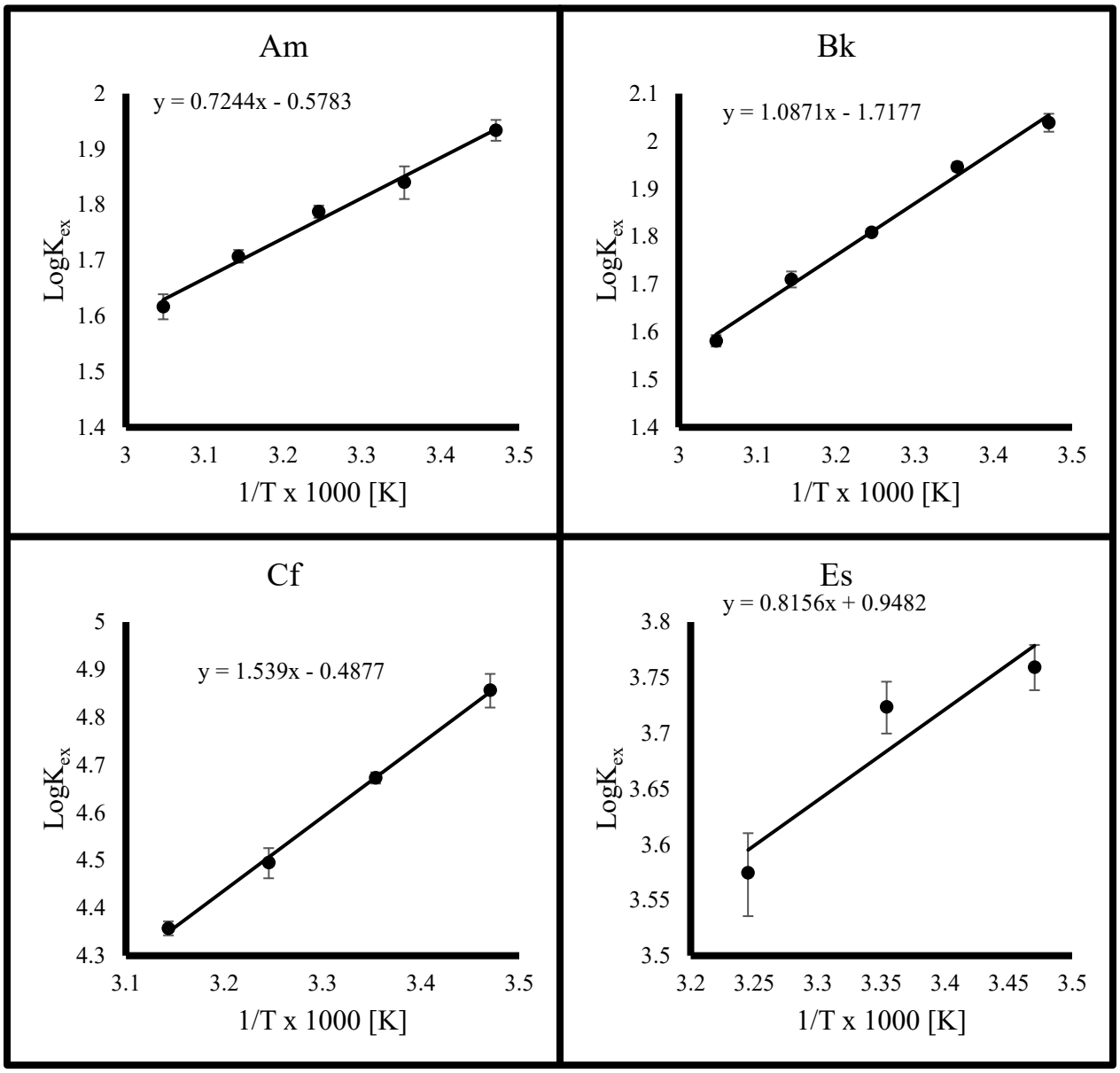

Figure 4.5: Van't Hoff analysis of extraction, I = 0.5 M, pcH = 2.5. Clockwise from top left: (A) Am-HDEHP, (B) Bk-HDEHP, (C) Cf-HDEHP, (D) Es-HDEHP.

As noted, however, the americium T = 25°C line does not comply with the supposition that the distribution ratio has third power dependence on the extractant concentration. Therefore, it is necessary to perform a Van't Hoff analysis on the remaining four temperature sets and interpolate the T = 25°C extraction constant, and compare the results. Using only the four remaining temperature datasets, the enthalpy of extraction is -14.1 kJ/mol and the entropy is -11.9 J/mol·K. Interpolating the extraction constant for T = 25°C yields K_{ex} = 71.8. This is well within the error of the extraction constant calculated using the T = 25°C dataset. Therefore, analysis of competition studies of americium used the extraction constant values listed in Table 4.1.

From the Van't Hoff analysis, berkelium has an enthalpy change of extraction of -20.8 kJ/mol and an entropy change of -32.9 J/mol·K. Figure 4.5 shows the Van't Hoff analysis. These extraction constants are an order of magnitude higher than results from Dr. Shafer's dipicolinic acid experiments with californium. However, the thermodynamic values are similar to her results, with an enthalpy change of -18.6 kJ/mol and an entropy change of -27.07 J/mol·K. Dr. Shafer's work yielded an enthalpy change of -14.3 kJ/mol and an entropy change of 11 J/mol·K. Due to the failure of this experiment to produce accurate results, extraction constants from Dr. Jenifer Shafer's previous work with californium had to be used in competition studies. Her constants were gathered at different temperatures, but the same ionic strength. These results are shown in Table 4.5.

Table 4.5: Dr. Shafer's californium extraction constants gathered in I = 0.5 M sodium perchlorate media. (Unpublished research from Dr. Jenifer Shafer)

Temperature (°C)	K_{ex}	Error
8	1739	33
15.5	1430	9
25	1175	2
35	1016	12
45.5	827	8

The Van't Hoff analysis produces an enthalpy change of -12 kJ/mol and an entropy change of 30.4 J/mol·K, without the T = 45°C data set. Without the T = 55°C data set, the change in enthalpy is -22.6 kJ/mol and the entropy change is -5.6 J/mol·K. With only T = 15°C, 25°C, and 35°C, the enthalpy change is -15.6 kJ/mol and the entropy change is 18.2 J/mol·K. The final analysis is most likely correct, and the results of the analysis and extrapolation are visualized in Figure 4.5. Einsteinium extraction constants are listed in Table 4.6, while extraction constants obtained from Dr. Braley are listed in Table 4.7 for comparison.

Table 4.6: Einsteinium extraction constants, T = 45°C and T = 55°C extrapolated. T = 15°C to T = 35°C is instrumental error. I = 0.5 M.

Temperature (°C)	K_{ex}	Error
15	5,700	270
25	5,300	280
35	3,800	320
45	3,300	310
55	2,700	310

Table 4.7: Dr. Shafer's einsteinum extraction constants. (Unpublished research from Dr. Jenifer Braley)

Temperature (°C)	K_{ex}	Error
15	5950	60
20	5300	300
25	4490	70
35	3710	80
45	2800	100

4.1.3 Extraction thermodynamic results

Extraction coefficients for all studied metals are listed in Table 4.8, while thermodynamic information is listed in Table 4.9.

Table 4.8: Consolidated extraction constants. Cf extraction constants interpolated from Dr. Shafer's DPA studies.

	15°C	25°C	35°C	45°C	55°C
Am (I = 0.5 M)	86(4)	69 (5)	61.3(1.6)	51.0(1.3)	41.4(2.1)
Bk	102(4)	76 (4)	59.4(1.2)	43.8(1.8)	33.8(0.6)
Cf	1,470(30)	1,203.0(9)	997.1(2)	840(10)	708.9(8)
Es	5,747(300)	5,293(284)	3,754(322)	3,250(306)	2,715(306)

Table 4.9: Consolidated thermodynamic parameters of extraction. Cf thermodynamic parameters from Dr. Shafer's DPA studies. Error values at 1σ, calculated using equation 10b except for Cf, calculated using 10 a.

	ΔH° (kJ/mol)	ΔS° (J/mol·K)	ΔG° (kJ/mol)
Am (I = 0.5 M)	-13.9(0.8)	-11.1(2.6)	-10.5086(2E-04)
Bk	-20.8(1)	-32.9(3.2)	-11.114(2E-03)
Cf	-14 (1)	11.0(3.0)	-18(3)
Es	-16(6)	18.2(19.7)	-21.257328(2E-06)

4.2 Competition Studies

Previous literature indicated that NTA forms a 1:1 complex with trivalent metal ions, and a 1:2 complex was hypothesized to possibly form but was not observed (Shah, 1980). HEDTA and CDTA complexes with berkelium are not indicated in the literature, but both can be expected to form 1:1 complexes only. DTPA can be expected to form protonated complexes as well as 1:1 complexes. The change in the distribution ratio as a function of the concentration of the ligand complex indicates the stoichiometry of the metal-ligand complex. Metal complexes can be modeled as

$$M^{3+} + L^{3-} \leftrightarrow ML \quad \beta_{101} = \frac{[ML]}{[M^{3+}][L^{3-}]} \tag{11}$$

$$M^{3+} + 2L^{3-} \leftrightarrow ML_2^{3-} \; \beta_{102} = \frac{[ML_2^{3-}]}{[M^{3+}][L^{3-}]^2} \quad (12)$$

where L^{3-} represents the fully deprotonated ligand anion, either NTA or HEDTA (Heathman & Nash, 2012). CDTA and DTPA may be modeled the same way, but it should be noted that different charges are associated with each ligand, CDTA being -4, and DTPA being -5. An aqueous phase mass balance expression may be used, along with the stability constant models, to calculate the free metal ion concentrations.

$$[M^{3+}]_{aq} = [M^{3+}]_{free} + [ML] + [ML_2^{3+}] \quad (13)$$

Substitution of the stability constants provides equation 14.

$$[M^{3+}]_{aq} = [M^{3+}]_{free}(1 + \beta_{101}[L^{3-}] + \beta_{102}[L^{3-}]^2) \quad (14)$$

Another substitution of the mass balance into the extraction equation provides equation 15 (Heathman & Nash, 2012).

$$\frac{D_o}{D} - 1 = \beta_{101}[L^{3-}] + \beta_{102}[L^{3-}]^2 \quad (15)$$

This expression relies on the assumptions that the ligand concentration is in excess of the metal ion concentration, the ligand does not partition into the organic phase, and the organic extractant does not partition into the aqueous phase. The first assumption works well due to the use of radiotracers in all experiments, ensuring that ligand concentrations will be well above metal ion concentrations. The studied ligands also poorly partition into the organic phase due to the poor organic solubility of the carboxylic acid functional groups present on all studied ligands. Even the NTA, which with one metal ion forms a charge neutral species, did not partition into the organic phase when tested with n-dodecane and no HDEHP. Metal-protonated ligand species

were assumed to not form at the pcHs studied save for DTPA. To test for metal protonated species with DTPA, solvent extraction studies at different pcHs were conducted.

A model was created using equation 15, and compared to the data using QtiPlot to calculate the stability constants of the metal-ligand complexes using an instrumental fit. Instrumental fit is the weighting the program gives to the data, calculated by the square of the reciprocal of the error values. Instrumental fit is useful when errors introduced in the system are possibly due to using an instrument to measure values, in this case scales, pH meters, and detectors. Stability constants can be used to determine the changes in enthalpy and entropy of complexation using equation 4. Natural logarithms may be converted to base ten logarithms by multiplying the natural logarithm by a factor of 2.303. Data for NTA, HEDTA, and CDTA were analyzed using equation 16, a modified equation 15 that omits the 1:2 complex.

$$\frac{D_o}{D} - 1 = \beta_{101}[L^{3-}] \tag{16}$$

4.3 NTA Complexation Studies

NTA reactions with trivalent metals are expected to be exothermic and favorable. These stability constants are expected to be the lowest constants of the ligands studied, due to the small molecule size unable to wrap around the metal ion fully. Further, the least amount of HDEHP was required to produce usable distribution data.

4.3.1 NTA-Am Studies

Americium-NTA stability constants conducted in I = 0.5 M sodium perchlorate media are listed in Table 4.10.

Table 4.10: Americium-NTA stability constants, evaluated for 1:1 and 1:2 species.

Temp (°C)	$Log\beta_{101}$	$Log\beta_{102}$
15	11.66(0.03)	22.5(0.2)
25	Does not refine	Does not refine
35	11.506(0.005)	21.49(0.02)
45	11.10(0.05)	22.1.91(0.02)
55	10.8(0.7)	23.0(0.2)

These values obtained from the least squares fit of equation 16 reflect poor agreement with established literature stability constants of Am-NTA complexes. Moreover, values fit poorly when manually inserted into equation 15. Finally, the T = 25°C dataset produces a non-physical β_{102} stability constant, not listed in Table 4.10. Therefore, it is reasonable to assume, under the conditions studied, that the Am-NTA systems presented produced only a 1:1 complex with NTA, or the 1:2 complex is insignificant compared to the 1:1 complex. Results of an analysis of the datasets with equation 16 are listed in Table 4.11.

Table 4.11: Am-NTA stability constants reflecting 1:1 complexes I = 0.5 M.

Temp (°C)	$Log\beta_{101}$
15	11.73(0.01)
25	11.62(0.01)
35	11.589(0.007)
45	11.55(0.02)
55	11.514(0.008)

These stability constants can now be analyzed to obtain thermodynamic information of the complex of Am-NTA. The plot is depicted in Figure 4.6, showing an exothermic reaction. Thermodynamic parameters from the Van't Hoff analysis are listed in Table 4.12.

.

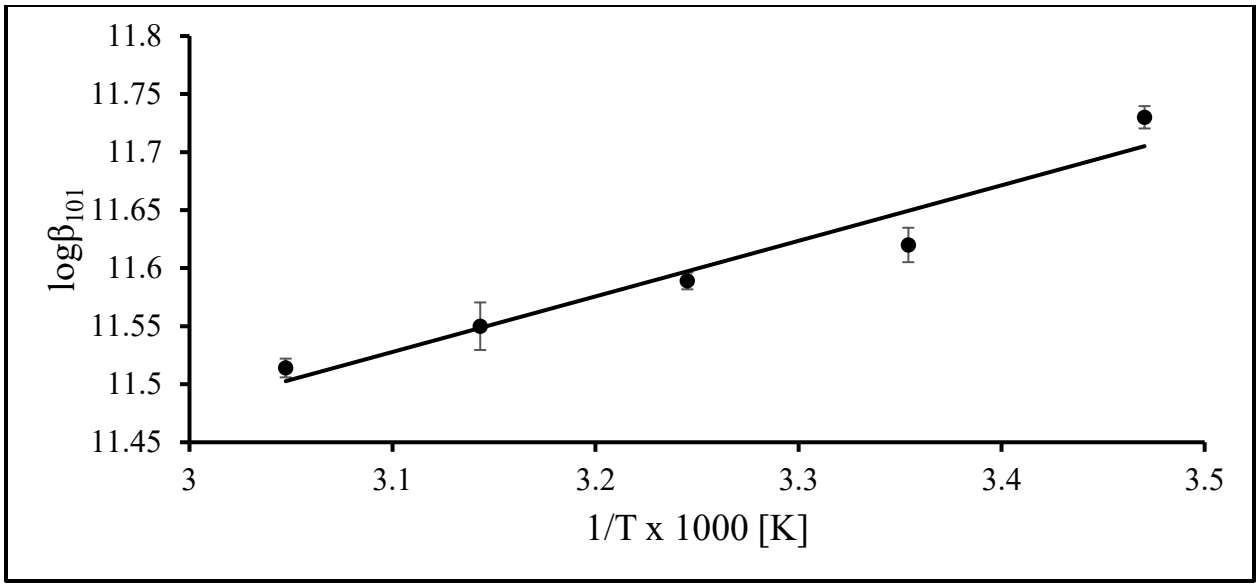

Figure 4.6: Am-NTA Van't Hoff plot (I = 0.5 M)

Table 4.12: Thermodynamic parameters for Am-NTA I = 0.5 M

	ΔH° (kJ/mol)	ΔS° (J/mol·K)	ΔG° (kJ/mol)
Am-NTA (I = 0.5M)	-9(1)	192(5)	-66.5033(0.0006)

Values for the enthalpy and entropy of Am-NTA were lower than reported by Shah or Choppin (see appendix B for comparison values, table 68). However, this can be explained by their use of different methods in Choppin's case (calorimetry), and the use of different solvents and extractant in Shah's case (n-heptane and dinonly-napthalenesulfonic acid). Values for the Gibbs free energy are similar to Shah's calculations, however.

4.2.2 Bk-NTA Studies

Berkelium-NTA stability constants are listed in Table 4.13. The first two stability constants are refined using the 1:1 and 1:2 species, while the final column listed the stability constant with only the 1:1 species refined.

Table 4.13: Bk-NTA stability constants I = 0.5 M.

Temp (°C)	$Log\beta_{101}$ (1:1 & 1:2)	$Log\beta_{102}$	$Log\beta_{101}$ (only 1:1)
15	12.6(0.1)	21.5(0.1)	12.0317(0.0001)
25	11.8(0.1)	22.2(0.2)	12.01(0.02)
35	11.8(0.1)	22.0(0.1)	11.958(0.004)
45	11.6(0.2)	21.9(0.2)	11.85(0.03)
55	11.4(0.2)	21.9(0.1)	11.91(0.01)

The 1:1 constants refined from both species show a clear exothermic trend, but the 1:2 constants do not refine well and only show a trend from T = 35°C to T = 55°C. Both 1:1 species

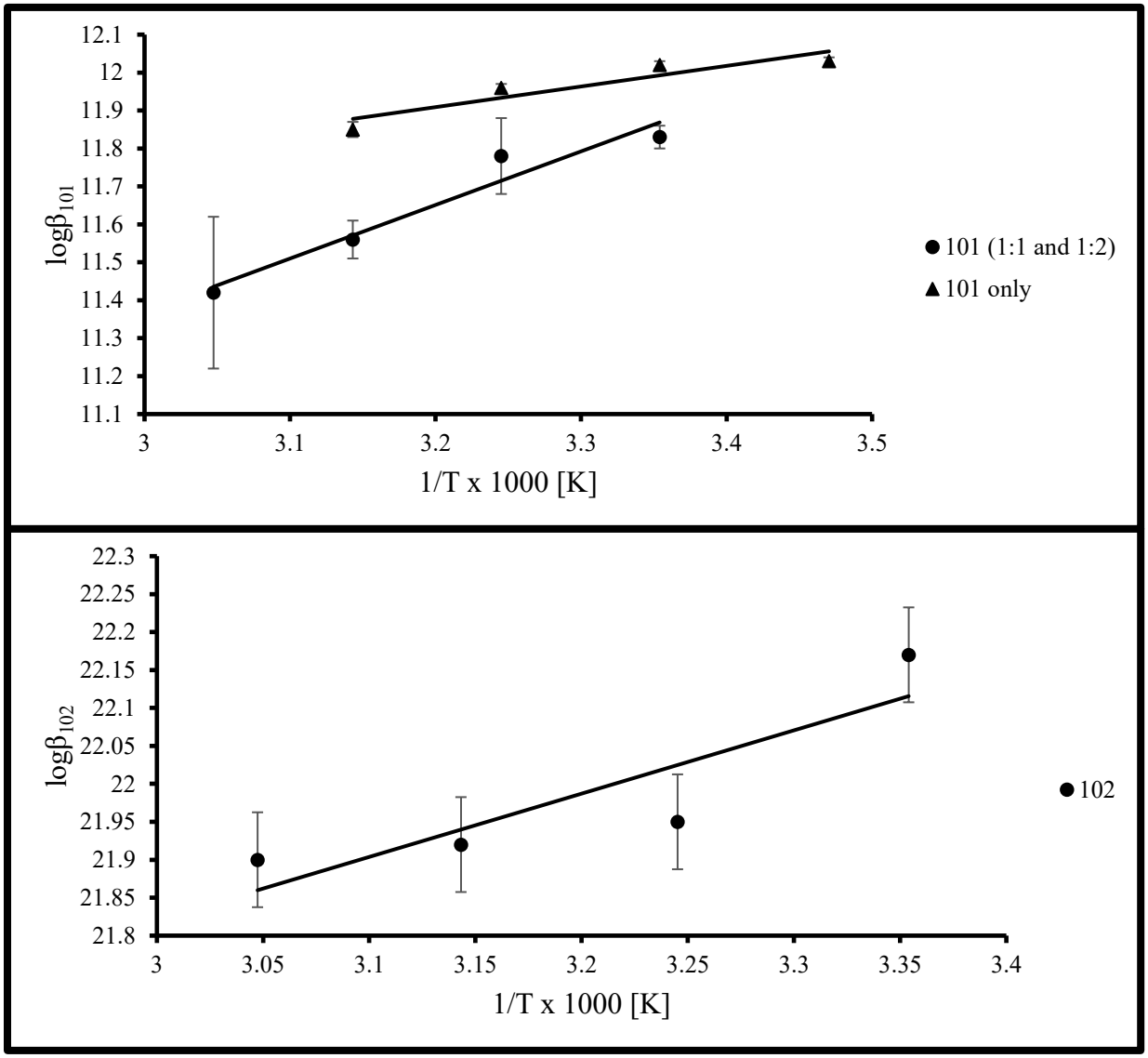

Figure 4.7: Bk-NTA Van't Hoff analysis. 4.7a is the 1:1 species and 4.7b is the 1:2 species.

datasets are analyzed in Figure 4.7a, while the 1:2 species is analyzed in Figure 4.7b. In the analysis, the T = 55°C stability constant is excluded for the 1:1 species only, the T = 15°C stability constant is excluded from both the 1:1 and 1:2 species since the data fit much better without them, indicating slower kinetics at that temperature.

The thermodynamic parameters are listed in Table 4.14.

Table 4.14: Bk-NTA standard thermodynamic parameters, I = 0.5 M.

	ΔH° (kJ/mol)	ΔS° (J/mol·K)	ΔG° (kJ/mol)
Bk-NTA	-27(5)	140(15)	-68(16)
Bk-NTA_2	-16(6)	370(20)	-130(21)
Bk-NTA only	-11(3)	194(9)	-68.4517(8E-04)

From the table and the analysis, it is unlikely that the Bk-NTA system has an appreciable 1:2 species at these conditions. Therefore, it is likely that those results may be excluded and only the 1:1 species should be considered. Berkelium-NTA has similar thermodynamic properties to americium-NTA, in that the reaction is exothermic and favorable.

4.2.3 Californium-NTA Studies

Californium-NTA stability constants are listed in Table 4.15. Both the 1:1 species and 1:2 species were clearly available in this experiment, so the 1:1 species alone was not calculated.

Table 4.15: Cf-NTA stability constants I = 0.5 M for 1:1 and 1:2 species.

Temp (°C)	$Log\beta_{101}$	$Log\beta_{102}$
15	11.78(0.06)	22.43(0.01)
25	11.76(0.03)	22.303(0.007)
35	11.670(0.002)	22.118(0.008)
45	11.96(0.08)	22.03(0.05)
55	11.73(0.06)	21.8(0.1)

The 1:1 stability constants show a clear trend from T = 15°C to T = 35°C, but the T = 45°C and T = 55°C deviate from this trend. It is likely that the Cf-NTA species shows little temperature dependence. The 1:2 stability constants show a clear trend from all temperatures sets. It is likely that the 1:2 species is favored.

The Van't Hoff analysis is plotted in Figure 4.8.

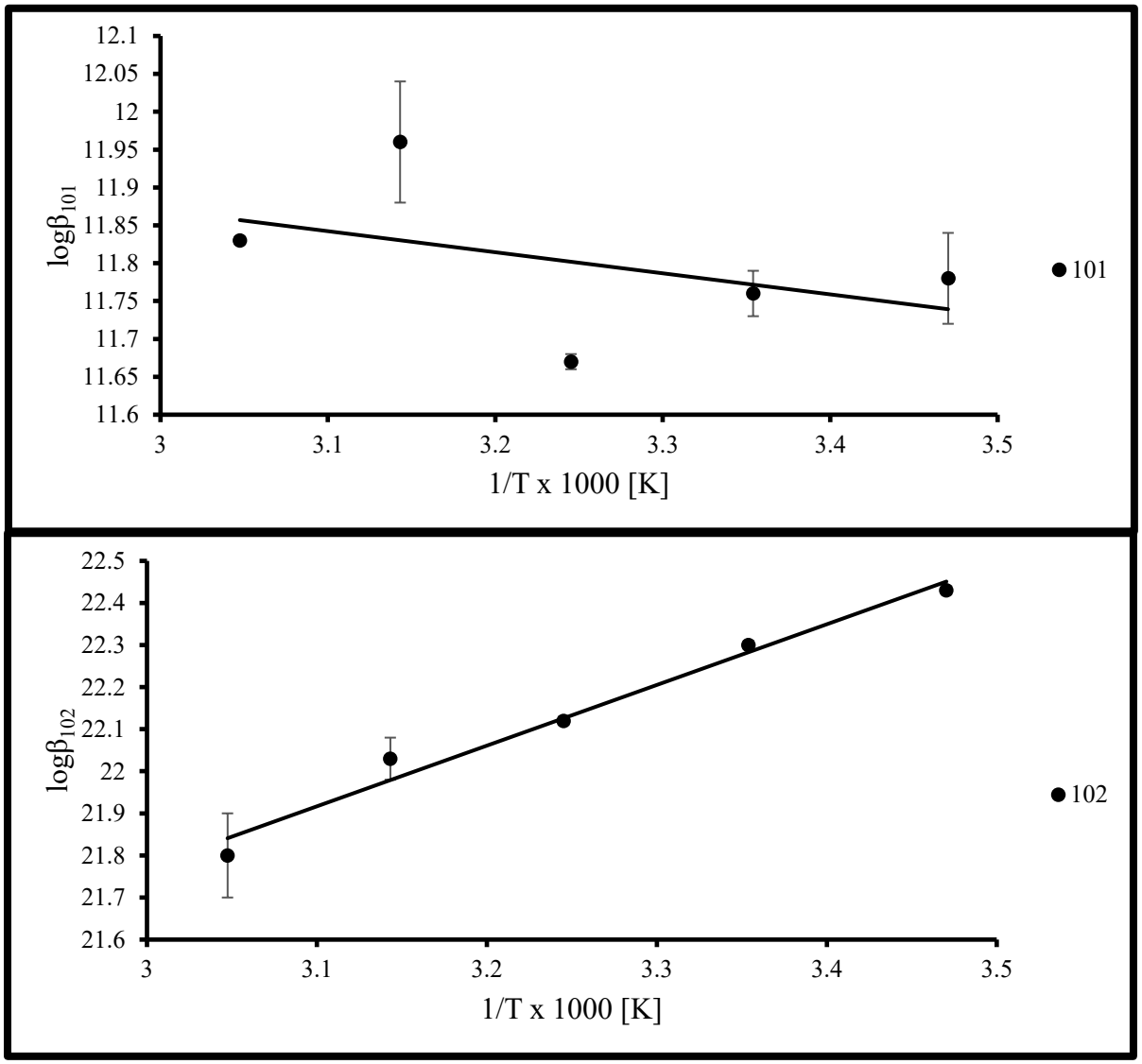

Figure 4.8: Cf-NTA Van't Hoff analysis plots. Figure 4.8a (top) is the 1:1 species, and figure 4.8b (bottom) is the 1:2 species.

Cf-NTA shows little temperature dependence in the 1:1 species, while a strong exothermic dependence in the 1:2 species. The thermodynamic parameters are listed in Table 4.16.

Table 4.16: Cf-NTA thermodynamic parameters

	ΔH° (kJ/mol)	ΔS° (J/mol·K)	ΔG° (kJ/mol)
Cf-NTA	2(7)	230(20)	-67.193(0.001)
Cf-NTA_2	-27(2)	333(8)	-127.2107(0.0001)

The enthalpic change in the 1:1 species presents a higher error than the change itself. This is probably indicating no temperature dependence for the 1:1 species, but it is possible that the change in enthalpy is endothermic, as indicated by Shah. However, the entropy change and the Gibbs free energy are both comparable to other actinide values, indicating a favorable reaction. The 1:2 species has a negative enthalpy change, indicating an exothermic reaction. The larger entropic change indicates more hydration waters are removed from the hydration sphere on the metal ion. The 1:2 Gibbs free energy is more favorable than the 1:1 species.

4.2.4 Einsteinium-NTA Studies

Einsteinium-NTA stability constants are listed in Table 4.17.

Table 4.17: Es-NTA stability constants I = 0.5 M.

Temp (°C)	$Log\beta_{101}$	$Log\beta_{102}$
15	11.93(0.02)	22.89(0.03)
25	12.07(0.02)	22.80(0.03)
35	11.97(0.02)	22.91(0.01)
45	11.96(0.06)	22.5(0.1)
55	12.26(0.03)	22.45(0.06)

The 1:1 and 1:2 constants show no clear trend, but the 1:2 constants seem to reflect an exothermic reaction. The Van't Hoff analysis is plotted in Figure 4.9.

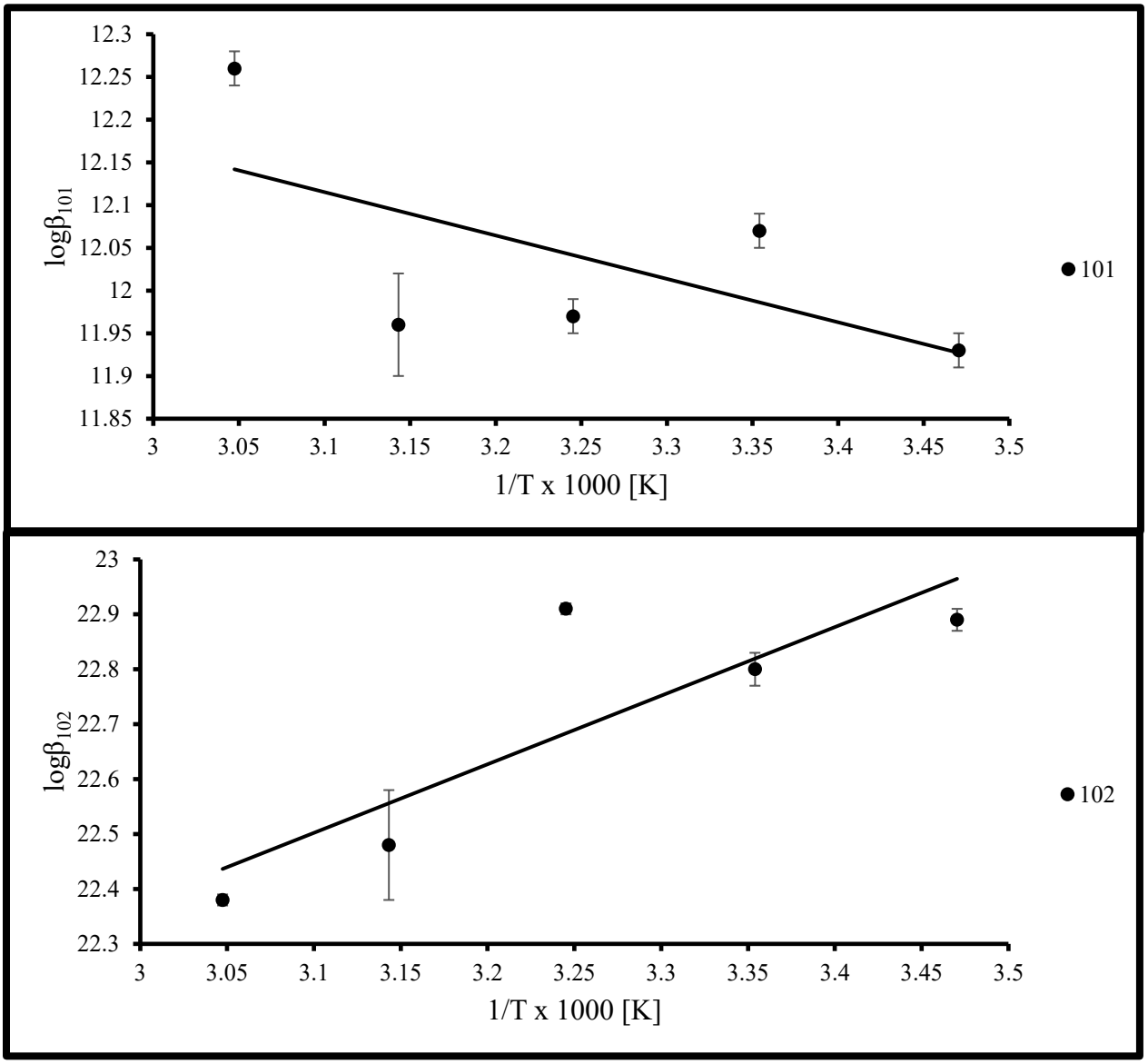

Figure 4.9: Es-NTA Van't Hoff Analysis, I = 0.5 M.

The Van't Hoff analysis again shows an exothermic trend in the 1:2 stability constants, but no clear trend in the 1:1 stability constants. It is possible that Es-NTA presents endothermic or temperature independent complexation behavior, depending on whether or not one includes the T = 55°C stability constant. The thermodynamic parameters are listed in Table 4.18.

Table 4.18: Es-NTA thermodynamic parameters

	ΔH° (kJ/mol)	ΔS° (J/mol·K)	ΔG° (kJ/mol)
Es-NTA	9(7)	260(20)	-68.4260(0.0008)
Es-NTA_2	-20(8)	370(30)	-130.2861(0.0005)

Es-NTA shows an endothermic change in enthalpy, but more likely there is no clear temperature dependence similar to Cf-NTA. If the T = 55°C stability constant is excluded from the analysis, the 1:1 species becomes temperature independent. However, the reaction becomes unfavorable as the change in Gibbs free energy becomes positive, and the entropy change becomes negative. It is unlikely that the system becomes more ordered as the waters in the hydration sphere surrounding the metal ion detach, however. This means that the T = 55°C stability constant is important in the analysis, and must be included for the results to make sense. Es-NTA_2, however, shows a clear exothermic trend.

4.4 HEDTA Competition Studies

HEDTA is expected to produce higher stability constants than NTA due to the fact that HEDTA is a larger molecule and more able to wrap around and hold metal ions than NTA. The extra amine group may also play a role in providing additional stability to the systems studied. Choppin's work included 1:2 complexes along with 1:1 complexes (Choppin et al, 2006). However, 1:2 complexes were only seen with Am-HEDTA at higher temperatures in this study, suggesting the addition of a second complex is a kinetically slower step.

4.4.1 Americium-HEDTA

Stability constants for the Am-HEDTA system are compiled in Table 4.19. Stability constants for the 1:1 and 1:2 species were only calculated for the T = 45°C and T = 55°C sets, as the kinetics of the 1:2 addition step most likely were too slow at the lower temperatures to resolve.

Table 4.19: Am-HEDTA stability constants, I = 0.5 M.

Temp (°C)	$Log\beta_{101}$	$Log\beta_{102}$	$Log\beta_{101}$ only
15			16.216(0.002)
25			16.170(0.009)
35			16.040(0.007)
45	15.8(0.1)	30.2(0.1)	15.88(0.03)
55	15.5(0.1)	29.8(0.1)	15.4(0.1)

Since the 1:2 step did not present in this experiment at all temperatures, only the 1:1 species is used in the Van't Hoff analysis in Figure 4.10.

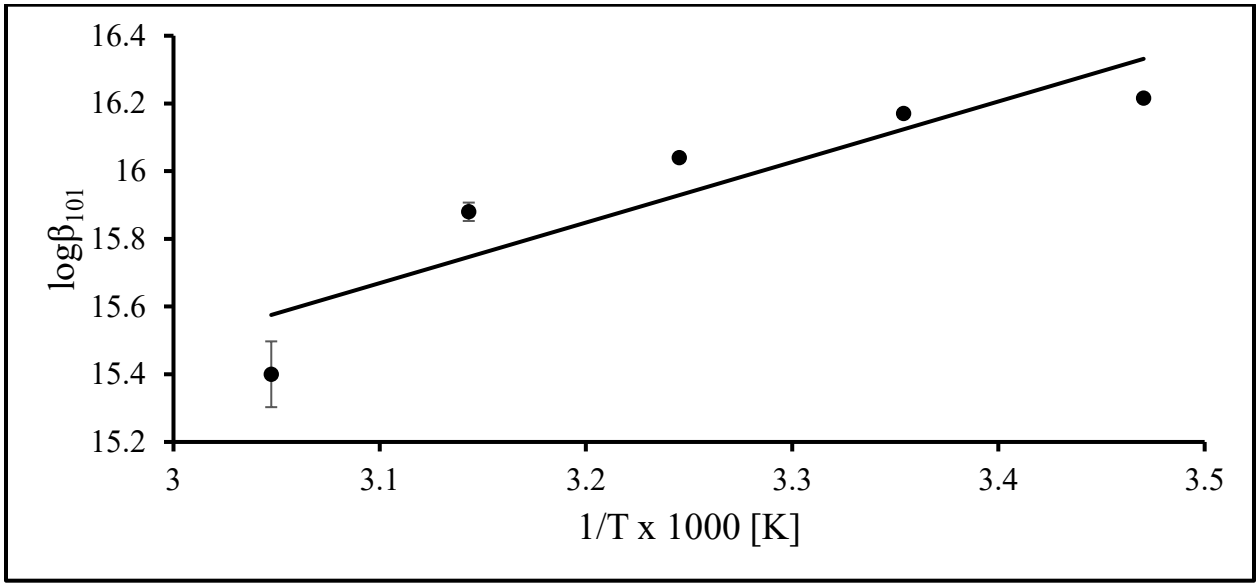

Figure 4.10: Am-HEDTA Van't Hoff analysis. I = 0.5 M.

The results of the analysis are presented in Table 4.20.

Table 4.20: Am-HEDTA thermodynamic parameters. I = 0.5 M.

	ΔH° (kJ/mol)	ΔS° (J/mol·K)	ΔG° (kJ/mol)
Am-HEDTA	-34(9)	190(30)	-92.0451(0.0003)

The 1:1 reaction presents as exothermic, and highly favorable.

4.4.2 Bk-HEDTA

Stability constants for the Bk-HEDTA system are compiled in Table 4.21. Only the 1:1 species was observed in this system.

Table 4.21: Bk-HEDTA stability constants I = 0.5 M.

Temp (°C)	$Log\beta_{101}$
15	15.795(0.001)
25	15.518(0.002)
35	15.40(0.01)
45	15.13(0.02)
55	15.165(0.003)

No data exists to compare Bk-HEDTA complexes. However, Bk-HEDTA appears to follow the trend set by Am-HEDTA, with larger stability constants than NTA, but lower than the Am-HEDTA complex.

The Van't Hoff plot is presented in Figure 4.11.

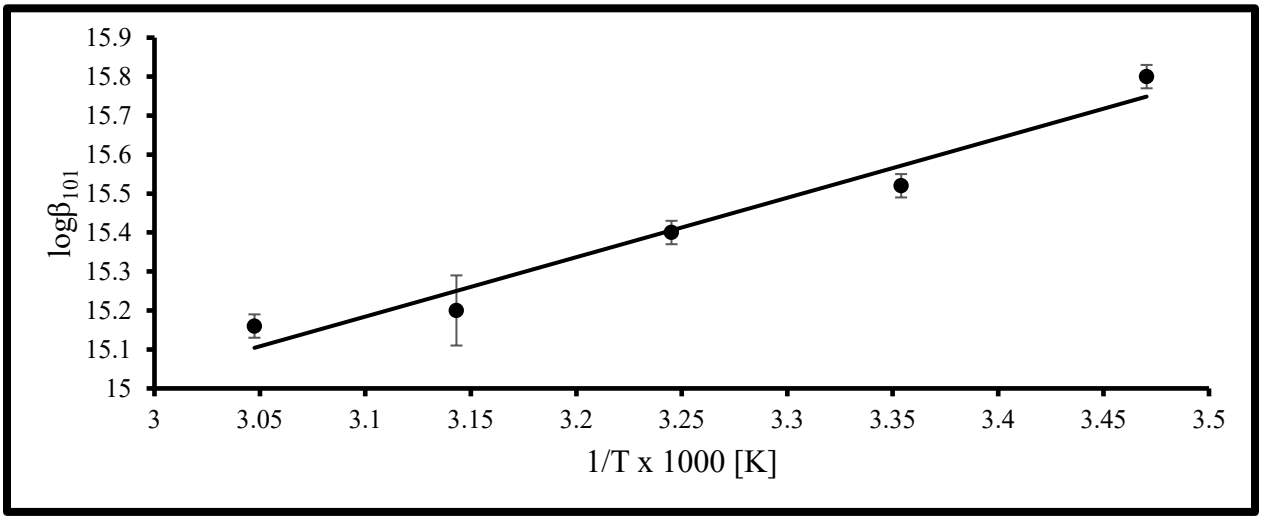

Figure 4.11: Bk-HEDTA Van't Hoff Analysis, I = 0.5 M.

Bk-HEDTA appears to follow the exothermic trend. The results of the analysis are presented in Table 4.22.

Table 4.22: Bk-HEDTA thermodynamic constants I = 0.5 M.

	ΔH° (kJ/mol)	ΔS° (J/mol·K)	ΔG° (kJ/mol)
Bk-HEDTA	-30(5)	200(16)	-88.83823(7E-05)

The reaction is presented as exothermic, and highly favorable, though slightly less exothermic and favorable than Am-HEDTA in absolute terms. When errors are accounted for, Am-HEDTA's and Bk-HEDTA's enthalpic changes are statistically identical.

4.4.3 Cf-HEDTA

The californium-HEDTA stability constants are presented in Table 4.23.

Table 4.23: Cf-HEDTA stability constants I = 0.5 M.

Temp (°C)	$Log\beta_{101}$
15	16.120(0.003)
25	16.12(0.02)
35	15.92(0.04)
45	15.68(0.05)
55	15.32(0.01)

Cf-HEDTA stability constants are slightly higher than the Bk-HEDTA stability constants.

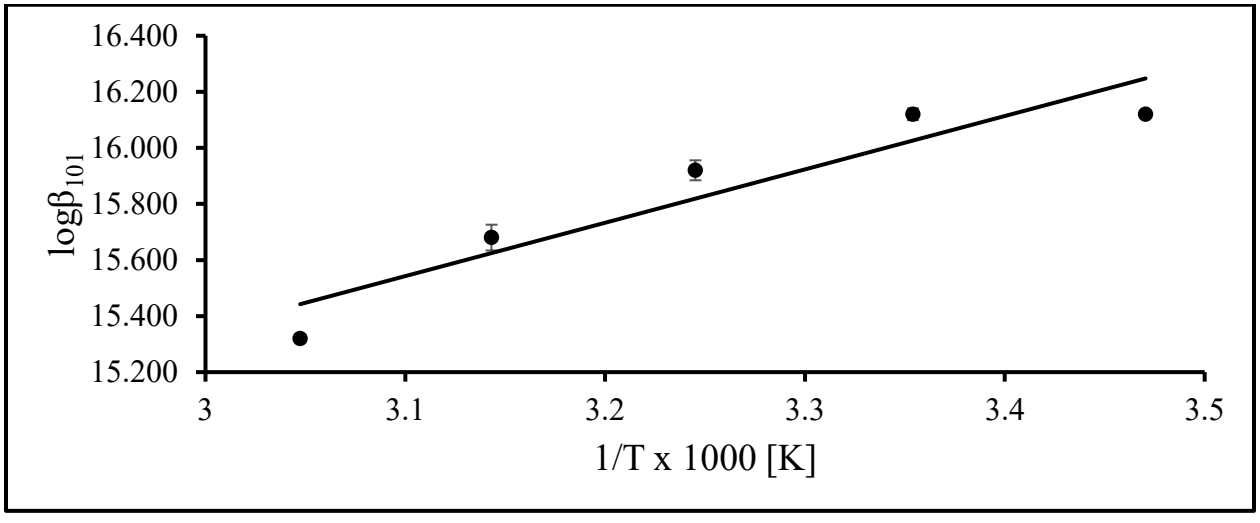

Figure 4.12: Cf-HEDTA Van't Hoff analysis I = 0.5 M.

The reaction is shown to be exothermic, though less so in absolute terms than Bk-HEDTA. The thermodynamic constants are in Table 4.24.

Table 4.24: Cf-HEDTA thermodynamic properties I = 0.5 M.

	ΔH° (kJ/mol)	ΔS° (J/mol·K)	ΔG° (kJ/mol)
Cf-HEDTA	-36(8)	180(25)	-91.4889(0.0006)

Cf-HEDTA presents as more exothermic than Bk-HEDTA, and more favorable.

4.4.4 Es-HEDTA

The Es-HEDTA stability constants are shown in Table 4.25.

Table 4.25: Es-HEDTA stability constants I = 0.5 M.

Temp (°C)	$Log\beta_{101}$
15	16.127(0.008)
25	16.17(0.01)
35	16.036(0.005)
45	15.7355(0.0005)
55	15.69(0.01)

The T = 15°C dataset is lower than expected. This could be due to kinetics issues and the set not reaching equilibrium. Therefore, the dataset was excluded from the Van't Hoff analysis in Figure 4.13 on the following page. The series is still comparable to Cf-HEDTA with a large enthalpic change and error, but still exothermic.

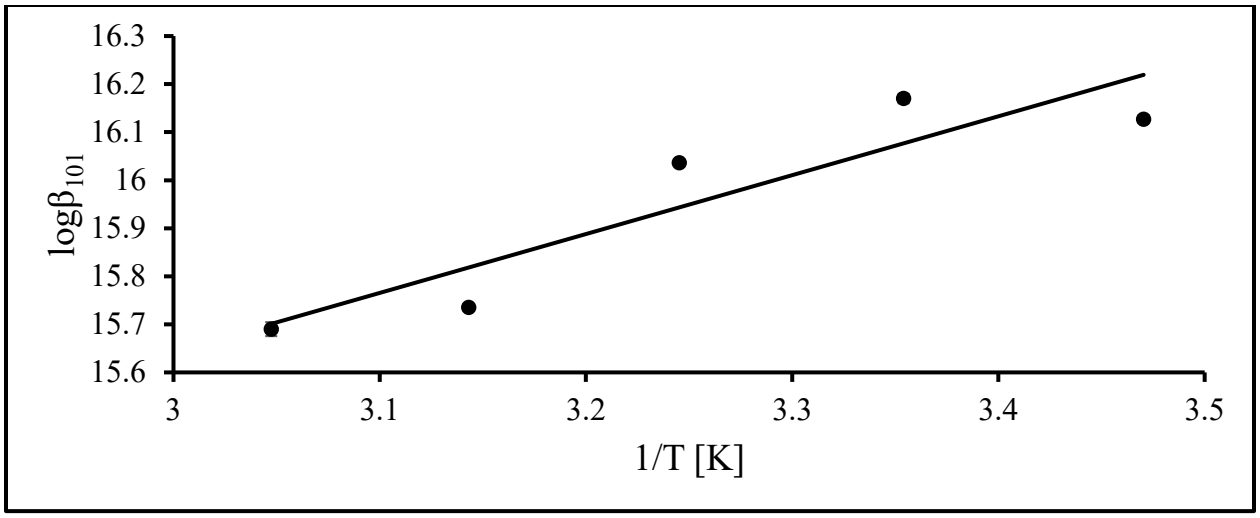

Figure 4.13: Es-HEDTA Van't Hoff analysis I = 0.5 M.

The thermodynamic parameters are listed in Table 4.26.

Table 4.26: Es-HEDTA thermodynamic parameters, I = 0.5 M.

	ΔH° (kJ/mol)	ΔS° (J/mol·K)	ΔG° (kJ/mol)
Es-HEDTA	-33(6)	200(19)	-92.3395(0.0003)

The change in enthalpy decreases from the maximum at Cf-HEDTA, but the other parameters are about the same.

4.5 CDTA Competition Studies

CDTA is expected to chelate with trivalent metals better than EDTA and HEDTA, due to the one possible conformation of the ligand. Only 1:1 complexes of this hexadentate molecule are observed due to steric hindrance.

4.5.1 Bk-CDTA

The Bk-CDTA stability constants are shown in Table 4.27.

Table 4.27: Bk-CDTA stability constants I = 0.5 M.

Temp (°C)	$Log\beta_{101}$
25	20.135(0.009)
30	20.081(0.004)
35	20.066(0.002)
45	19.952(0.001)
55	19.8407(0.0006)

The datasets conform to one another and show an exothermic trend. The Van't Hoff analysis is depicted in Figure 4.14.

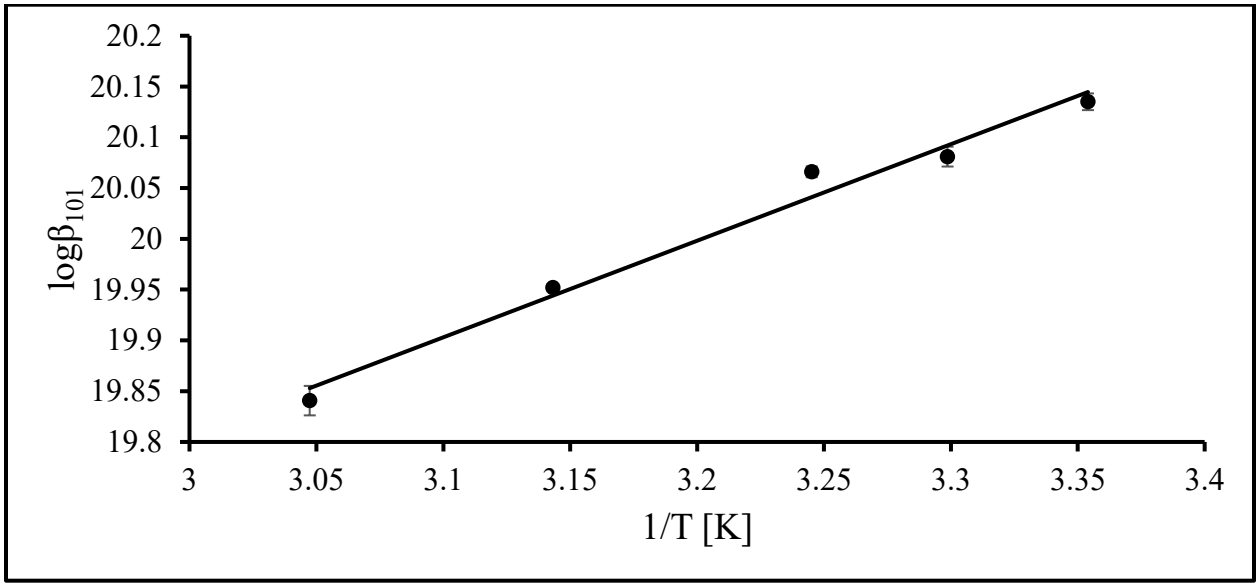

Figure 4.14: Bk-CDTA Van't Hoff analysis I = 0.5 M.

The thermodynamic parameters are listed in Table 4.28.

Table 4.28: Bk-CDTA thermodynamic parameters

	ΔH° (kJ/mol)	ΔS° (J/mol·K)	ΔG° (kJ/mol)
Bk-CDTA (I = 0.5M)	-18(1)	325(5)	-114.9997(0.0001)

The favorability is larger than other ligand systems due to the fact that CDTA can only form one conformation with metal ions, and that conformation is much more favorable than most systems.

4.5.2 Cf-CDTA

Cf-CDTA stability constants are listed in Table 4.29.

Table 4.29: Cf-CDTA stability constants I = 0.5 M.

Temp (°C)	$Log\beta_{101}$
15	22.53(0.05)
25	21.5332(0.0008)
35	20.63(0.06)
45	20.52(0.01)
55	20.33(0.01)

These constants span a wider range than thought, as shown in Figure 4.15. The T = 15°C and T = 25°C data sets yield stability constants that are much higher than the rest of the temperature sets. This is most likely due to slower kinetics at lower temperatures, and the T = 15°C and T = 25°C data sets not achieving equilibrium. Therefore, in the Van't Hoff analysis, these sets are excluded.

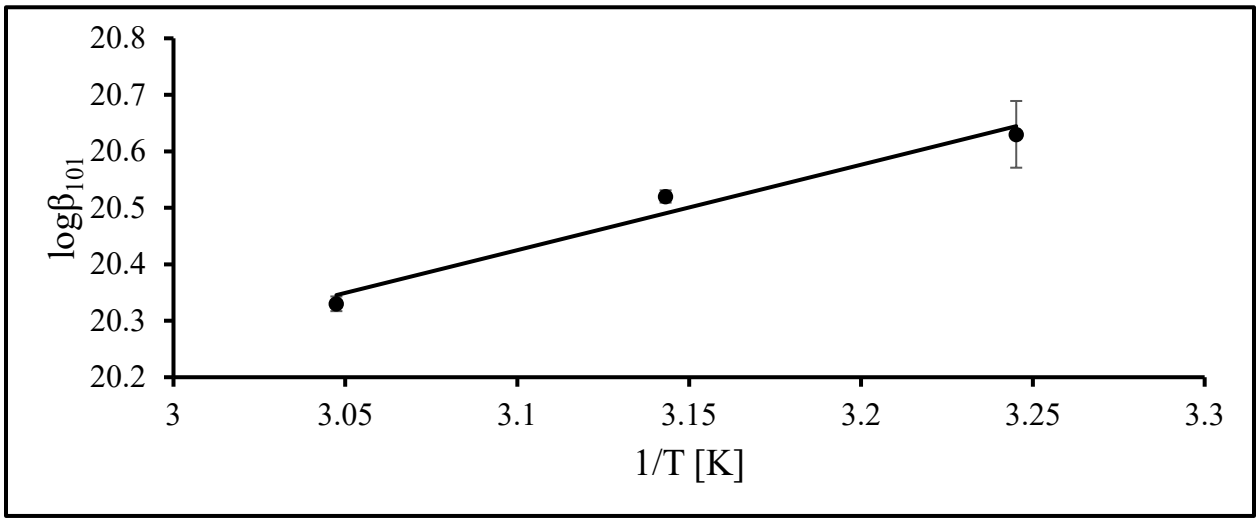

Figure 4.15: Cf-CDTA Van't Hoff analysis, I = 0.5 M.

This analysis yields the thermodynamic parameters in Table 4.30.

Table 4.30: Cf-CDTA thermodynamic parameters, I = 0.5 M.

	ΔH° (kJ/mol)	ΔS° (J/mol·K)	ΔG° (kJ/mol)
Cf-CDTA (I = 0.5M)	-29(5)	300(16)	-118.79282(0.00002)

These parameters seem to indicate that the reaction between californium and CDTA is highly exothermic and highly favorable. However, a literature survey indicates that, while Gibbs free energy values are similar, the stability constants for Cf-CDTA are higher than reported (Baybarz, 1965). Further, Choppin reports that the CDTA actinide complex is endothermic (Choppin et al., 2006).

4.5.3 Es-CDTA

The stability constants for Es-CDTA are listed in Table 4.31.

Table 4.31: Es-CDTA stability constants, I = 0.5 M.

Temp (°C)	$\log\beta_{101}$
15	21.38(0.08)
25	21.39(0.09)
35	20.490(0.007)
45	20.19(0.02)
55	20.1(0.2)

These values are similar to the Cf-CDTA stability constants in that there is a wide range between temperature sets, although the Es-CDTA range is not as wide as the Cf-CDTA range. Once again, the T = 15°C and the T = 25° reflect slow kinetics and are excluded from the analysis. The Van't Hoff analysis is depicted in Figure 4.16.

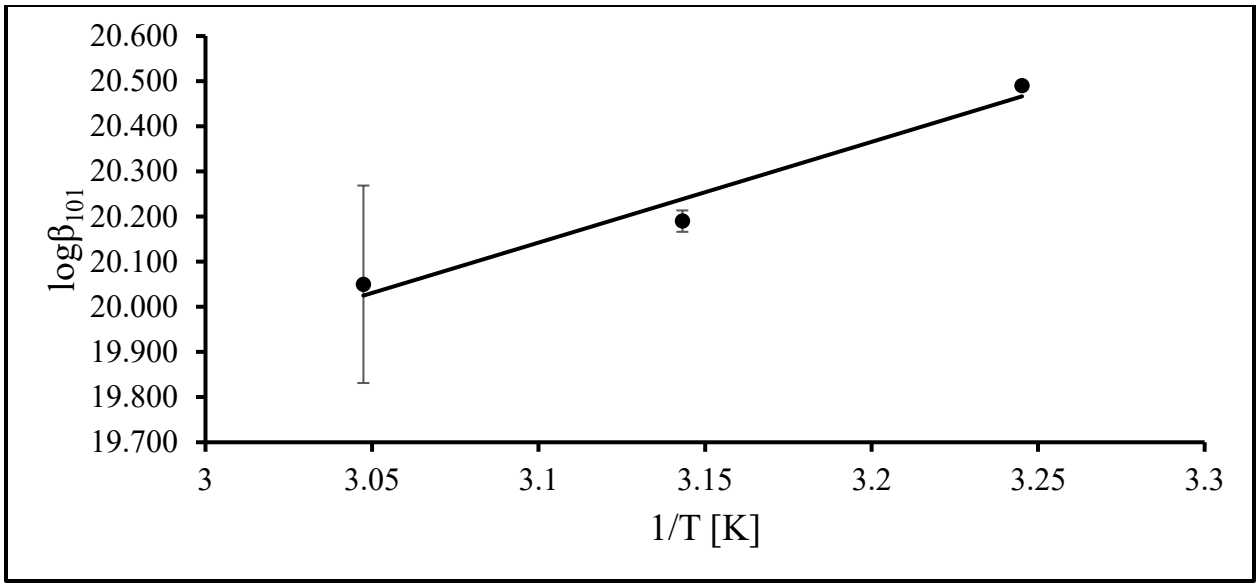

Figure 4.16: Es-CDTA Van't Hoff analysis, I = 0.5 M.

With these adjustments, the thermodynamic parameters are listed in Table 4.32.

Table 4.32: Es-CDTA thermodynamic parameters I = 0.5 M

	ΔH° (kJ/mol)	ΔS° (J/mol·K)	ΔG° (kJ/mol)
Es-CDTA (I = 0.5M)	-43(8)	250(26)	-118.224(0.002)

While these values are similar to the Cf-CDTA system analyzed previously, they do not reflect the work performed by Baybarz and Choppin. One possible explanation for this phenomenon is that Baybarz and Choppin did not operate under the same conditions as this work. Their hydrogen ion concentrations are lower than this work, and they use different organic extractants and diluents.

4.6 DTPA Complexation Studies

DTPA requires more analysis than the previous ligands in that at the operating conditions, both a protonated species and deprotonated species form complexes with metal

cations. Shanbhag and Choppin describe the method to solve for the protonated and deprotonated stability constants (Shanhbag & Choppin, 1981).

Equation 16 must be modified by accounting for both species. Equation 17 shows the modification of the addition of the β_{111} stability constant. This constant represents the protonated species, or the DTPA ligand with one hydrogen ion attached that bonds to the metal ion in competition with the deprotonated ligand.

$$\frac{D_o}{D} - 1 = (\beta_{101} + \beta_{111}[H^+])[L^{5-}] \quad (17)$$

To solve for each stability constant, an overall conditional constant, called β_1, must first be solved for. This constant is defined in equation 18.

$$\beta_1 = \beta_{101} + \beta_{111}[H^+] \quad (18)$$

This conditional constant is solved for using non-linear least squares analysis of equation 19.

$$\frac{D_o}{D} - 1 = \beta_1[L^{5-}] \quad (19)$$

By performing solvent extractions over a range of hydrogen ion concentrations and solving for β_1 for each set, a plot of β_1 vs. hydrogen ion concentration may be created. The slope of this plot is the stability constant for the protonated complex while the intercept is the stability constant for the deprotonated complex.

4.6.1 Bk-DTPA

The results of the Bk-DTPA study are listed in Table 4.33.

Table 4.33: Bk-DTPA conditional stability constants, $\beta_{1.}$

Temp °C	pcH = 1.9	2.1	2.3	2.5
25	22.66(0.02)	23.11(0.01)	22.47(0.02)	22.9(0.1)
35	23.0(0.1)	22.66(0.01)	22.77(0.02)	22.46(0.02)
45	22.843(0.004)	22.71(0.02)	23.1947(0.0002)	22.72(0.01)
55	23.17(0.02)	22.50(0.02)	22.77(0.03)	22.30(0.01)

These constants may now be used to solve for the protonated and deprotonated stability constants using equation 18. However, care must be taken to ensure nonphysical constants are not obtained. Generally, the higher the amount of hydrogen ions in solution, the higher the conditional stability constant is. Due to the large variance in pcH of some DTPA solutions used and the large variance of the pH probe used to measure the pcH, some constants may be unusable in this study. The T = 35°C data set's pcH = 2.1 conditional stability constant, the T = 45°C data set's pcH = 2.3 stability constant, and the T = 55°C data set's pcH = 2.1 conditional stability constant are all excluded as they do not fit the trend of the data. Through equation 18, the 1:0:1 and the 1:1:1 stability constants may be determined. The stability constants for each temperature are listed in Table 4.34.

Table 4.34: Bk-DTPA stability constants, I = 0.5 M

Temp °C	β_{101}	β_{111}
25	22.7(0.4)	24.5(0.5)
35	22.0(0.4)	24.9(0.1)
45	22.7(0.1)	24.1(0.4)
55	22.5(0.1)	25.3(0.1)

No literature comparison may be made, as Baybarz neglected the protonated species since the difference between the deprotonated and protonated stability constants of Am-DTPA was only 5.75 (Baybarz, 1965). The difference between the T = 25°C stability constants in this study is only 1.8, showing the equilibrium strongly shifted to the deprotonated species.

Therefore, while the protonated species may be detected, the thermodynamic constants of the DTPA were not calculated. A thermodynamic analysis of the 1:0:1 formation is provided in Table 4.35. The T = 35°C dataset does not appear to follow the general trend, the stability constant is excluded in this analysis.

Table 4.35: Bk-DTPA thermodynamic parameters, I = 0.5 M.

	ΔH° (kJ/mol)	ΔS° (J/mol·K)	ΔG° (kJ/mol)
Bk-DTPA	-10(9)	400(30)	-129.744(0.002)

The large error in the change in enthalpy indicates that the reaction is probably temperature independent. However, the reaction is still favorable due to the large Gibbs free energy change. These values are very close to Baybarz's listed stability constant, indicating his supposition that the deprotonated species dominates the equilibrium is most likely correct (Baybarz, 1965).

4.6.2 Cf-DTPA

The results of the Cf-DTPA study are listed in Table 4.36.

Table 4.36: Cf-DTPA conditional stability constants, I = 0.5 M.

Temp °C	pcH=1.9	2.1	2.3	2.5
25	222.72(0.03)	22.671(0.003)	22.721(0.009)	22.895(0.006)
35	22.1(0.4)	22.0(0.4)	21.007(0.004)	22.23(0.04)
45	23.1(0.1)	22.4(0.3)	21(1)	22.08(0.08)
55	21.9(0.4)	21.9(0.4)	20.9(0.6)	21.71(0.01)

The data present a large amount of variability. For T = 25°C and T = 35°C, the pcH = 1.9, pcH = 2.1, and pcH = 2.3 conditional stability constants may be used to obtain a line with the possible stability constants. For the T = 45°C dataset, the pcH = 1.9 and pcH = 2.1 constants yield usable information, while the pcH = 2.3 conditional stability constant should be excluded from the T =

55°C data set due to the point's poor fit. From these sets, presents the stability constants for Cf-DTPA. From the conditional stability constants, the protonated and deprotonated stability constants may be obtained. These constants are listed in Table 4.37.

Table 4.37: Cf-DTPA stability constants, I = 0.5 M.

Temp °C	β_{101}	β_{111}
25	23.8(0.1)	25.6(0.2)
35	23.3(0.2)	25.0(0.4)
45	23.3(0.1)	24.8(0.1)
55	23.26(0.05)	24.2(0.5)

Cf-DTPA seems to present an exothermic reaction. The protonated species also forms, but like Bk-DTPA, the equilibrium is dominated by the deprotonated species. The deprotonated stability constant is an order of magnitude larger than Baybarz's Cf-DTPA stability constant, possibly due to differing conditions (Baybarz, 1965). The stability constant is also an order of magnitude lower than the Cf-DTPA stability constant reported by Brandau, who questioned Baybarz's work (Brandau, 1971). Brandau posited that the reaction mechanism proceeded through the protonated species to the deprotonated species. However, both Brandau and Baybarz neglected the sixth protonation constant of DTPA in their calculations. This constant is important because it represents the proton attached to the most acidic site, a carboxylate group. This constant is not calculated in the literature until 1979. This may account for the discrepancies in both Baybarz's and Brandau's calculations.

The thermodynamic parameters are listed in Table 4.38.

Table 4.38: Cf-DTPA thermodynamic parameters

	$\Delta H°$ (kJ/mol)	$\Delta S°$ (J/mol·K)	$\Delta G°$ (kJ/mol)
Cf-DTPA (I = 0.5M)	-30(15)	350(47)	-135.112(0.004)

The Cf-DTPA system exhibits exothermic and favorable behavior. The enthalpic change is more exothermic than the possibly temperature independent Bk-DTPA complex, possibly indicating different interactions between orbitals of californium and the amine heavy DTPA.

4.6.3 Es-DTPA

The results of the Es-DTPA study are listed in Table 4.39.

Table 4.39: Es-DTPA conditional stability constants.

Temp °C	pcH=1.9	2.1	2.3
25	23.27(0.05)	23.31(0.06)	23.1462(0.0006)
35	22.96(0.04)	22.987(0.006)	22.90(0.04)
45	22.58(0.03)	22.61(0.05)	23.0(0.1)

The trend in the data is opposite what is expected, yielding a negative slope. This means that the protonated species is not present in the system, a surprising result. The intercept of the trend line may still be calculated from the data sets. From these sets, Table 4.40 presents the stability constants for Es-DTPA.

Table 4.40: Es-DTPA stability constants

Temp °C	β_{101}
25	24.04(0.01)
35	23.65(0.07)
45	23.67(0.01)

Es-DTPA seems to present an exothermic reaction like Cf-DTPA. The thermodynamic parameters are listed in Table 4.41.

Table 4.41: Es-DTPA thermodynamic parameters, I = 0.5 M.

	ΔH° (kJ/mol)	ΔS° (J/mol·K)	ΔG° (kJ/mol)
Es-DTPA	-30(20)	350(70)	-136.871(0.001)

The Es-DTPA system exhibits slightly more exothermic and favorable behavior than the Cf-DTPA system.

CHAPTER 5

DISCUSSION

Conclusions about the data obtained in chapter 4 will be discussed in sections beginning with each ligand compared between metal ions, and an overall comparison between actinide complexes studied and their lanthanide analogues.

5.1 NTA

Standard stability constants and thermodynamic parameters for NTA complexes obtained in this study are listed in Table 5.1.

Table 5.1: NTA thermodynamic constants obtained at T = 25°C and I = 0.5 M. 1:2 data tabulated as available.

Metal	Logβ T=25°C	ΔH° (kJ/mol)	ΔS° (J/mol·K)	ΔG° (kJ/mol)
Am	11.62(0.01)	-9(1)	192(4)	-66.5033(0.0005)
Bk	12.01(0.02)	-11(3)	194(9)	-68.4517(0.0008)
Cf	11.76(0.03)	2(7)	230(23)	-67.193(0.001)
	22.303(0.007)	-28(2)	333(8)	-130.2861(0.0005)
Es	12.07(0.02)	10(7)	260(22)	-68.4260(0.0008)
	22.80(0.03)	-21(8)	370(30)	-130.2861(0.0005)

There is no apparent trend in the 1:1 stability constants between the actinides, shown in Figure 5.1, though the 1:2 constants increase from Cf-NTA to Es-NTA.

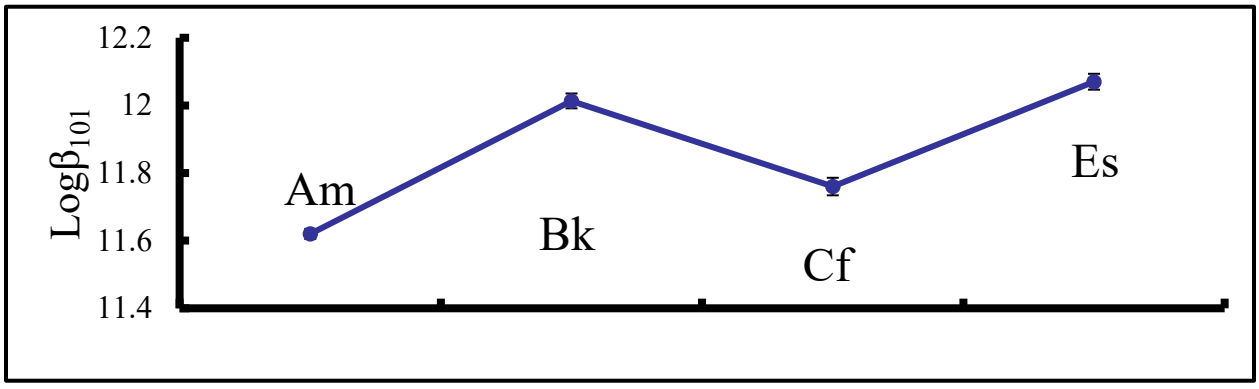

Figure 5.1: Stability Constant Trends, An-NTA

Trends in the changes in enthalpy, entropy, and Gibbs free energy are shown in Figure 5.2, Figure 5.3, and Figure 5.4, respectively.

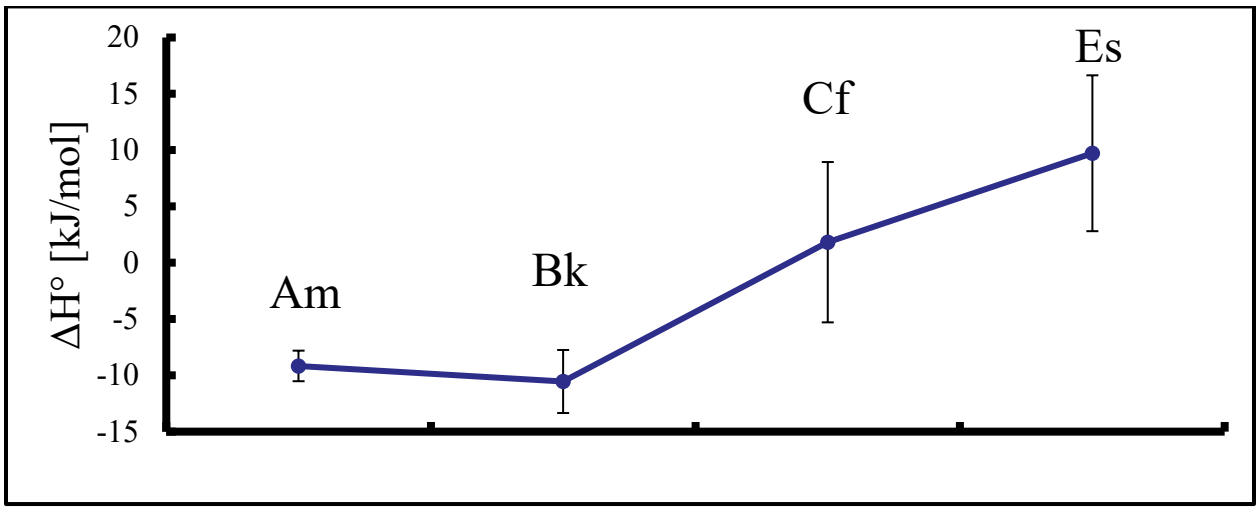

Figure 5.2: Trend in enthalpy changes, An-NTA

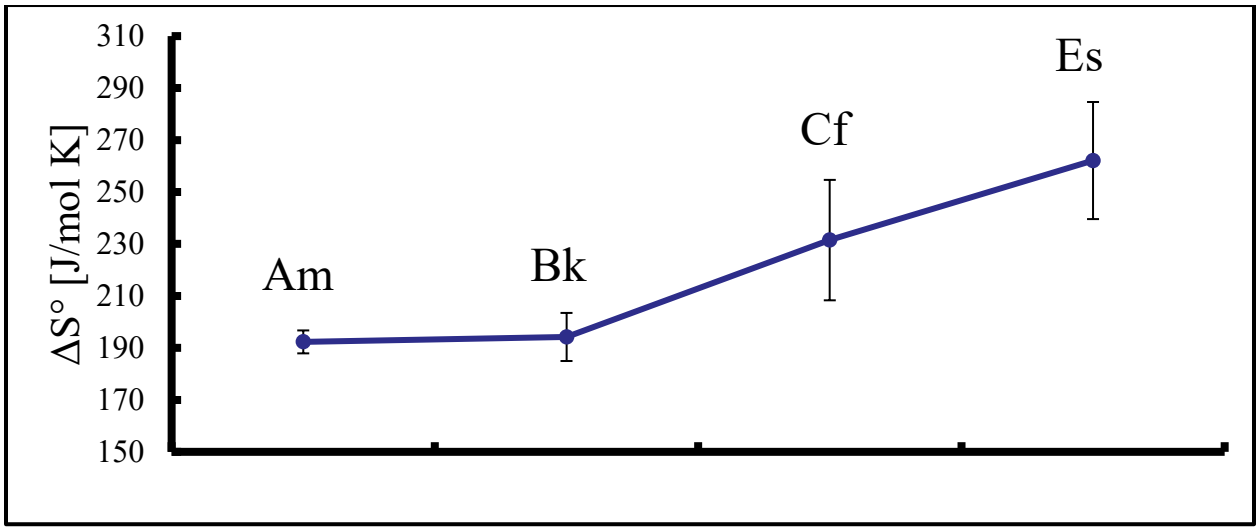

Figure 5.3: Trends in entropy changes, An-NTA

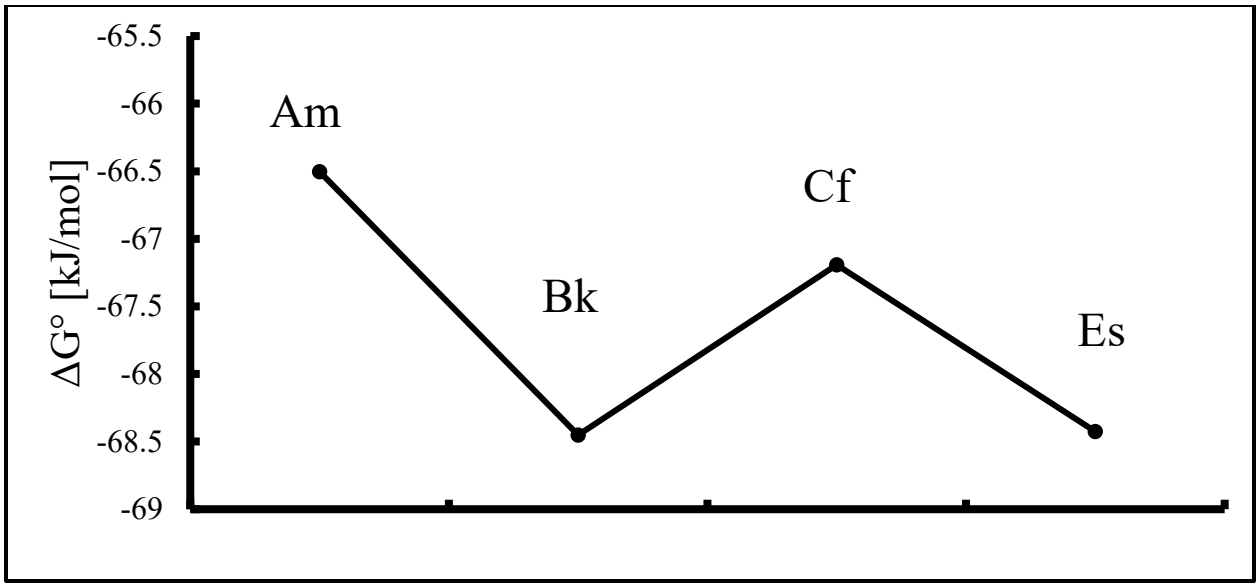

Figure 5.4: Trends in Gibbs free energy changes, An-NTA

The reactions become more endothermic from Cf-NTA to Es-NTA, though since the errors are so high, it is difficult to find a pattern. The reactions also become more entropically favorable across the series. However, there is not clear trend in the favorability of the reactions.

The most interesting finding is the clear appearance of the 1:2 species at californium continuing to einsteinium. The 1:2 species of Cf-NTA is clearly more exothermic than all the other NTA species in this study, and highly favorable. Es-NTA_2 is also exothermic, but less so than the Cf-NTA. However, if one compares the reaction conditions of Cf-NTA and Am-NTA as shown in Figure 5.5, one notices that, due to the lower amounts of NTA used in the americium

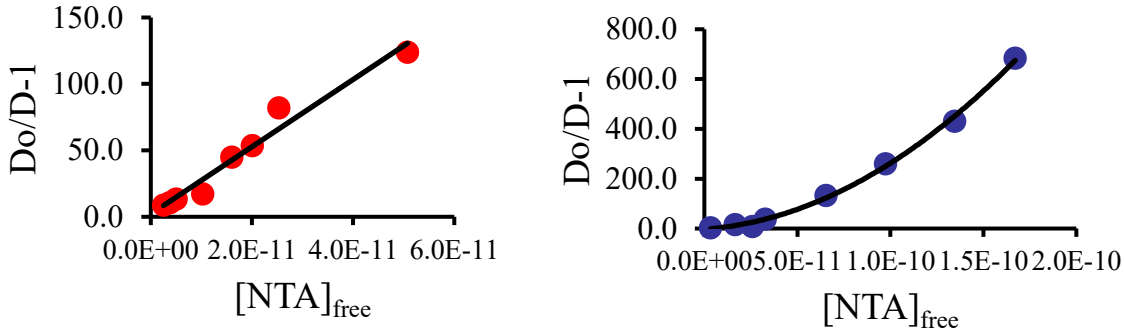

Figure 5.5: Comparison between (A) Am-NTA (left) and (B) Cf-NTA (right)

system and the higher hydrogen ion concentration, the two systems are not comparable. It is possible that americium and berkelium may form 1:2 complexes with NTA if more NTA were present in the system. Therefore, the 1:2 reactions may be a result of the reaction conditions rather than any different chemistry happening between the late trivalent actinides californium and einsteinium.

5.2 HEDTA

Standard stability constants and thermodynamic parameters for HEDTA complexes obtained in this study are listed in Table 5.2.

Table 5.2: HEDTA thermodynamic constants obtained at T = 25°C and I = 0.5 M.

Metal	$Log\beta_{101}$ T=25°C	ΔH°	ΔS°	ΔG°
Am	16.170(0.009)	-34(9)	190(30)	-92.0451(0.0003)
Bk	15.581(0.002)	-30(5)	200(16)	-88.83823(7E-05)
Cf	16.12(0.02)	-36(8)	190(25)	-91.4889(0.0006)
Es	16.17(0.01)	-33(6)	200(19)	-92.3395(0.0003)

HEDTA complexes with metal ions better than NTA due to the larger molecule being able to better wrap around the ion. There is a minimum in the stability constants at berkelium, while the californium and einsteinium stability constants increase, as shown in Figure 5.6.

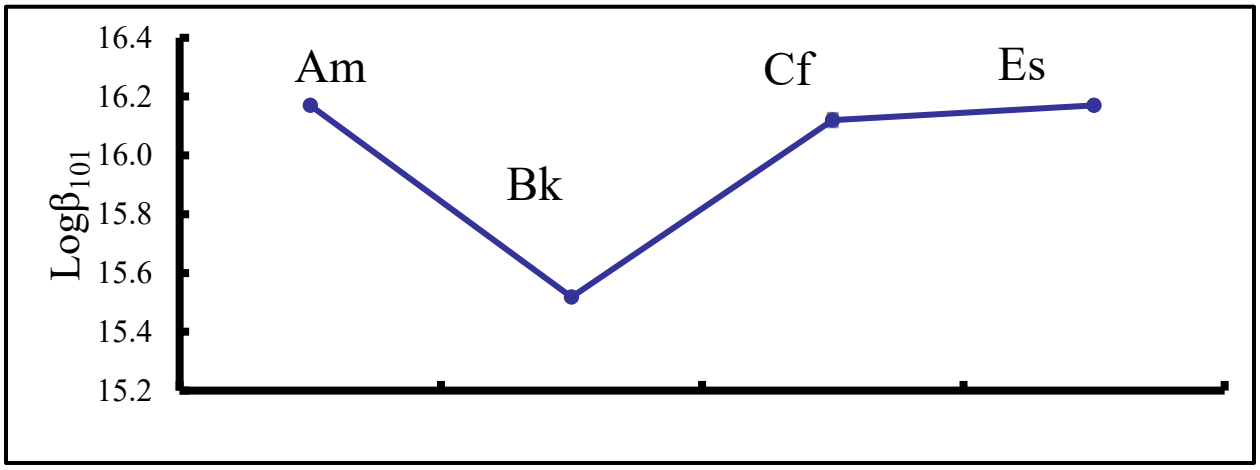

Figure 5.6: Trend in stability constants for An-HEDTA

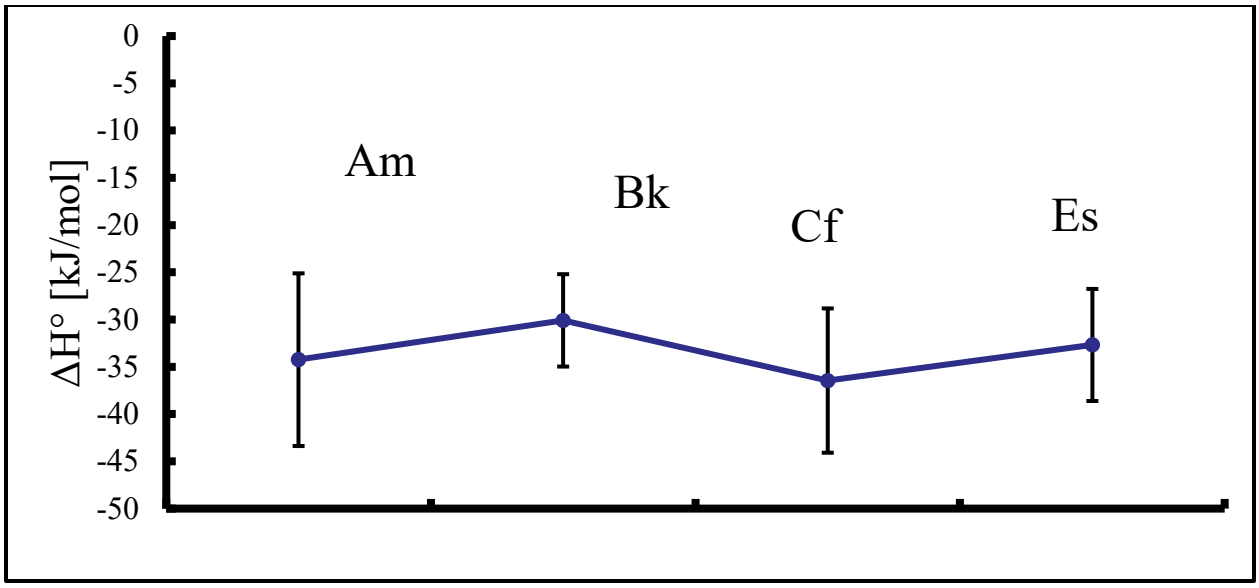

Figure 5.7: Trend in enthalpy change for An-HEDTA

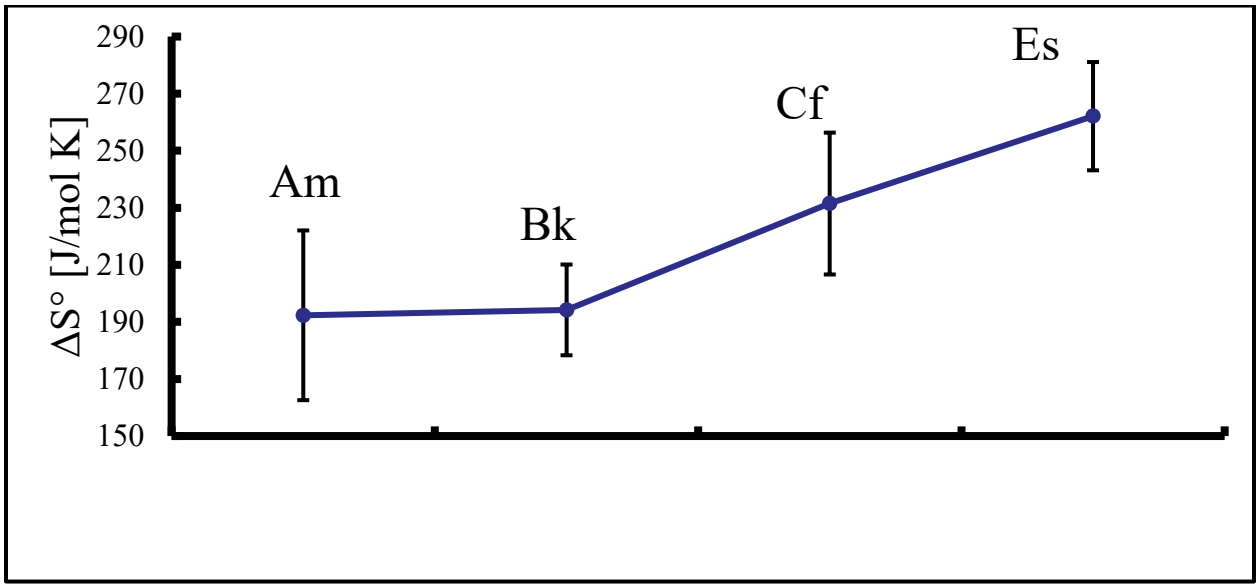

Figure 5.8: Trend in change in entropy for An-HEDTA

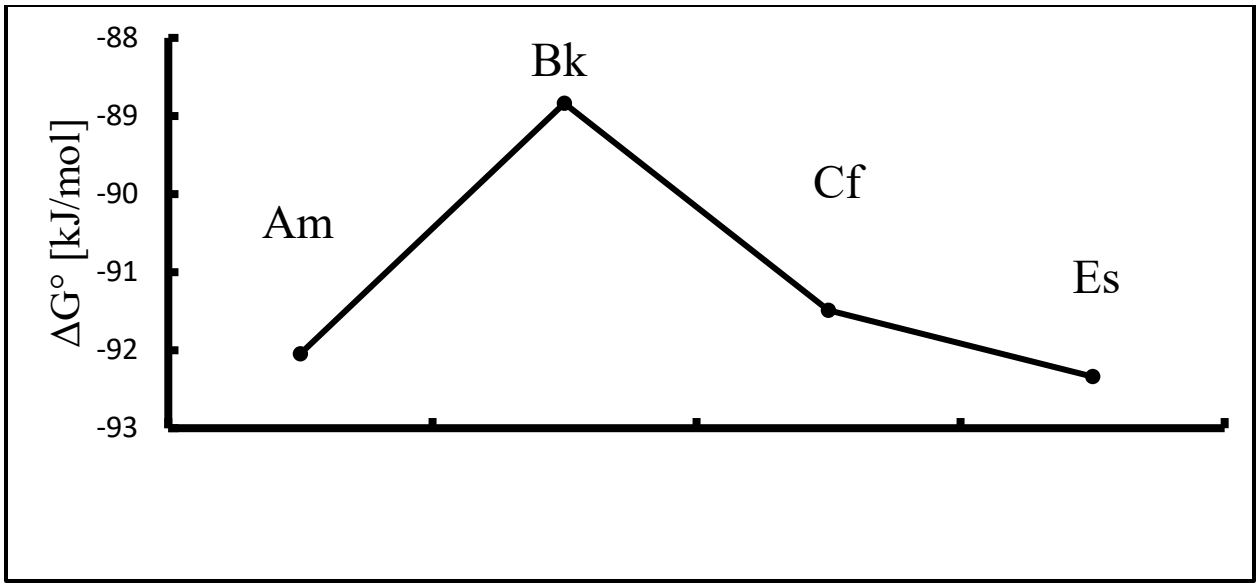

Figure 5.9: Trend in Gibbs free energy change for An-HEDTA

Californium represents the minimum enthalpy change, while einsteinium represents a larger change than any of the other metal ions. However, from Figure 5.7, the enthalpy change for the reactions is statistically identical across the series. Entropy changes across the series tend to increase, as shown in Figure 5.8. The Gibbs free energy enters a minimum at berkelium, representing a relatively unfavorable reaction compared to the rest of the series. However, all reactions remain very favorable, as shown in Figure 5.9.

It is likely that the Bk-HEDTA complex represents the beginning of a change in chemical behavior of the actinide series since it is the minimum of the series in all thermodynamic parameters. This possibly compares favorably to Albrecht-Schmitt's work with Bk-DPA representing the change in chemical behavior of the actinide series (Albrecht-Schmitt et al., 2016).

5.3 CDTA

Standard stability constants and thermodynamic parameters for CDTA complexes obtained in this study are listed in Table 5.3.

Table 5.3: CDTA thermodynamic constants obtained at T = 25°C and I = 0.5 M. The Cf-CDTA and Es-CDTA stability constants are extrapolated from the thermodynamic parameters due to slow kinetics.

Metal	$Log\beta_{101}$ T=25°C	ΔH°	ΔS°	ΔG°
Bk	20.081(0.004)	-18(1)	325(5)	-114.9997(0.0001)
Cf	20.8090(0.0008)	-30(5)	300(16)	-118.79282(2E-05)
Es	20.71(0.09)	-43(8)	250(26)	-118.224(0.002)

The trans-1,2 CDTA ligand is only able to complex with a metal ion in one conformation due to the rigid cyclohexane ring connecting to the amine groups (Thakur, et al. 2007). This is why the stability constants increase dramatically from HEDTA to CDTA, despite only increasing the number of carboxylic acid groups by one. The trend in stability constants, Figure 5.10, is unclear.

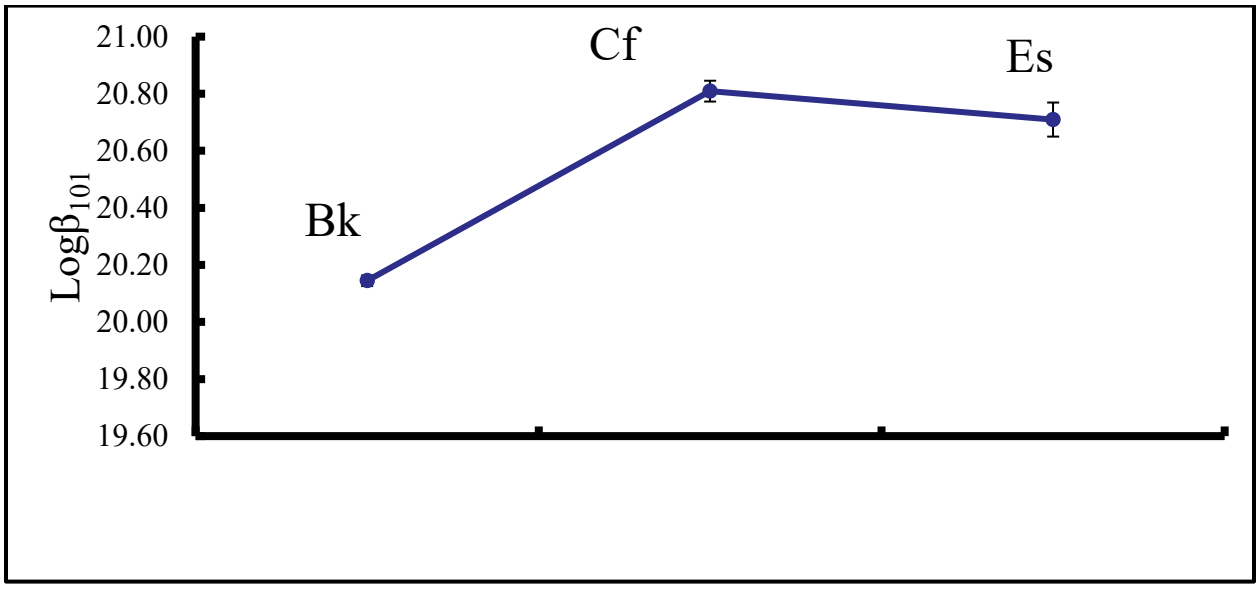

Figure 5.10: Stability constant trend for An-CDTA

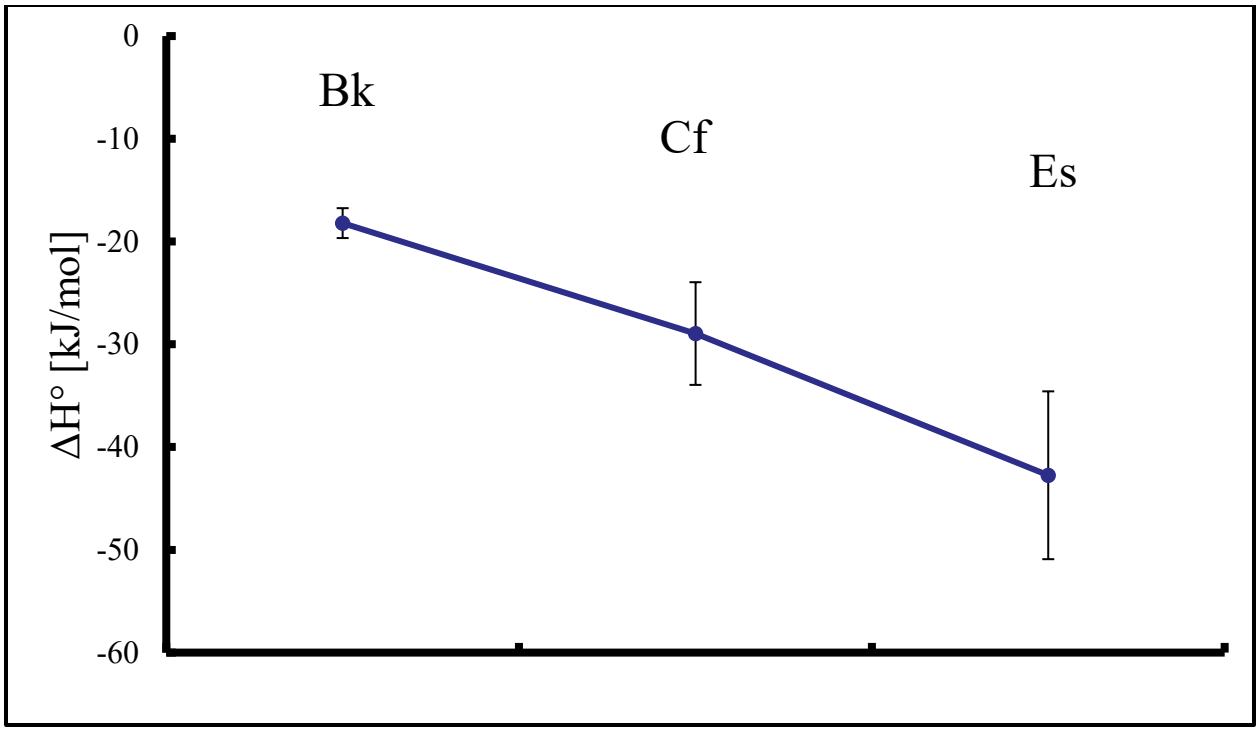

Figure 5.11: Enthalpy change trend for An-CDTA

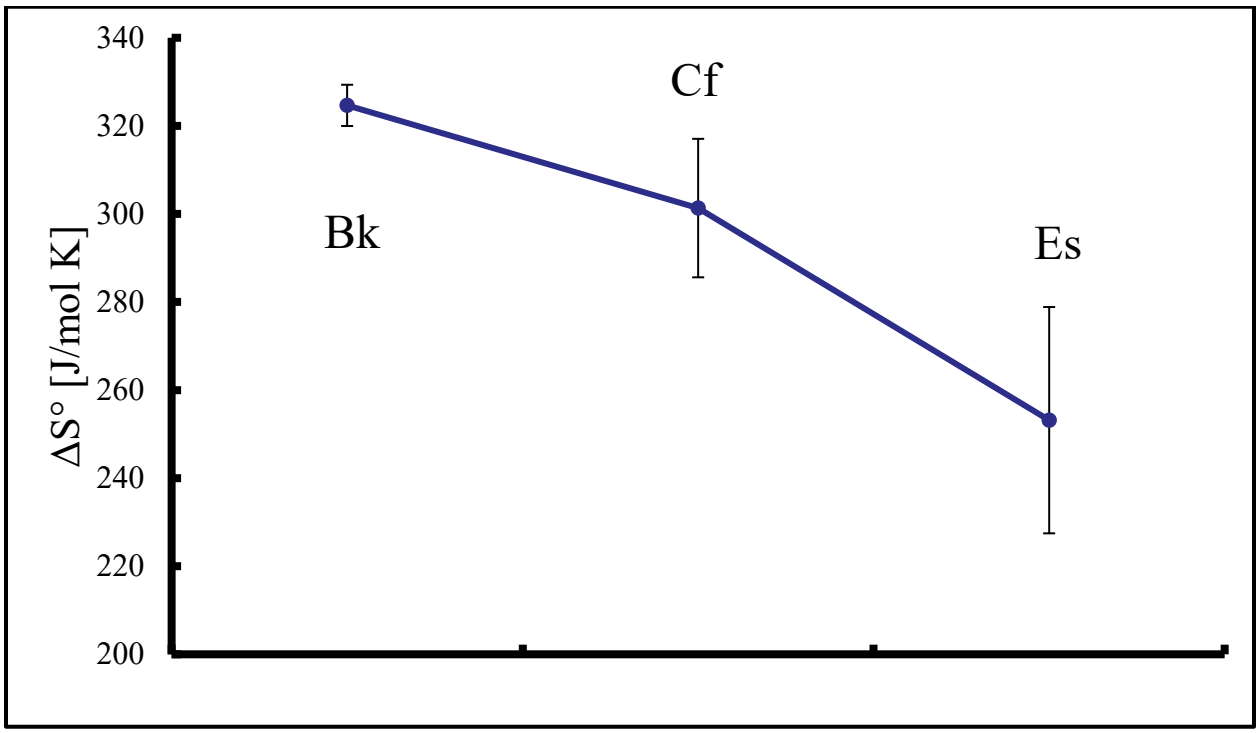

Figure 5.12: Trend in entropy change, An-CDTA

The enthalpy change (Figure 5.11) increases across the series while entropy changes decrease from Bk-CDTA (Figure 5.12). Berkelium seems to lose the most waters in its hydration sphere while complexing with CDTA, though, which explains why the entropy change is so high. Californium and einsteinium lose less water when binding with CDTA. The Gibbs free energy change (Figure 5.13) seems to increase slightly at californium and stays constant at einsteinium.

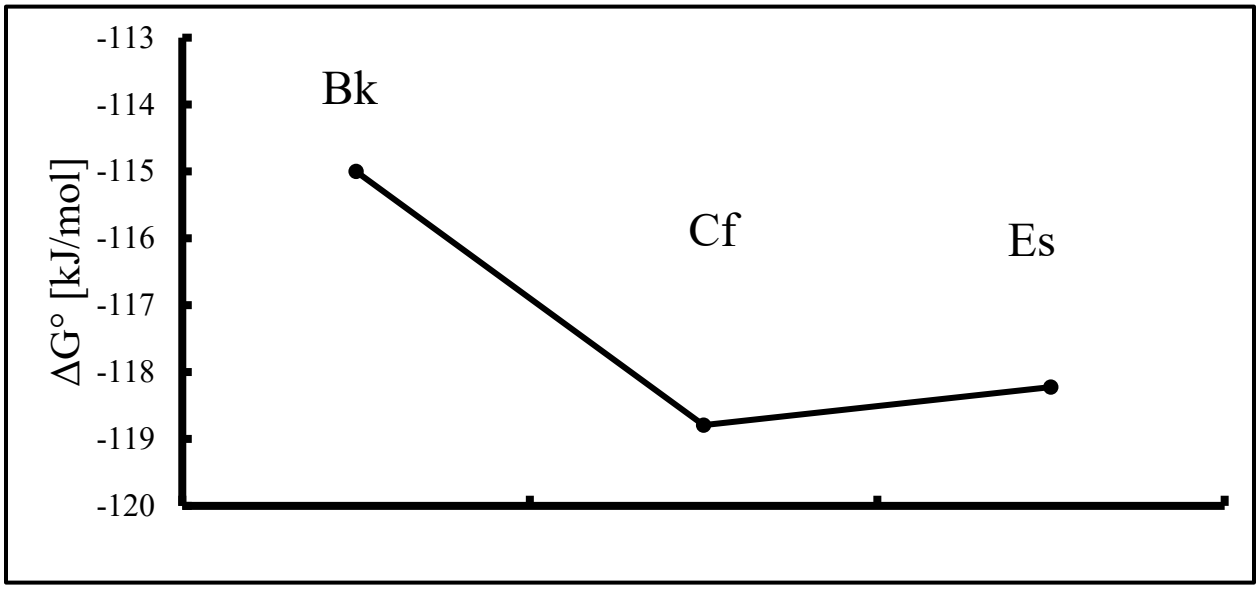

Figure 5.13: Trend in Gibbs free energy change, An-CDTA

5.4 DTPA

Standard stability constants and thermodynamic parameters for DTPA complexes obtained in this study are listed in Table 5.4.

Table 5.4: DTPA thermodynamic constants obtained at T = 25°C and I = 0.5 M.

Metal	$Log\beta_{101}$ T=25°C	ΔH°	ΔS°	ΔG°
Bk	22.7(0.4)	-10(9)	400(30)	-129.744(0.002)
Cf	23.8(0.1)	-30(15)	350(50)	-135.112(0.004)
Es	24.04(0.01)	-30(21)	350(70)	-136.871(0.001)

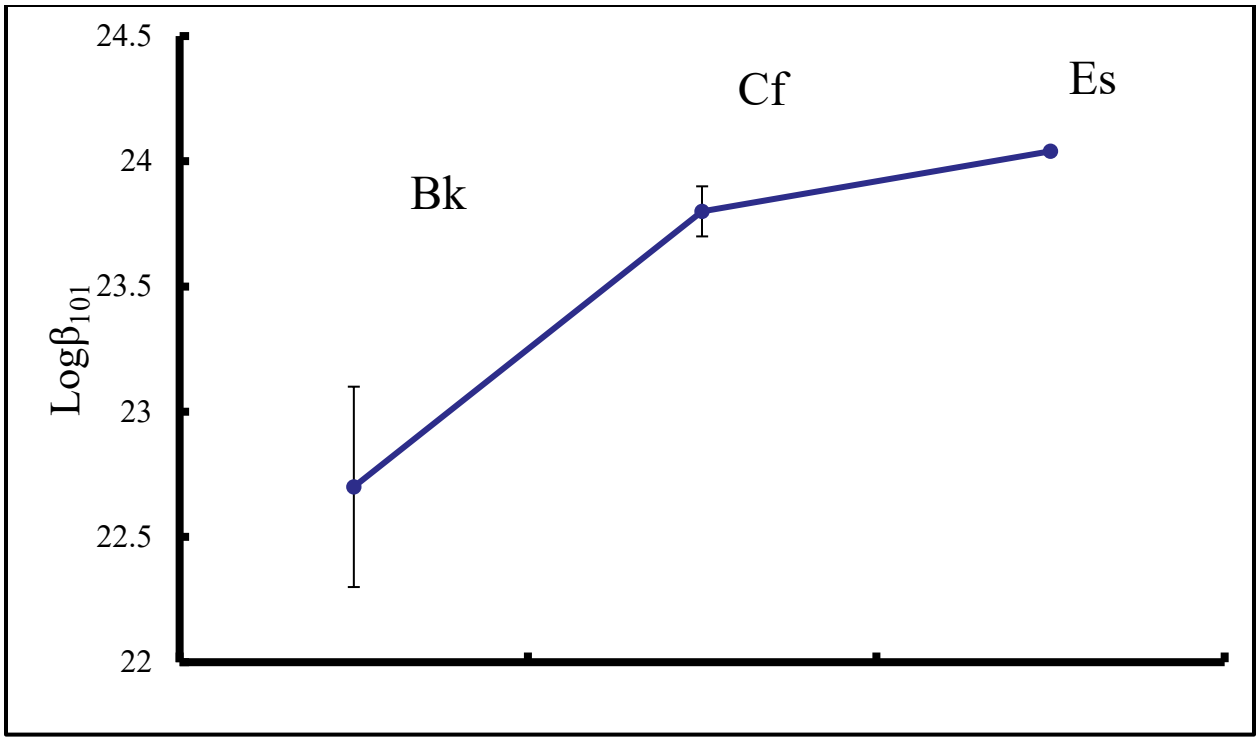

Figure 5.14: Stability constant series trend, An-DTPA

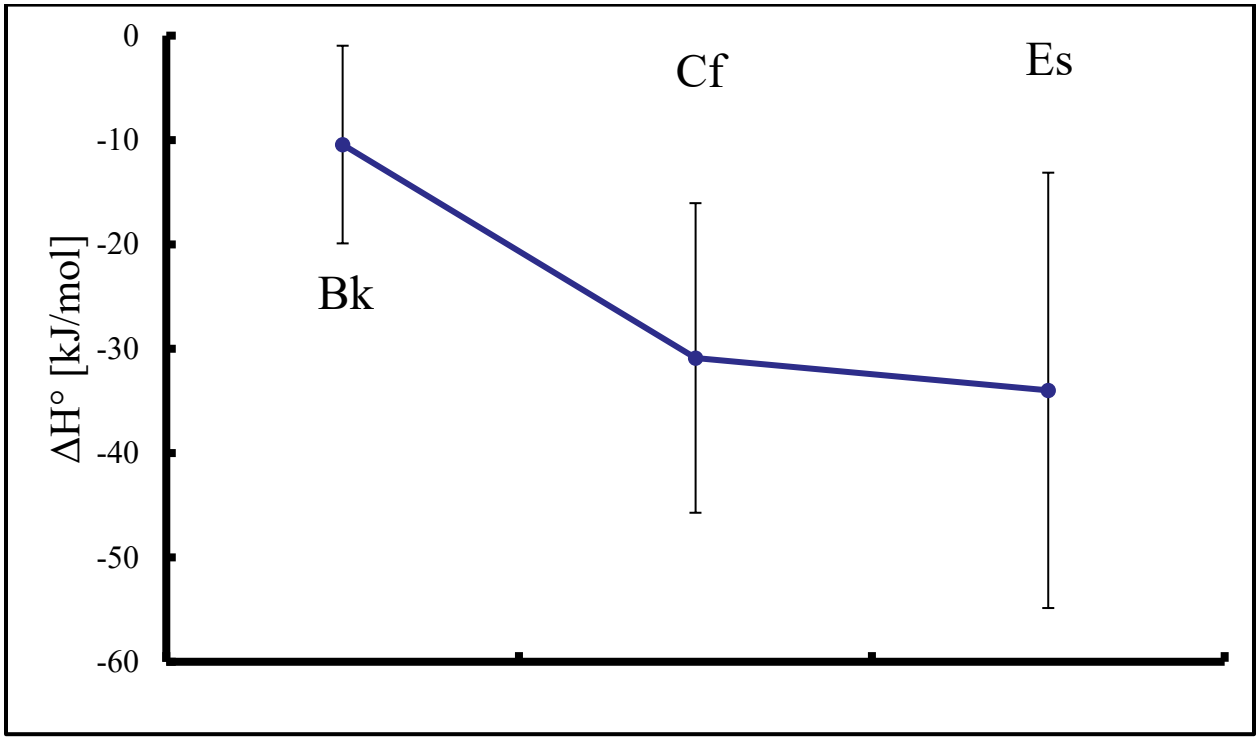

Figure 5.15: Enthalpy change series trend, An-DTPA

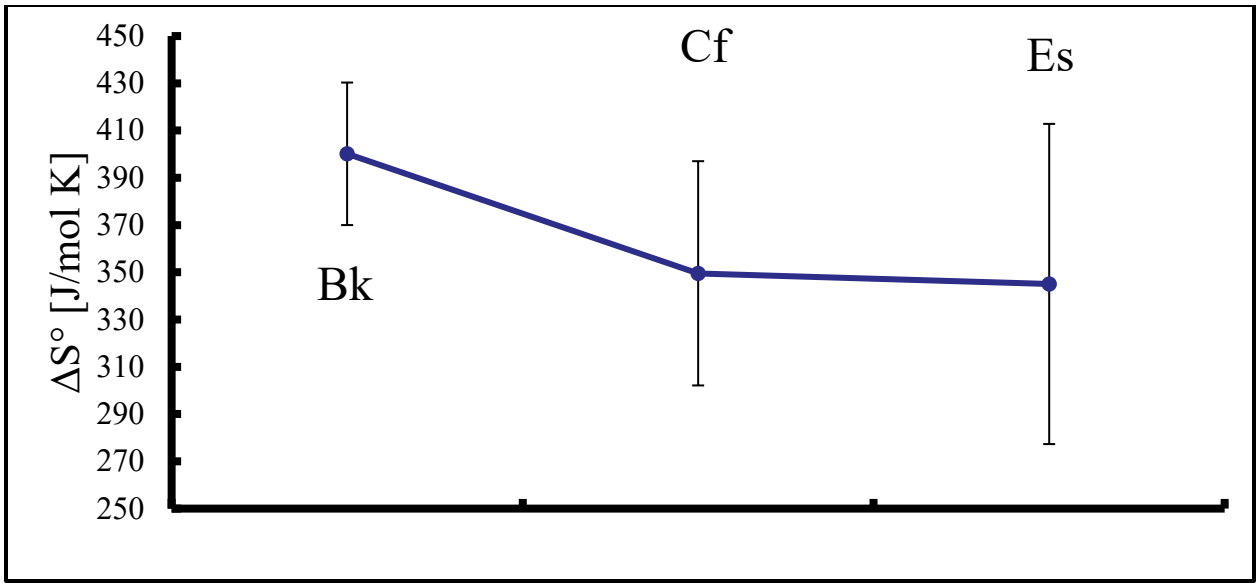

Figure 5.16: Entropy change series trend, An-DTPA

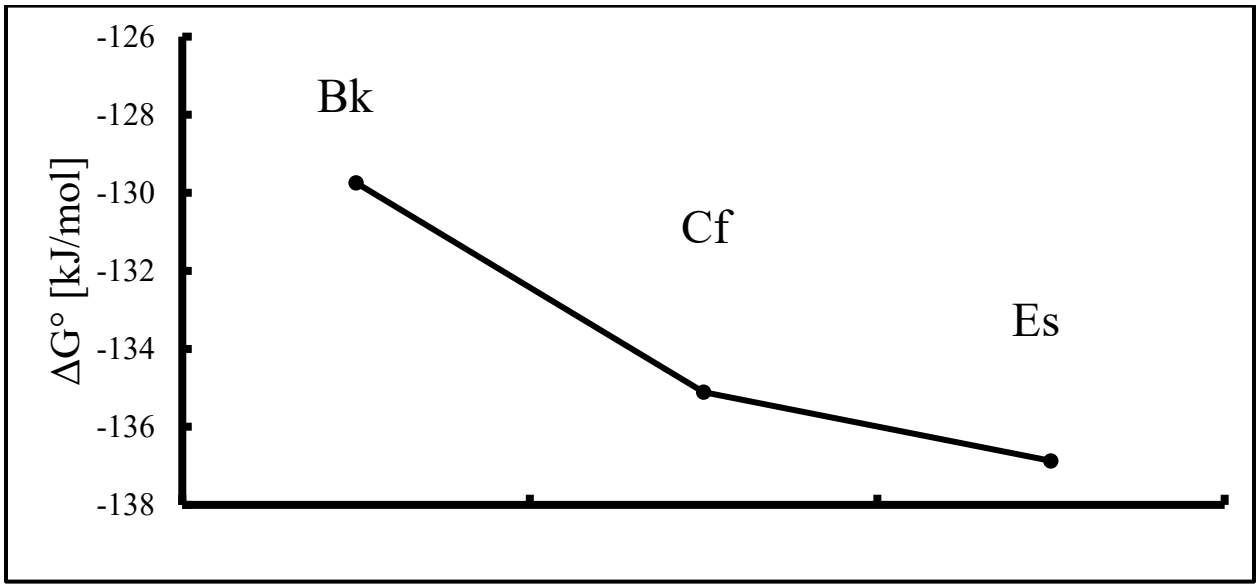

Figure 5.17: Gibbs free energy series trend, An-DTPA

DTPA complexes the best out of all ligands studied. A strange occurrence is the berkelium complex's possibly enthalpically neutral behavior. Bk-DTPA displays the least exothermicity (Figure 5.15) than the other complexes and the smallest stability constant (Figure 5.14). It is interesting to note that the Cm-DTPA complex as evaluated by Baybarz is slightly higher than the Bk-DTPA complex, indicating that Bk-DTPA may represent a minimum in

stability constants of the actinide series with DTPA (Baybarz, 1966). It is likely that berkelium represents the beginning of the shift in actinide behavior, and it takes stronger ligands like DTPA and DPA to bring this behavior to light. Cf-DTPA confirms this shift with stronger complexing and exothermic behavior, while Es-DTPA also increases these parameters. All thermodynamic parameters tend to change in the same way across the series; meaning that the enthalpy change, entropy change, and Gibbs free energy change curves all resemble each other in a way not seen in previous ligands.

An odd finding was that einsteinium has a tendency to not form the protonated species, as seen in Figure 5.18. This may be evidence of different chemistry occurring at einsteinium, but is likely due to pH conditions, though differences in the Cf-DTPA and Es-DTPA systems were negligible.

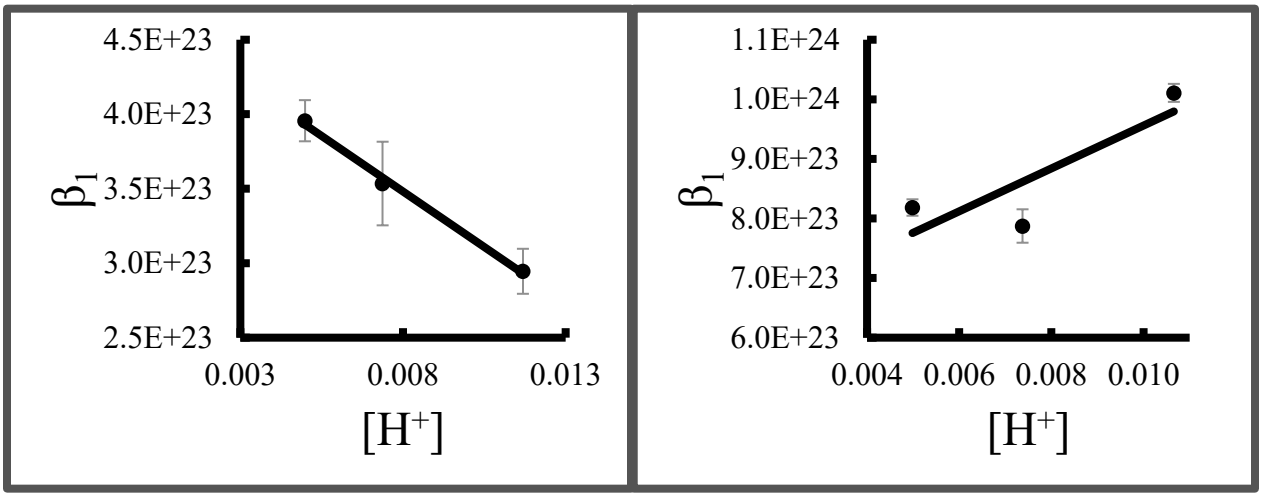

Figure 5.18: Comparison between einsteinium-DTPA (left) and californium-DTPA (right)

5.5 Comparison to Lanthanides

Trivalent actinides and lanthanides are very similar in ionic radii and valence state. Radii and lanthanide analogues are listed in Table 5.5, comparing the studied actinides with their closest lanthanide counterpart.

Table 5.5: Actinide-lanthanide ionic radii comparison. Es not reliably measured and not listed. (Braley, 2013)

Actinide	Ionic Radii (pm)	Lanthanide	Ionic Radii (pm)
Am	99	Nd	99.5
Bk	96	Sm	95.8
Cf	95	Eu	94.7
Es	--	Gd	93.8

Comparison of the bonding behavior of the late actinides and their lanthanide analogues can elucidate bonding differences between similar sized ions, and possibly shed light on selective interactions between actinides and soft donor bases. First, general trends in stability constants are illustrated in Figure 5.19 (lanthanide stability constants listed in Table 5.6). Lanthanides follow a general trend of decreasing stability constant from samarium to gadolinium for NTA, and reaching a maximum at europium for HEDTA, CDTA, and DTPA. By contrast, there is no clear trend in stability constants for the actinides.

Another comparison that may be made is a linear free energy relationship. A linear free energy relationship is a correlation between similar sized ions to quantify the relationship between structure and activity. The stability constants of the actinides are plotted against the lanthanide stability constants at the same temperature and ionic strength (where available). All lanthanide stability constants are obtained from Choppin's research of lanthanide APCs at T = 25° C and I = 0.5 M $NaClO_4$ (Choppin, 1977) and listed in Table 5.6.

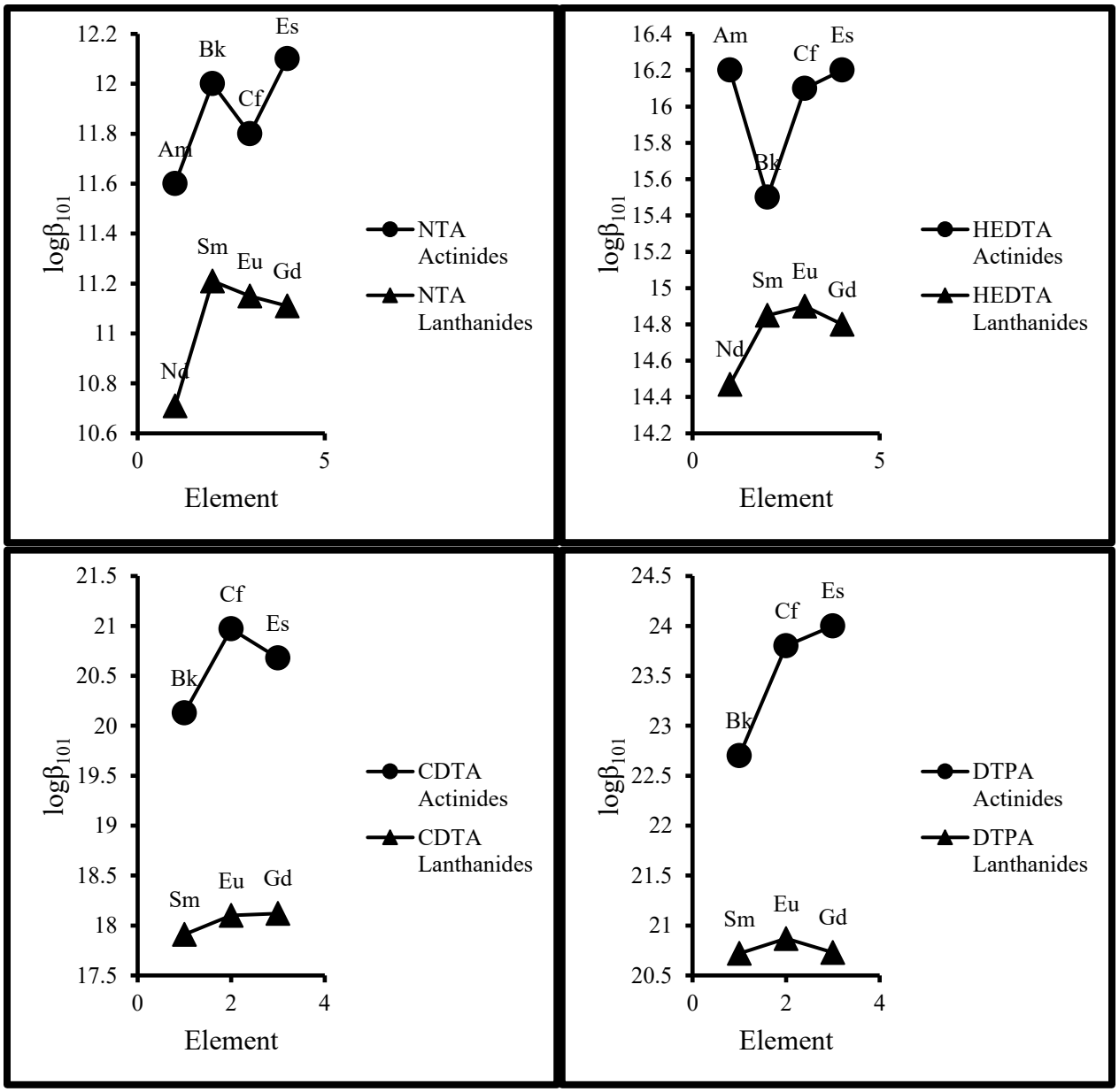

Figure 5.19: Comparisons between APC stability constants for actinides and lanthanides. CDTA and DTPA Am and Nd constants omitted.

Table 5.6: Lanthanide stability constants, logarithmic form (Choppin, 1977)

Lanthanide	NTA	HEDTA	CDTA	DTPA
Nd	10.71	14.47	17.16	20.09
Sm	11.21	14.85	17.91	20.72
Eu	11.15	14.90	18.10	20.87
Gd	11.11	14.80	18.12	20.73

Americium and neodymium are shown in Figure 5.20. Even though only two points were available in this study, a comparison may be made between the actinide-lanthanide systems.

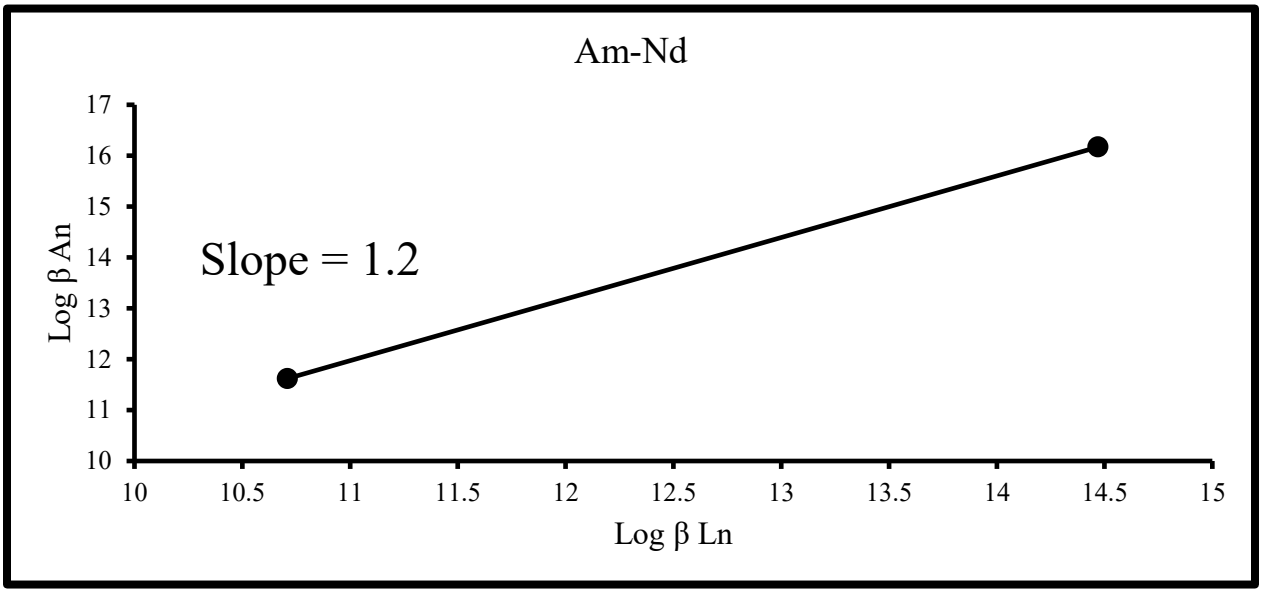

Figure 5.20: Americium-neodymium linear free energy relationship. Only HEDTA and NTA were analyzed.

Americium is the control relationship for this analysis, in that any deviations from the Am-Nd APC bonding relationship may show changes in covalent behavior across the later actinide series. The slope of the line between the two elements' stability constants may be interpreted as a baseline for comparison between systems. Stability constants for Am-APCs are higher than Nd-APCs, indicating americium has a selectivity for APCs. This difference may be interpreted as a general preference of the actinides to bond with the APCs, possibly due to the 5f orbital interactions.

Berkelium and samarium are shown in Figure 5.21.

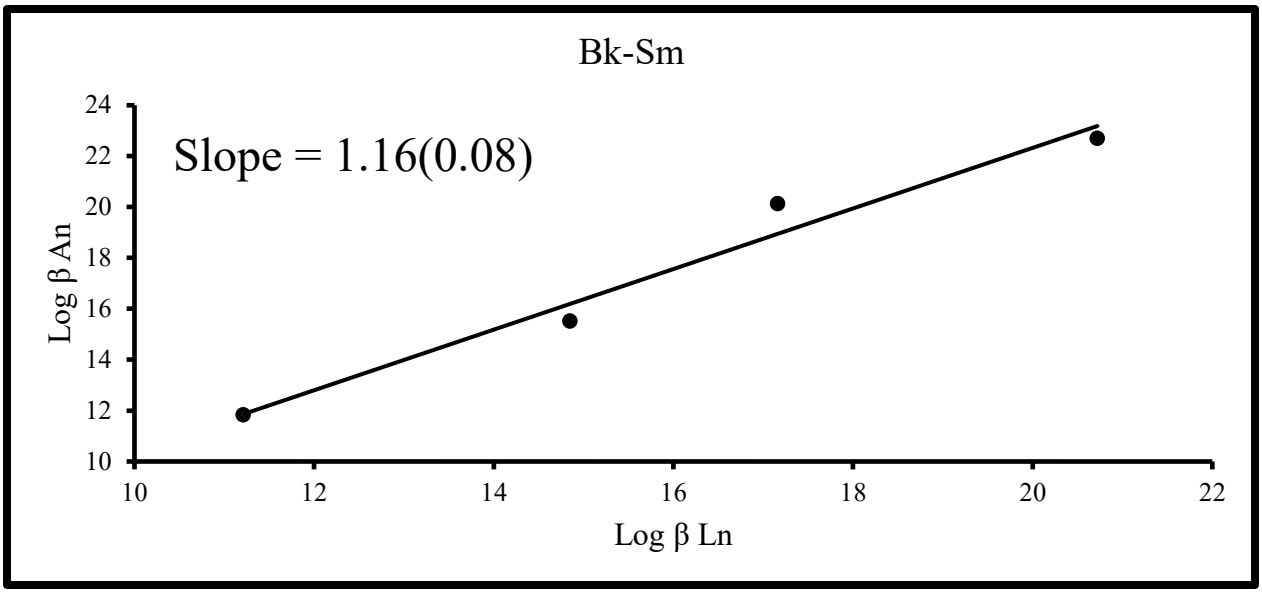

Figure 5.21: Berkelium-samarium linear free energy relationship

This relationship shows no deviation from the slope of the Am/Nd line in statistical terms. This may be due to the low Bk-HEDTA stability constants in relation to the other actinides, judging from the slope of a best fit line. There are large differences between Sm-CDTA and Bk-CDTA, and Sm-DTPA and Bk-DTPA. Other works have shown similar stability constants for Sm-CDTA at different ionic strength, but there is a wide variance between Sm-DTPA stability constants. Choppin reports the lowest value for Sm-DTPA, 20.72 (Choppin et al., 1977), while Zakrzewski and Geisler report a constant of 20.99 and a constant of 21.5 (Zakrzewski & Geisler, 1987), and Moeller and Thomson report a constant of 22.34 (Moeller & Thomson, 1962). Further, Choppin's DTPA measurements were taken with a pH electrode, and no mention of the protonated species was made. A later paper was also found by Choppin and Shanbhag where they describe how to find the protonated and deprotonated stability constants of DTPA using solvent extraction, meaning it is likely that Choppin did not find the deprotonated stability constants of the lanthanide DTPA complexes in his 1977 paper (Shanbhag & Choppin,

1982). If the constant used were changed to 20.99, the difference in slope does not change. Therefore, we can conclude that berkelium shows no special selectivity with the aliphatic APCs.

The californium and europium linear free energy relationship is shown in Figure 5.22.

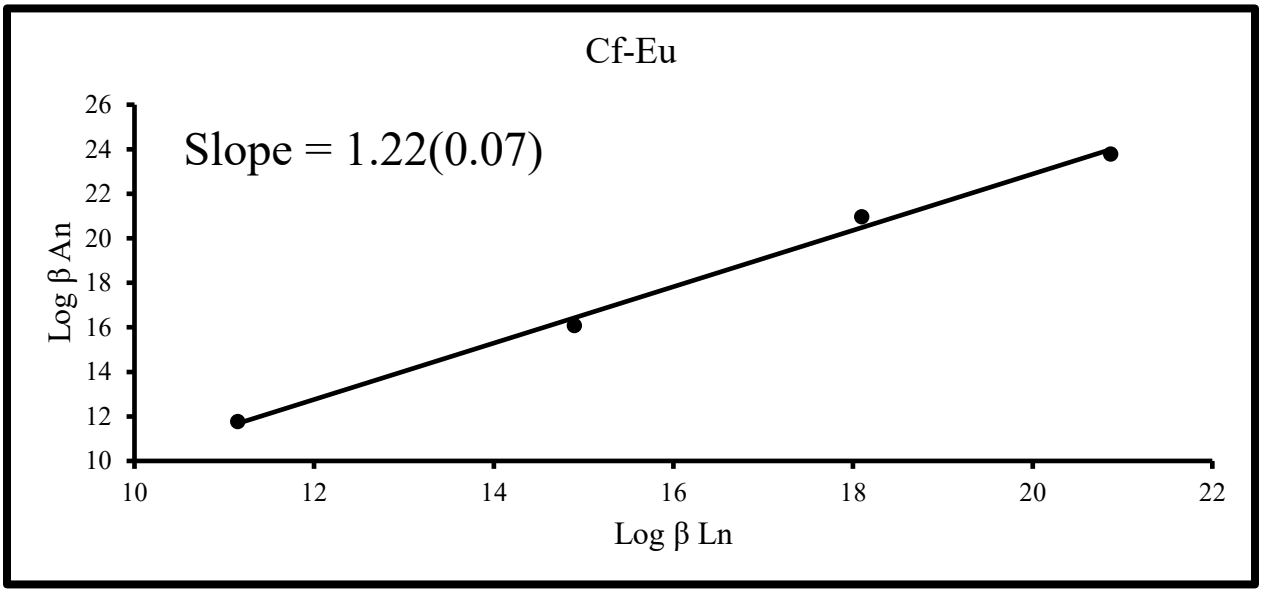

Figure 5.22: Californium-Europium linear free energy relationship

Californium APCs show a difference in selectivity from europium by about 2% in absolute terms when compared to the Am-Nd system. However, in statistical terms, the Cf-Eu system is identical to the Am-Nd system.

A further comparison may be made between Cf-NTA_2 and Eu-NTA_2. Unfortunately, Choppin failed to include the 1:2 species in his work with lanthanide stability constants (Choppin, 1987). Collange and Thomas, however, used similar conditions to find the stability constants of Eu-NTA and Eu-NTA_2 (Collange & Thomas, 1973). Their logarithmic stability constants for the Eu-NTA system are 10.51 and 19.51 for the 1:1 and 1:2 species. This is a difference of three orders of magnitude between the lanthanide and actinide complexes. Moeller and Ferrus report values of 11.52 and 20.70 for the 1:1 and 1:2 species, respectively under and

ionic strength of 0.1 M (Moeller & Ferrus, 1962). It is unwise to try and correct any value above 0.3 M ionic strength, so values may be compared directly. The 1:1 NTA complexes are similar in stability constant, but the 1:2 species are still two orders of magnitude apart. It is likely that this is more evidence for actinide selectivity in bonding with the APCs.

The linear free energy relationship between einsteinium and gadolinium is plotted in Figure 5.23.

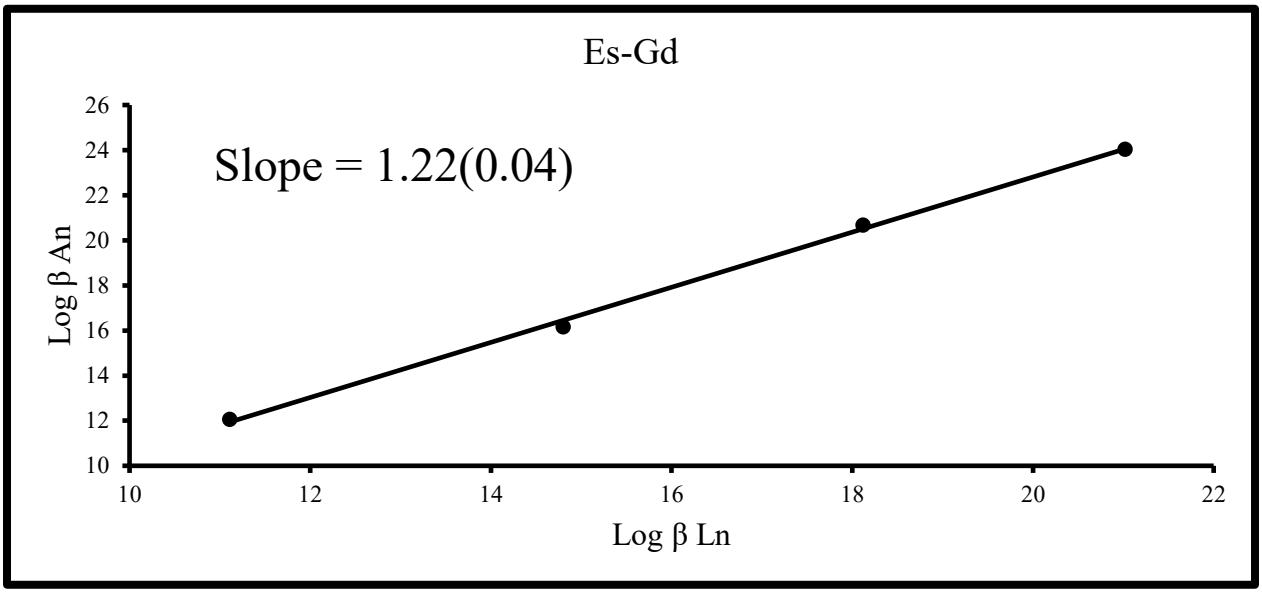

Figure 5.23: Einsteinium-gadolinium linear free energy relationship

This plot again shows a 2% absolute deviation from the Am-Nd system. However, like the other systems, the error precludes any judgements about the change in selectivity from the early trivalent actinides to the later trivalent actinides.

For further comparison, Anderegg and Moeller and Ferrus report similar stability constants for Gd-NTA_2, both at 0.1 M ionic strength (Anderegg, 1965) (Moeller & Ferrus, 1962). Anderegg reports a $\log\beta_{101}$ of 11.43 and a $\log\beta_{102}$ of 20.78. Moeller and Ferrus report a $\log\beta_{101}$ of 11.54 and a $\log\beta_{102}$ of 20.80. Both of these values are two orders of magnitude smaller than the Es-NTA_2 stability constant reported in this work. As with the Cf-NTA system, caution must be

used when comparing systems of different ionic strength. However, it is likely that this is more evidence for selectivity between the actinides as a whole for the APCs when compared to the lanthanide APCs.

Berkelium, californium, and einsteinium all exhibit large differences in stability constants from their lanthanide counterparts. It is of note that the actinide stability constants deviate from the lanthanide stability constants most with the ligands CDTA and DTPA. CDTA has two amine groups like HEDTA, but four carboxylic acid groups instead of three, and a rigid conformation that only allows bonding with metal ions in one way. DTPA is the ligand with three amines and five carboxylic acid groups. It seems that the more carboxylic acids and amines a ligand has, the more the trivalent actinide ions preferentially bond over the lanthanides. The actinides may preferentially bond due to the combination of hard and soft donors. Further, the size of the ligand and its ability to completely wrap around the metal ion may contribute to preferential bonding of the 5f orbital to the ligand. This ability to wrap around the ion may expose the metal ion to the amine groups more than other ligands can, possibly improving bonding through orbital degeneracy or covalent interactions.

However, it is unlikely that a change in the selectivity exists in the actinides, since the only evidence is the 1:2 bonding between NTA and californium and einsteinium which may be explained by having a greater free ligand concentration in solution, and californium's and einsteinium's 2% absolute selectivity increase over the Am-Nd relationship. It is difficult to tell without knowing the error between the Am-Nd system, though, and the errors in the Cf-Eu and Es-Gd systems preclude any judgements as well.

Since there is little difference between the baseline case of the Am-Nd relationship and the later actinide APCs, it is likely that the hypothesis of this thesis may be answered in the

negative, and the late trivalent actinides show no change in selectivity with the aliphatic amines in aminopolycarboxylates relative to their lanthanide counterparts.

CHAPTER 6

SUMMARY AND CONCLUSIONS

Solvent extraction experiments were conducted with americium, berkelium, californium, and einsteinium with the APC ligands NTA, HEDTA, CDTA, and DTPA to provide evidence for selectivity in bonding between the soft donor amine and the metal ion. While americium and berkelium provided no evidence for selectivity, californium and einsteinium displayed unique chemical interactions that may be explained by selective interactions with the amine groups. Californium and einsteinium displayed a tendency to form 1:2 complexes with NTA where other actinides did not at reasonable lengths of time, though the Am-NTA and Bk-NTA systems contained less free NTA ligand than the Cf-NTA and Es-NTA systems. Berkelium, californium, and einsteinium also all yielded stability constants with CDTA and DTPA at least two orders of magnitude greater than their lanthanide counterparts. These facts provide more pieces of evidence for selective interactions between soft donor bases and the late trivalent actinides californium and einsteinium. However, no clear trends were observed, and since there was little deviation from the baseline case of Am-Nd except in absolute terms, the conclusion that the late actinides represent a break in periodicity from the earlier trivalent actinides cannot be supported with the work of this thesis.

This work also proved that there are ligands that can be used in solvent extraction processes to separate actinides from lanthanides of similar ionic radii if kinetics limitations are accounted for. HEDTA is already considered for use in the ALSEP process as well as DTPA. Refined thermodynamic parameters are now available for comparison between APCs and other ligands that may be considered in separations processes.

The late actinides may have uses yet to be discovered, and in the case of californium, it is already produced for use in industry. Production of these nuclides must involve high flux reactors and separations processes that can differentiate between trivalent actinides and lanthanide fission products. The four APCs studied in this thesis can provide the basis for separations processes of these nuclides from lanthanides if they are required. Further, Cf-249 and Cf-251 constitute sinks that the later actinides, when created, decay to since their half-lives are 351 years and 898 years, respectively. This means that if a nation were to move to an aggressive fuel cycle where used nuclear fuel is constantly reprocessed into MOX and used in thermal spectrum reactors, Cf-249 and Cf-251 will build up in the system. These nuclides would require separations similar to americium and curium and can be burned in reactors or partitioned with other waste products. The APCs offer a route for separations from the trivalent lanthanides. These may also be used to create Cf-252, a neutron emitter used in well logging, imaging, and many other applications.

Other applications of this work include use of APCs in decontaminating trivalent actinides by removing the metal ions from surfaces. APCs may be used for this process provided enough time is taken to allow the metal ions to overcome kinetics issues of the APC ligands. Further, all APC ligands considered in this work are major ingredients in detergents used worldwide. This means a handy supply of decontamination material is always readily available.

The understanding of the fundamental chemistry of the late actinides is underway. Already, some unique chemical interactions have been observed, and may be taken advantage of. More research into this area using different ligands, different methods, and higher actinides may yet reveal a completely new understanding of the periodic table.

CHAPTER 7

FUTURE WORK

Future explorations should consider probing the trivalent actinides with EDTA to complete the linear free energy relationship and compare the thermodynamics of the similar sized ligands HEDTA and EDTA. An interesting comparison can be made between the two ligands, as HEDTA and EDTA both have two amine groups but EDTA has one more acetate group that interacts with the metal ion.

More experiments should be conducted with aromatic amines since the aliphatic amines showed little difference from the baseline case in the linear free energy relationships. Aromatic amines may be more able to access the f-orbitals of the late actinides, and also have access to more electron density through the use of the aromatic ring. Since this study started with discoveries made using aromatic amines and californium and berkelium, aromatic amines may show more selectivity than aliphatic amines.

Curium must be studied with these APCs to complete our understanding of the trivalent actinides and investigate the actual breaking point of the actinide series. The stock of curium available to this study was found to be contaminated with plutonium, skewing extraction results and providing nonsensical stability constants. A fresh stock studied with NTA and HEDTA would help complete understanding of the early trivalent actinide series. However, investigations into curium have already been conducted and further laboratory experiments should be confined to seeing if there is a difference between americium and curium selectivities.

Further studies must be conducted to elucidate the interactions between later actinides like fermium, mendelevium, nobelium, and lawrencium and APCs. If the trends revealed in this

work hold, our fundamental understanding of the actinide series and its chemistry may be changed. However, the difficulty in obtaining enough of these elements to conduct tracer studies cannot be understated. Further, the longest half-life of fermium is 3 days, mendelevium 51 days, nobelium 58 minutes, and lawrencium 39 minutes. These nuclides must be obtained in massive quantities to have enough time to conduct all required kinetics, extraction, and competition studies to illuminate the chemistry between the late actinides and APCs, especially if complexation chemistry is kinetically limited to where the nuclide can undergo several half-lives during an experiment. Calorimetry may help speed the process. However, production of these elements is limited, even at ORNL.

Finally, computational investigations into orbital interactions between APCs and the late actinides will help reveal the way these elements' orbitals mix and interact with different ligands, and quantify the degree of orbital interactions. This would especially be useful in investigating the californium and einsteinium complexes with NTA, as well as helping to understand why berkelium and americium do not exhibit the same degree and type of complexation that the aforementioned elements do with NTA.

REFERENCES

Albrecht-Schmitt, T. E. et al. “Unusual Structure, Bonding, and Properties in a Californium Borate.” s.l. : Nature Chemistry, 2014, Vol. 6. 10.1038/NCHEM1896.

Albrecht-Schmitt, T. E. et al. “Emergence of Californium as the Second Transitional Element in the Actinide Series.” s.l. : Nature Communications, 2015, Vol. 6. 10.1038/ncomms7827.

Albrecht-Schmitt, T. E. et al. “Characterization of Berkelium(III) Dipicolinate and Borate Compounds in Solution and the Solid State.” Science, 2016. Vol. 353, Issue 6302, pp. 888.

Anderegg, G. “Entropiebedingte Komplexbildung Thermodynamische Daten der Komplexbildung mit dem Tripolyphosphat-Ion”. Helvetica Chimica Acta, 1965. Vol. 48, pp. 825.

Baybarz, R. D. “Dissociation Constants of the Transplutonium Element Chelates of the Diethylenetriaminepenta-acetic Acid (DTPA) and the Application of DTPA Chelates to Solvent Extraction Separations of Transplutonium Elements from the Lanthanide Elements.” Journal of Inorganic Chemistry, 1965, Vol. 27, pp. 1831-1839.

Baybarz, R. D. “Dissociation Constants of the Trans-Plutonium Element Chelates of 1,2-Diaminocyclohexanetetraacetic Acid.” Journal of Inorganic Nuclear Chemistry, 1966. Vol 28, pp. 1055-1061.

Braley, Jenifer. “Actinide N-Donor Thermodynamics: Expanding the f-element Covalency Dialogue.” Golden, CO : DOE, 2013. PRE-0000003125.

Brandau, E. “Stabilitatskonstanten Der Komplexe Von Am(III), Cm(III), und Cf(III) mit Diathylentriaminpentaessigsaure.” 1971, Inorganic Nuclear Chemistry Letters, Vol. 7, pp. 1177-1181.

Brown, M. Alex, Wardle, Kent, Lumetta, Gregg, Gelis, Artem. “Accomplishing Equilibrium in ALSEP: Demonstrations of Modified Process Chemistry on 3-D Printed Enhanced Annular Centrifugal Contactors.” Procedia Chemistry 21 (2016): 167-173.

Choppin, Gregory. “Covalency in f-element bonds.” 1-2, s.l. : Journal of Alloys and Compounds, 2002, Vol. 344, pp. 55-59. 10.1016/S0925-8388(02)00305-5.

Choppin, Gregory. “Solution Chemistry of the Actinides.” Radiochimica Acta., 1982, Vol. 32. 0033-8230.

Choppin, Gregory, Schneider, Joan. “The Acetate Complexing by Trivalent Actinide Ions.” Journal of Inorganic Nuclear Chemistry, 1970, Vol. 32m pp.3283-88.

Choppin, G. R., Goedken, M. P., Gritmon, T. F. “The Complexation of Lanthanides by Aminoolycarboxylate Ligands-II.” Journal of Inorganic Nuclear Chemistry, 1977, Vol. 39, pp. 2025-2030.

Choppin, Gregory., Rydberg, Jan. and Liljenzin, J. Radiochemistry and Nuclear Chemistry. Woburn, MA: Butterworth-Heinemann; 3rd edition, 2001.

Choppin, G., Thakur, P. and Mathur, J. N. “Complexation Thermodynamics and Structural Aspects of Actinide-Aminopolycarboxylates.” Coordination Chemistry Reviews, 2006, Vol. 250.

Collange, E., Thomas, G. “Complexes de l'europium(II) avec les acides iminodiacétique et nitrilotriacétique en solution aqueuse”. Analytica Chimica Acta, 1973, Vol. 65, pp. 87.

Fuger, J. “Ion Exchange Behavior and Dissociation Constants of Americium, Curium, and Californium Complexes with Ethylenediaminetetraacetic Acid.” 1958, J. Inorg. Nucl. Chem., Vol. 5, pp. 332-338.

Gousetis, C. and Opgenorth, H.-J. 2000. Nitrilotriacetic Acid. Ullmann's Encyclopedia of Industrial Chemistry. .

Heathman, C. R. and Nash, K. L. “Characterization of Europium and Americium Dipicolinate Complexes.” 14-15, Pullman, WA : Separation Science and Technology, 2012, Vol. 47. 01496395.2012.704225.

IAEA 2017. Nuclear Share of Electricity Generation in 2016. IAEA. Accessed 27 June 2017. https://www.iaea.org/PRIS/WorldStatistics/NuclearShareofElectricityGeneration.aspx.

King, L., Bigelow, J. and Collins, E. “Experience in the Separation and Purification of Transplutonium Elements in the Transuranium Processing Plant at the Oak Ridge National Laboratory.” San Francisco, CA : ACS, 1980. CONF-800814-21.

Y. Marcus and A. S. Kertes, "Ion Exchange and Solvent Extraction of Metal Complexes", Wiley-Interscience. 1969, Chapter 8 and references therein.

Moeller, T., Chu, Shu-Kung. “The Stabilities and Thermodynamic Functions for the Formation of Aluminium and Mercury (II) Chelates of certain Polyaminepolyacetic Acids.” Journal of Inorganic Nuclear Chemistry, 1966, Vol. 28, pp. 153-159.

Moeller, T., Ferrus, R. “Observations on the Rare Earths. LXXIV. The Enthalpy and Entropy of Formation of the 1:1 and 1:2 Chelates of Nitrilotriacetic Acid with Tripositive Cations”. Inorganic Chemistry. 1962. Vol. 1, pp. 55.

Moeller, T., Hseu, T. “Observations on the rare earths—LXXVI(1): The stabilities of the trans-1,2-diaminocyclohexane-N,N′-tetraacetic acid chelates of the tri-positive ions”, Journal of Inorganic and Nuclear Chemistry, 1962, Vol. 24, pp. 1635.

Moeller, T., Thomson, L. “Observations on the rare earths—LXXV(1): The stabilities of diethylenetriaminepentaacetic acid chelates”. Journal of Inorganic Nuclear Chemistry, 1962, Vol 24, pp. 499.

Neidig, Michael, Clark, David and Martin, Richard. “Covalency in f-element Complexes.” 2013, Coordination Chemistry Reviews, Vol. 257, pp. 394-406.

Osborne-Lee, Irvin and Alexander, C. “Californium-252: A Remarkable Versatile Isotope.” Oak Ridge, TN : Oak Ridge National Laboratory - Martin Marietta, 1995. ORNL/TM-12706.

Rousseau, Ronald. Handbook of Separation Process Technology. New York, NY: John Wiley & Sons, 1987.

Rydberg, Jan, Musikas, Claude, Choppin, Gregory. Principles and Practices of Solvent Extraction. New York, NY: Marcel Dekker, Inc, 1992.

Schwarzenbach, G., Gut, R., Anderegg, G. “Komplexone XXV. Die polarographische Untersuchung von Austauschgleichgewichten. Neue Daten der Bildungskonstanten von Metallkomplexen der Äthylendiamin-tetraessigsäure und der 1,2-Diaminocyclohexan-tetraessigsäure”. Helvetica Chimica Acta, 1954. Vol. 37, pp. 937.

Seaborg, G. T. and Street, K. Jr. “The Separation of Americium and Curium from the Rare Earth Elements.” 6, Berkeley, CA : Journal of American Chemical Society, 1950, Vol. 72. 10.1021/ja01162a530.

Shanbhag, S. M., Choppin, G. R. “Determination of the Stability Constant for MHL Formation by a Tracer Method.” Inorganic Chemistry, 19823. Vol. 21, pp. 1696-1697.

Thakur, P., Mathur, J. N., Choppin, G. R. “Complexation Thermodynamics and the Structure of the Binary and the Ternary Complexes of Am^{3+}, Cm^{3+}, and Eu^{3+} with CDTA and CDTA + IDA.” Inorganica Chimica Acta, 2007. Col. 360, pp. 3688-3698.

Tsoulfanidis, Nicholas. The Nuclear Fuel Cycle. Bellingham, WA : Quantum Publishing Services, 2013.

Zakrzewski, A. Geisler, J. Chemia Anaitychna, 1987, Vol. 32, pp. 151.

Zhang, Sarah. “The US Is Playing a Dangerous Game of Musical Chairs With Nuclear Waste.” [Electronic News Article] s.l. : Conde Nast, 2016.

Zhengshui, H., Ying, P., Wanwu, M., Xun, F. “Purification of Organophosphorus Acid Extractants.” Solvent Extraction and Ion Exchange, 1995, Vol. 13, Number 5, pp. 965-976.

APPENDIX A

INDIVIDUAL VAN'T HOFF PLOTS OF EXTRACTIONS

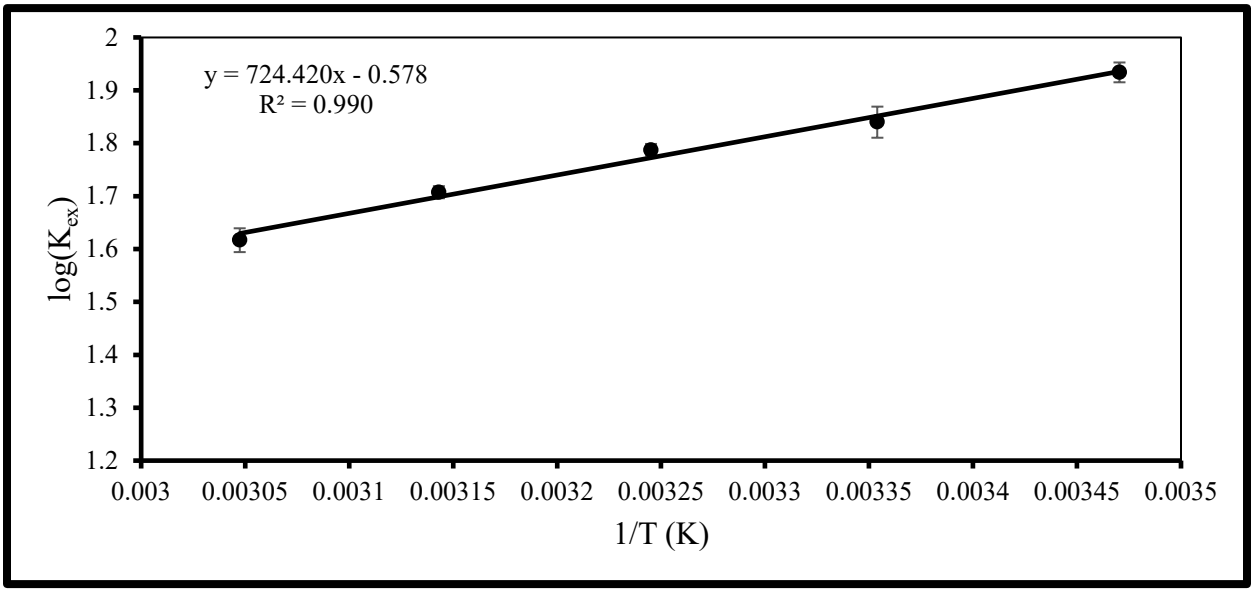

Figure A.1: Americium extraction Van't Hoff plot

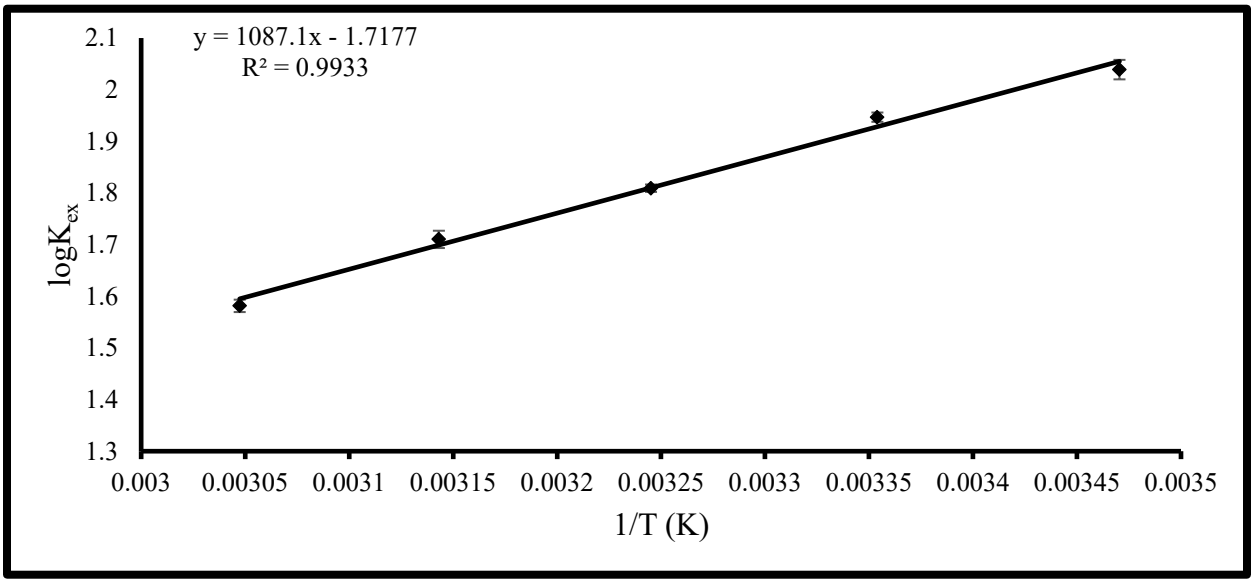

Figure A.2: Berkelium extraction Van't Hoff plot

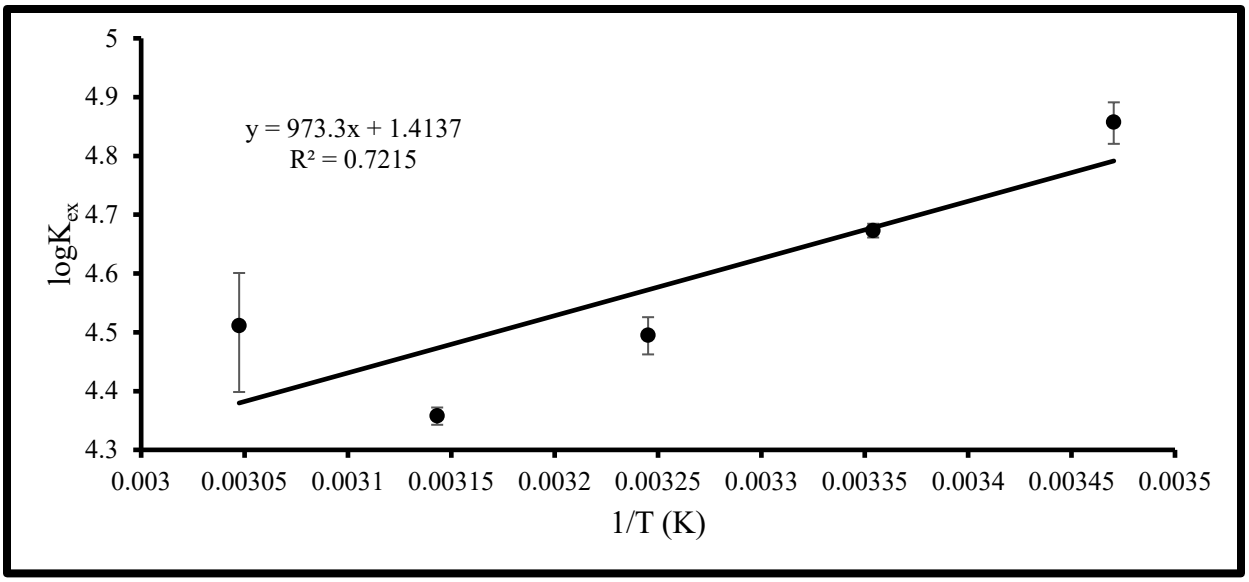

Figure A.3: Californium extraction Van't Hoff plot

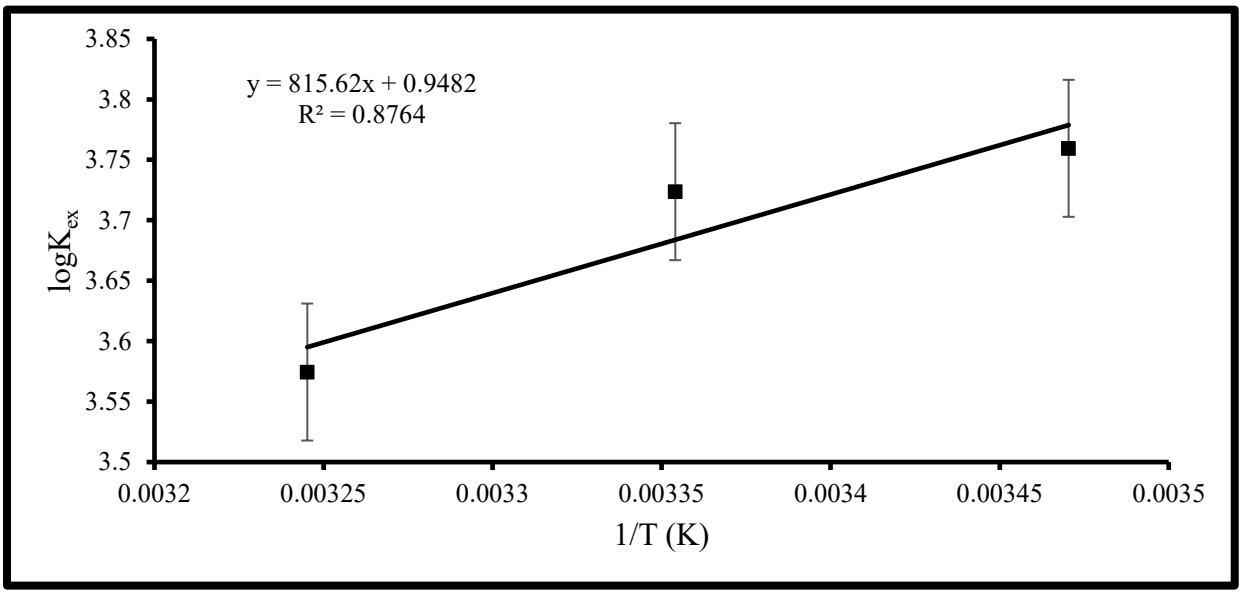

Figure A.4: Einsteinium extraction Van't Hoff plot

APPENDIX B

ACID DISSOCIATION CONSTANTS AND STABILITY CONSTANTS

Table B.1: NTA protonation constants used in calculations (Choppin, 1977)

NTA	pKa1	pKa2	pKa3	pKa4
15°C	9.730	2.580	1.514	0
25°C	9.570	2.641	1.569	0
35°C	9.420	2.698	1.621	0
45°C	9.280	2.751	1.669	0
55°C	9.148	2.801	1.715	1.000

Table B.2: NTA protonation thermodynamic constants (Choppin, 1977)

NTA	ΔH°	ΔS°
pKa1	-24.2	102
pKa2	0	44.7
pKa3	2	41

Table B.3: HEDTA protonation constants used in calculations (Choppin, 1977)

HEDTA	pKa1	pKa2	pKa3	pKa4
15°C	9.96	5.47	2.68	1.028
25°C	9.79	5.40	2.71	1.028
35°C	9.63	5.33	2.73	1.028
45°C	9.48	5.26	2.76	1.028
55°C	9.34	5.20	2.78	1.028

Table B.4: HEDTA protonation thermodynamic constants (Choppin, 1977)

HEDTA	ΔH°	ΔS°
pKa1	-28	93.3
pKa2	-12	59.4
pKa3	4.6	65.6
pKa4	0	0

Table B.5: CDTA protonation constants used in calculations (Choppin, 1977)

CDTA	pKa1	pKa2	pKa3	pKa4	pKa5
15°C	11.54	6.58	3.02	2.39	1.65
25°C	11.30	6.51	3.01	2.38	1.65
35°C	11.08	6.45	3.00	2.37	1.65
45°C	10.88	6.40	3.00	2.36	1.65
55°C	10.68	6.34	2.99	2.35	1.65

Table B.6: CDTA protonation thermodynamic parameters (Choppin, 1977)

CDTA	ΔH°	ΔS°
pKa1	-28	143
pKa2	-9	87.4
pKa3	-1	55
pKa4	-1	40
pKa5	0	0

Table B.7: DTPA protonation constants (Choppin, 1977)

DTPA	pKa1	pKa2	pKa3	pKa4	pKa5	pKa6
25°C	9.90	8.32	4.10	2.70	2.10	1.60
35°C	9.71	8.22	4.07	2.69	2.11	1.60
45°C	9.53	8.13	4.03	2.69	2.12	1.60
55°C	9.37	8.04	4.00	2.68	2.13	1.60

Table B.8: DTPA protonation thermodynamic constants (Choppin, 1977)

DTPA	ΔH°	ΔS°
pKa1	-28	89
pKa2	-18	104
pKa3	-6	25
pKa4	-1	25
pKa5	2	45
pKa6	0	0

Table B.9: Lanthanide stability constants, I = 0.5 M (Choppin, 1977)

	NTA	HEDTA	CDTA	DTPA
Nd	10.71	14.47		
Sm	11.21	14.85	17.91	20.72
Eu	11.15	14.9	18.1	20.87
Gd	11.11	14.8	18.12	21.02

Table B.10: Thermodynamic parameters for various NTA complexes, all gathered at I = 0.5 M.

Complex	ΔH	ΔS	ΔG	Source
Am-NTA	-12.6(0.6)	172(2)	-63.9(0.3)	Choppin, 2006
Cf-NTA	0.8(2)	229(2)	-67.5(0.3)	Choppin, 2006
Es-NTA	-7.5(1.7)	188(6)	-66.0(0.3)	Choppin, 2006
Am-NTA	15.6(0.9)	267(1)	-63.9(0.3)	Shah, 1980
Bk-NTA	-	-	-64.9(0.4)	Shah, 1980
Cf-NTA	25(2)	309(2)	-67.5(0.3)	Shah, 1980
Es-NTA	26(2)	308(2)	-66.0(0.3)	Shah, 1980

APPENDIX C

EXAMPLE STABILITY CONSTANT DETERMINATIONS

Determination of stability constants for NTA, HEDTA, and CDTA followed the same general pattern. Once distribution values were determined through gamma or liquid scintillation counting, the molal concentration of the aqueous phase and the pcH were determined and used along with the pKa values of the ligands calculate the amount of free ligand available to complex with the metal ion. For HEDTA, this is calculated using equation 20.

$$[L^{3-}]_{free} = \frac{[L^{3-}]_{total}}{1 + Ka_1 * [H^+] + Ka_2 * [H^+]^2 + Ka_3 * [H^+]^3} \quad (20)$$

To find the free ligand concentration, the equilibria equations are combined and rearranged. The free ligand concentration may now be used to solve for the extraction constants using equations 15 or 16, depending on whether or not multiple ligands are expected to complex with the metal ion. A table of inputs to the non-linear least squares analysis is provided.

Table C.1: Einsteinium-HEDTA inputs, T = 25°C

Free ligand Concentration (m)	(Do/D)-1	Distribution Error
6.47e-15	116.2	1.086
1.28e-14	237.1	3.824
3.78e-14	605.4	6.321
6.42e-14	985.5	0.813
1.01e-13	1415.9	1.755

These inputs are fitted to either equation 15 or 16. QTIplot plots a best non-linear fit to the data, seen in Figure C.1. QTIplot also calculates the slope and error of the fit line, pictured in Figure C.2.

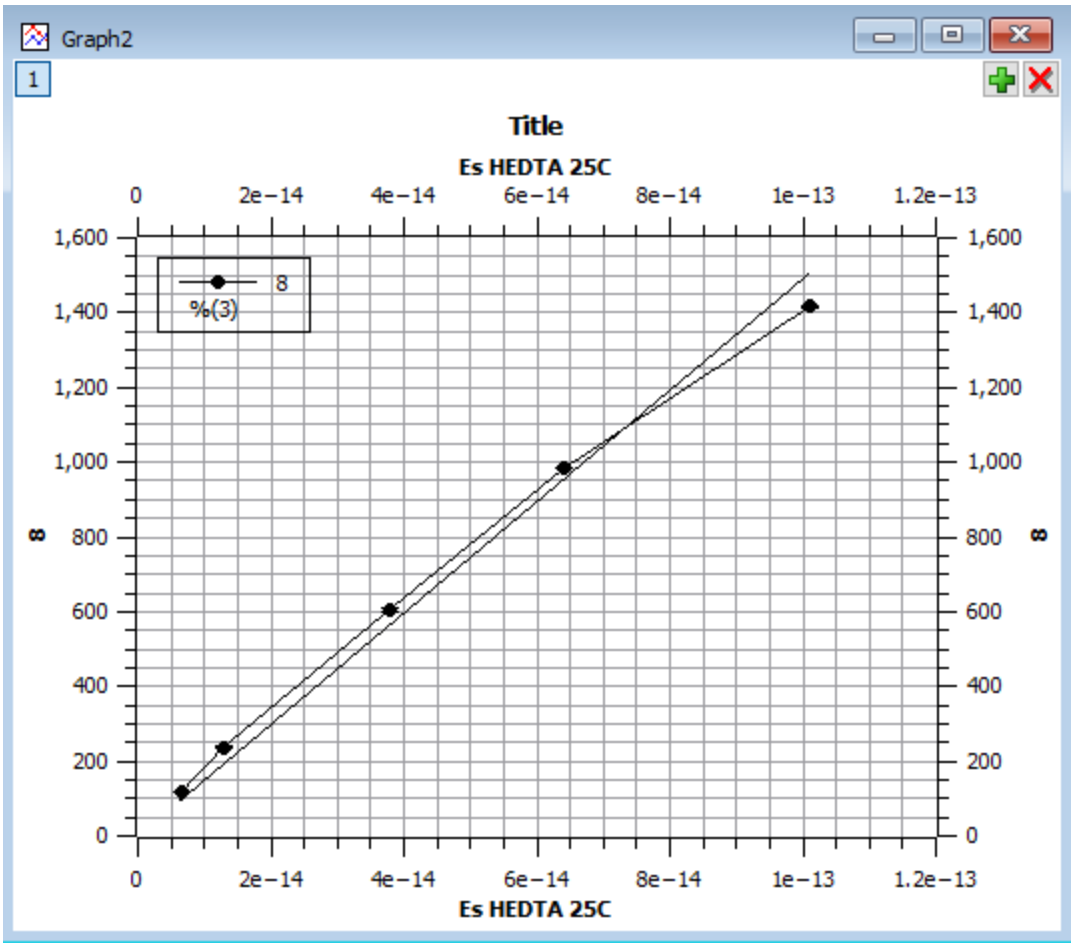

Figure C.1: Einsteinium-HEDTA best fit

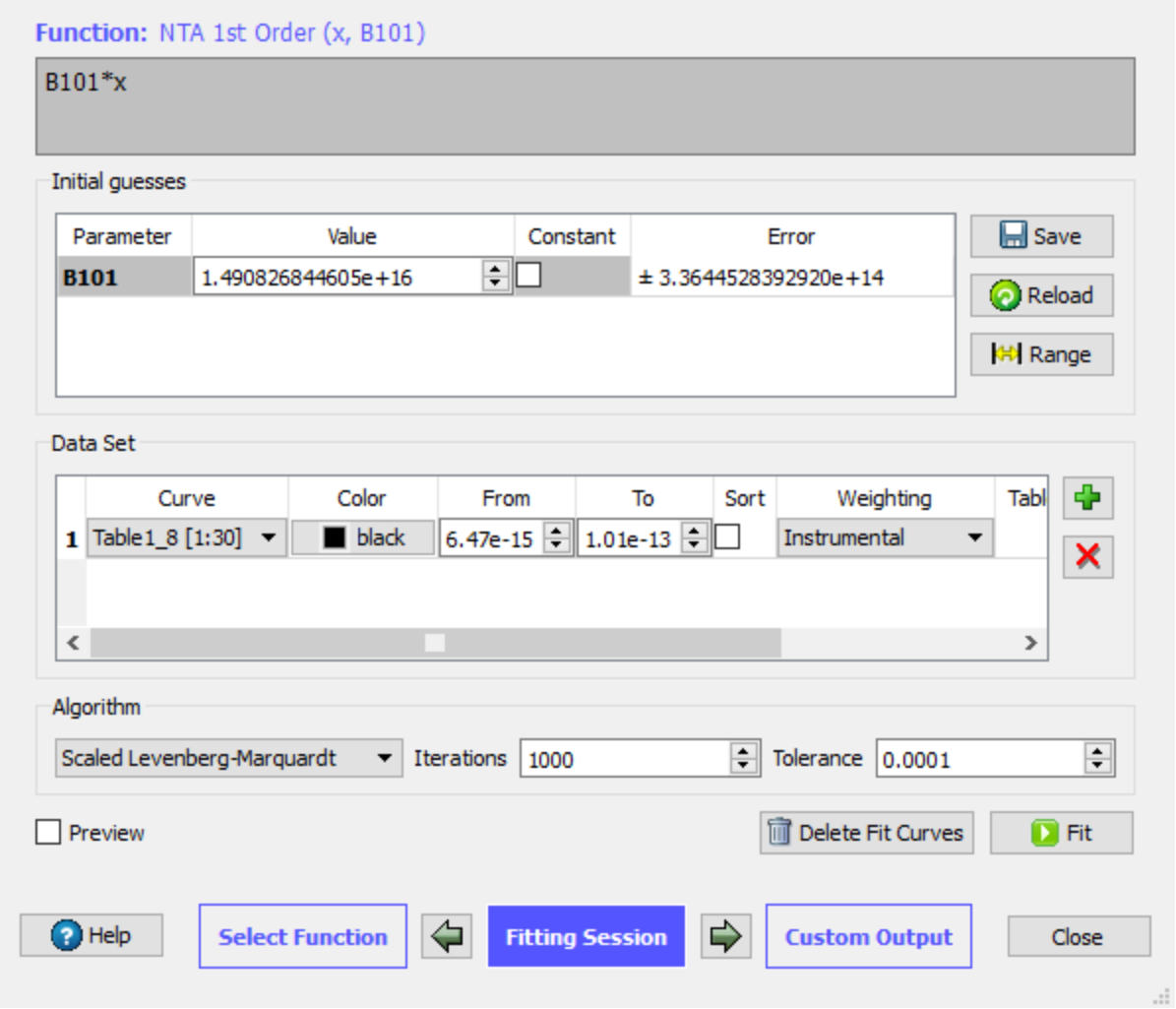

Figure C.2: QTIplot output

DTPA fits are calculated in the same manner, only the QTIplot fits an apparent or conditional stability constant. The constants must be fit to hydrogen ion concentration, creating a line. The slope of this line is the protonated stability constant, while the intercept is the deprotonated stability constant.

APPENDIX D

RAW DATA

D. 1 Americium-NTA

Table D.1: Am-NTA T = 15°C Raw Data

pcH	D	D error	[NTA] (m)	$[NTA]_{free}$	Do	Do/D-1	Do/D error
2.05	1.87	0.05	4.93E-05	2.03E-13	1.90	1.6E-04	9.28E-06
2.06	1.86	0.06	7.43E-05	3.20E-13	2.03	9.5E-02	9.47E-05
2.05	1.58	0.05	9.75E-05	3.93E-13	1.83	0.1580	1.77E-04
2.04	1.33	0.08	2.00E-04	7.89E-13	1.77	0.336	1.19E-03
2.05	1.13	0.08	3.13E-04	1.29E-12	1.90	0.679	3.41E-03
2.02	0.90	0.05	3.93E-04	1.41E-12	1.54	0.719	1.83E-03
2.04	0.87	0.03	4.96E-04	1.95E-12	1.77	1.036	1.59E-03
2.00	0.48	0.03	9.96E-04	3.26E-12	1.34	1.813	9.08E-03

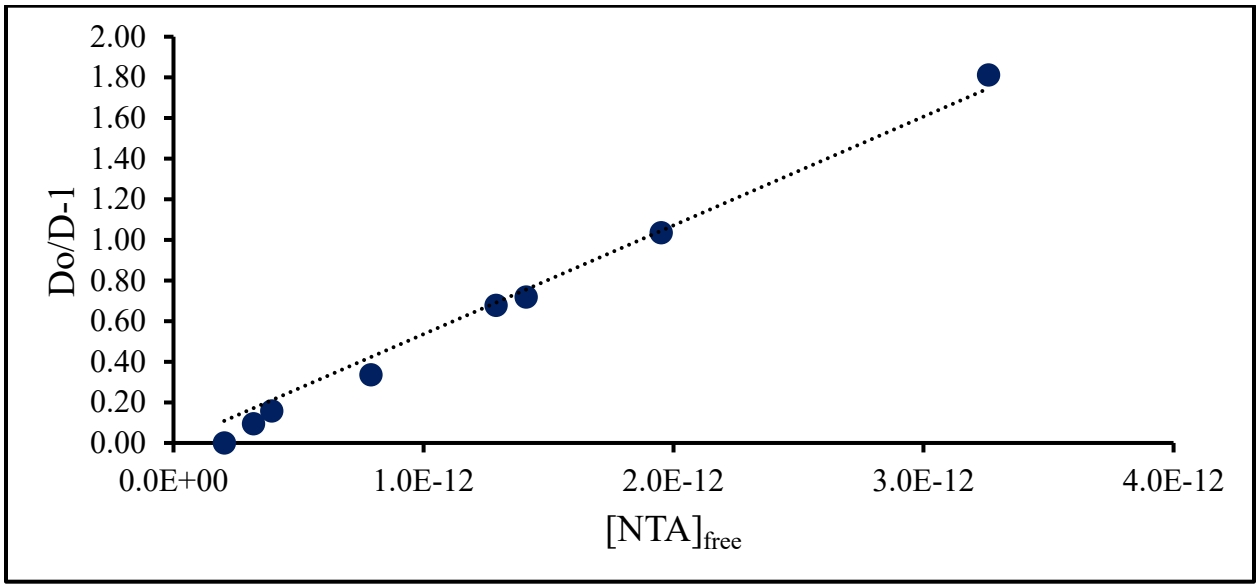

Figure D.1: Fit of Am-NTA T = 15°C data

Table D.2: Am-NTA T = 25°C Raw Data

pcH	D	D error	[NTA] (m)	$[NTA]_{free}$	Do	Do/D-1	Do/D error
2.60	43.23	0.06	4.93E-05	2.51E-12	74.41	0.722000	1.23E-06
2.60	35.88	0.03	7.43E-05	3.79E-12	74.41	1.074000	6.09E-07
2.60	29.615	0.008	9.75E-05	4.97E-12	74.41	1.513000	1.04E-07
2.60	23.2	0.3	2.00E-04	1.02E-11	74.41	2.2110	2.70E-04
2.60	9.24	0.03	3.13E-04	1.60E-11	74.41	7.04700	7.07E-05
2.60	7.76	0.09	3.93E-04	2.01E-11	74.41	8.592	1.20E-03
2.60	5.12	0.02	4.96E-04	2.53E-11	74.41	13.5430	2.96E-04
2.60	3.40	0.01	9.96E-04	5.08E-11	74.41	20.9010	3.41E-04

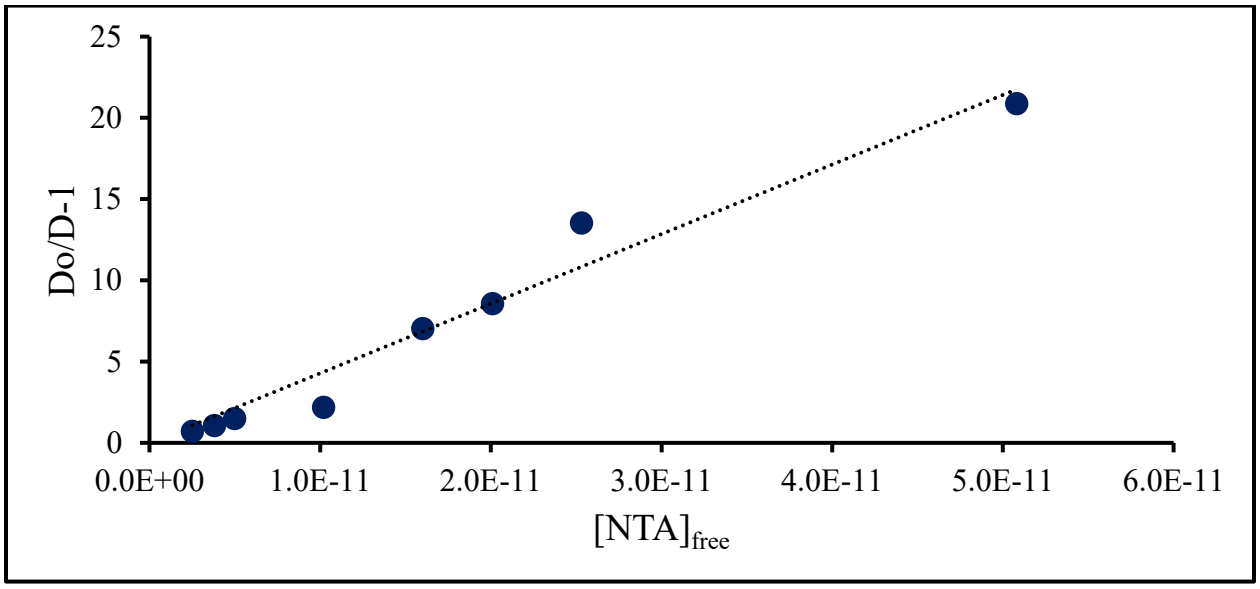

Figure D.2: Fit of Am-NTA T = 25°C data

Table D.3: Am-NTA T = 35°C Raw Data

pcH	D	D error	[NTA] (m)	$[NTA]_{free}$	Do	Do/D-1	Do/D error
2.33	6.18	0.04	4.93E-05	1.26E-12	10.20	0.65200	2.57E-05
2.33	5.90	0.06	7.43E-05	1.89E-12	10.20	0.72900	6.68E-05
2.33	5.366	0.008	9.75E-05	2.49E-12	10.20	0.901000	2.05E-06
2.36	4.089	0.03	2.00E-04	5.75E-12	12.55	2.06900	8.93E-05
2.44	3.78	0.03	3.13E-04	1.22E-11	21.81	4.7720	2.22E-04
2.41	2.71	0.04	3.93E-04	1.37E-11	17.73	5.532	1.48E-03
2.45	2.709	0.002	4.96E-04	2.00E-11	23.37	7.627000	3.91E-06
2.42	1.153	0.009	9.96E-04	3.59E-11	18.99	15.4690	9.78E-04

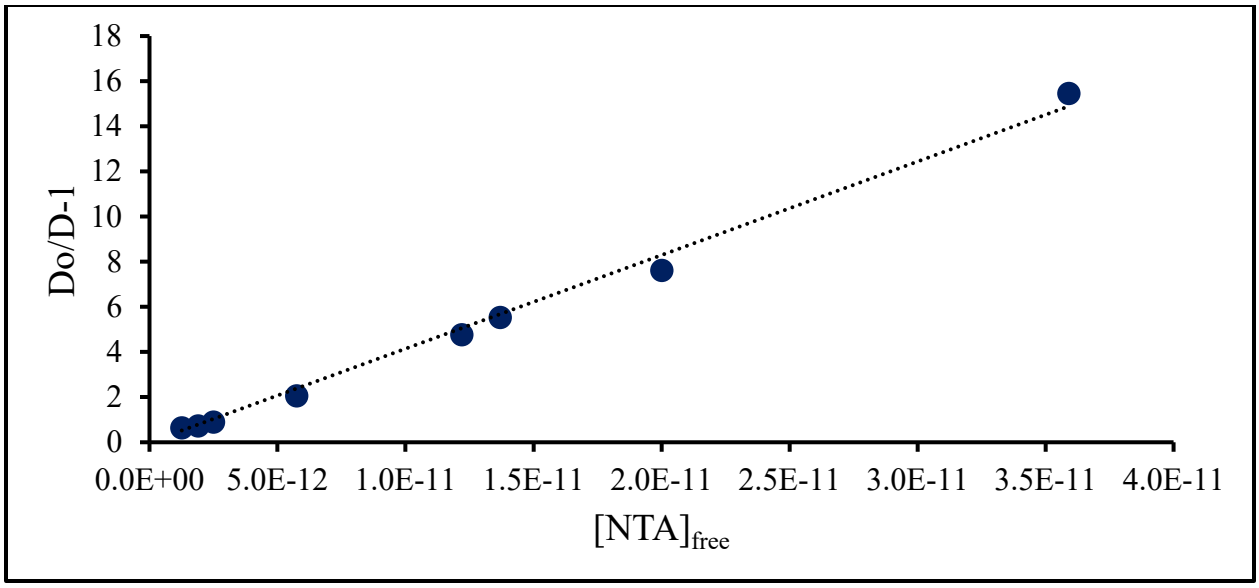

Figure D.3: Fit of Am-NTA T = 35°C data

Table D.4: Am-NTA T = 45°C Raw Data

pcH	D	D error	[NTA] (m)	$[NTA]_{free}$	Do	Do/D-1	Do/D error
2.35	5.14	0.05	4.93E-05	1.51E-12	55.54	9.811	1.00E-03
2.35	5.15	0.06	7.43E-05	2.28E-12	55.54	9.783	1.11E-03
2.35	5.17	0.01	9.75E-05	2.99E-12	55.54	9.75300	7.02E-05
2.35	3.61	0.03	2.00E-04	6.16E-12	55.54	14.389	1.27E-03
2.35	3.39	0.04	3.13E-04	9.62E-12	55.54	15.383	1.86E-03
2.35	2.12	0.03	3.93E-04	1.21E-11	55.54	25.156	4.78E-03
2.35	2.053	0.005	4.96E-04	1.52E-11	55.54	26.0590	1.28E-04
2.35	0.780	0.004	9.96E-04	3.06E-11	55.54	70.223	1.69E-03

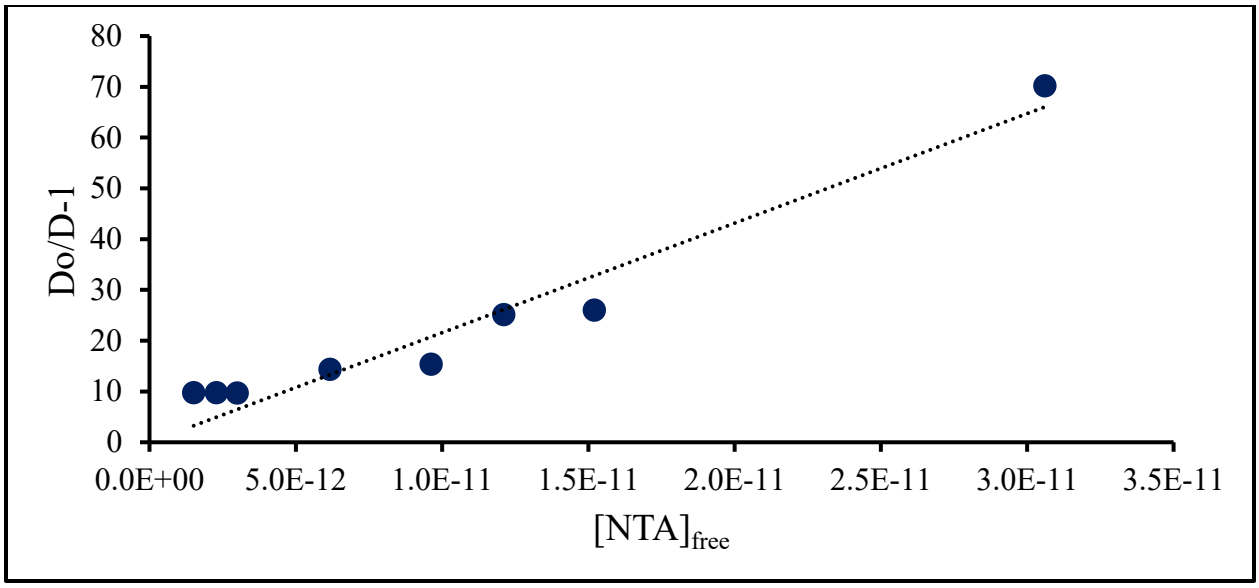

Figure D.4: Fit of Am-NTA T = 45°C data

Table D.5: Am-NTA T = 55°C Raw Data

pcH	D	D error	[NTA] (m)	$[NTA]_{free}$	Do	Do/D-1	Do/D error
2.00	0.79	0.01	4.93E-05	1.25E-12	4.02	4.0890	9.26E-04
2.00	0.83	0.02	7.43E-05	1.88E-12	4.02	3.854	3.13E-03
2.00	0.85	0.09	9.75E-05	2.47E-12	4.02	3.74	4.14E-02
2.00	0.58	0.02	2.00E-04	5.07E-12	4.02	5.965	5.77E-03
2.00	0.28	0.02	3.13E-04	7.93E-12	4.02	13.57	9.78E-02
2.00	0.31	0.03	3.93E-04	9.95E-12	4.02	12.1	1.29E-01
2.00	0.32	0.02	4.96E-04	1.25E-11	4.02	11.85	2.55E-02
2.00	0.111	0.002	9.96E-04	2.52E-11	4.02	35.25	1.38E-02

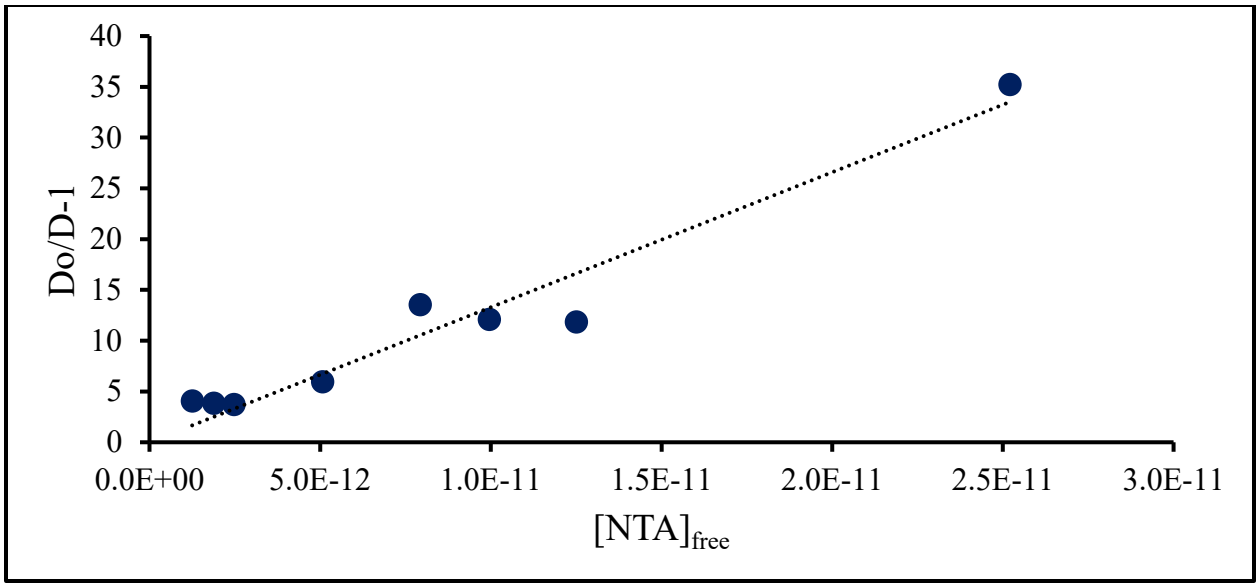

Figure D.5: Fit of Am-NTA T = 55°C data

D.2 Americium-HEDTA

Table D.6: Am-HEDTA T = 15°C Raw Data

pcH	D	D error	[HEDTA] (m)	$[HEDTA]_{free}$	Do	Do/D-1	Do/D error
1.85	1.44	0.04	1.01E-05	1.44E-17	1.56	0.08200	6.80E-05
1.85	1.08	0.03	2.51E-05	3.61E-17	1.58	0.4580	3.24E-04
1.85	0.71	0.02	4.92E-05	7.09E-17	1.58	1.231	1.15E-03
1.84	0.60	0.03	7.47E-05	1.03E-16	1.50	1.520	4.12E-03
1.85	0.44	0.04	9.99E-05	1.48E-16	1.63	2.70	1.70E-02
1.85	0.209	0.004	2.48E-04	3.53E-16	1.56	6.493	2.51E-03
1.84	0.162	0.009	3.46E-04	4.80E-16	1.52	8.38	2.80E-02
1.84	0.1234	0.0004	4.96E-04	6.85E-16	1.51	11.2760	1.13E-04

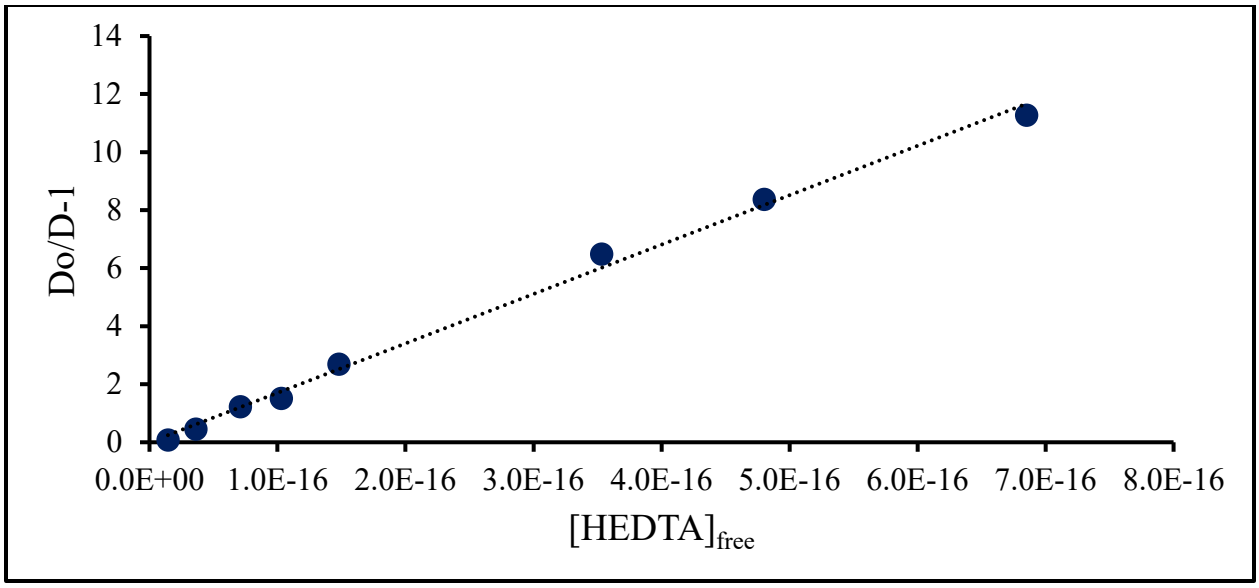

Figure D.6: Fit of Am-HEDTA T = 15°C data

Table D.7: Am-HEDTA T = 25°C Raw Data

pcH	D	D error	[HEDTA] (m)	$[HEDTA]_{free}$	Do	Do/D-1	Do/D error
1.85	0.9	0.1	1.01E-05	2.01E-17	1.17	0.263	0.003
1.85	0.78	0.03	2.51E-05	5.04E-17	1.19	0.521	0.001
1.85	0.58	0.03	4.92E-05	9.89E-17	1.19	1.053	0.002
1.84	0.42	0.05	7.47E-05	1.43E-16	1.13	1.71	0.02
1.85	0.33	0.02	9.99E-05	2.06E-16	1.22	2.75	0.01
1.85	0.146	0.001	2.48E-04	4.92E-16	1.17	7.042	0.001
1.84	0.097	0.001	3.46E-04	6.70E-16	1.14	10.741	0.002
1.84	0.076	0.001	4.96E-04	9.56E-16	1.14	14.042	0.003

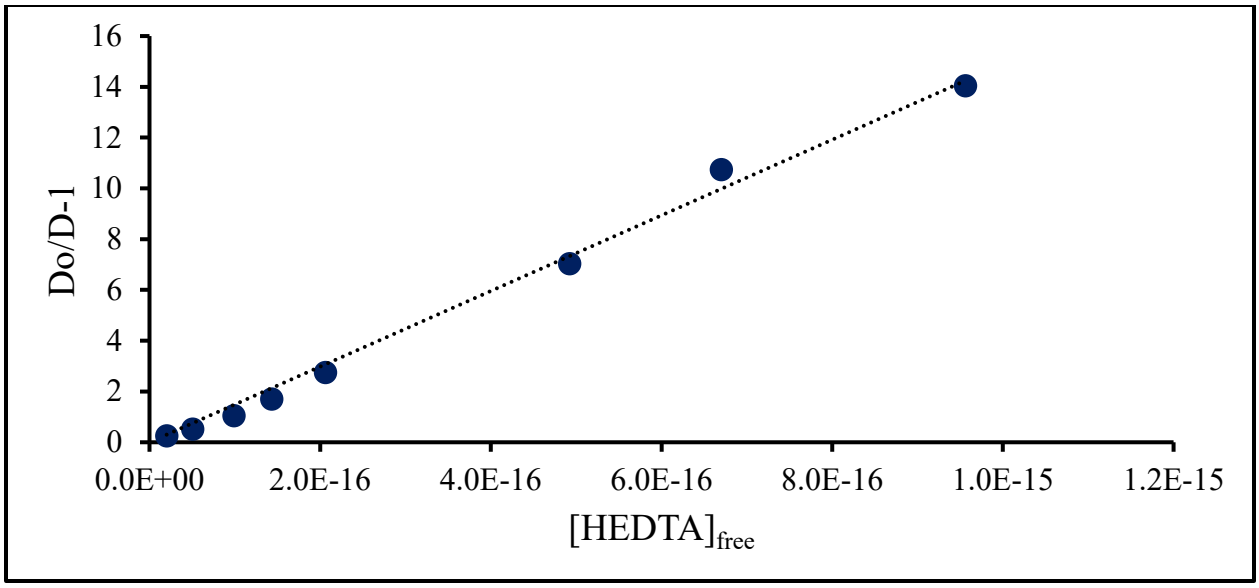

Figure D.7: Fit of Am-HEDTA T = 25°C data

Table D.8: Am-HEDTA T = 35°C Raw Data

pcH	D	D error	[HEDTA] (m)	$[HEDTA]_{free}$	Do	Do/D-1	Do/D error
1.85	0.51	0.03	1.01E-05	3.14E-17	0.72	0.413	1.29E-03
1.85	0.38	0.03	2.51E-05	7.89E-17	0.73	0.887	5.35E-03
1.85	0.25	0.02	4.92E-05	1.55E-16	0.73	1.902	6.70E-03
1.84	0.198	0.002	7.47E-05	2.24E-16	0.69	2.4920	3.46E-04
1.85	0.17	0.02	9.99E-05	3.23E-16	0.75	3.48	6.81E-02
1.85	0.077	0.002	2.48E-04	7.71E-16	0.72	8.343	4.34E-03
1.84	0.062	0.001	3.46E-04	1.05E-15	0.70	10.182	4.21E-03
1.84	0.045	0.002	4.96E-04	1.50E-15	0.69	14.52	3.11E-02

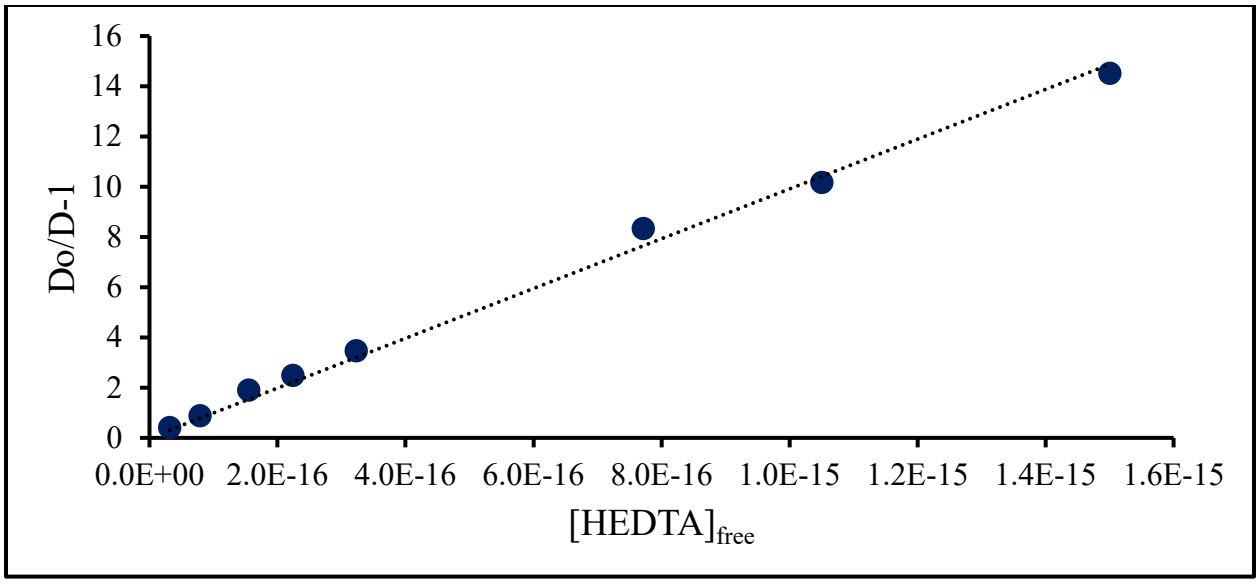

Figure D.8: Fit of T = 35°C data

Table D.9: Am-HEDTA T = 45°C Raw Data

pcH	D	D error	[HEDTA] (m)	$[HEDTA]_{free}$	Do	Do/D-1	Do/D error
1.85	0.73	0.06	1.01E-05	4.47E-17	0.91	0.243	0.001
1.85	0.6	0.1	2.51E-05	1.12E-16	0.92	0.46	0.01
1.85	0.43	0.02	4.92E-05	2.20E-16	0.92	1.163	0.003
1.84	0.32	0.02	7.47E-05	3.19E-16	0.88	1.712	0.008
1.85	0.233	0.006	9.99E-05	4.60E-16	0.95	3.076	0.002
1.85	0.093	0.005	2.48E-04	1.10E-15	0.91	8.79	0.02
1.84	0.063	0.001	3.46E-04	1.49E-15	0.89	13.212	0.007
1.84	0.041	0.002	4.96E-04	2.13E-15	0.88	20.37	0.04

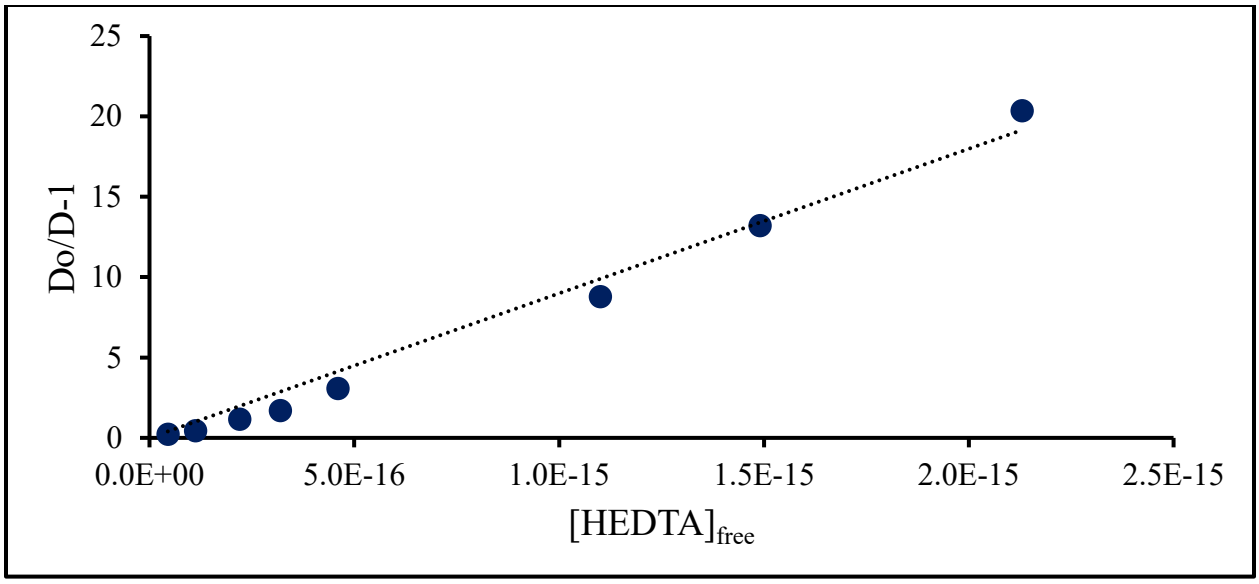

Figure D.9: Fit of Am-HEDTA T = 45°C data

Table D.10: Am-HEDTA T = 55°C Raw Data

pcH	D	D error	[HEDTA] (m)	$[HEDTA]_{free}$	Do	Do/D-1	Do/D error
1.85	0.68	0.06	1.01E-05	7.94E-17	0.74	0.0900	0.0006
1.85	0.57	0.02	2.51E-05	1.99E-16	0.75	0.3080	0.0003
1.85	0.39	0.02	4.92E-05	3.91E-16	0.75	0.906	0.002
1.84	0.289	0.009	7.47E-05	5.67E-16	0.72	1.478	0.001
1.85	0.199	0.009	9.99E-05	8.17E-16	0.77	2.892	0.006
1.85	0.043	0.003	2.48E-04	1.95E-15	0.74	16.28	0.09
1.84	0.054	0.002	3.46E-04	2.65E-15	0.72	12.34	0.02
1.84	0.035	0.001	4.96E-04	3.78E-15	0.72	19.620	0.009

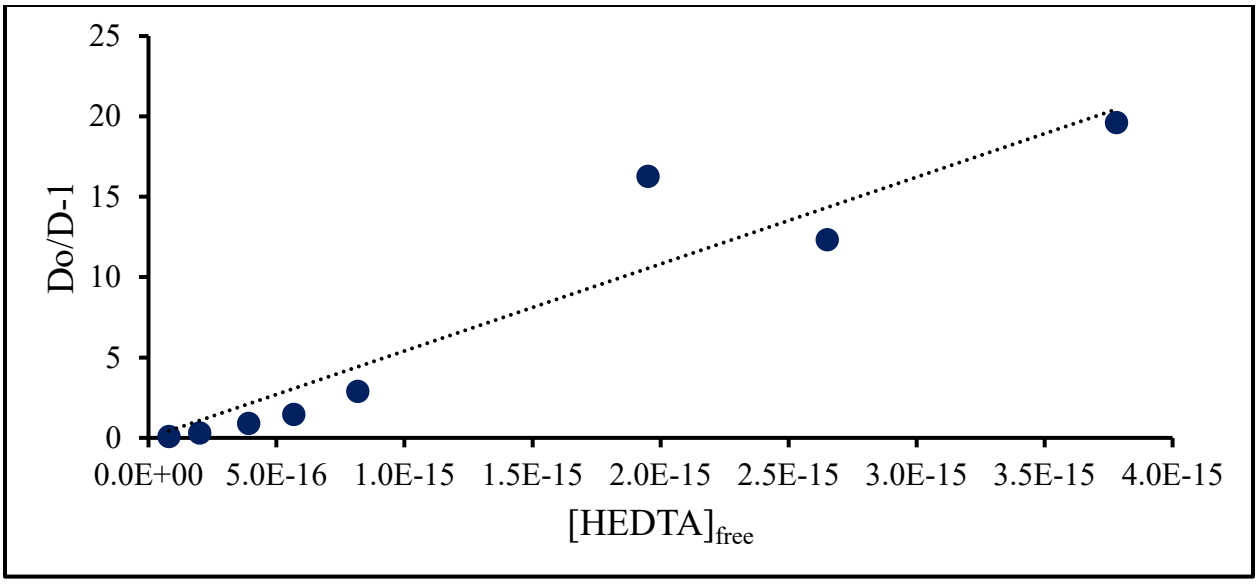

Figure D.10: Fit of Am-HEDTA T = 55°C data

D.3 Berkelium-NTA

Table D.11: Bk-NTA T = 15°C Raw Data

pcH	D	D error	[NTA] (m)	$[NTA]_{free}$	Do	Do/D-1	Do/D error
2.53	22.5118	0.7	9.87E-05	2.91E-12	98.74	3.400	0.003
2.50	10	1	2.48E-04	6.52E-12	79.74	7.4	0.2
2.47	5.00	0.08	5.05E-04	1.20E-11	66.03	12.200	0.003
2.43	2.67	0.08	7.53E-04	1.55E-11	50.71	18.00	0.02
2.42	2.2	0.3	1.01E-03	1.94E-11	45.29	19.2	0.5
2.49	6.1	0.4	3.94E-04	9.88E-12	73.02	10.90	0.06
2.46	3.922	0.006	5.88E-04	1.32E-11	59.71	14.20000	0.00003
2.41	1.9	0.1	1.08E-03	2.00E-11	42.00	21.10	0.06
2.36	1.38	0.04	1.23E-03	1.90E-11	30.67	21.20	0.02
2.33	1.07	0.03	1.48E-03	2.06E-11	25.72	23.00	0.02

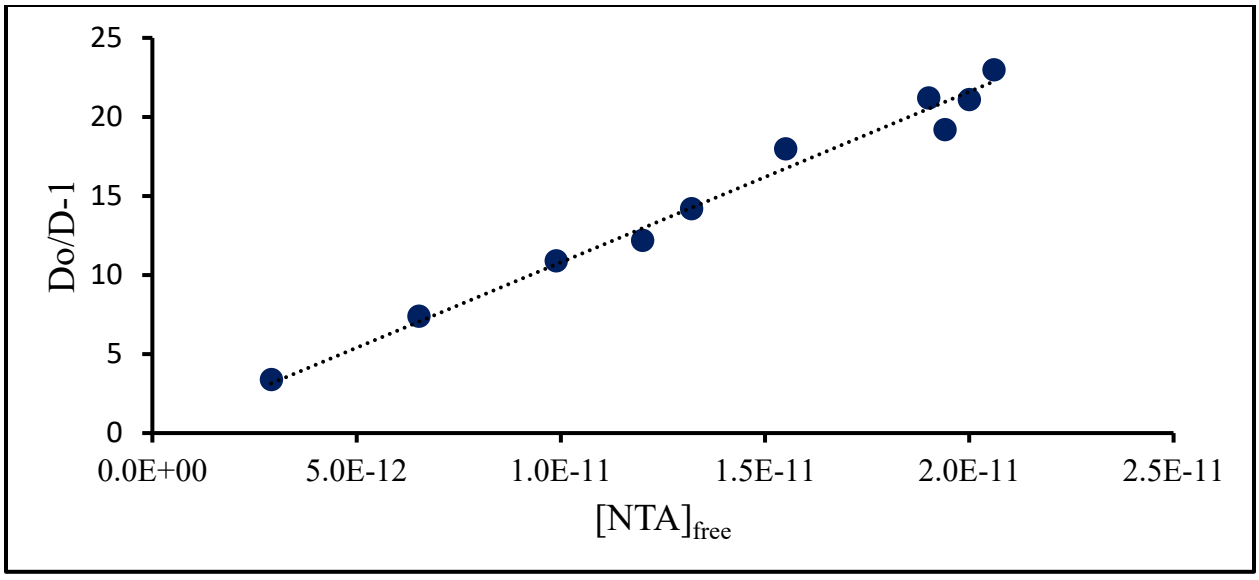

Figure D.11: Fit of Bk-NTA T = 15°C data

Table D.12: Bk-NTA T = 25°C Raw Data

pcH	D	D error	[NTA] (m)	$[NTA]_{free}$	Do	Do/D-1	Do/D error
2.53	13.0	0.2	9.87E-05	3.86E-12	73.27	4.600	0.001
2.50	7.0	0.5	2.48E-04	8.62E-12	59.17	7.50	0.04
2.47	3.50	0.06	5.05E-04	1.58E-11	49.00	13.000	0.003
2.43	2.09	0.06	7.53E-04	2.03E-11	37.63	17.00	0.02
2.42	1.40	0.07	1.01E-03	2.54E-11	33.60	23.10	0.05
2.49	3.87	0.09	3.94E-04	1.31E-11	54.18	13.000	0.007
2.46	2.49	0.05	5.88E-04	1.74E-11	44.31	16.800	0.005
2.41	1.08	0.02	1.08E-03	2.62E-11	31.16	27.900	0.009
2.36	0.79	0.07	1.23E-03	2.48E-11	22.76	27.7	0.2
2.33	0.583	0.008	1.48E-03	2.68E-11	19.08	31.700	0.005

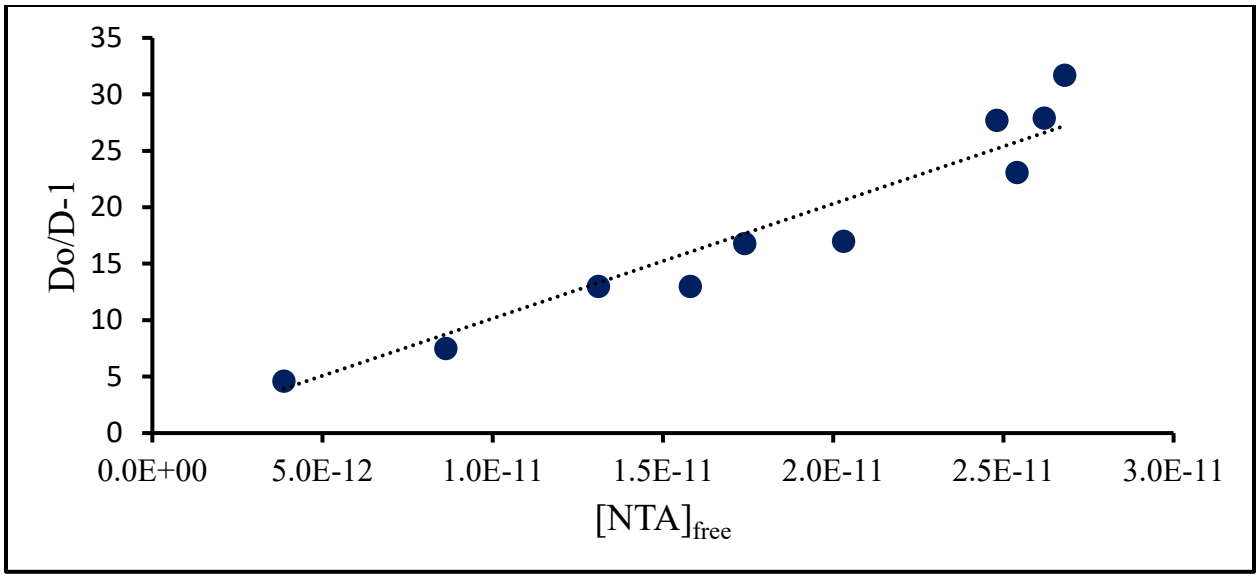

Figure D.12: Fit of Bk-NTA T = 25°C data

Table D.13: Bk-NTA T = 35°C Raw Data

pcH	D	D error	[NTA] (m)	$[NTA]_{free}$	Do	Do/D-1	Do/D error
2.53	8.8	0.9	9.87E-05	5.36E-12	57.05	5.50	0.05
2.50	4.2	0.1	2.48E-04	1.20E-11	46.07	9.90	0.01
2.47	2.29	0.07	5.05E-04	2.21E-11	38.16	15.60	0.02
2.43	1.29	0.06	7.53E-04	2.85E-11	29.30	21.70	0.05
2.42	0.86	0.05	1.01E-03	3.59E-11	26.17	29.3	0.1
2.49	2.97	0.09	3.94E-04	1.82E-11	42.19	13.20	0.01
2.46	1.88	0.09	5.88E-04	2.43E-11	34.50	17.30	0.04
2.41	0.71	0.04	1.08E-03	3.71E-11	24.27	33.1	0.1
2.36	0.533	0.004	1.23E-03	3.53E-11	17.72	32.200	0.002
2.33	0.40	0.02	1.48E-03	3.84E-11	14.86	35.70	0.05

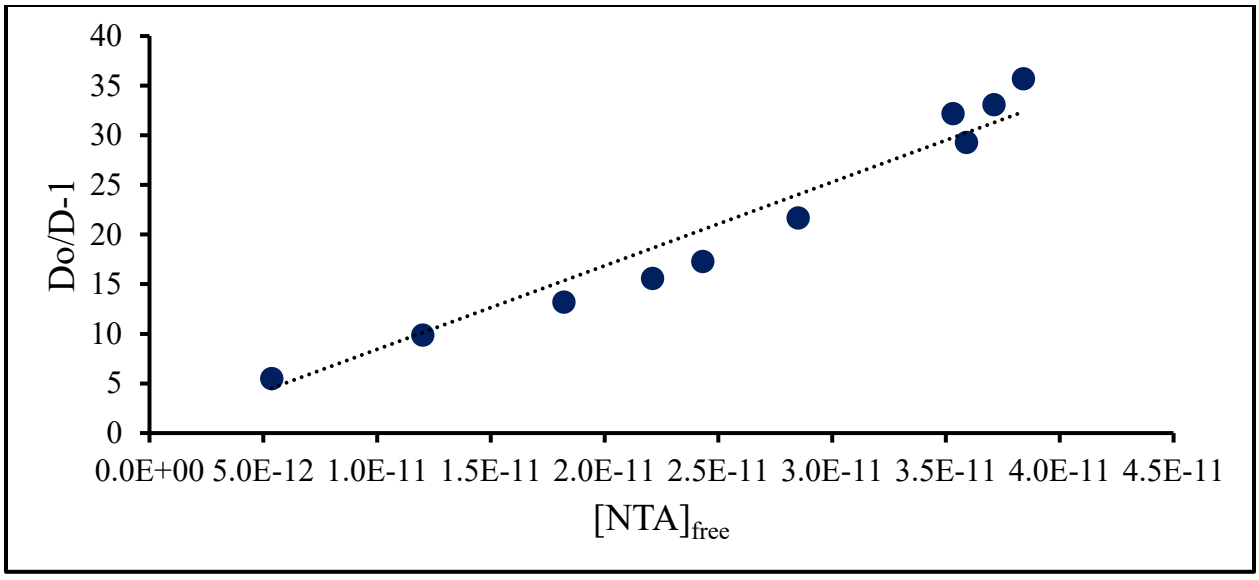

Figure D.13: Fit of Bk-NTA T = 35°C data

Table D.14: Bk-NTA T = 45°C Raw Data

pcH	D	D error	[NTA] (m)	$[NTA]_{free}$	Do	Do/D-1	Do/D error
2.53	9	2	9.87E-05	6.87E-12	42.05	3.5	0.1
2.50	3.3	0.2	2.48E-04	1.54E-11	33.96	9.30	0.04
2.47	1.83	0.03	5.05E-04	2.82E-11	28.12	14.400	0.005
2.43	0.99	0.04	7.53E-04	3.64E-11	21.60	20.90	0.04
2.42	0.71	0.03	1.01E-03	4.57E-11	19.29	26.20	0.06
2.49	1.90	0.08	3.94E-04	2.33E-11	31.10	15.40	0.03
2.46	1.17	0.05	5.88E-04	3.11E-11	25.43	20.60	0.04
2.41	0.44	0.03	1.08E-03	4.71E-11	17.88	39.4	0.2
2.36	0.34	0.03	1.23E-03	4.48E-11	13.06	37.0	0.2
2.33	0.274	0.003	1.48E-03	4.87E-11	10.95	39.000	0.006

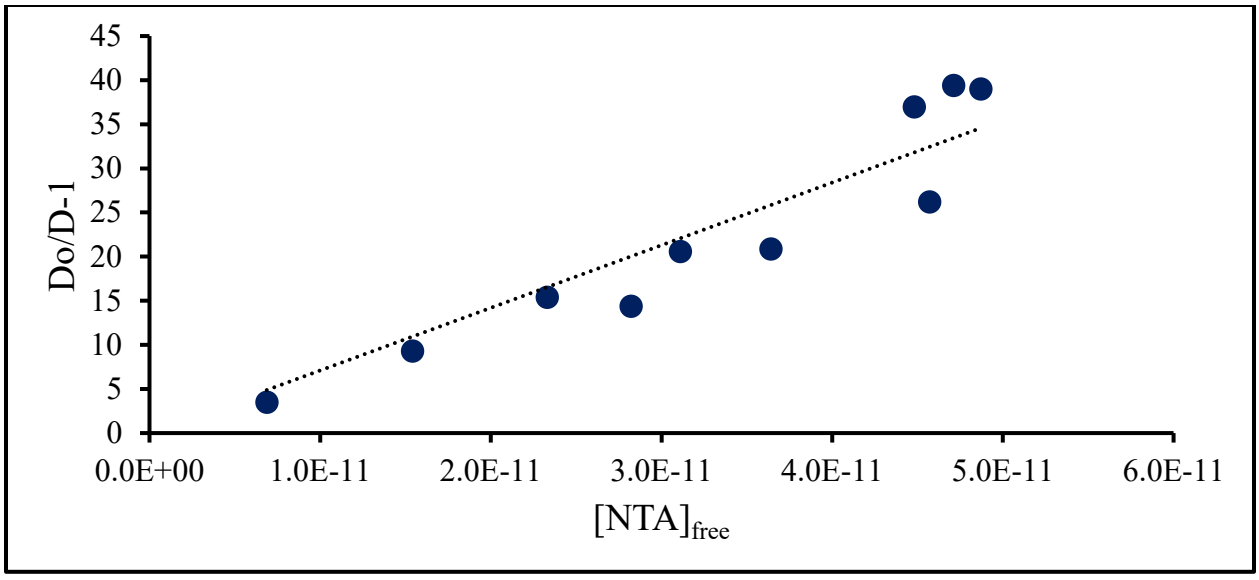

Figure D.14: Fit of Bk-NTA T = 45°C data

Table D.15: Bk-NTA T = 55°C Raw Data

pcH	D	D error	[NTA] (m)	$[NTA]_{free}$	Do	Do/D-1	Do/D error
2.53	8.1	0.4	9.87E-05	8.65E-12	32.52	3.000	0.007
2.50	2.70	0.04	2.48E-04	1.93E-11	26.26	8.700	0.002
2.47	1.15	0.02	5.05E-04	3.54E-11	21.75	17.900	0.004
2.43	0.60	0.01	7.53E-04	4.56E-11	16.70	27.100	0.009
2.42	0.402	0.004	1.01E-03	5.71E-11	14.92	36.200	0.005
2.49	1.42	0.05	3.94E-04	2.93E-11	24.05	16.00	0.02
2.46	0.81	0.03	5.88E-04	3.90E-11	19.67	23.40	0.03
2.41	0.334	0.007	1.08E-03	5.89E-11	13.83	40.50	0.02
2.36	0.215	0.001	1.23E-03	5.59E-11	10.10	46.1000	0.0003
2.33	0.170	0.006	1.48E-03	6.06E-11	8.47	48.80	0.06

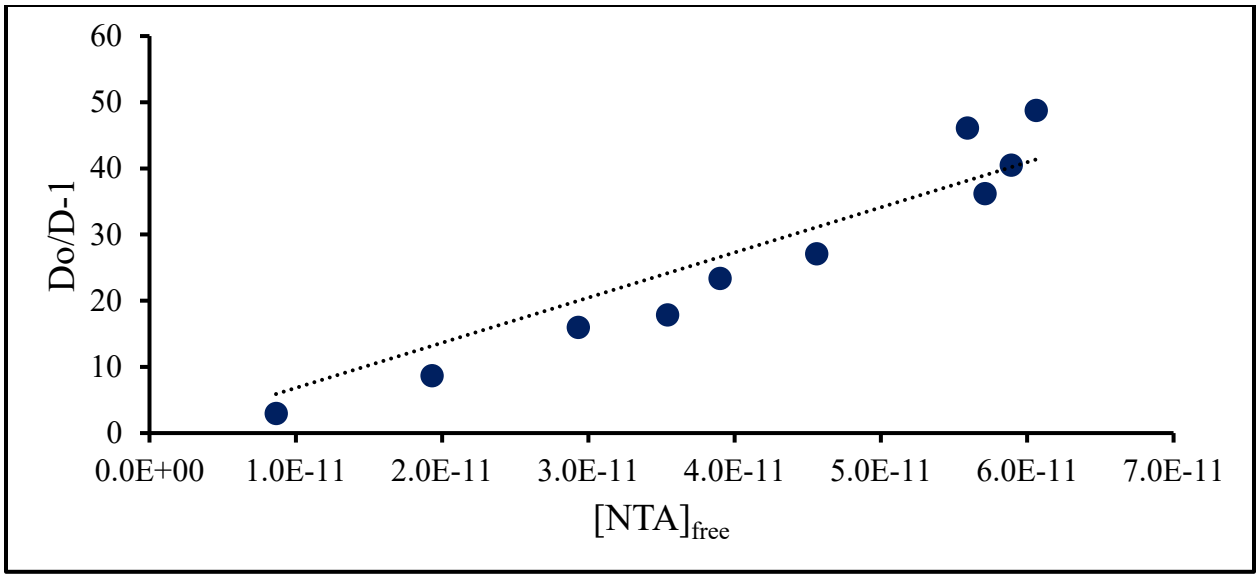

Figure D.15: Fit of Bk-NTA T = 55°C data

D.4 Berkelium-HEDTA

Table D.16: Bk-HEDTA T = 15°C Raw Data

pcH	D	D error	[HEDTA] (m)	$[HEDTA]_{free}$	Do	Do/D-1	Do/D error
2.53	33	2	4.79E-05	9.24E-16	191.97	4.8	0.02
2.54	15	2	9.68E-05	1.95E-15	201.87	12.9	0.3
2.53	5.3	0.4	2.88E-04	5.38E-15	184.86	33.9	0.2
2.52	2.98	0.04	4.85E-04	8.48E-15	171.43	56.60	0.01
2.51	2.19	0.09	6.79E-04	1.15E-14	165.08	74.5	0.1
2.49	1.6	0.1	9.67E-04	1.42E-14	140.19	88.0	0.7
2.45	0.76	0.03	1.91E-03	2.29E-14	110.40	144.1	0.2
2.41	0.477	0.002	2.91E-03	2.67E-14	81.65	170.100	0.002
2.39	0.364	0.001	3.84E-03	3.05E-14	69.34	189.600	0.001
2.37	0.284	0.005	4.81E-03	3.41E-14	61.15	214.30	0.08

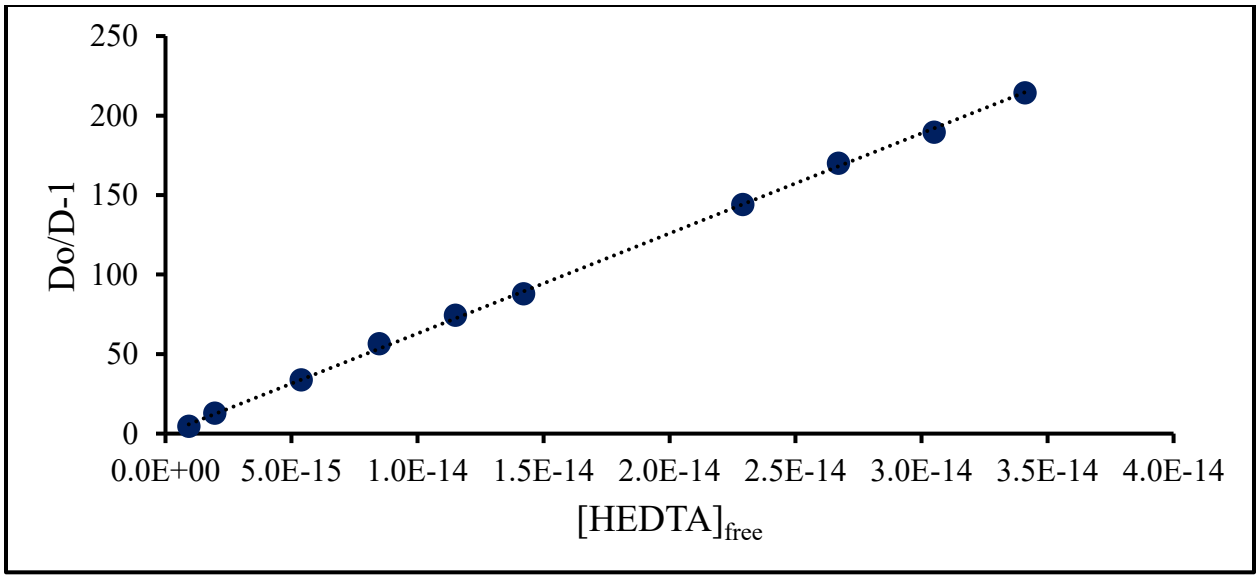

Figure D.16: Fit of Bk-HEDTA T = 15°C data

Table D.17: Bk-HEDTA T = 25°C Raw Data

pcH	D	D error	[HEDTA] (m)	$[HEDTA]_{free}$	Do	Do/D-1	Do/D error
2.53	24	1	4.79E-05	1.54E-15	155.18	5.40	0.02
2.54	12.7	0.6	9.68E-05	3.16E-15	163.18	11.80	0.03
2.53	3.9	0.1	2.88E-04	9.17E-15	149.44	37.00	0.03
2.52	2.33	0.09	4.85E-04	1.51E-14	138.58	58.50	0.08
2.51	1.61	0.05	6.79E-04	2.10E-14	133.45	82.10	0.09
2.49	1.02	0.03	9.67E-04	2.84E-14	113.33	109.9	0.1
2.45	0.516	0.002	1.91E-03	5.21E-14	89.25	172.000	0.003
2.41	0.33	0.01	2.91E-03	7.14E-14	66.00	198.8	0.3
2.39	0.240	0.004	3.84E-03	8.87E-14	56.05	233.00	0.07
2.37	0.19	0.01	4.81E-03	1.06E-13	49.43	261.4	0.8

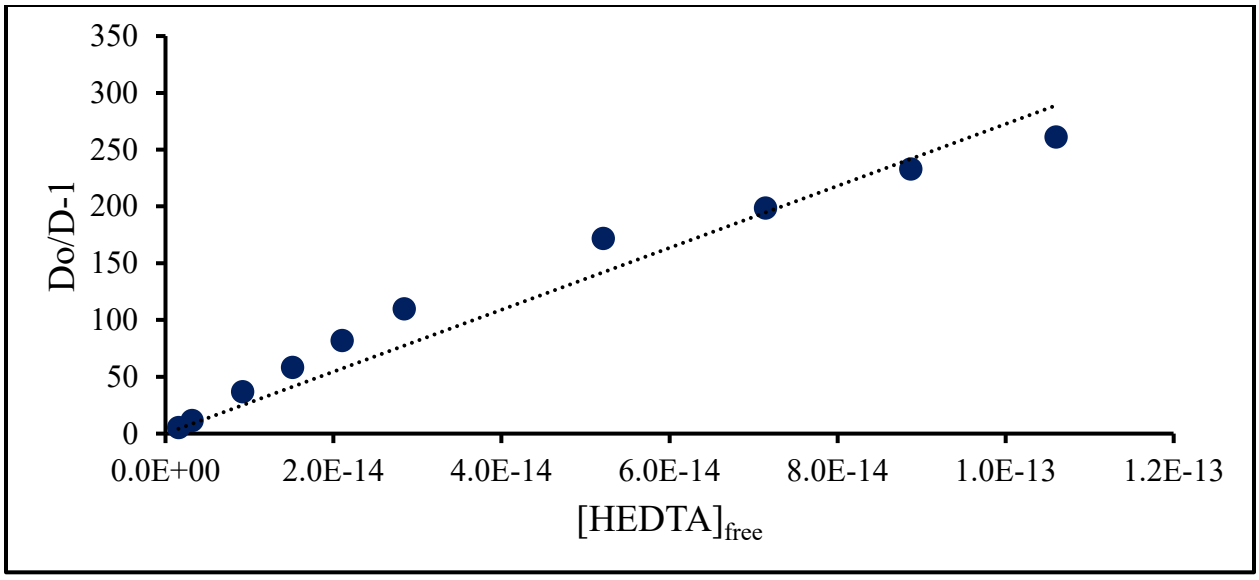

Figure D.17: Fit of Bk-HEDTA T = 25°C data

Table D.18: Bk-HEDTA T = 35°C Raw Data

pcH	D	D error	[HEDTA] (m)	$[HEDTA]_{free}$	Do	Do/D-1	Do/D error
2.53	18.6	0.9	4.79E-05	2.55E-15	113.05	5.10	0.01
2.54	9.5	0.5	9.68E-05	5.22E-15	118.88	11.50	0.03
2.53	2.79	0.08	2.88E-04	1.52E-14	108.86	38.00	0.04
2.52	1.56	0.02	4.85E-04	2.50E-14	100.95	63.700	0.006
2.51	1.084	0.006	6.79E-04	3.47E-14	97.22	88.700	0.003
2.49	0.76	0.02	9.67E-04	4.71E-14	82.56	107.30	0.06
2.45	0.36	0.02	1.91E-03	8.65E-14	65.02	180.5	0.4
2.41	0.229	0.007	2.91E-03	1.19E-13	48.08	209.3	0.2
2.39	0.162	0.002	3.84E-03	1.48E-13	40.83	251.00	0.05
2.37	0.123	0.004	4.81E-03	1.76E-13	36.01	291.5	0.3

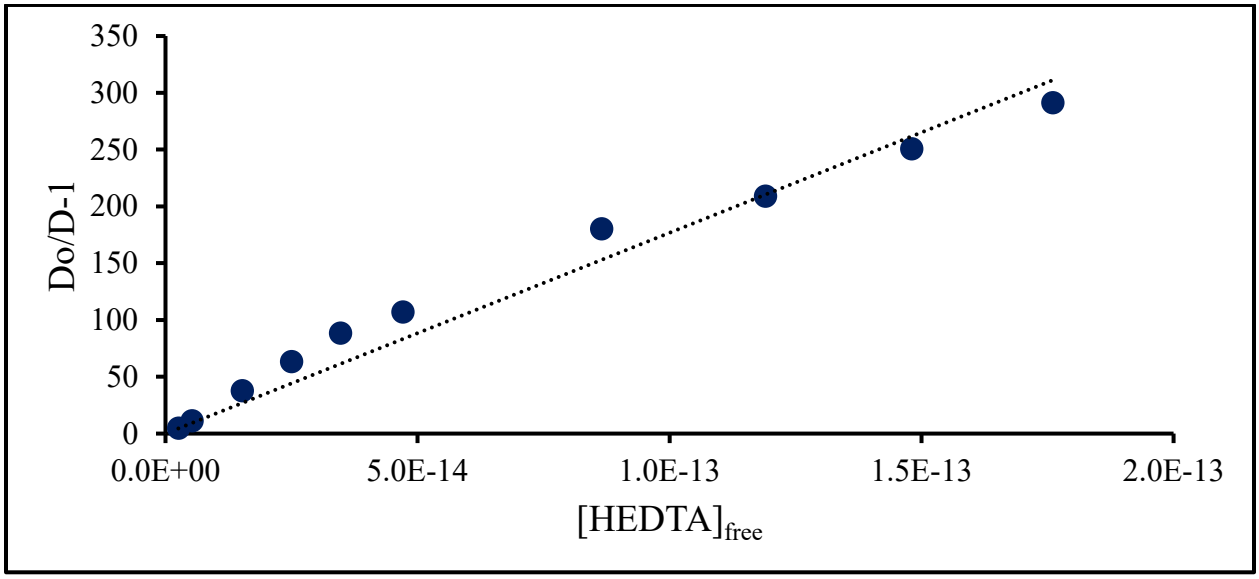

Figure D.18: Fit of Bk-HEDTA T = 35°C data

Table D.19: Bk-HEDTA T = 45°C Raw Data

pcH	D	D error	[HEDTA] (m)	$[HEDTA]_{free}$	Do	Do/D-1	Do/D error
2.53	21.9	0.9	4.79E-05	4.05E-15	59.72	1.700	0.003
2.54	9.1	0.2	9.68E-05	8.56E-15	62.80	5.900	0.003
2.53	2.25	0.01	2.88E-04	2.36E-14	57.51	24.600	0.001
2.52	1.16	0.04	4.85E-04	3.71E-14	53.33	45.10	0.06
2.51	0.81	0.02	6.79E-04	5.03E-14	51.36	62.30	0.06
2.49	0.57	0.02	9.67E-04	6.21E-14	43.61	76.00	0.09
2.45	0.244	0.001	1.91E-03	9.94E-14	34.35	139.900	0.001
2.41	0.16	0.01	2.91E-03	1.16E-13	25.40	155.1	0.8
2.39	0.113	0.002	3.84E-03	1.32E-13	21.57	190.70	0.08
2.37	0.086	0.002	4.81E-03	1.47E-13	19.02	219.6	0.1

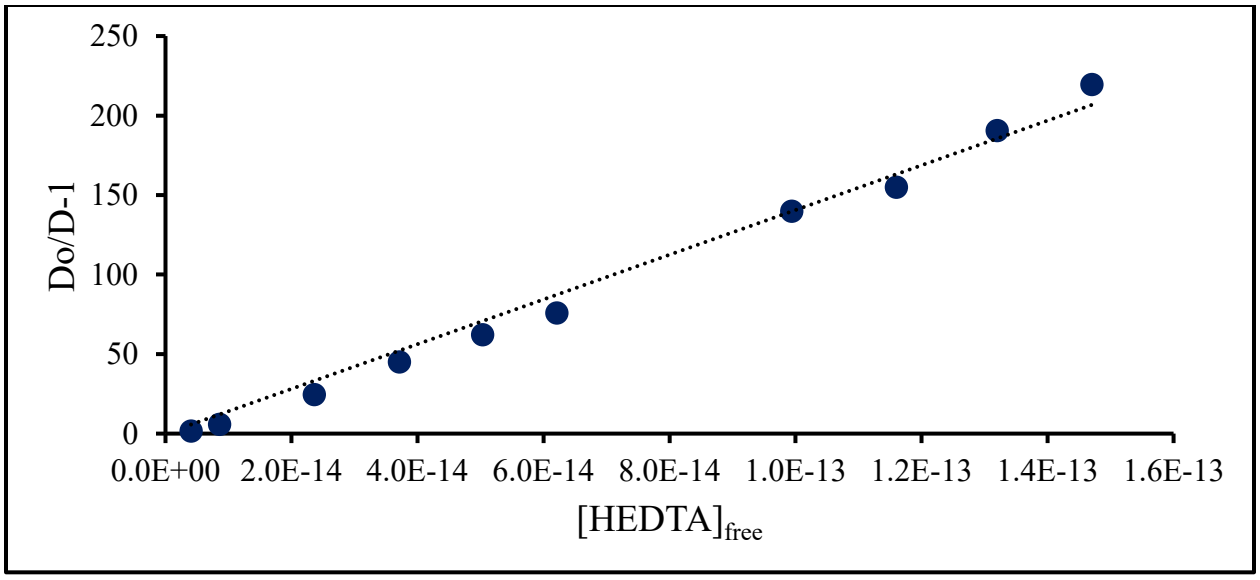

Figure D.19: Fit of Bk-HEDTA T = 45°C data

Table D.20: Bk-HEDTA T = 55°C Raw Data

pcH	D	D error	[HEDTA] (m)	$[HEDTA]_{free}$	Do	Do/D-1	Do/D error
2.53	11.0	0.8	4.79E-05	6.24E-15	66.92	5.10	0.03
2.54	5.9	0.4	9.68E-05	1.32E-14	70.37	10.90	0.06
2.53	1.61	0.05	2.88E-04	3.63E-14	64.44	39.10	0.04
2.52	0.88	0.03	4.85E-04	5.72E-14	59.76	66.80	0.07
2.51	0.57	0.01	6.79E-04	7.74E-14	57.55	100.90	0.03
2.49	0.388	0.009	9.67E-04	9.55E-14	48.87	124.80	0.06
2.45	0.171	0.001	1.91E-03	1.53E-13	38.49	224.100	0.007
2.41	0.111	0.006	2.91E-03	1.77E-13	28.46	256.1	0.7
2.39	0.076	0.001	3.84E-03	2.02E-13	24.17	317.5	0.1
2.37	0.062	0.001	4.81E-03	2.26E-13	21.32	345.3	0.1

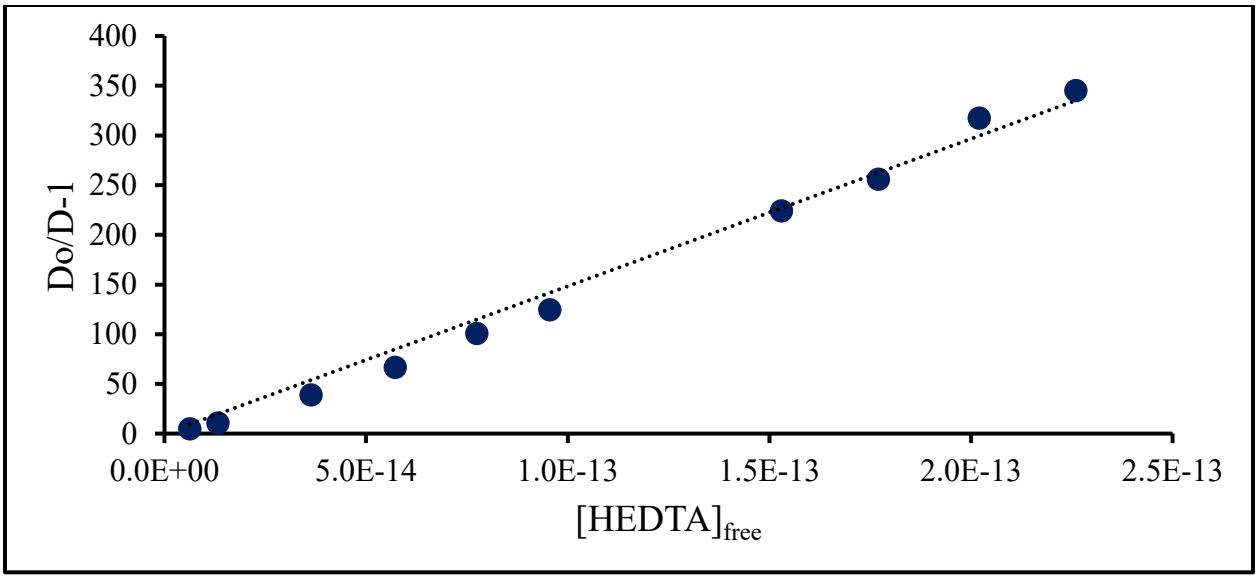

Figure D.20: Fit of Bk-HEDTA T = 55°C data

D.5 Berkelium-CDTA

Table D.21: Bk-CDTA T = 25°C Raw Data

pcH	D	D error	[CDTA] (m)	$[CDTA]_{free}$	Do	Do/D-1	Do/D error
2.34	21	1	1.01E-05	6.97E-20	1009.02	48.0	0.2
2.25	16.5	0.6	2.93E-05	1.16E-19	541.88	31.90	0.04
2.30	16.1	0.6	4.96E-05	2.73E-19	765.42	46.60	0.06
2.45	12	1	9.87E-05	1.08E-18	2157.26	181	3
2.46	5.12	0.01	2.97E-04	3.34E-18	2311.54	450.600	0.002
2.40	2.1	0.1	5.09E-04	4.66E-18	1527.22	735	2
2.40	1.1	0.1	1.02E-03	9.35E-18	1527.22	1390	15

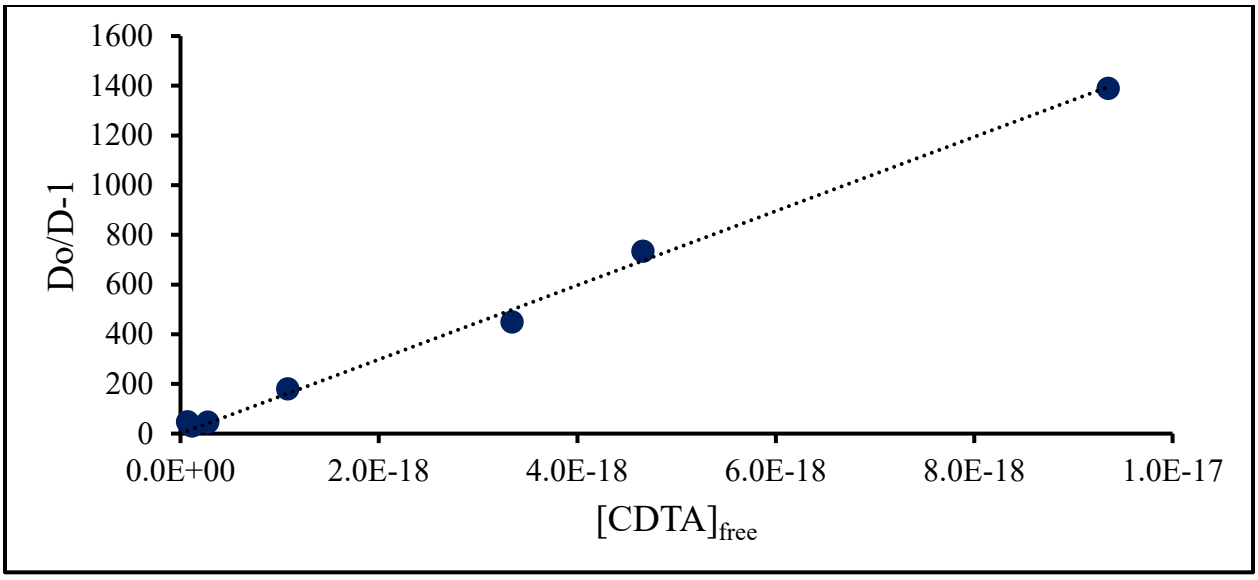

Figure D.21: Fit of Bk-CDTA T = 25°C data

Table D.22: Bk-CDTA T = 30°C Raw Data

pcH	D	D error	[CDTA] (m)	$[CDTA]_{free}$	Do	Do/D-1	Do/D error
2.34	17.1547	0.5	1.01E-05	9.57E-20	831.18	47.50	0.05
2.25	13.6726	0.3	2.93E-05	9.77E-20	286.05	19.900	0.009
2.30	13.6687	0.6	4.96E-05	2.07E-19	347.67	24.40	0.04
2.45	10.2256	0.2	9.87E-05	5.50E-19	457.74	43.80	0.02
2.46	3.9640	0.1	2.97E-04	1.48E-18	411.02	102.70	0.06
2.40	1.4395	0.02	5.09E-04	4.08E-18	675.42	468.20	0.09
2.40	0.6619	0.02	1.02E-03	6.90E-18	556.97	840.4	0.4

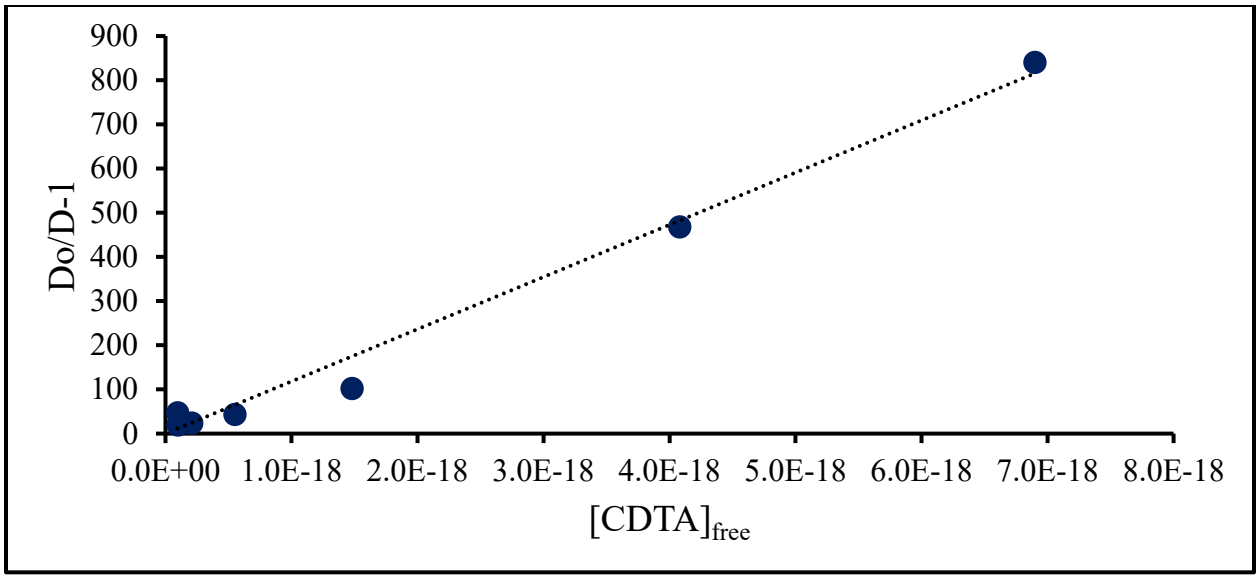

Figure D.22: Fit of Bk-CDTA T = 30°C data

Table D.23: Bk-CDTA T = 35°C Raw Data

pcH	D	D error	[CDTA] (m)	$[CDTA]_{free}$	Do	Do/D-1	Do/D error
2.34	16	1	1.01E-05	1.32E-19	725.71	43.3	0.3
2.25	11.3	0.1	2.93E-05	1.35E-19	249.76	21.100	0.003
2.30	11.1	0.3	4.96E-05	2.85E-19	303.56	26.40	0.02
2.45	8.3	0.4	9.87E-05	7.59E-19	399.66	47.3	0.1
2.46	2.63	0.07	2.97E-04	2.04E-18	358.87	135.60	0.09
2.40	0.95	0.01	5.09E-04	5.63E-18	589.72	621.00	0.09
2.40	0.439	0.003	1.02E-03	9.51E-18	486.30	1107.90	0.04

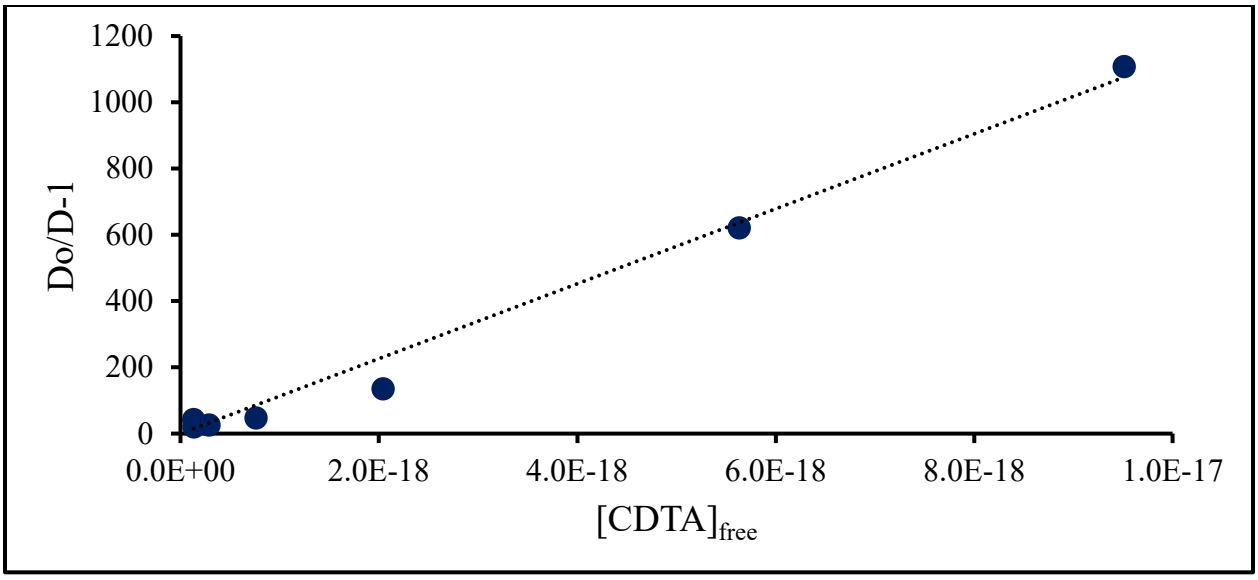

Figure D.23: Fit of Bk-CDTA T = 35°C data

Table D.24: Bk-CDTA T = 45°C Raw Data

pcH	D	D error	[CDTA] (m)	$[CDTA]_{free}$	Do	Do/D-1	Do/D error
2.34	11.9	0.1	1.01E-05	2.51E-19	578.00	47.500	0.003
2.25	9.6	0.2	2.93E-05	2.58E-19	198.92	19.700	0.007
2.30	9.8	0.3	4.96E-05	5.45E-19	241.77	23.70	0.02
2.45	6.9	0.2	9.87E-05	1.45E-18	318.31	45.00	0.04
2.46	1.59	0.06	2.97E-04	3.90E-18	285.83	179.2	0.2
2.40	0.55	0.02	5.09E-04	1.07E-17	469.69	853.6	0.9
2.40	0.239	0.002	1.02E-03	1.81E-17	387.32	1621.5	0.1

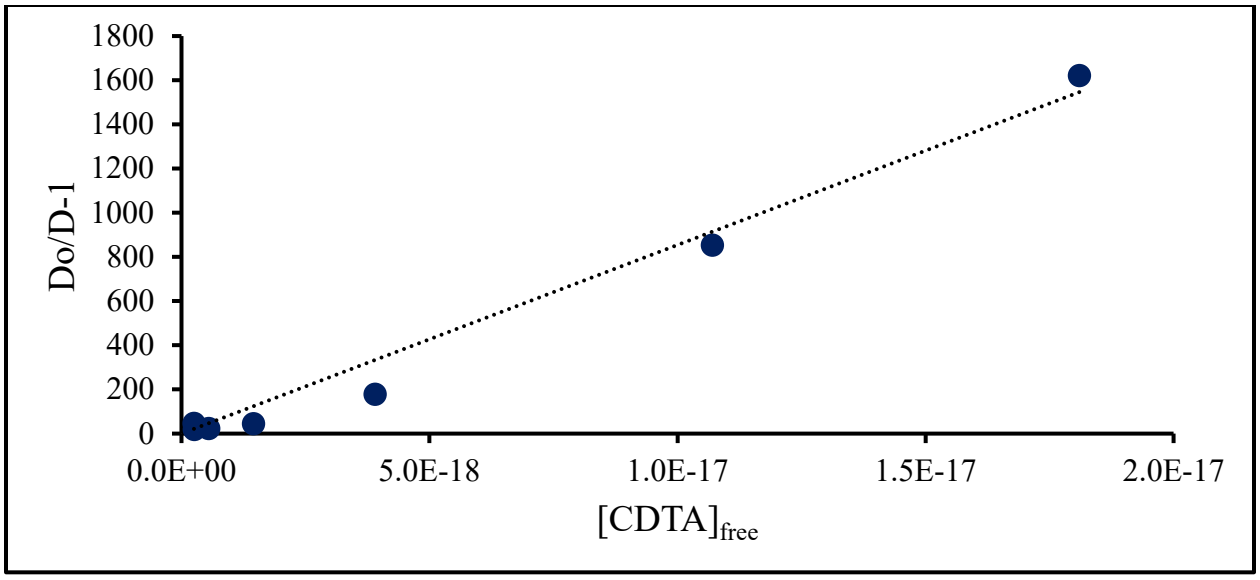

Figure D.24: Fit of Bk-CDTA T = 45°C data

Table D.25: Bk-CDTA T = 55°C Raw Data

pcH	D	D error	[CDTA] (m)	$[CDTA]_{free}$	Do	Do/D-1	Do/D error
2.34	9.2	0.3	1.01E-05	4.57E-19	429.60	45.70	0.04
2.25	9.12	0.09	2.93E-05	4.75E-19	147.85	15.200	0.001
2.30	9.5	0.2	4.96E-05	1.00E-18	179.70	17.9	0.01
2.45	6.7	0.5	9.87E-05	2.65E-18	236.58	34.5	0.2
2.46	0.82	0.03	2.97E-04	7.16E-18	212.44	259.4	0.4
2.40	0.26	0.01	5.09E-04	1.96E-17	349.09	1329	2
2.40	0.125	0.001	1.02E-03	3.32E-17	287.87	2301.0	0.3

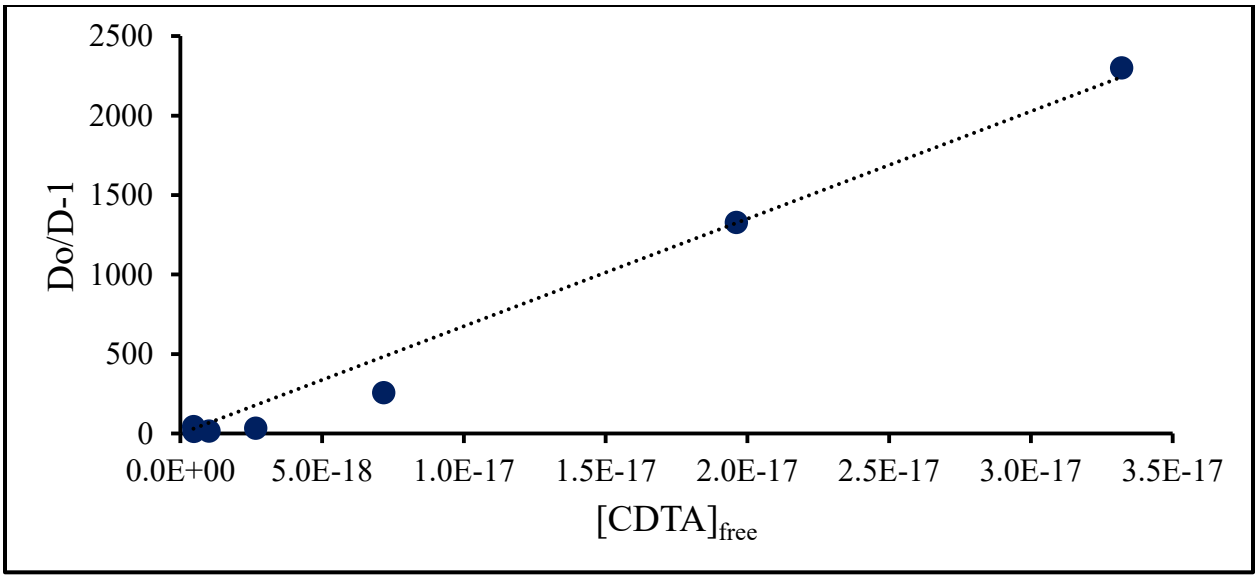

Figure D.25: Fit of Bk-CDTA T = 55°C data

D.6 Berkelium-DTPA

Table D.26: Bk-DTPA T = 25°C pcH = 2.1

pcH	D	D error	[DTPA] (m)	$[DTPA]_{free}$	Do	Do/D-1	Do/D error
2.01	9.2	0.1	9.90E-05	4.06E-22	216.49	77	3
2.01	9.12	0.02	5.08E-04	2.08E-21	216.49	400	16
2.01	9.53	0.01	1.04E-03	4.28E-21	216.49	610	25
2.01	6.672	0.002	2.14E-03	8.76E-21	216.49	1150	46
2.01	0.816	0.001	3.05E-03	1.25E-20	216.49	1650	66
2.01	0.263	0.002	3.99E-03	1.64E-20	216.49	2030	82
2.01	0.125	0.001	4.89E-03	2.01E-20	216.49	2350	94

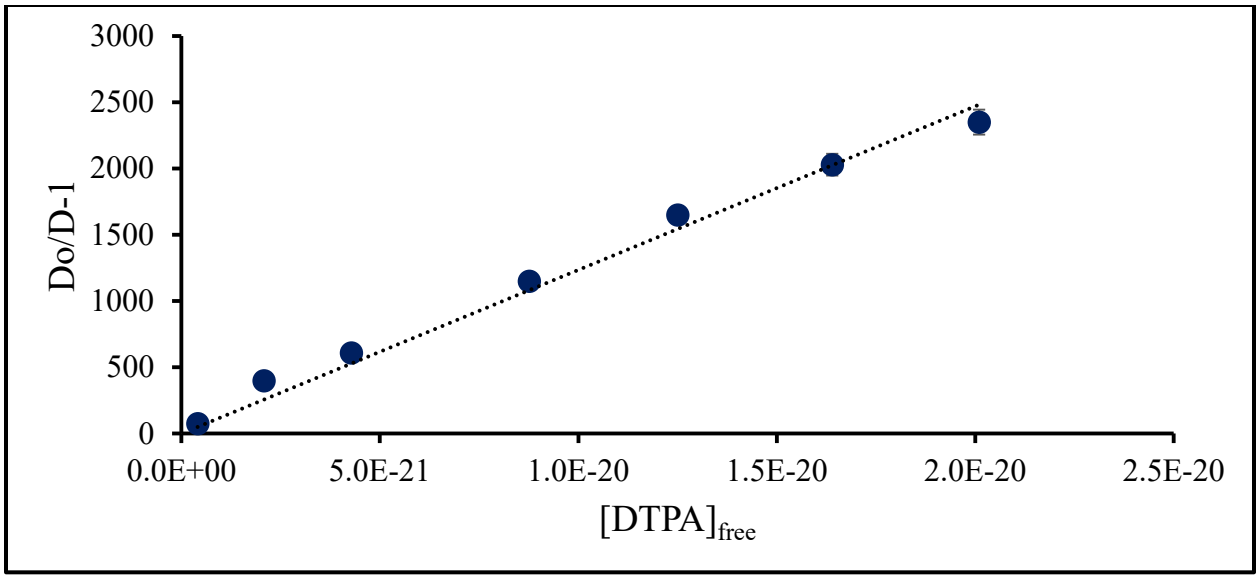

Figure D.26: Fit of Bk-DTPA T = 25°C pcH = 2.1

Table D.27: Bk-DTPA T = 25°C pcH = 1.9

pcH	D	D error	[DTPA] (m)	$[DPTA]_{free}$	Do	Do/D-1	Do/D error
1.99	13.5	0.4	1.00E-05	3.25E-23	188.56	13.0	0.5
1.99	12.3	0.2	4.91E-05	1.66E-22	188.56	14.3	0.6
1.99	10.6	0.2	1.02E-04	3.34E-22	188.56	16.8	0.7
1.99	4.14	0.07	3.03E-04	1.00E-21	188.56	45	2
1.99	2.53	0.05	5.12E-04	1.71E-21	188.56	74	3

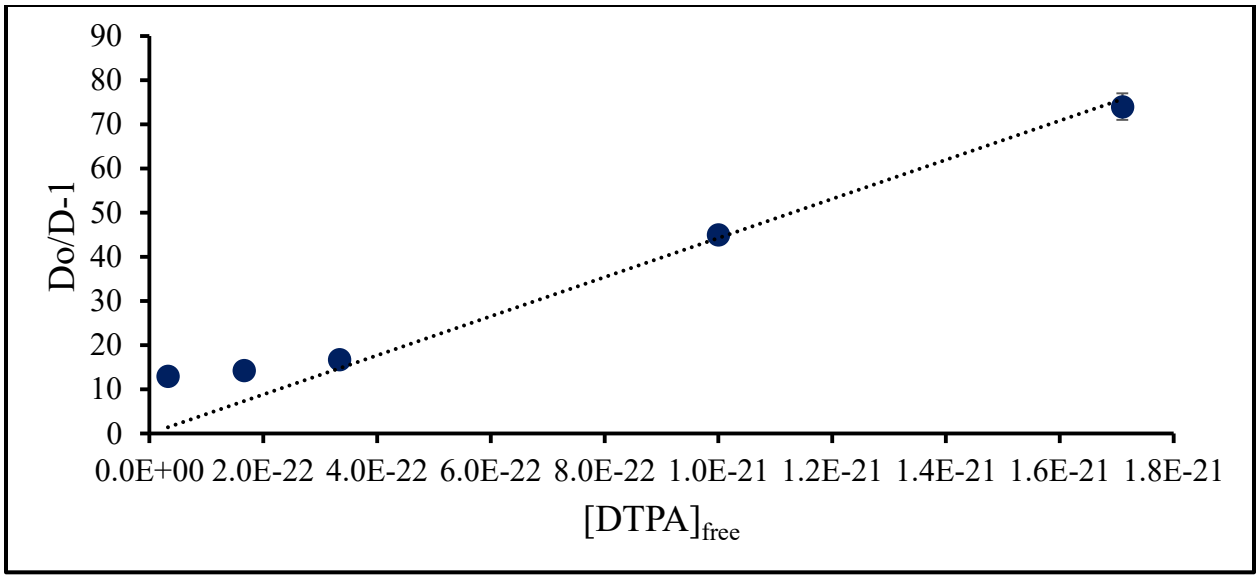

Figure D.27: Fit of Bk-DTPA T = 25°C, pcH = 1.9

Table D.28: Bk-DTPA T = 25°C pcH = 2.3

pcH	D	D error	[DPTA] (m)	$[DPTA]_{free}$	Do	Do/D-1	Do/D error
2.32	57.1	0.8	9.81E-06	9.60E-22	1842.7	31	1
2.32	14.4	0.6	5.01E-05	4.70E-21	1842.7	126	5
2.32	7.20	0.05	1.01E-04	9.72E-21	1842.7	250	10
2.32	1.85	0.02	3.03E-04	2.90E-20	1842.7	1000	40
2.32	1.28	0.02	5.17E-04	4.90E-20	1842.7	1440	60

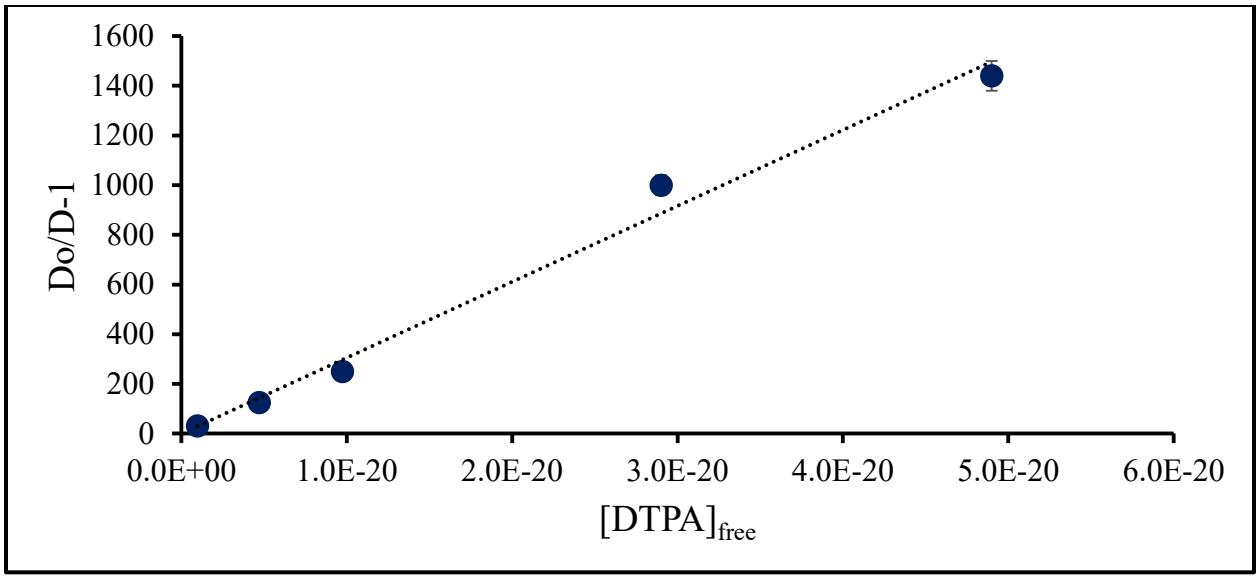

Figure D.28: Fit of Bk-DTPA T = 25°C, pcH = 2.3

Table D.29: Bk-DTPA T = 25°C pcH = 2.5

pcH	D	D error	[DPTA] (m)	$[DPTA]_{free}$	Do	Do/D-1	Do/D error
2.52	3.8	0.1	1.03E-05	6.28E-21	7335.8	1910	77
2.52	0.90	0.09	4.98E-05	3.04E-20	7335.8	8200	400
2.52	0.44	0.02	1.00E-04	6.11E-20	7335.8	16700	695
2.52	0.51	0.01	2.94E-04	1.79E-19	7335.8	14300	580
2.52	0.35	0.02	5.11E-04	3.11E-19	7335.8	21100	890

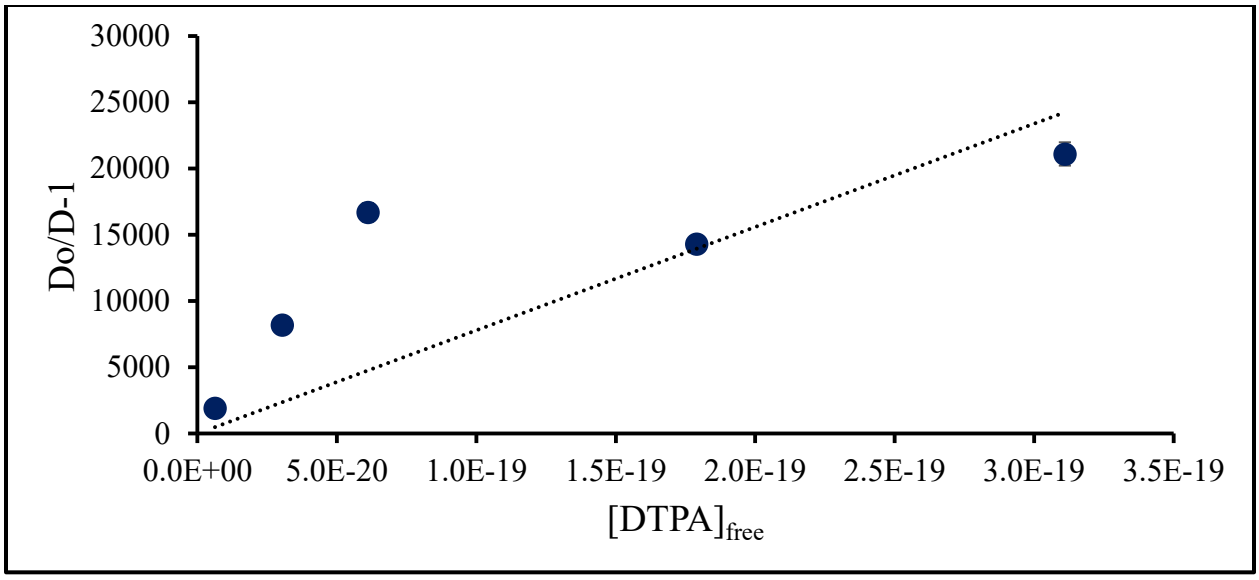

Figure D.29: Fit of Bk-DTPA T = 25°C, pcH = 2.5 data

Table D.30: Bk-DTPA T = 35°C pcH = 2.1

pcH	D	D error	[DPTA] (m)	$[DPTA]_{free}$	Do	Do/D-1	Do/D error
2.01	1.7	0.1	9.90E-05	8.58E-22	96.10	56.3	0.4
2.01	0.32	0.02	5.08E-04	4.40E-21	96.10	304	1
2.01	0.20	0.01	1.04E-03	9.05E-21	96.10	476	2
2.01	0.1092	0.002	2.14E-03	1.85E-20	96.10	879.1	0.3
2.01	0.079	0.001	3.05E-03	2.65E-20	96.10	1215.3	0.4
2.01	0.063	0.002	3.99E-03	3.46E-20	96.10	1535	2
2.01	0.055	0.001	4.89E-03	4.24E-20	96.10	1757.7	0.9

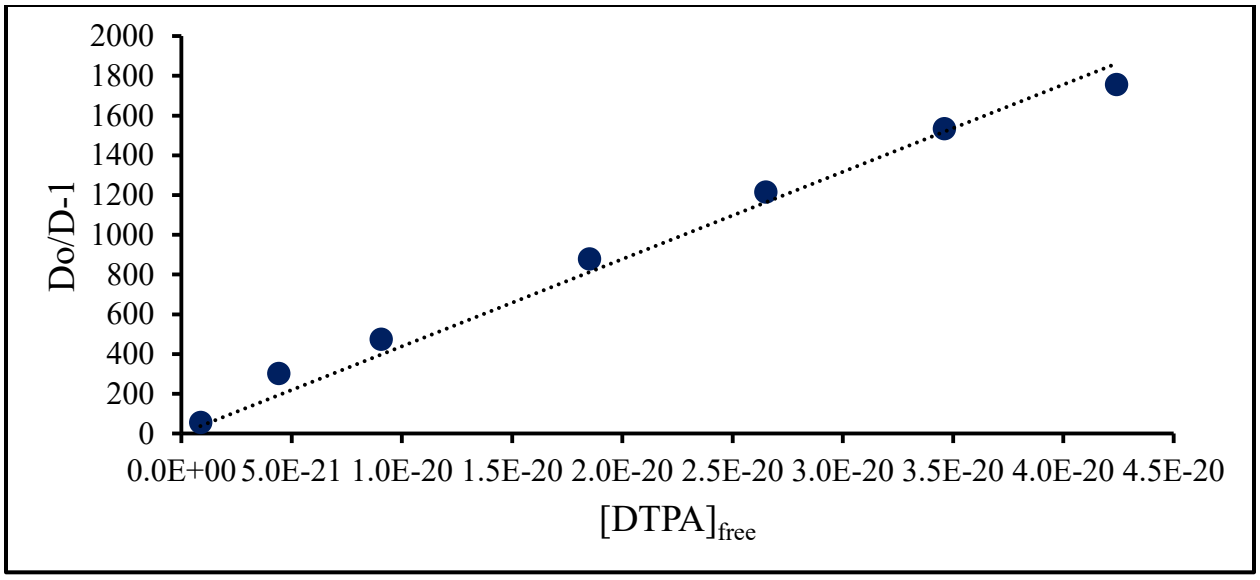

Figure D.30: Fit of Bk-DTPA T = 35°C, pcH = 2.1 data

Table D.31: Bk-DTPA T = 35°C pcH = 1.9

pcH	D	D error	[DPTA] (m)	$[DPTA]_{free}$	Do	Do/D-1	Do/D error
1.99	8.2	0.8	1.00E-05	7.01E-23	83.70	9.20	0.08
1.99	3.3	0.1	4.91E-05	3.43E-22	83.70	24.50	0.04
1.99	0.72	0.02	1.02E-04	7.10E-22	83.70	115.1	0.1
1.99	2.67	0.03	3.03E-04	2.11E-21	83.70	30.300	0.004
1.99	0.969	0.002	5.12E-04	3.58E-21	83.70	85.400	0.003

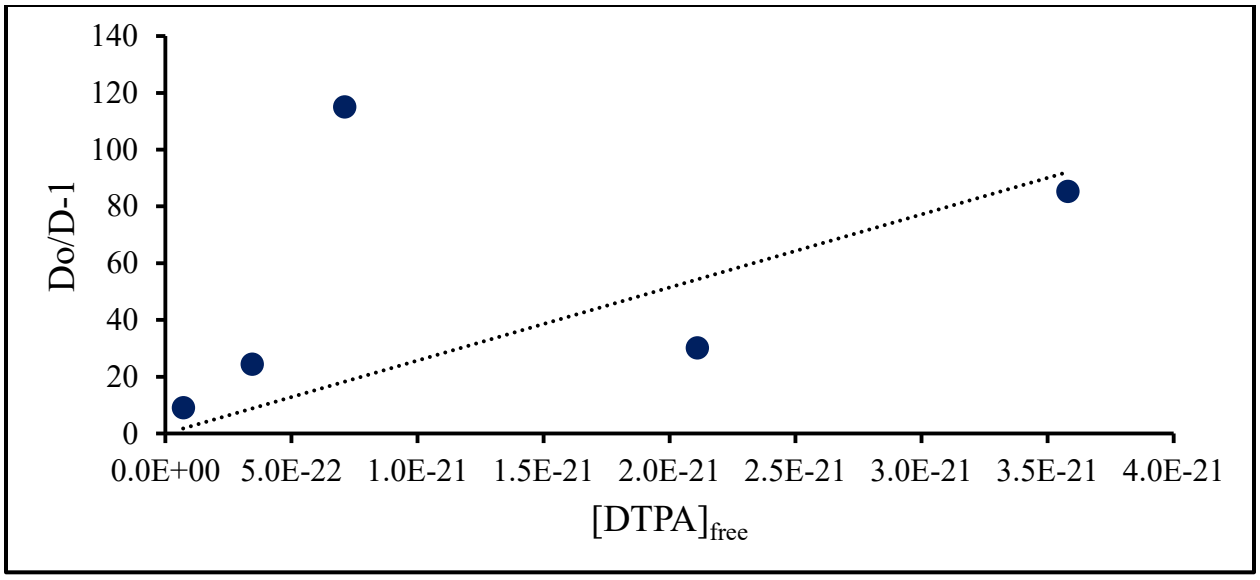

Figure D.31: Fit of Bk-DTPA T = 35°C, pcH = 1.9 data. Middle point excluded from fit analysis.

Table D.32: Bk-DTPA T = 35°C pcH = 2.3

pcH	D	D error	[DPTA] (m)	$[DPTA]_{free}$	Do	Do/D-1	Do/D error
2.32	0.29	0.02	9.81E-06	1.99E-21	817.96	2869	8
2.32	1.385	0.002	5.01E-05	1.02E-20	817.96	589.80	0.02
2.32	0.677	0.001	1.01E-04	2.05E-20	817.96	1207.70	0.04
2.32	0.175	0.001	3.03E-04	6.14E-20	817.96	4670.5	0.4
2.32	1.53	0.03	5.17E-04	1.05E-19	817.96	534.3	0.3

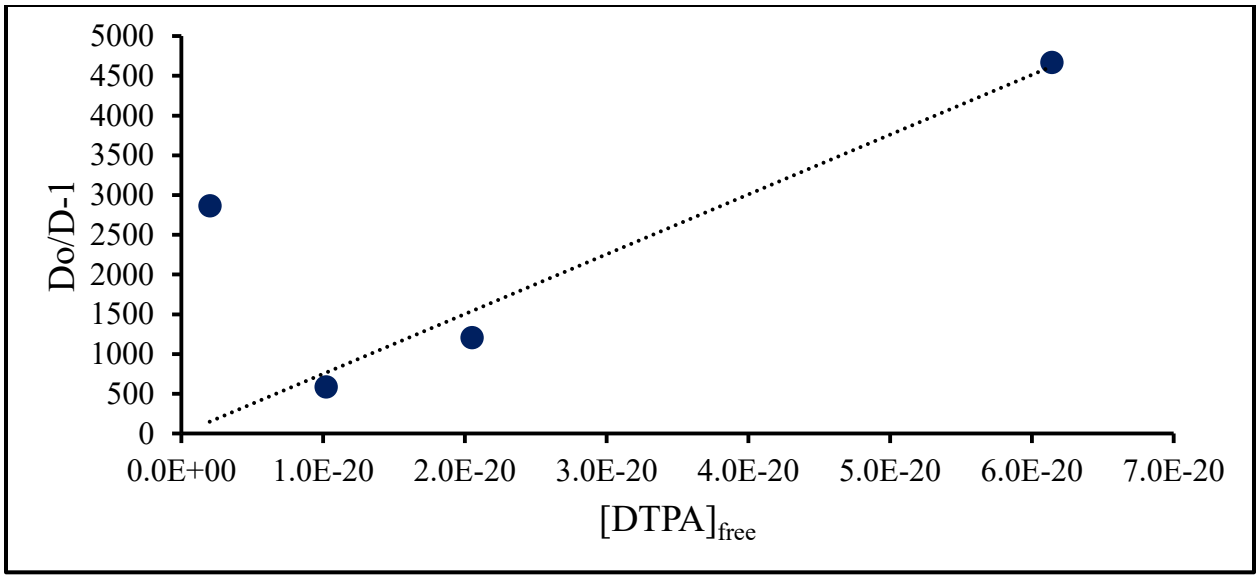

Figure D.32: Fit of Bk-DTPA T = 35°C, pcH = 2.3 data. Last point omitted for fit.

Table D.33: Bk-DTPA T = 35°C pcH = 2.5

pcH	D	D error	[DPTA] (m)	$[DPTA]_{free}$	Do	Do/D-1	Do/D error
2.52	0.42	0.01	1.03E-05	1.33E-20	3256.4	7763	8
2.52	0.187	0.004	4.98E-05	6.44E-20	3256.4	17394	8
2.52	0.892	0.007	1.00E-04	1.30E-19	3256.4	3649.0	0.4
2.52	0.298	0.003	2.94E-04	3.80E-19	3256.4	10937	1
2.52	0.144	0.002	5.11E-04	6.61E-19	3256.4	22680	5

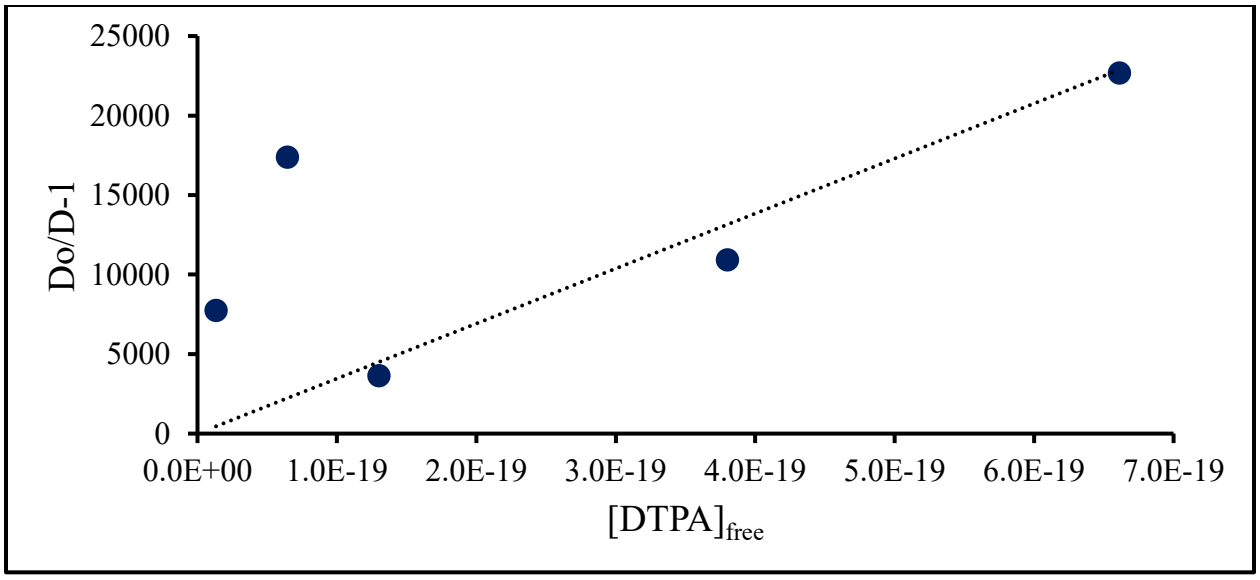

Figure D.33: Fit of Bk-DTPA T = 35°C, pcH = 2.5 data. Second point omitted from fit, but plotted.

Table D.34: Bk-DTPA T = 45°C pcH = 2.1

pcH	D	D error	[DPTA] (m)	$[DPTA]_{free}$	Do	Do/D-1	Do/D error
2.01	1.1	0.1	9.90E-05	1.70E-21	145.77	133	2
2.01	0.22	0.02	5.08E-04	8.74E-21	145.77	670	5
2.01	0.13	0.01	1.04E-03	1.80E-20	145.77	1127	9
2.01	0.072	0.002	2.14E-03	3.67E-20	145.77	2028	1
2.01	0.054	0.001	3.05E-03	5.25E-20	145.77	2683	2
2.01	0.044	0.002	3.99E-03	6.87E-20	145.77	3346	8
2.01	0.039	0.001	4.89E-03	8.42E-20	145.77	3730	3

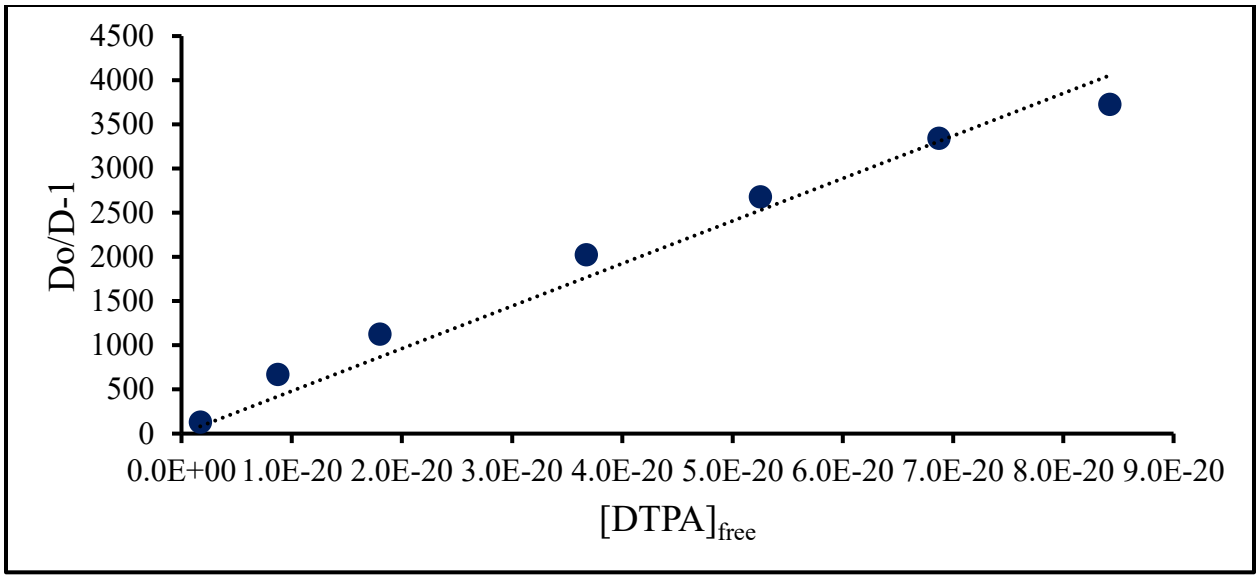

Figure D.34: Fit of Bk-DTPA T = 45°C, pcH = 2.1 data

Table D.35: Bk-DTPA T = 45°C pcH = 1.9

pcH	D	D error	[DPTA] (m)	$[DPTA]_{free}$	Do	Do/D-1	Do/D error
1.99	2.29	0.08	1.00E-05	1.39E-22	126.96	54.30	0.07
1.99	0.93	0.06	4.91E-05	6.80E-22	126.96	136.1	0.7
1.99	0.43	0.07	1.02E-04	1.41E-21	126.96	298	7
1.99	0.72	0.02	3.03E-04	4.19E-21	126.96	175.2	0.1
1.99	0.2561	0.0002	5.12E-04	7.10E-21	126.96	494.800	0.008

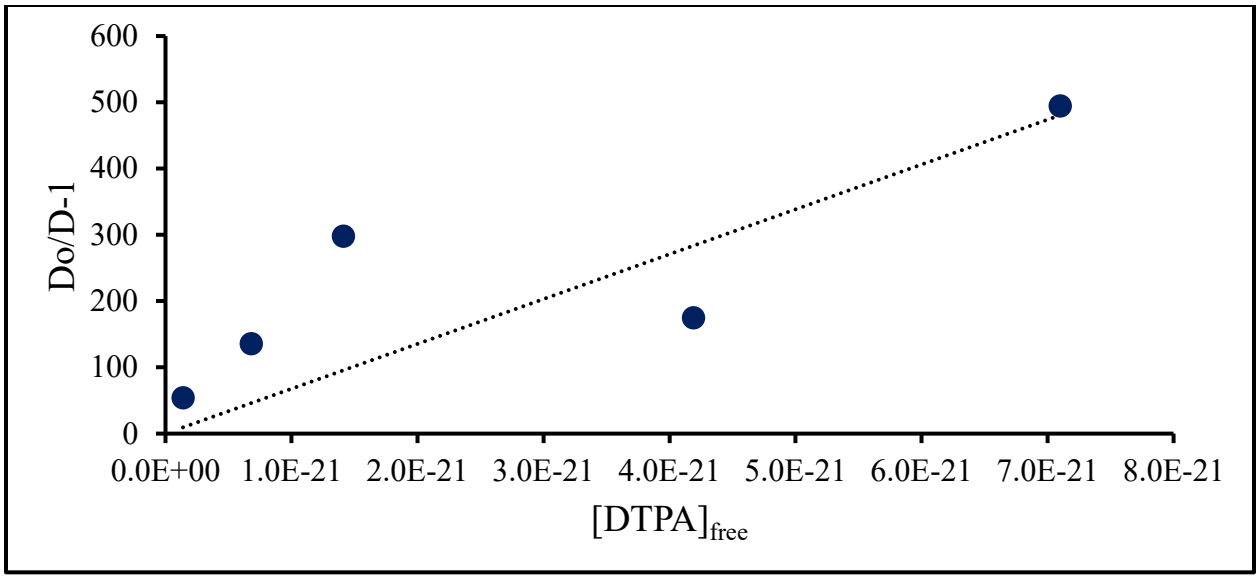

Figure D.35: Fit of Bk-DTPA T = 45°C, pcH = 1.9 data

Table D.36: Bk-DTPA T = 45°C pcH = 2.3

pcH	D	D error	[DPTA] (m)	$[DPTA]_{free}$	Do	Do/D-1	Do/D error
2.32	0.13	0.02	9.81E-06	3.97E-21	1240.7	9400	200
2.32	0.390	0.001	5.01E-05	2.03E-20	1240.7	3178.50	0.08
2.32	0.19	0.01	1.01E-04	4.09E-20	1240.7	6690	35
2.32	0.080	0.009	3.03E-04	1.23E-19	1240.7	15600	200
2.32	0.48	0.02	5.17E-04	2.09E-19	1240.7	2595	3

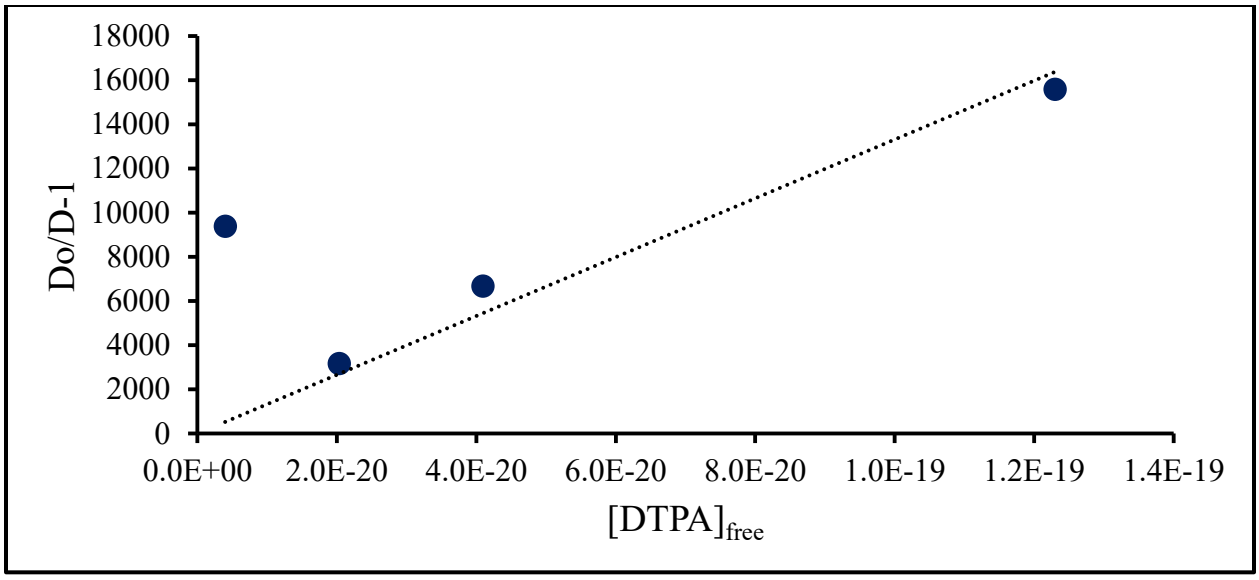

Figure D.36: Fit of Bk-DTPA T = 45°C, pcH = 2.3 data. Last point omitted due to poor fit.

Table D.37: Bk-DTPA T = 45°C pcH = 2.5

pcH	D	D error	[DPTA] (m)	$[DPTA]_{free}$	Do	Do/D-1	Do/D error
2.52	0.12	0.01	1.03E-05	2.66E-20	4939.2	39700	300
2.52	0.063	0.003	4.98E-05	1.29E-19	4939.2	78900	150
2.52	0.366	0.005	1.00E-04	2.59E-19	4939.2	13483	3
2.52	0.11	0.01	2.94E-04	7.59E-19	4939.2	45700	540
2.52	0.053	0.003	5.11E-04	1.32E-18	4939.2	92800	275

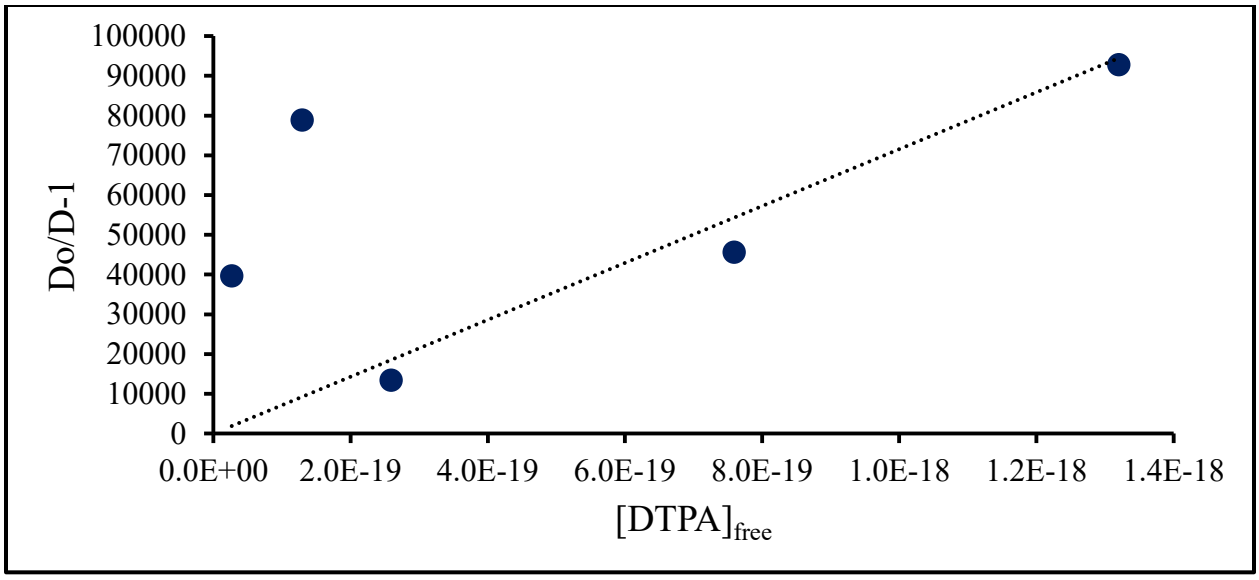

Figure D.37: Fit of Bk-DTPA T = 45°C, pcH = 2.5 data

Table D.38: Bk-DTPA T = 55°C pcH = 2.1

pcH	D	D error	[DPTA] (m)	$[DPTA]_{free}$	Do	Do/D-1	Do/D error
2.01	0.8	0.1	9.90E-05	3.31E-21	108.34	140	5
2.01	0.13	0.02	5.08E-04	1.70E-20	108.34	820	15
2.01	0.08	0.01	1.04E-03	3.49E-20	108.34	1340	30
2.01	0.043	0.002	2.14E-03	7.14E-20	108.34	2531	4
2.01	0.033	0.001	3.05E-03	1.02E-19	108.34	3245	5
2.01	0.027	0.002	3.99E-03	1.33E-19	108.34	4070	30
2.01	0.024	0.001	4.89E-03	1.64E-19	108.34	4520	11

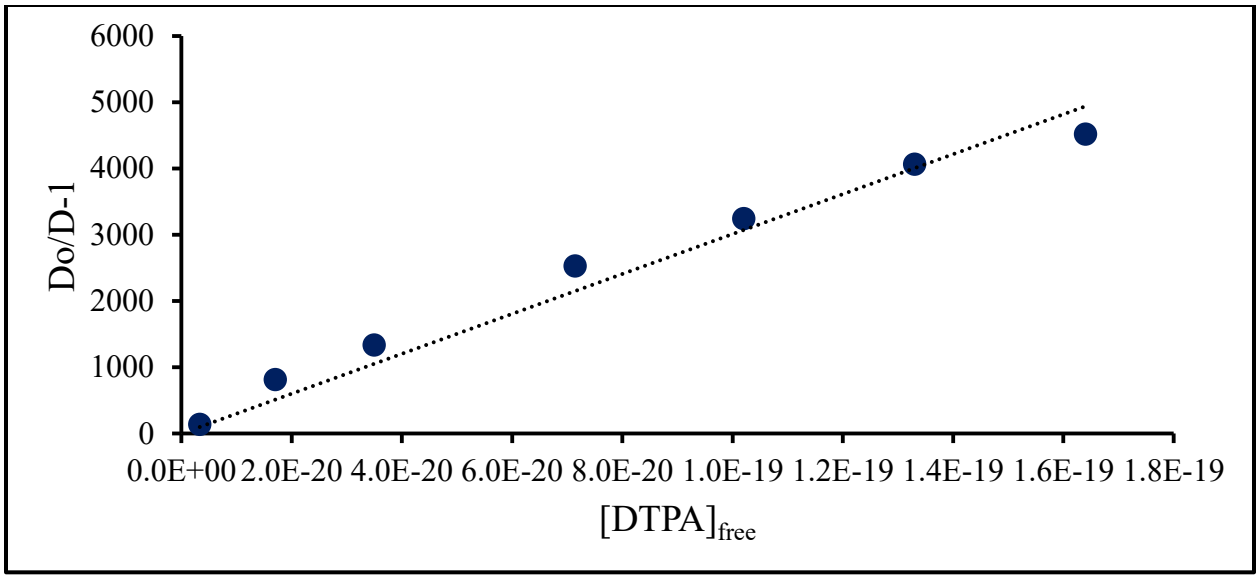

Figure D.38: Fit of Bk-DTPA T = 55°C, pcH = 2.1 data

Table D.39: Bk-DTPA T = 55°C pcH = 1.9

pcH	D	D error	[DPTA] (m)	$[DPTA]_{free}$	Do	Do/D-1	Do/D error
1.99	1.731	0.004	1.00E-05	2.70E-22	94.36	53.500	0.002
1.99	0.59	0.02	4.91E-05	1.32E-21	94.36	158.0	0.1
1.99	0.27	0.02	1.02E-04	2.74E-21	94.36	353	2
1.99	0.56	0.01	3.03E-04	8.14E-21	94.36	167.00	0.08
1.99	0.24	0.05	5.12E-04	1.38E-20	94.36	400	19

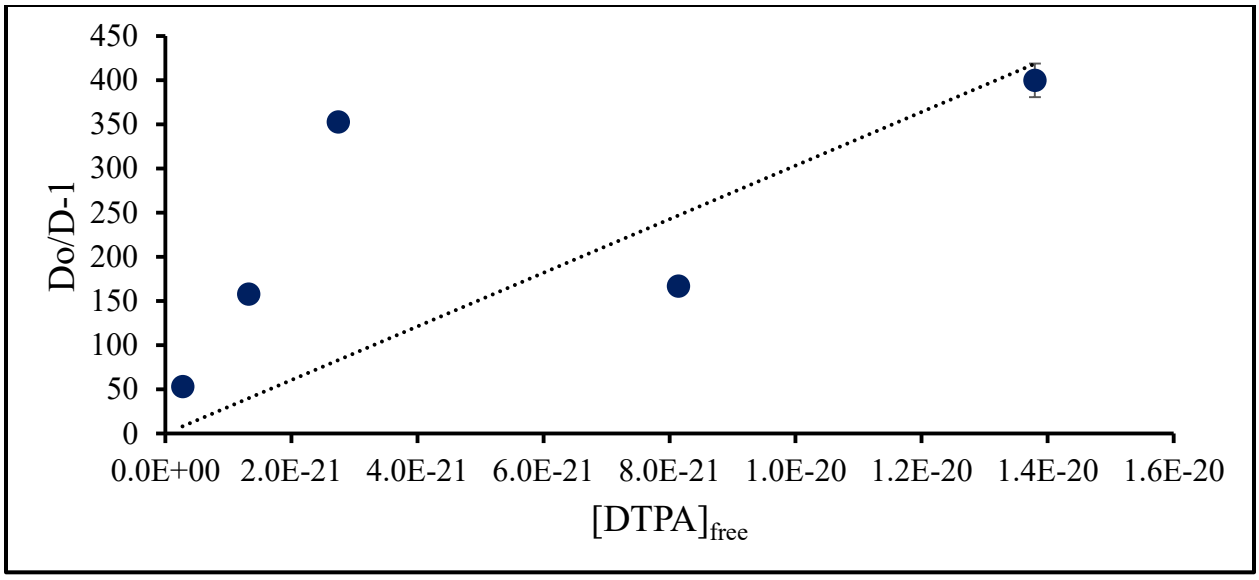

Figure D.39: Fit of Bk-DTPA T = 55°C, pcH = 1.9 data

Table D.40: Bk-DTPA T = 55°C pcH = 2.3

pcH	D	D error	[DPTA] (m)	$[DPTA]_{free}$	Do	Do/D-1	Do/D error
2.32	0.09	0.01	9.81E-06	7.73E-21	922.12	10600	200
2.32	0.33	0.04	5.01E-05	3.95E-20	922.12	2760	50
2.32	0.155	0.004	1.01E-04	7.96E-20	922.12	5943	3
2.32	0.061	0.002	3.03E-04	2.39E-19	922.12	15140	20
2.32	0.379	0.002	5.17E-04	4.07E-19	922.12	2434.0	0.1

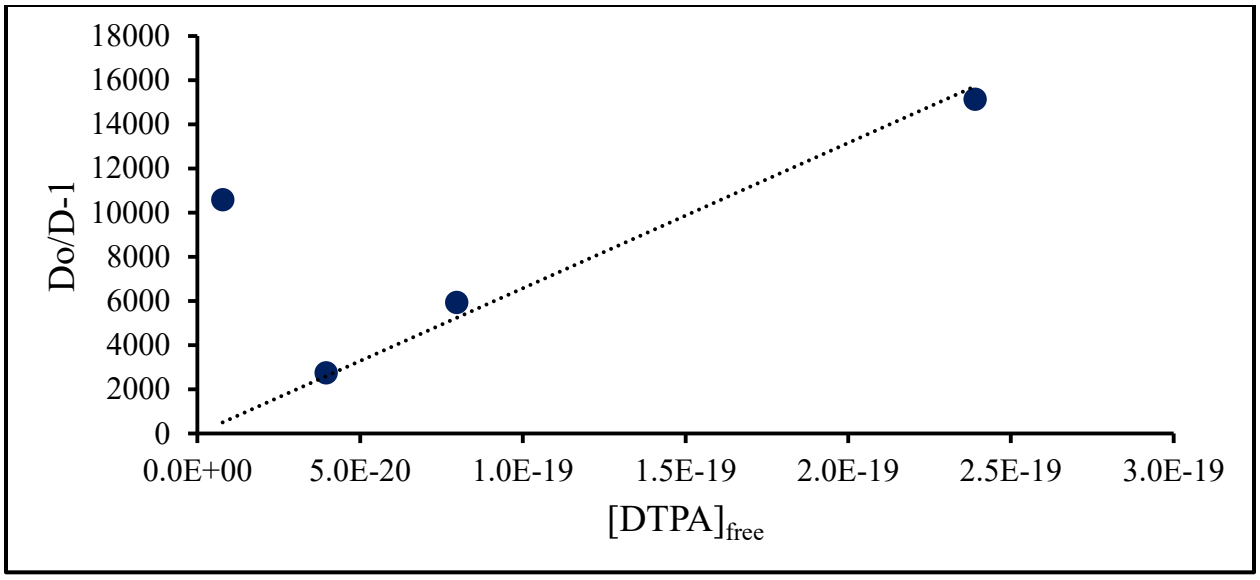

Figure D.40: Fit of Bk-DTPA T = 55°C, pcH = 2.3 data

Table D.41: Bk-DTPA T = 55° C pcH = 2.5

pcH	D	D error	[DPTA] (m)	$[DPTA]_{free}$	Do	Do/D-1	Do/D error
2.52	0.090	0.003	1.03E-05	5.18E-20	3671.0	40860	40
2.52	0.047	0.004	4.98E-05	2.50E-19	3671.0	77700	500
2.52	0.269	0.006	1.00E-04	5.04E-19	3671.0	13638	8
2.52	0.082	0.008	2.94E-04	1.48E-18	3671.0	44800	400
2.52	0.040	0.002	5.11E-04	2.57E-18	3671.0	92100	300

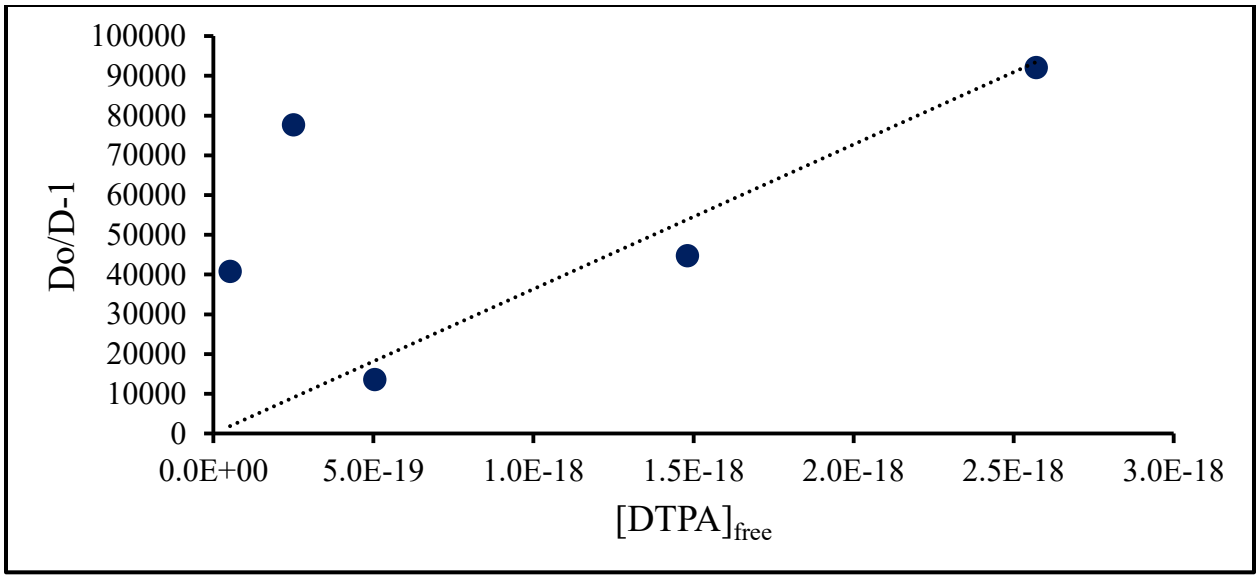

Figure D.41: Fit of Bk-DTPA T = 55°C, pcH = 2.5 data

D.7 Californium-NTA

Table D.42: Cf-NTA T = 15° C Raw Data

pcH	D	D error	[NTA] (m)	$[NTA]_{free}$	Do	Do/D-1	Do/D error
2.49	13	2	9.79E-05	2.50E-12	34.63	1.70	0.05
2.49	2.44	0.02	4.88E-04	1.25E-11	34.63	13.200	0.001
2.49	3.87	0.09	7.66E-04	1.96E-11	34.63	8.000	0.005
2.49	0.98	0.03	9.71E-04	2.48E-11	34.63	34.30	0.04
2.49	0.34	0.02	1.94E-03	4.95E-11	34.63	102.2	0.3
2.49	0.175	0.002	2.88E-03	7.36E-11	34.63	196.80	0.02
2.49	0.106	0.004	3.99E-03	1.02E-10	34.63	325.2	0.4
2.49	0.065	0.001	4.95E-03	1.26E-10	34.63	530.60	0.05

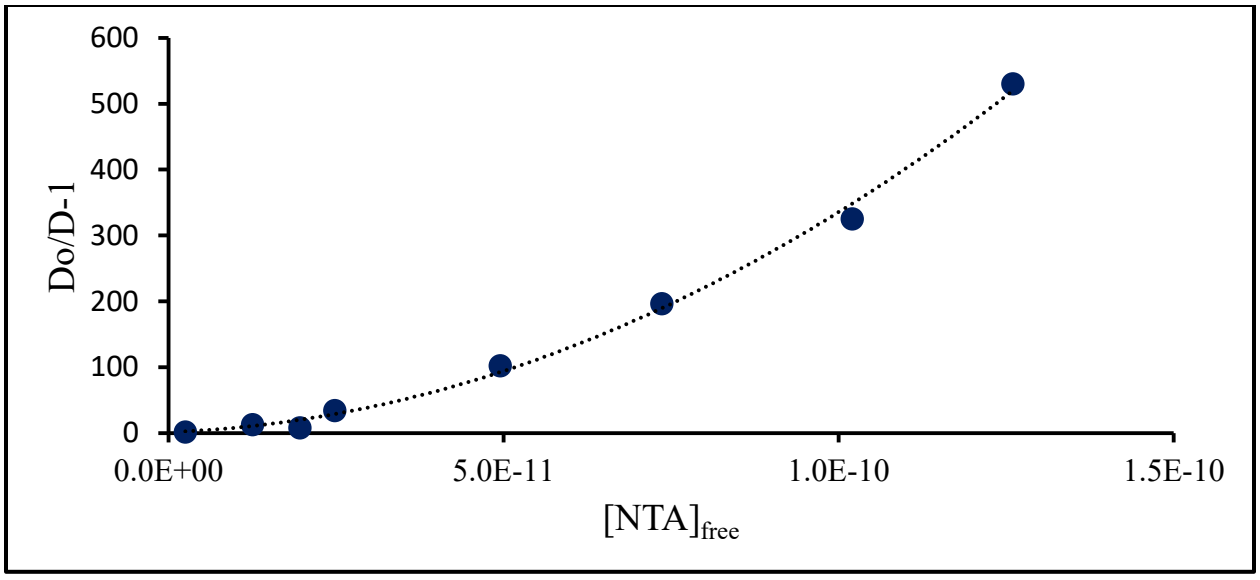

Figure D.42: Fit of Cf-NTA, T = 15°C data

Table D.43: Cf-NTA T = 25° C Raw Data

pcH	D	D error	[NTA] (m)	$[NTA]_{free}$	Do	Do/D-1	Do/D error
2.49	6.6897	5	9.79E-05	3.30E-12	28.46	3	2
2.49	1.72	0.04	4.88E-04	1.65E-11	28.46	15.50	0.01
2.49	3.12	0.06	7.66E-04	2.59E-11	28.46	8.100	0.003
2.49	0.73	0.06	9.71E-04	3.27E-11	28.46	38.0	0.3
2.49	0.21	0.01	1.94E-03	6.55E-11	28.46	133.2	0.5
2.49	0.109	0.002	2.88E-03	9.73E-11	28.46	259.8	0.1
2.49	0.0660	0.001	3.99E-03	1.35E-10	28.46	430.90	0.05
2.49	0.042	0.002	4.95E-03	1.67E-10	28.46	683.4	0.9

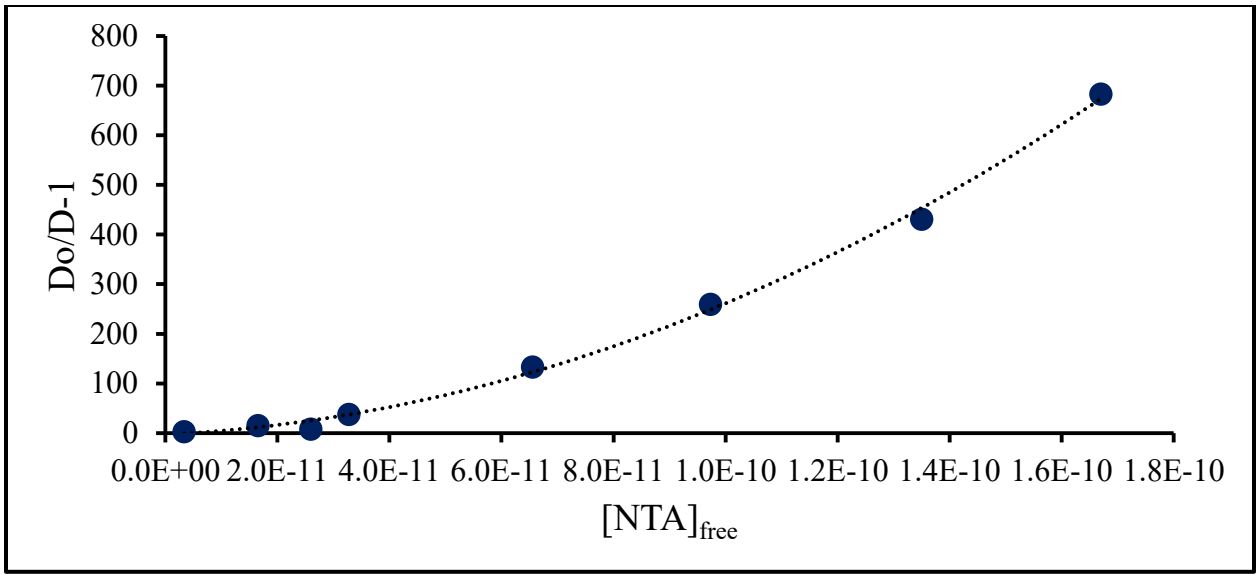

Figure D.43: Fit of Cf-NTA T = 25°C data

Table D.44: Cf-NTA T = 35° C Raw Data

pcH	D	D error	[NTA] (m)	$[NTA]_{free}$	Do	Do/D-1	Do/D error
2.49	7.30	0.02	9.79E-05	4.26E-12	24.61	2.40000	0.00002
2.49	0.95	0.03	4.88E-04	2.13E-11	24.61	24.90	0.02
2.49	1.83	0.06	7.66E-04	3.34E-11	24.61	12.40	0.01
2.49	0.41	0.01	9.71E-04	4.23E-11	24.61	59.00	0.07
2.49	0.146	0.004	1.94E-03	8.45E-11	24.61	167.2	0.1
2.49	0.078	0.002	2.88E-03	1.26E-10	24.61	314.2	0.1
2.49	0.050	0.0004	3.99E-03	1.74E-10	24.61	495.60	0.03
2.49	0.029	0.002	4.95E-03	2.16E-10	24.61	836	3

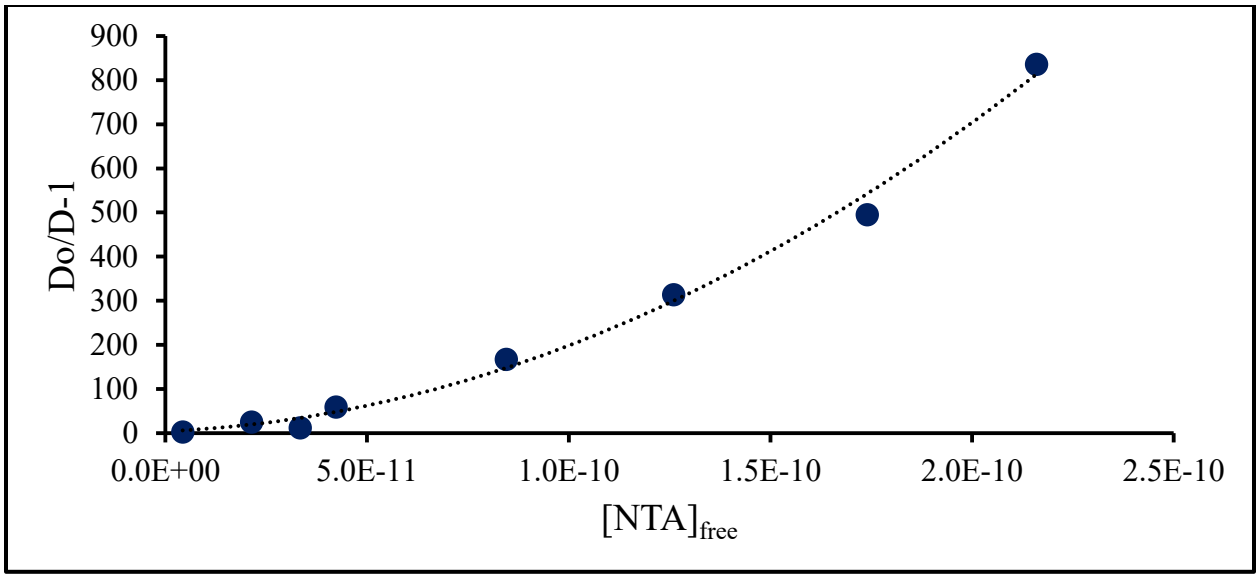

Figure D.44: Fit of Cf-NTA T = 35°C data

Table D.45: Cf-NTA T = 45° C Raw Data

pcH	D	D error	[NTA] (m)	$[NTA]_{free}$	Do	Do/D-1	Do/D error
2.49	5	1	9.79E-05	1.21E-11	85.57	18.0	0.9
2.49	0.64	0.01	4.88E-04	6.03E-11	85.57	133.10	0.03
2.49	1.13	0.05	7.66E-04	9.47E-11	85.57	74.5	0.2
2.49	0.248	0.006	9.71E-04	1.20E-10	85.57	344.2	0.2
2.49	0.088	0.002	1.94E-03	2.40E-10	85.57	970.8	0.5
2.49	0.047	0.003	2.88E-03	3.56E-10	85.57	1820	10
2.49	0.028	0.002	3.99E-03	4.93E-10	85.57	3030	13
2.49	0.023	0.002	4.95E-03	6.12E-10	85.57	3720	25

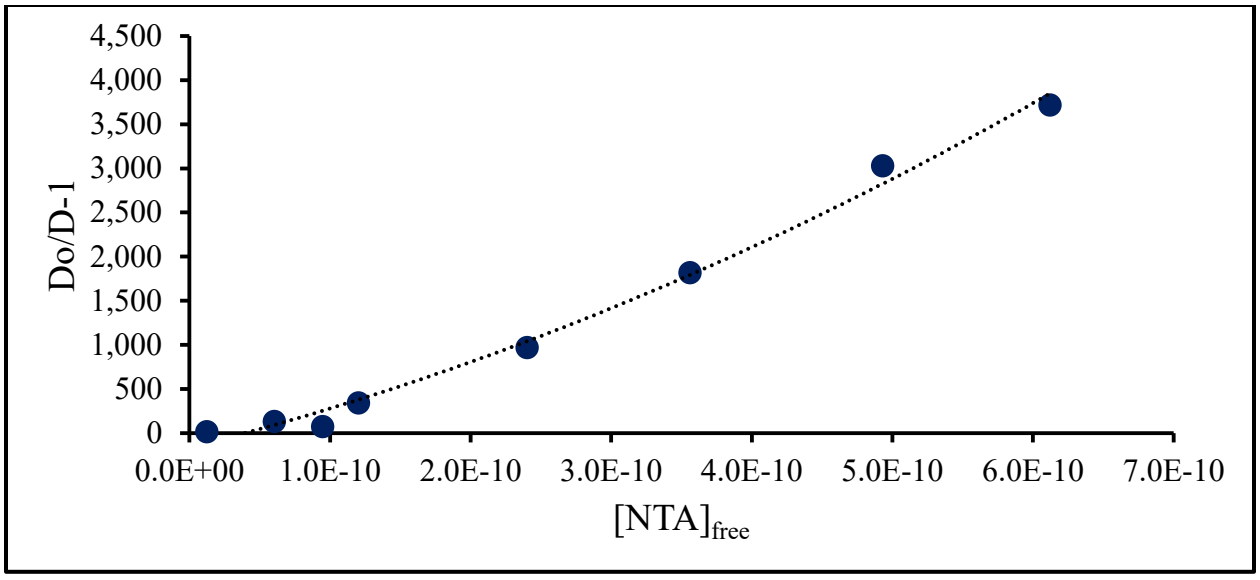

Figure D.45: Fit of Cf-NTA T = 45°C data

Table D.46: Cf-NTA T = 55° C Raw Data

pcH	D	D error	[NTA] (m)	$[NTA]_{free}$	Do	Do/D-1	Do/D error
2.49	4.1	0.3	9.79E-05	1.59E-11	78.51	18.3	0.1
2.49	0.46	0.04	4.88E-04	7.96E-11	78.51	169	1
2.49	0.87	0.03	7.66E-04	1.25E-10	78.51	89.10	0.07
2.49	0.209	0.008	9.71E-04	1.58E-10	78.51	374.6	0.5
2.49	0.076	0.002	1.94E-03	3.16E-10	78.51	1037.5	0.7
2.49	0.044	0.003	2.88E-03	4.70E-10	78.51	1780	8
2.49	0.029	0.002	3.99E-03	6.50E-10	78.51	2750	11
2.49	0.021	0.001	4.95E-03	8.07E-10	78.51	3790	11

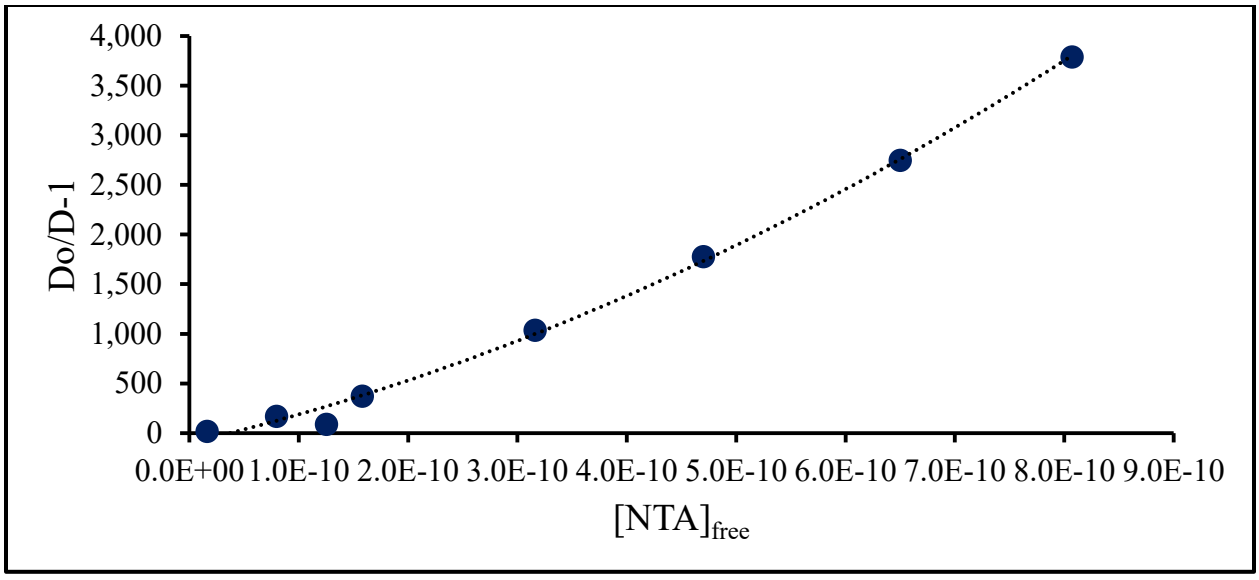

Figure D.46: Fit of Cf-NTA T = 55°C data

D.8 Californium-HEDTA

Table D.47: Cf-HEDTA T = 15° C Raw Data

pcH	D	D error	[HEDTA] (m)	$[HEDTA]_{free}$	Do	Do/D-1	Do/D error
2.51	19	4	1.03E-04	1.76E-15	966.97	50	2
2.39	12	3	2.49E-04	2.02E-15	409.90	34	2
2.46	7	2	5.07E-04	6.51E-15	692.57	101	6
2.57	5	1	7.52E-04	1.82E-14	1450.2	320	16
2.37	3	1	1.00E-03	7.31E-15	363.84	110	12
2.39	1.2	0.2	2.96E-03	2.39E-14	409.90	352	6
2.34	0.73	0.02	5.03E-03	3.06E-14	297.10	403.8	0.4
2.37	0.49	0.03	7.90E-03	5.88E-14	372.62	766	3

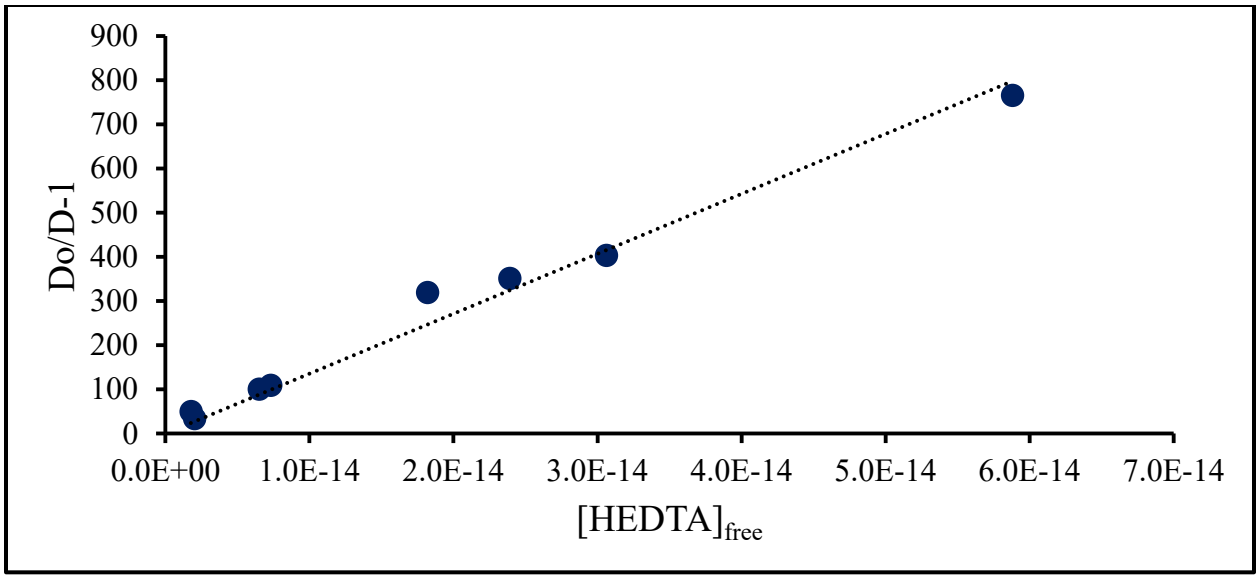

Figure D.47: Fit of Cf-HEDTA T = 15°C data

Table D.48: Cf-HEDTA T = 25 ° C Raw Data

pcH	D	D error	[HEDTA] (m)	$[HEDTA]_{free}$	Do	Do/D-1	Do/D error
2.51	2	6	1.03E-04	2.94E-15	791.09	33	3
2.39	8	2	2.49E-04	6.70E-15	335.35	40	2
2.46	4.2	0.2	5.07E-04	1.62E-14	566.60	134.5	0.2
2.57	2.8	0.1	7.52E-04	4.07E-14	1186.4	416	1
2.37	2.37	0.07	1.00E-03	2.43E-14	297.67	124.70	0.09
2.39	0.76	0.02	2.96E-03	3.98E-14	335.35	442.3	0.3
2.34	0.46	0.01	5.03E-03	4.06E-14	243.07	529.8	0.3
2.37	0.323	0.002	7.90E-03	6.97E-14	304.85	943.10	0.06

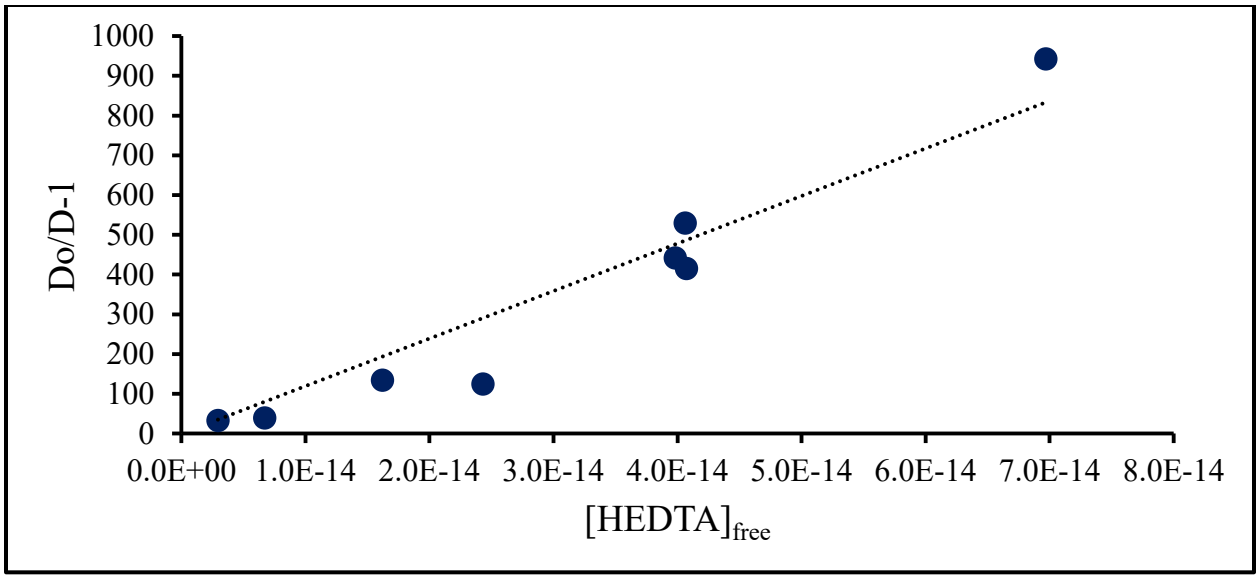

Figure D.48: Fit of Cf-HEDTA T = 25°C data

Table D.49: Cf-HEDTA T = 35° C Raw Data

pcH	D	D error	[HEDTA] (m)	$[HEDTA]_{free}$	Do	Do/D-1	Do/D error
2.51	18	2	1.03E-04	4.86E-15	655.69	35.9	0.4
2.39	6.9	0.4	2.49E-04	1.10E-14	277.95	39.1	0.1
2.46	3.7	0.1	5.07E-04	2.68E-14	469.62	126.1	0.2
2.57	2.3	0.1	7.52E-04	6.72E-14	983.36	418	1
2.37	1.76	0.03	1.00E-03	3.99E-14	246.72	139.60	0.05
2.39	0.55	0.02	2.96E-03	6.54E-14	277.95	508.5	0.5
2.34	0.342	0.007	5.03E-03	6.67E-14	201.46	588.5	0.2
2.37	0.245	0.002	7.90E-03	1.15E-13	252.67	1031.90	0.06

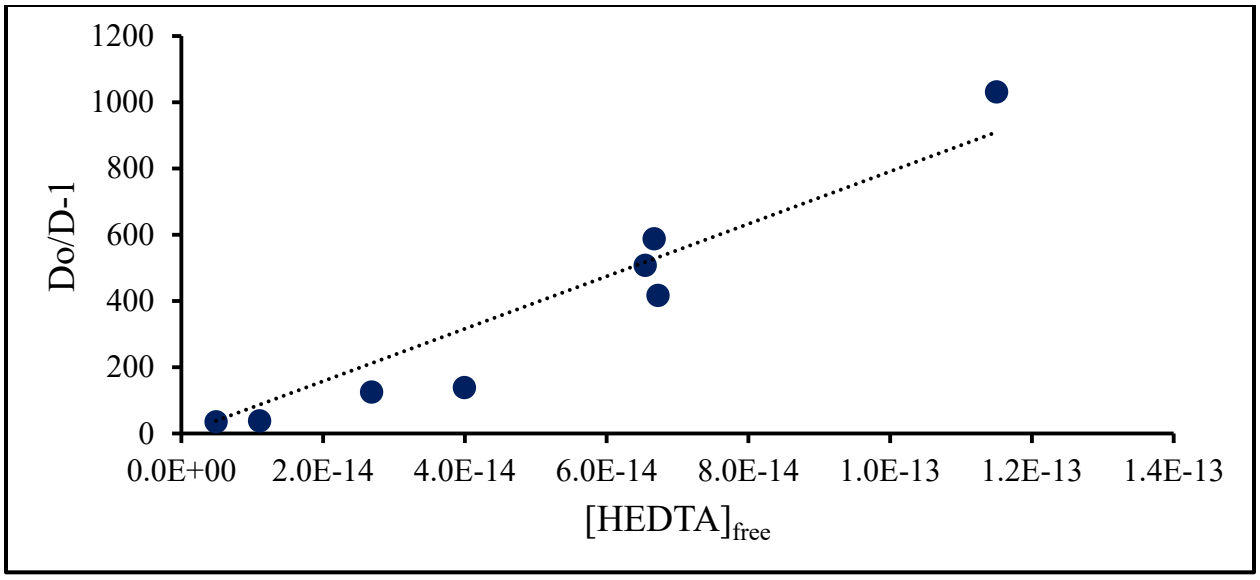

Figure D.49: Fit of Cf-HEDTA T = 35°C data

Table D.50: Cf-HEDTA T = 45° C Raw Data

pcH	D	D error	[HEDTA] (m)	$[HEDTA]_{free}$	Do	Do/D-1	Do/D error
2.51	10.7	0.7	1.03E-04	7.72E-15	549.92	50.5	0.2
2.39	4.4	0.2	2.49E-04	1.75E-14	233.11	51.60	0.07
2.46	2.40	0.03	5.07E-04	4.25E-14	393.86	163.20	0.02
2.57	1.66	0.02	7.52E-04	1.07E-13	824.72	496.70	0.06
2.37	1	1	1.00E-03	6.31E-14	206.92	150	160
2.39	0.372	0.006	2.96E-03	1.04E-13	233.11	626.3	0.2
2.34	0.227	0.003	5.03E-03	1.05E-13	168.96	742.2	0.1
2.37	0.166	0.002	7.90E-03	1.81E-13	211.91	1274.0	0.2

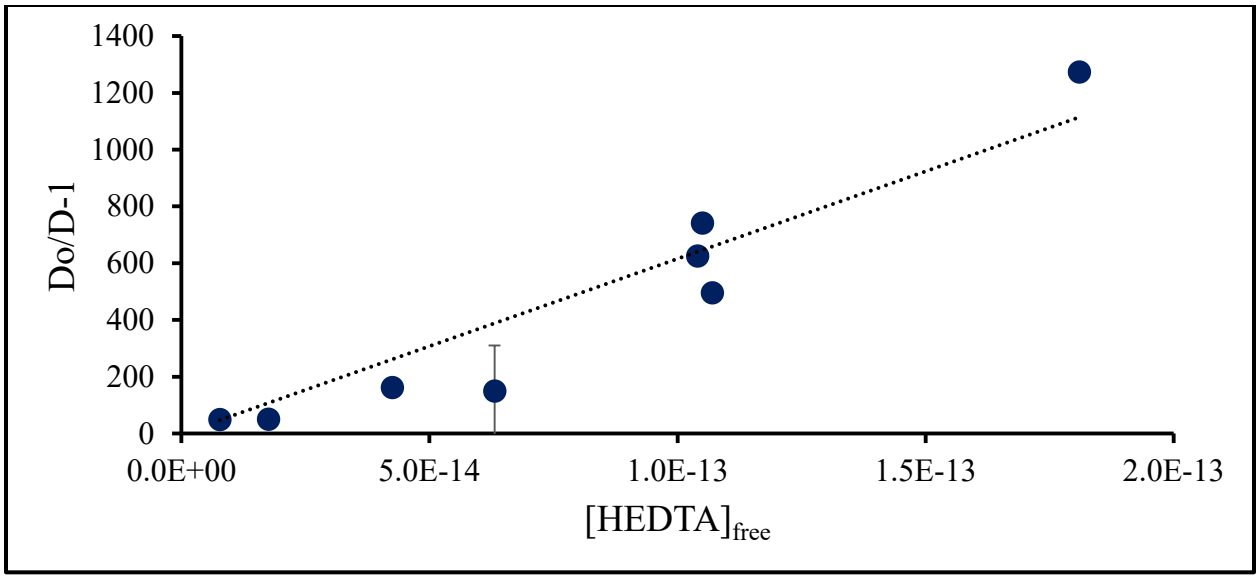

Figure D.50: Fit of Cf-HEDTA T = 45°C data

Table D.51: Cf-HEDTA T = 55° C Raw Data

pcH	D	D error	[HEDTA] (m)	$[HEDTA]_{free}$	Do	Do/D-1	Do/D error
2.51	10	2	1.03E-04	1.19E-14	465.37	43.6	0.9
2.39	3.2	0.1	2.49E-04	2.68E-14	197.27	60.60	0.07
2.46	1.72	0.07	5.07E-04	6.53E-14	333.31	193.0	0.3
2.57	1.09	0.04	7.52E-04	1.65E-13	697.93	640.3	0.8
2.37	0.877	0.009	1.00E-03	9.68E-14	175.11	198.70	0.02
2.39	0.284	0.009	2.96E-03	1.59E-13	197.27	694.1	0.7
2.34	0.168	0.009	5.03E-03	1.62E-13	142.99	850	2
2.37	0.131	0.005	7.90E-03	2.78E-13	179.33	1366	2

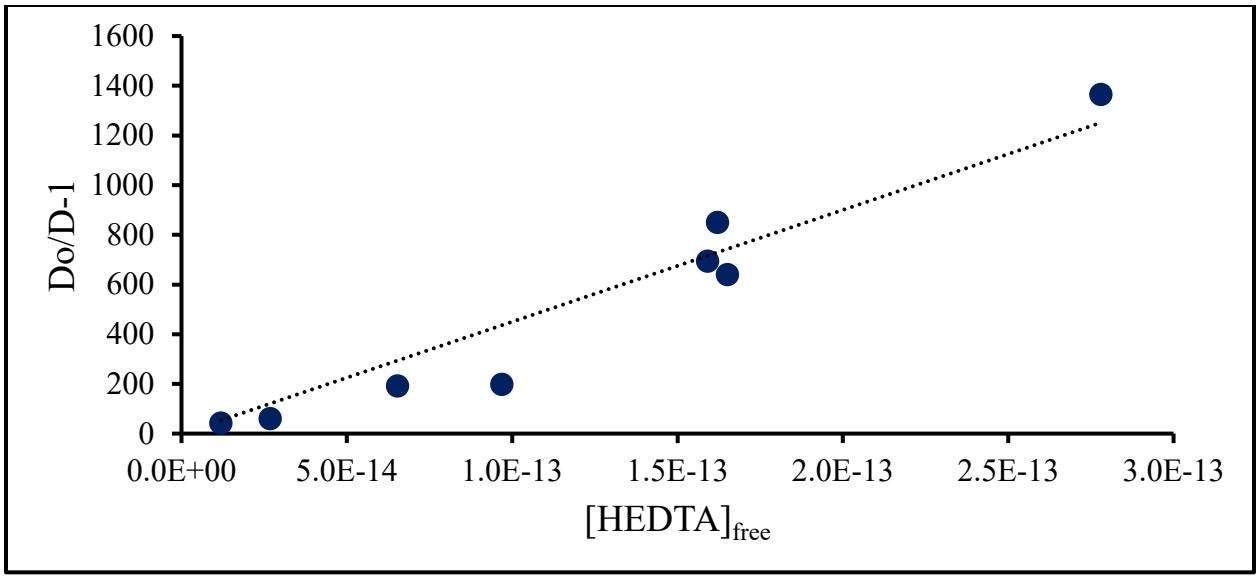

Figure D.51: Fit of Cf-HEDTA T = 55°C data

D.9 Californium-CDTA

Table D.52: Cf-CDTA T = 15° C Raw Data

pcH	D	D error	[CDTA] (m)	$[CDTA]_{free}$	Do	Do/D-1	Do/D error
2.27	33	2	1.01E-05	1.95E-20	24459	741	2
2.27	14	1	2.91E-05	5.60E-20	24459	1740	10
2.27	9.1	0.8	4.83E-05	9.31E-20	24459	2694	20
2.27	7.0	0.8	9.63E-05	1.85E-19	24459	3483	41
2.27	3.7	0.6	2.94E-04	5.67E-19	24459	6600	170
2.27	0.026	0.005	5.42E-04	1.04E-18	24459	937000	37000

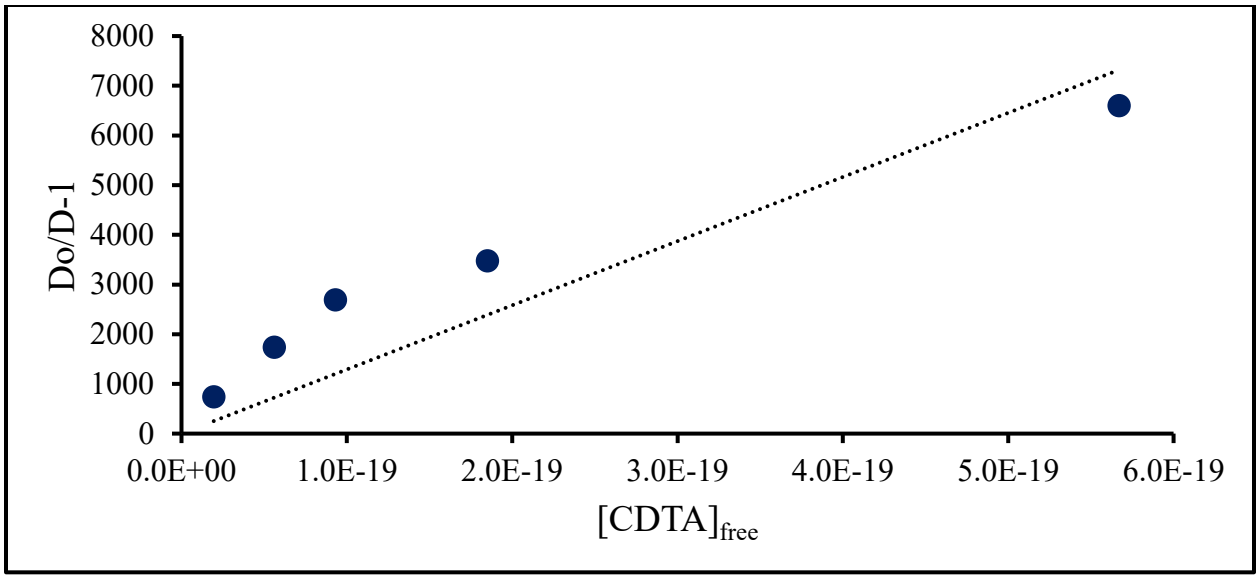

Figure D.52: Fit of Cf-CDTA T = 15°C data

Table D.53: Cf-CDTA T = 25° C Raw Data

pcH	D	D error	[CDTA] (m)	$[CDTA]_{free}$	Do	Do/D-1	Do/D error
2.27	21	1	1.01E-05	3.94E-20	20097	974	4
2.27	16.5	0.6	2.91E-05	1.13E-19	20097	1219	2
2.27	16.1	0.6	4.83E-05	1.88E-19	20097	1250	2
2.27	12	1	9.63E-05	3.75E-19	20097	1700	25
2.27	5.12	0.01	2.94E-04	1.15E-18	20097	3925.40	0.02
2.27	2.1	0.1	5.42E-04	2.11E-18	20097	9680	22

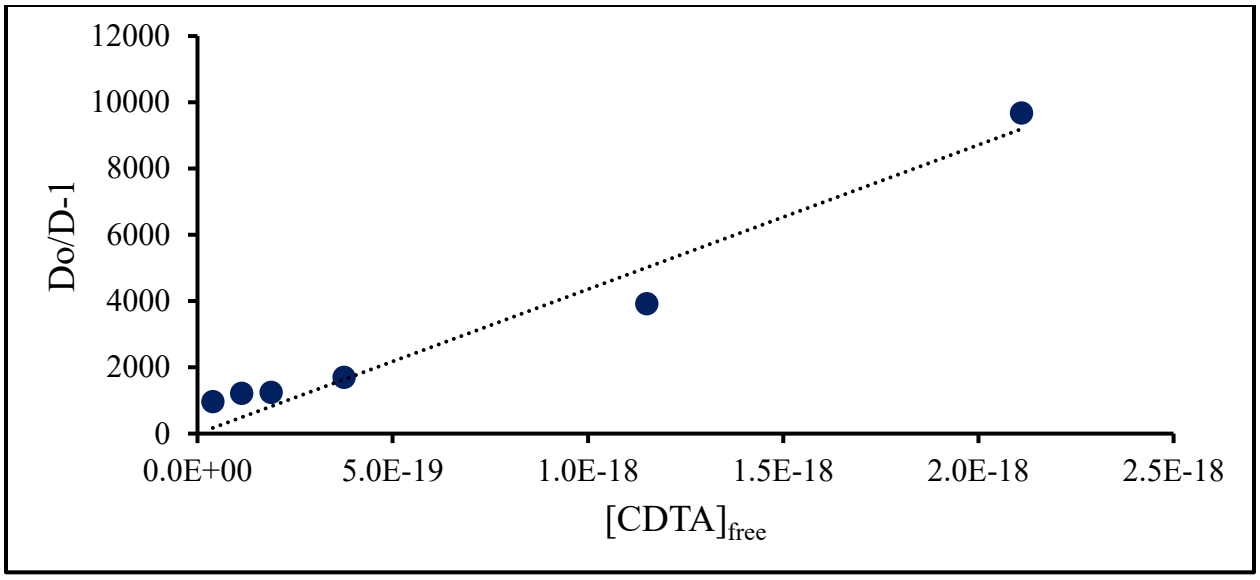

Figure D.53: Fit of Cf-CDTA T = 25°C data

Table D.54: T = 35° C Raw Data

pcH	D	D error	[CDTA] (m)	$[CDTA]_{free}$	Do	Do/D-1	Do/D error
2.30	410	90	1.01E-05	1.03E-19	2.17E+04	51.8	3
2.24	250	85	2.91E-05	2.05E-19	1.43E+04	56.7	7
2.25	71	60	4.83E-05	3.68E-19	1.55E+04	218.5	160
2.31	94	64	9.63E-05	1.00E-18	2.22E+04	234.2	110
2.35	13	5	2.94E-04	3.76E-18	2.96E+04	2216.6	320
3.26	0.038	0.005	5.42E-04	1.43E-17	1.62E+07	4250000	7500000

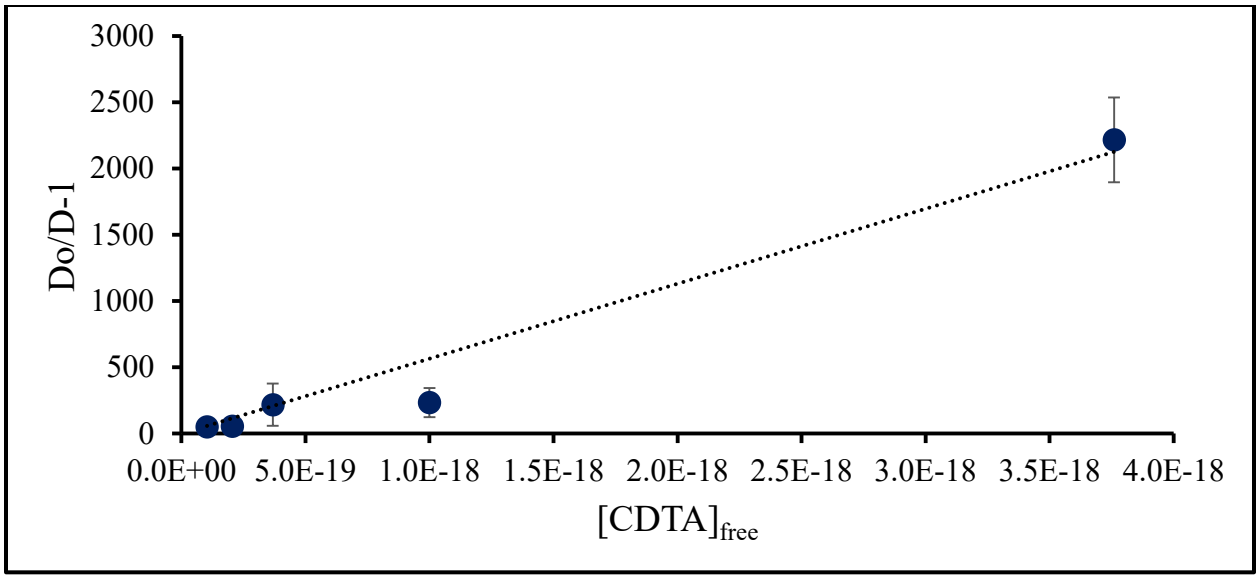

Figure D.54: Fit of Cf-CDTA T = 35°C data. Last point omitted for fit.

Table D.55: Cf-CDTA T = 45° C Raw Data

pcH	D	D error	[CDTA] (m)	$[CDTA]_{free}$	Do	Do/D-1	Do/D error
2.30	700	270	1.01E-05	1.92E-19	17652	24	4
2.24	230	120	2.91E-05	3.81E-19	11631	49	12
2.25	56	2	4.83E-05	6.86E-19	12643	223.3	0.4
2.31	26	5	9.63E-05	1.86E-18	18078	690	23
2.35	8.0	0.8	2.94E-04	6.97E-18	24066	3000	27
3.26	0.039	0.009	5.42E-04	2.63E-17	1.32E+07	3.38E+08	1.70E+07

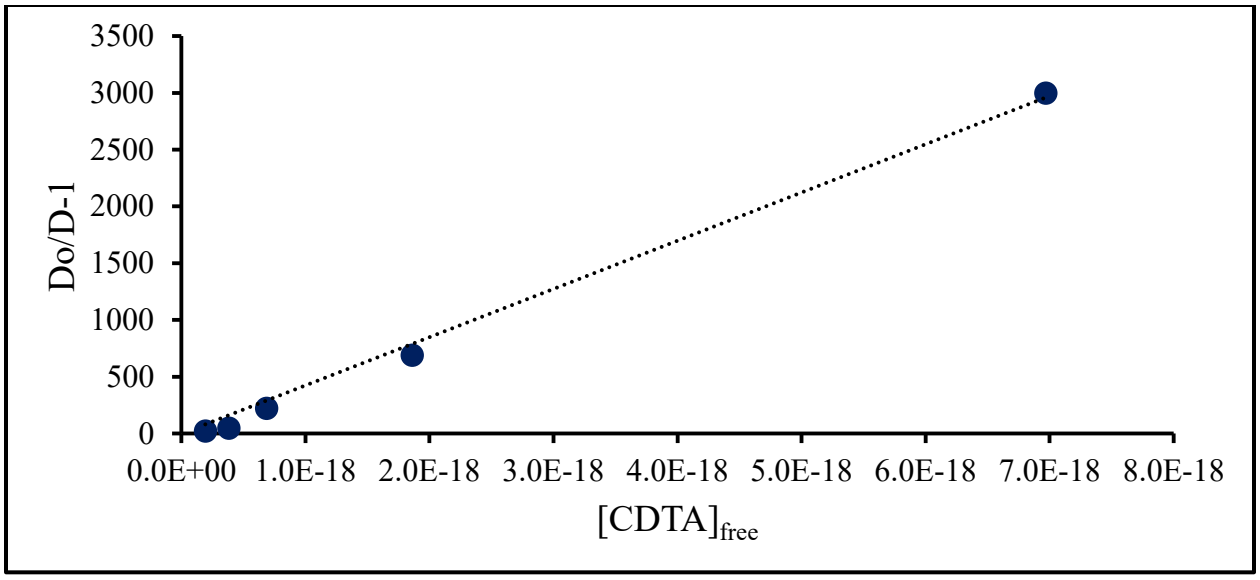

Figure D.55: Fit of Cf-CDTA T = 45°C data. Last point omitted for fit.

Table D.56: Cf-CDTA T = 55° C Raw Data

pcH	D	D error	[CDTA] (m)	$[CDTA]_{free}$	Do	Do/D-1	Do/D error
2.30	360	72	1.01E-05	3.50E-19	14941	40	2
2.24	230	61	2.91E-05	6.98E-19	9844	42	3
2.25	87	7	4.83E-05	1.26E-18	10701	122.5	0.7
2.31	19	7	9.63E-05	3.39E-18	15302	800	130
2.35	7	5	2.94E-04	1.27E-17	20370	2700	1120
3.26	0.044	0.001	5.42E-04	4.73E-17	1.11E+07	2.56E+08	163000

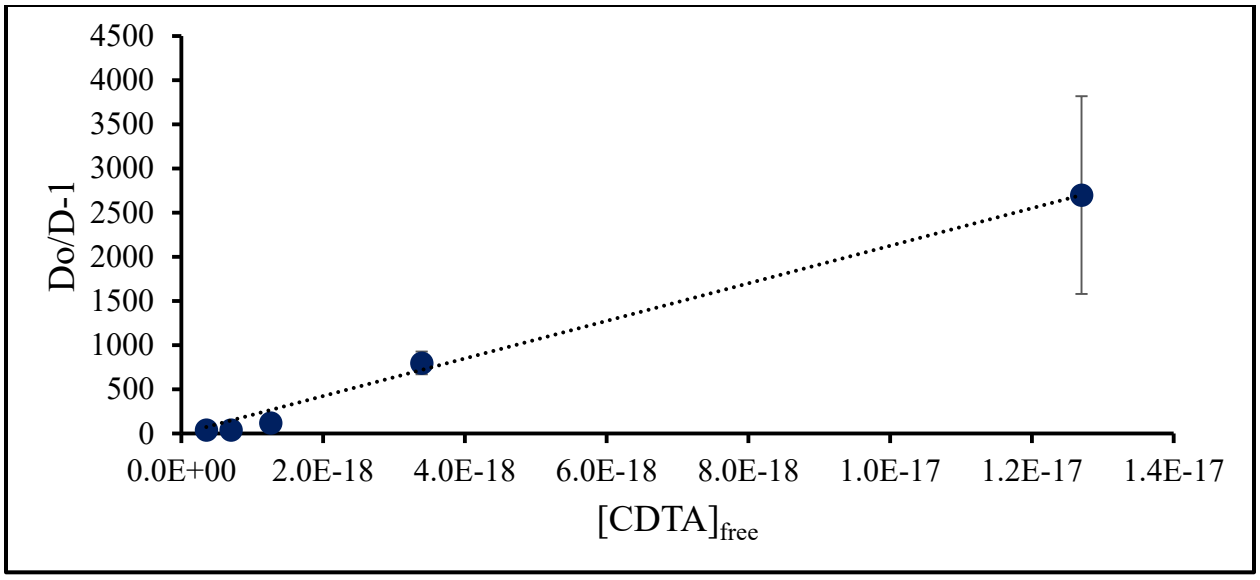

Figure D.56: Fit of Cf-CDTA T = 55°C data. Last point omitted for fit.

D.10 Californium-DTPA

Table D.57: Cf-DTPA T = 25° C pcH = 2.5

pcH	D	D error	[DPTA] (m)	$[DPTA]_{free}$	Do	Do/D-1	Do/D error
2.55	1.3	0.6	9.88E-05	7.86E-20	142380	110000	21000
2.55	0.5	0.2	2.96E-04	2.35E-19	142380	300000	74000
2.55	0.24	0.02	4.88E-04	3.88E-19	142380	597000	5000
2.55	0.23	0.08	6.84E-04	5.44E-19	142380	630000	84000
2.55	0.150	0.004	1.02E-03	8.08E-19	142380	951900	800

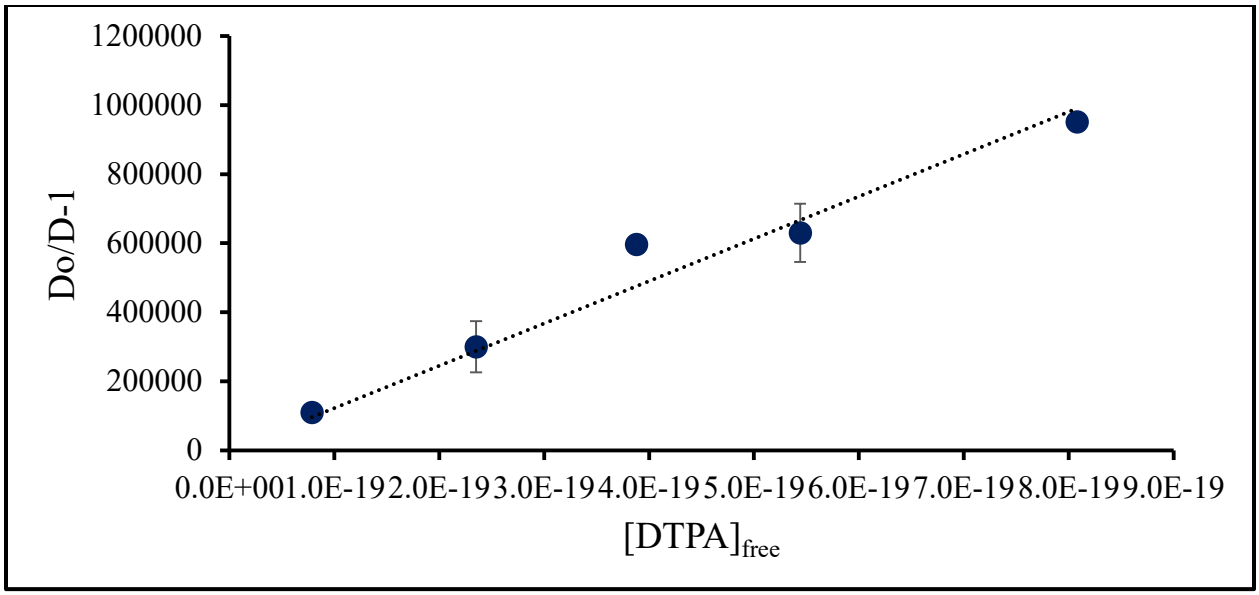

Figure D.57: Fit of Cf-DTPA T = 25°C, pcH = 2.5 data

Table D.58: Cf-DTPA T = 25° C pcH = 2.3

pcH	D	D error	[DPTA] (m)	$[DPTA]_{free}$	Do	Do/D-1	Do/D error
2.29	4.31	0.06	9.82E-05	7.03E-21	23630	5487.9	0.9
2.29	1.25	0.07	2.97E-04	2.13E-20	23630	18970	70
2.29	0.92	0.03	5.18E-04	3.71E-20	23630	25720	20
2.29	0.530	0.007	7.03E-04	5.03E-20	23630	44572	8
2.29	0.40	0.01	1.02E-03	7.28E-20	23630	58660	50

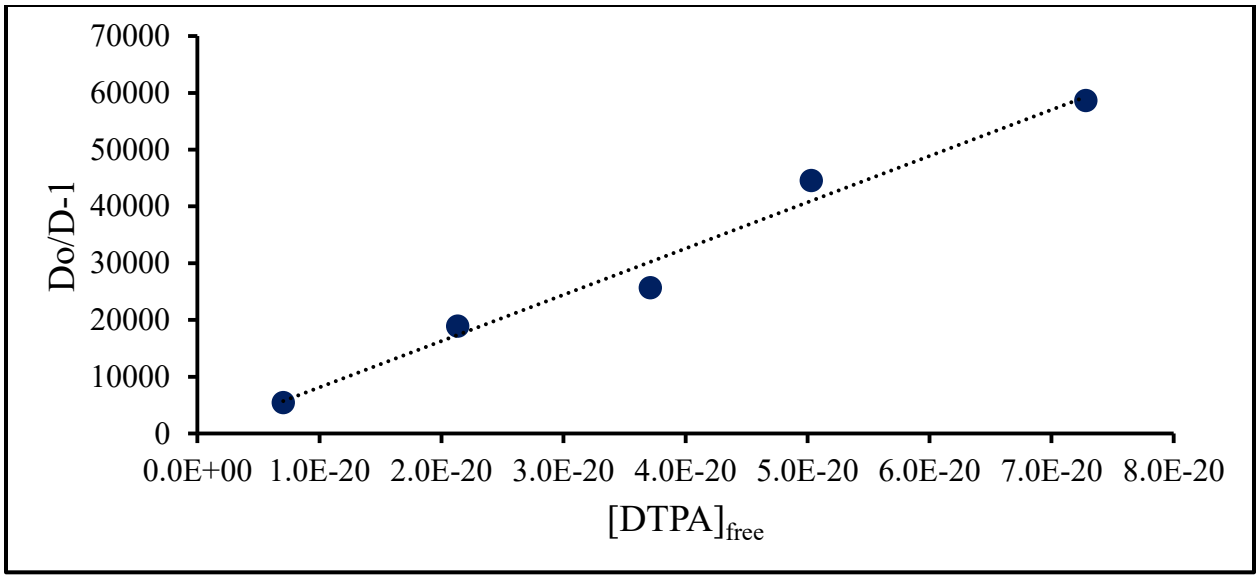

Figure D.58: Fit of Cf-DTPA T = 25°C, pcH = 2.3 data

Table D.59: Cf-DTPA T = 25° C pcH = 2.1

pcH	D	D error	[DPTA] (m)	$[DPTA]_{free}$	Do	Do/D-1	Do/D error
2.12	6.81	0.09	1.01E-04	7.03E-21	7302.3	1071.0	0.2
2.12	1.9	0.1	3.02E-04	2.13E-20	7302.3	3910	11
2.12	1.43	0.07	4.99E-04	3.71E-20	7302.3	5100	11
2.12	0.9	0.4	7.40E-04	5.03E-20	7302.3	8000	2000
2.12	0.75	0.01	1.00E-03	7.28E-20	7302.3	9708	3

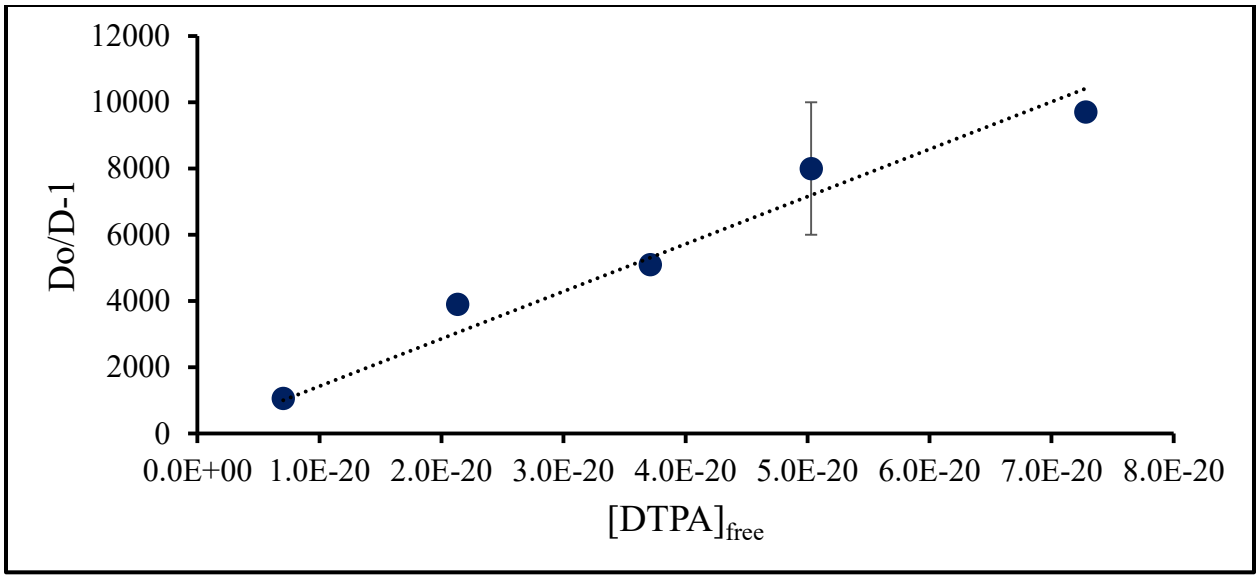

Figure D.59: Fit of Cf-DTPA T = 25°C, pcH = 2.1 data

Table D.60: Cf-DTPA T = 25° C pcH = 1.9

pcH	D	D error	[DPTA] (m)	$[DPTA]_{free}$	Do	Do/D-1	Do/D error
1.96	10.8	0.4	1.01E-04	2.40E-22	2418.0	222.3	0.3
1.96	3.28	0.02	3.03E-04	7.24E-22	2418.0	735.80	0.02
1.96	1.87	0.02	5.00E-04	1.19E-21	2418.0	1292.6	0.2
1.96	2.04	0.03	7.06E-04	1.69E-21	2418.0	1183.7	0.3
1.96	1.31	0.05	1.04E-03	2.48E-21	2418.0	1842	3

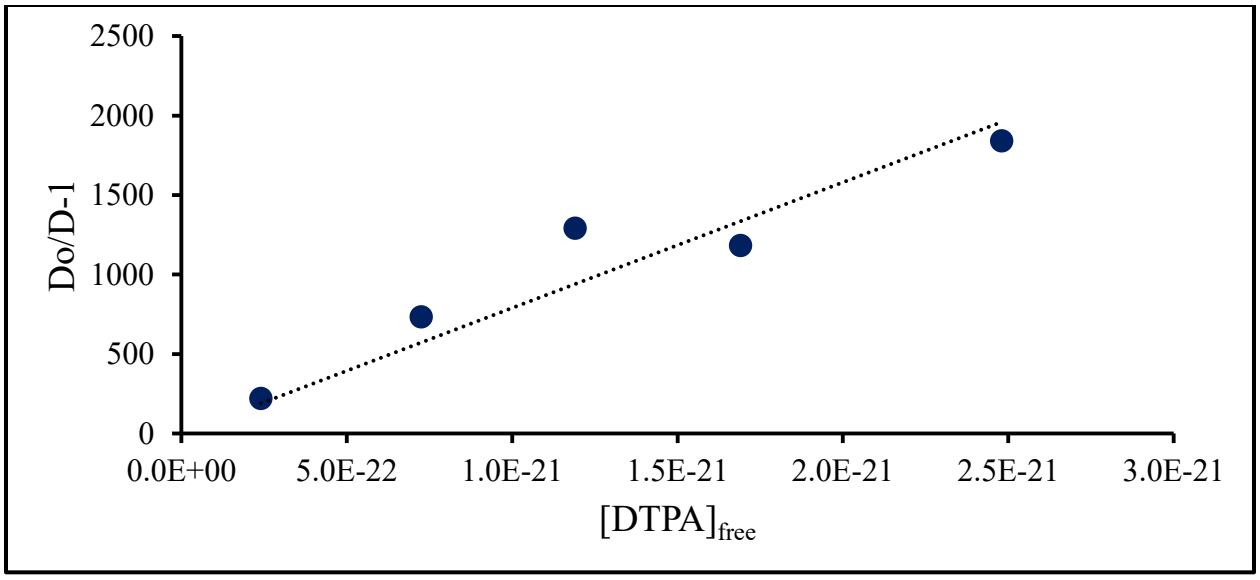

Figure D.60: Fit of Cf-DTPA T = 25°C, pcH = 1.9 data

Table D.61: Cf-DTPA T = 35° C pcH = 2.5

pcH	D	D error	[DPTA] (m)	$[DPTA]_{free}$	Do	Do/D-1	Do/D error
2.55	1.1	0.4	9.88E-05	1.67E-19	118010	100000	15000
2.55	0.22	0.04	2.96E-04	5.00E-19	118010	540000	20000
2.55	0.12	0.06	4.88E-04	8.24E-19	118010	990000	260000
2.55	0.09	0.09	6.84E-04	1.16E-18	118010	1300000	1200000
2.55	0.09	0.02	1.02E-03	1.71E-18	118010	1250000	30000

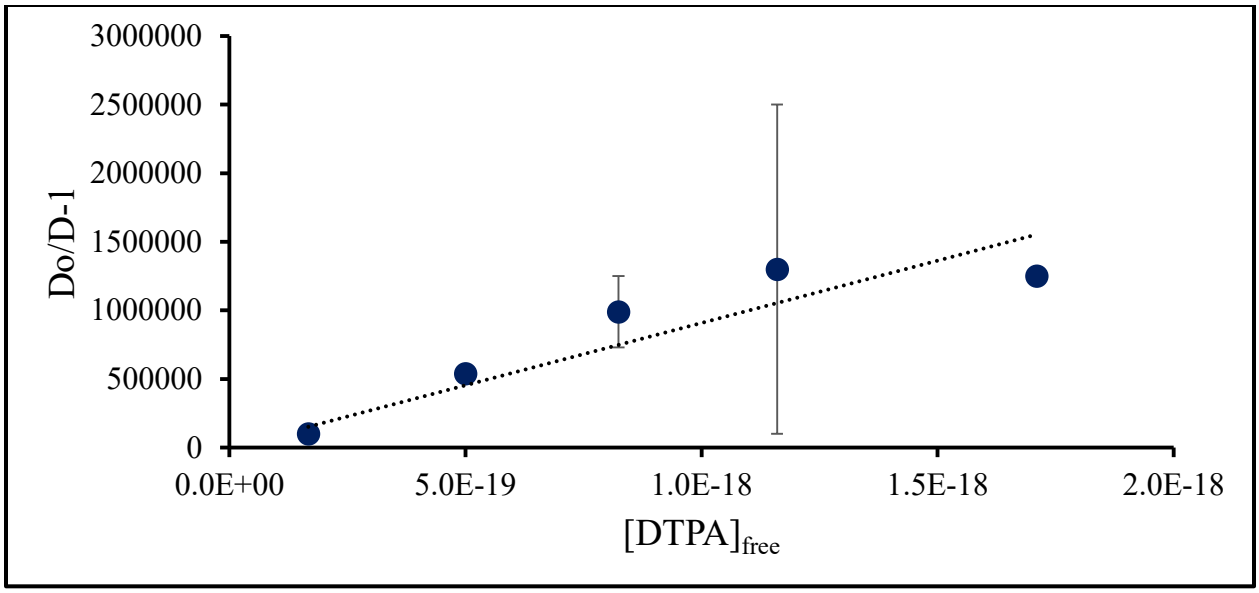

Figure D.61: Fit of Cf-DTPA T = 35°C, pcH = 2.5 data

Table D.62: Cf-DTPA T = 35° C pcH = 2.3

pcH	D	D error	[DPTA] (m)	$[DPTA]_{free}$	Do	Do/D-1	Do/D error
2.29	5.06	0.02	9.82E-05	1.49E-20	19585	3870.70	0.08
2.29	1.57060	0.00005	2.97E-04	4.51E-20	19585	12468.700	0.001
2.29	1.135	0.004	5.18E-04	7.86E-20	19585	17256.1	0.2
2.29	0.641	0.008	7.03E-04	1.07E-19	19585	30561	4
2.29	0.48	0.02	1.02E-03	1.54E-19	19585	41010	64

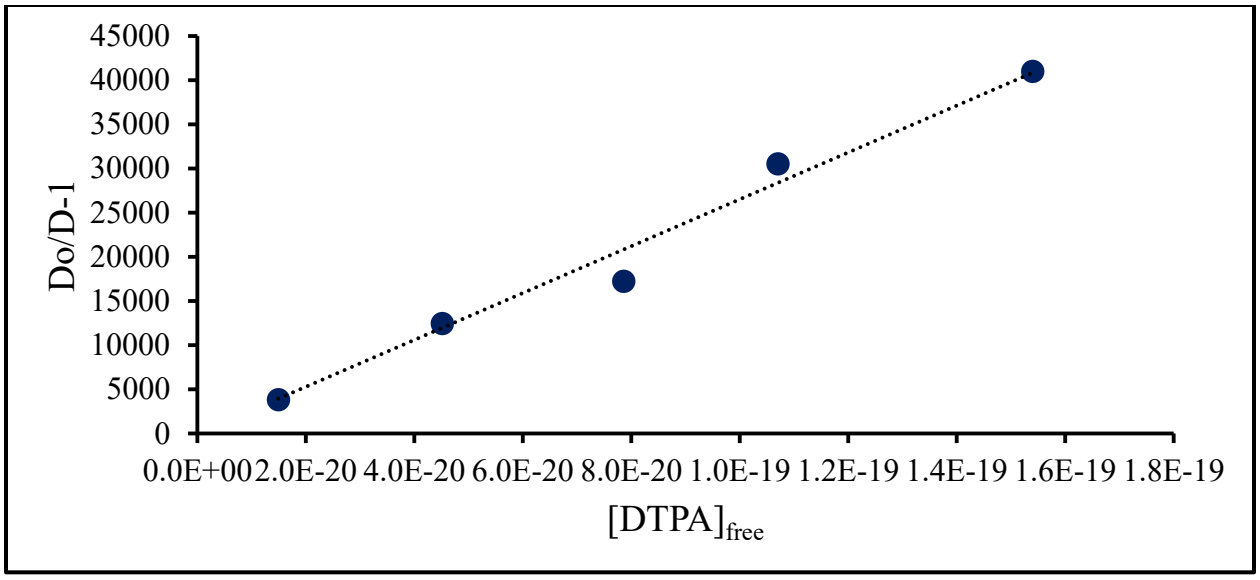

Figure D.62: Fit of Cf-DTPA T = 35°C, pcH = 2.3 free

Table D.63: Cf-DTPA T = 35° C pcH = 2.1

pcH	D	D error	[DPTA] (m)	$[DPTA]_{free}$	Do	Do/D-1	Do/D error
2.12	8.3	0.2	1.01E-04	2.80E-21	6052.4	730.7	0.3
2.12	2.1	0.1	3.02E-04	8.34E-21	6052.4	2821	6
2.12	1.907	0.005	4.99E-04	1.38E-20	6052.4	3172.90	0.02
2.12	1.40	0.05	7.40E-04	2.04E-20	6052.4	4335	6
2.12	0.90	0.02	1.00E-03	2.77E-20	6052.4	6717	4

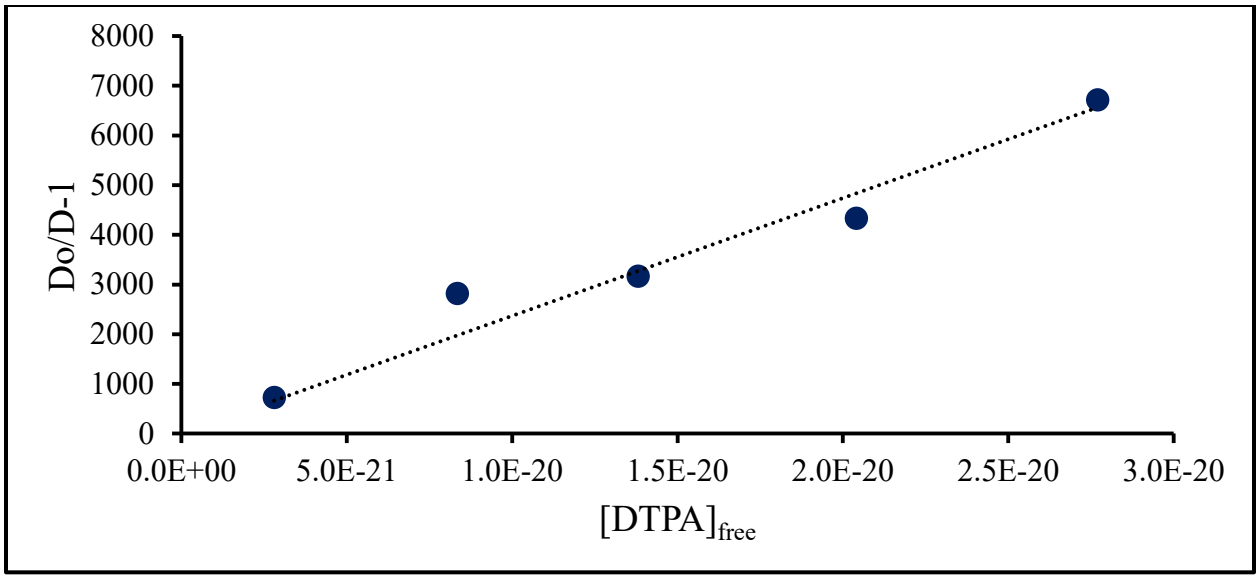

Figure D.63: Fit of Cf-DTPA T = 35°C, pcH = 2.1 data

Table D.64: Cf-DTPA T = 35° C pcH = 1.9

pcH	D	D error	[DPTA] (m)	$[DPTA]_{free}$	Do	Do/D-1	Do/D error
1.96	12.9	0.9	1.01E-04	5.07E-22	2004.2	154.3	0.7
1.96	3.98	0.04	3.03E-04	1.53E-21	2004.2	502.10	0.04
1.96	2.41	0.06	5.00E-04	2.52E-21	2004.2	829.9	0.4
1.96	2.47	0.07	7.06E-04	3.56E-21	2004.2	809.7	0.6
1.96	1.48	0.03	1.04E-03	5.24E-21	2004.2	1352.3	0.7

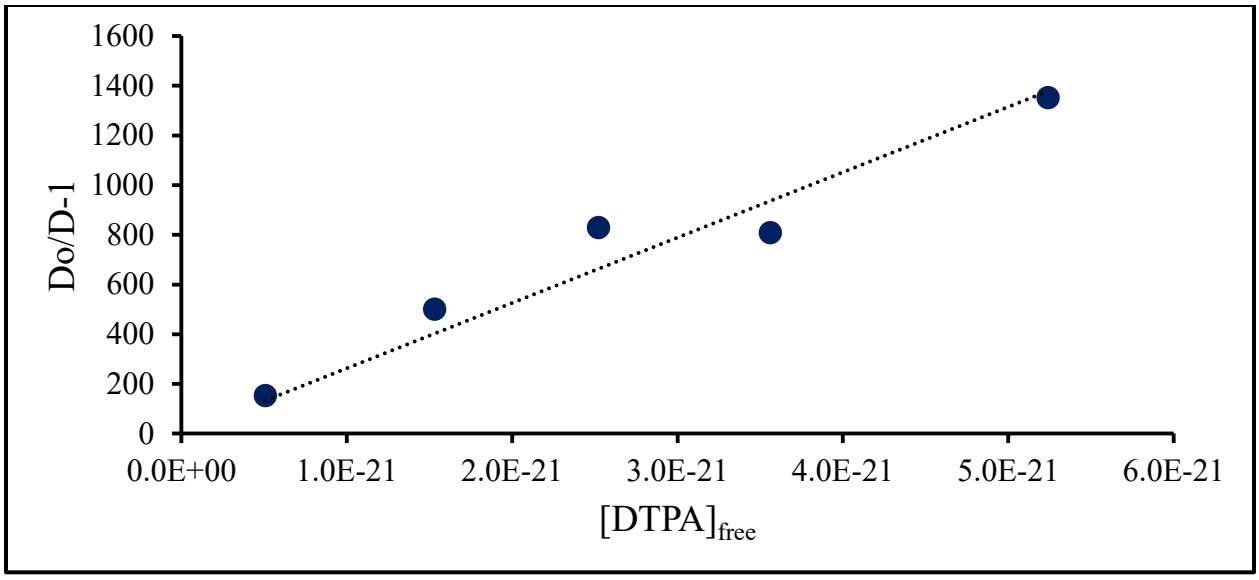

Figure D.64: Fit of Cf-DTPA T = 35°C, pcH = 1.9 data

Table D.65: Cf-DTPA T = 45° C pcH = 2.5

pcH	D	D error	[DPTA] (m)	$[DPTA]_{free}$	Do	Do/D-1	Do/D error
2.55	0.7	0.2	9.88E-05	3.33E-19	98975	150000	17000
2.55	0.11	0.07	2.96E-04	9.98E-19	98975	900000	300000
2.55	0.106	0.001	4.88E-04	1.64E-18	98975	938100	200
2.55	0.113	0.003	6.84E-04	2.31E-18	98975	873800	500
2.55	0.080	0.002	1.02E-03	3.42E-18	98975	1235900	600

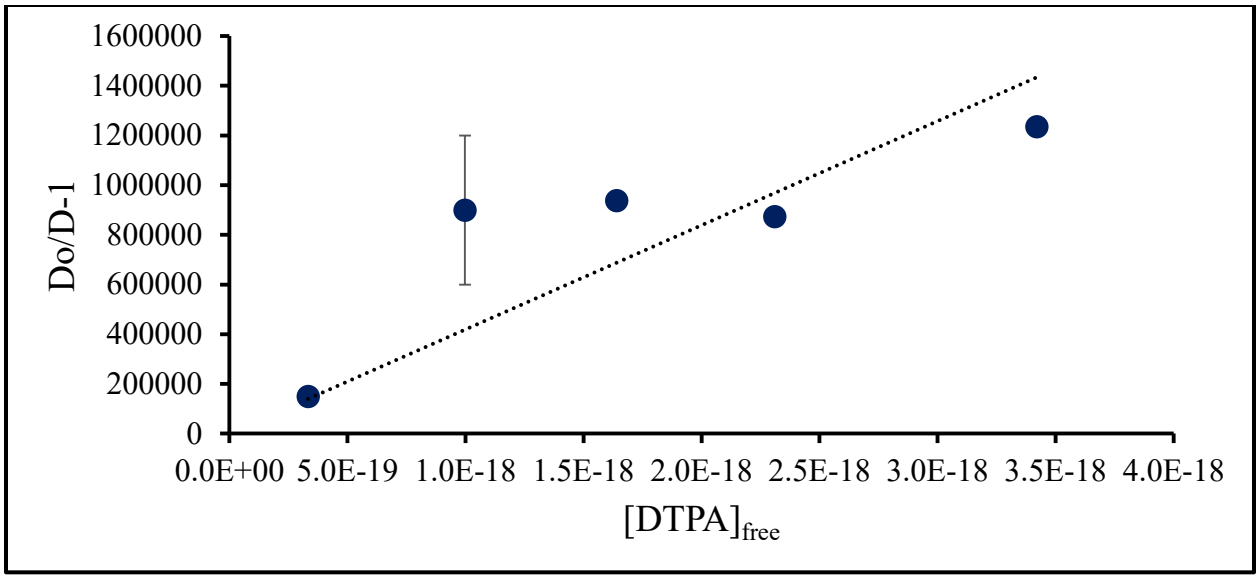

Figure D.65: Fit of Cf-DTPA T = 45°C, pcH = 2.5 data

Table D.66: Cf-DTPA T = 45° C pcH = 2.3

pcH	D	D error	[DPTA] (m)	$[DPTA]_{free}$	Do	Do/D-1	Do/D error
2.29	1.6	0.1	9.82E-05	2.97E-20	16425	10020	40
2.29	0.55	0.02	2.97E-04	8.98E-20	16425	29620	20
2.29	0.43	0.01	5.18E-04	1.57E-19	16425	38560	40
2.29	0.253	0.006	7.03E-04	2.13E-19	16425	64830	30
2.29	0.21	0.01	1.02E-03	3.08E-19	16425	77300	300

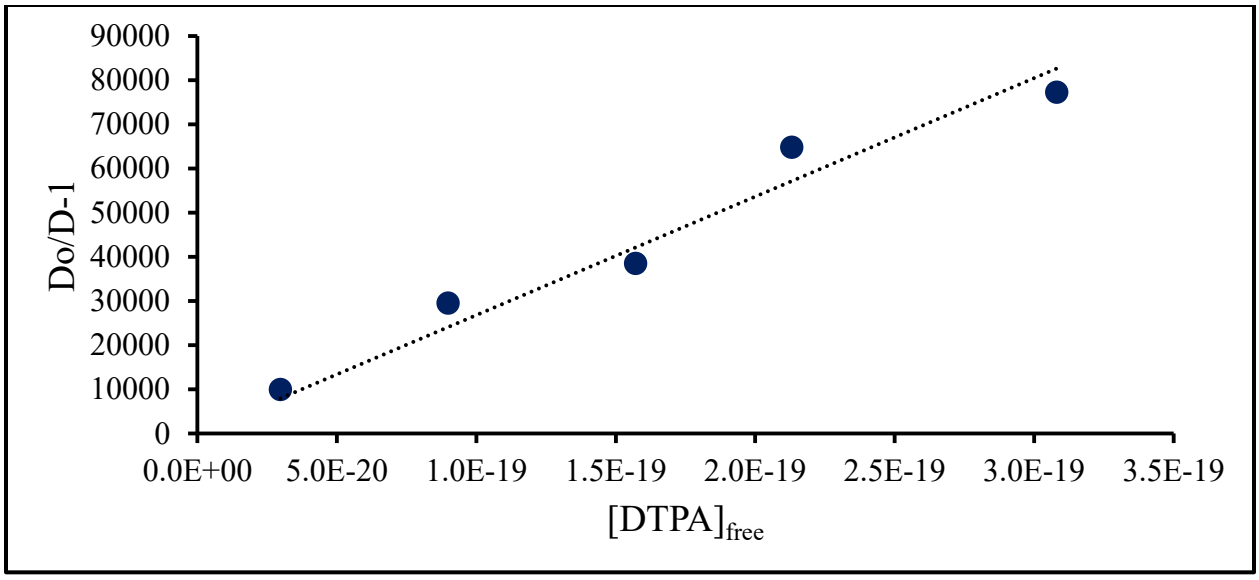

Figure D.66: Fit of Cf-DTPA T = 45°C, pcH = 2.3 data

Table D.67: Cf-DTPA T = 45° C pcH = 2.1

pcH	D	D error	[DPTA] (m)	$[DPTA]_{free}$	Do	Do/D-1	Do/D error
2.12	2.7	0.1	1.01E-04	5.58E-21	5076.1	1856	4
2.12	0.80	0.01	3.02E-04	1.66E-20	5076.1	6385	1
2.12	0.75	0.02	4.99E-04	2.74E-20	5076.1	6792	4
2.12	0.59	0.01	7.40E-04	4.06E-20	5076.1	8630	3
2.12	0.428	0.005	1.00E-03	5.50E-20	5076.1	11853	2

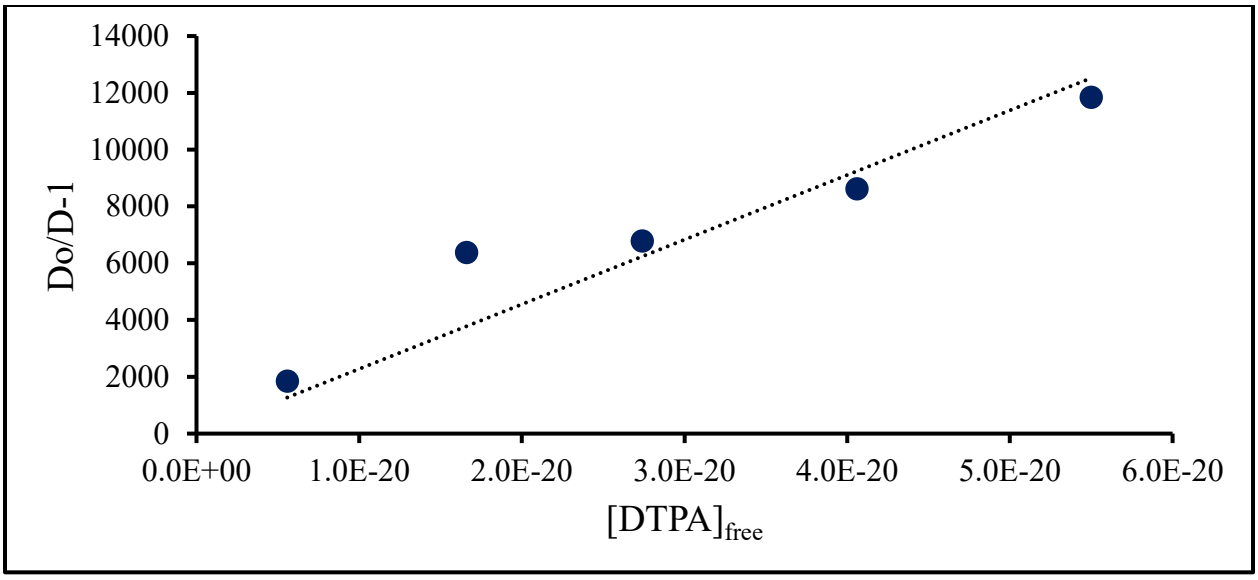

Figure D.67: Fit of Cf-DTPA T = 45°C, pcH = 2.1 data

Table D.68: Cf-DTPA T = 45° C pcH = 1.9

pcH	D	D error	[DPTA] (m)	$[DPTA]_{free}$	Do	Do/D-1	Do/D error
1.96	4.4	0.4	1.01E-04	1.01E-21	1680.8	380	3
1.96	1.46	0.1	3.03E-04	3.03E-21	1680.8	1151	5
1.96	0.91	0.06	5.00E-04	5.00E-21	1680.8	1844	8
1.96	1.17	0.07	7.06E-04	7.06E-21	1680.8	1442	6
1.96	0.73	0.01	1.04E-03	1.04E-20	1680.8	2294.8	0.8

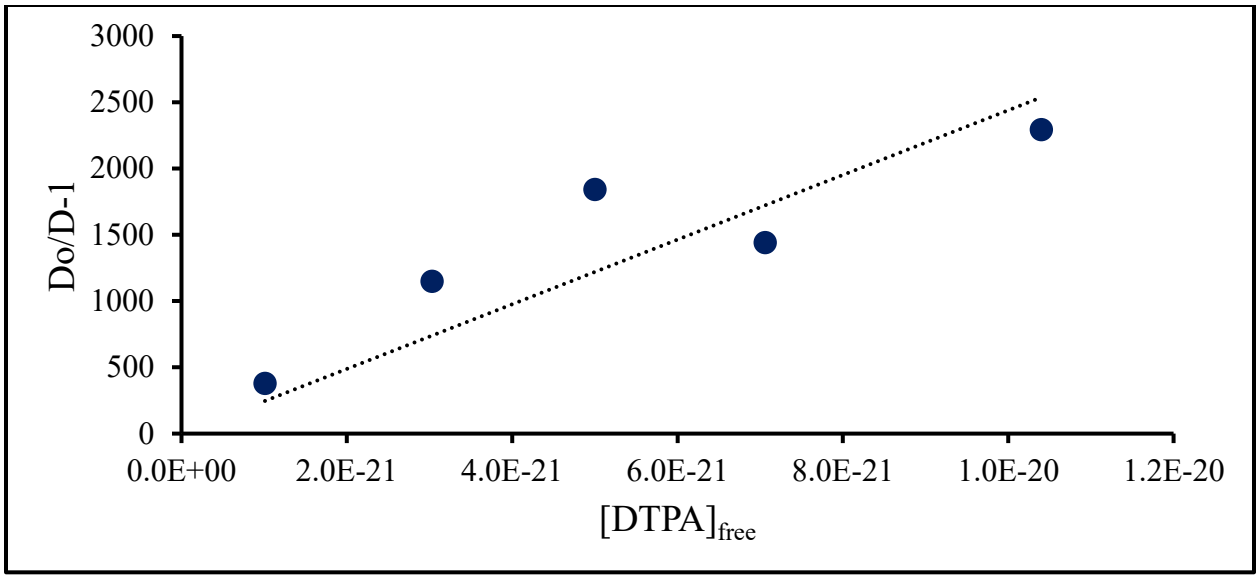

Figure D.68: Fit of Cf-DTPA T = 45°C, pcH = 1.9 data

Table D.69: Cf-DTPA T = 55° C pcH = 2.5

pcH	D	D error	[DPTA] (m)	$[DPTA]_{free}$	Do	Do/D-1	Do/D error
2.55	0.67	0.01	9.88E-05	6.48E-19	83904	125030	40
2.55	0.234	0.002	2.96E-04	1.94E-18	83904	359160	40
2.55	0.130	0.003	4.88E-04	3.20E-18	83904	645500	400
2.55	0.081	0.001	6.84E-04	4.49E-18	83904	1030200	300
2.55	0.053	0.002	1.02E-03	6.66E-18	83904	1572000	1300

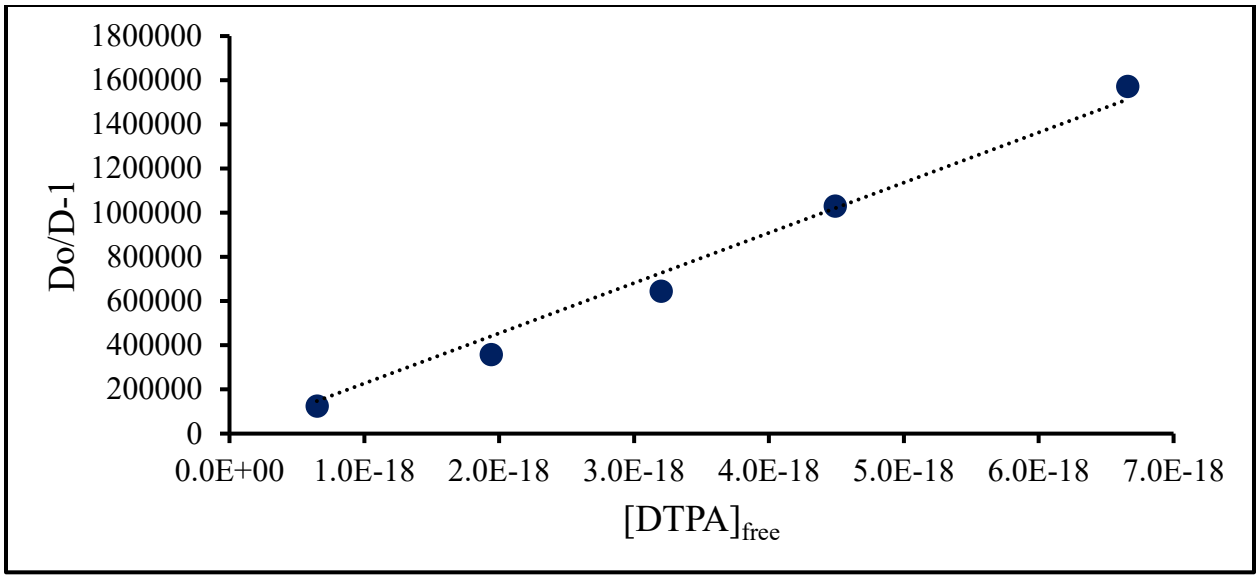

Figure D.69: Fit of Cf-DTPA T = 55°C, pcH = 2.5 data

Table D.70: Cf-DTPA T = 55° C pcH = 2.3

pcH	D	D error	[DPTA] (m)	$[DPTA]_{free}$	Do	Do/D-1	Do/D error
2.29	1.24	0.03	9.82E-05	5.79E-20	13924	11215	9
2.29	0.356	0.006	2.97E-04	1.75E-19	13924	39150	10
2.29	0.31	0.02	5.18E-04	3.05E-19	13924	44800	100
2.29	0.178	0.004	7.03E-04	4.14E-19	13924	78380	50
2.29	0.149	0.008	1.02E-03	5.99E-19	13924	93500	300

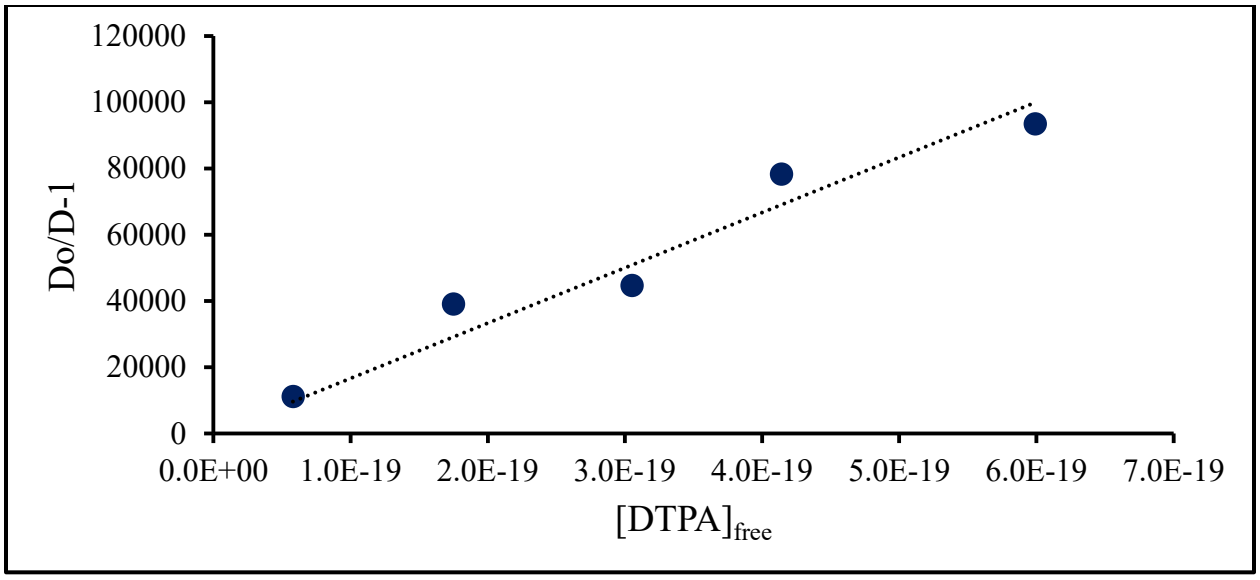

Figure D.70: Fit of Cf-DTPA T = 55°C, pcH = 2.3 data

Table D.71: Cf-DTPA T = 55° C pcH = 2.1

pcH	D	D error	[DPTA] (m)	$[DPTA]_{free}$	Do	Do/D-1	Do/D error
2.12	1.97	0.03	1.01E-04	1.08E-20	4303.1	2188.9	0.4
2.12	0.58	0.01	3.02E-04	3.23E-20	4303.1	7411	2
2.12	0.479	0.005	4.99E-04	5.33E-20	4303.1	8987	1
2.12	0.44	0.03	7.40E-04	7.90E-20	4303.1	9710	60
2.12	0.31	0.04	1.00E-03	1.07E-19	4303.1	14100	200

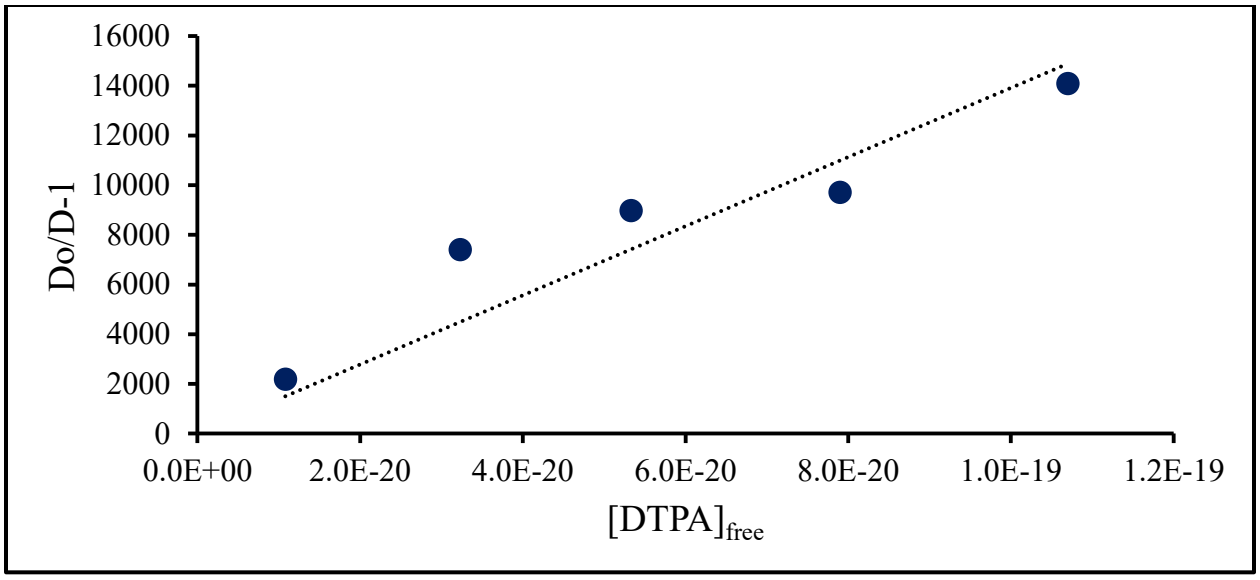

Figure D.71: Fit of Cf-DTPA T = 55°C, pcH = 2.1 data

Table D.72: Cf-DTPA T = 55° C pcH = 1.9

pcH	D	D error	[DPTA] (m)	$[DPTA]_{free}$	Do	Do/D-1	Do/D error
1.96	3.2	0.3	1.01E-04	1.95E-21	1424.9	446	5
1.96	1.1	0.1	3.03E-04	5.89E-21	1424.9	1330	10
1.96	0.67	0.04	5.00E-04	9.70E-21	1424.9	2121	9
1.96	0.8	0.1	7.06E-04	1.37E-20	1424.9	1720	20
1.96	0.52	0.06	1.04E-03	2.02E-20	1424.9	2730	40

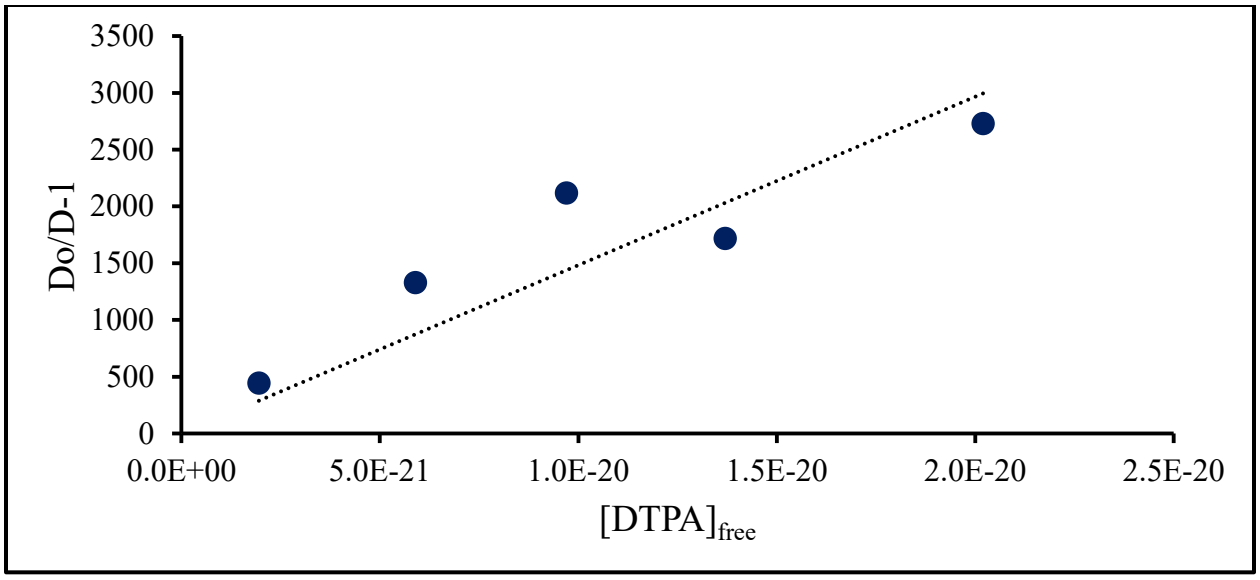

Figure D.72: Fit of Cf-DTPA T = 55°C, pcH = 1.9 data

D.11 Einsteinium-NTA

Table D.73: Es-NTA T = 15° C Raw Data

pcH	D	D error	[NTA] (m)	$[NTA]_{free}$	Do	Do/D-1	Do/D error
2.2	3.48	0.05	9.71E-04	7.75E-12	38.86	10.200	0.002
2.2	1.12	0.06	1.94E-03	1.55E-11	38.86	33.6	0.1
2.2	0.66	0.05	2.88E-03	2.30E-11	38.86	57.9	0.3
2.2	0.33	0.02	3.99E-03	3.18E-11	38.86	117.4	0.4
2.2	0.25	0.02	4.95E-03	3.95E-11	38.86	157	1

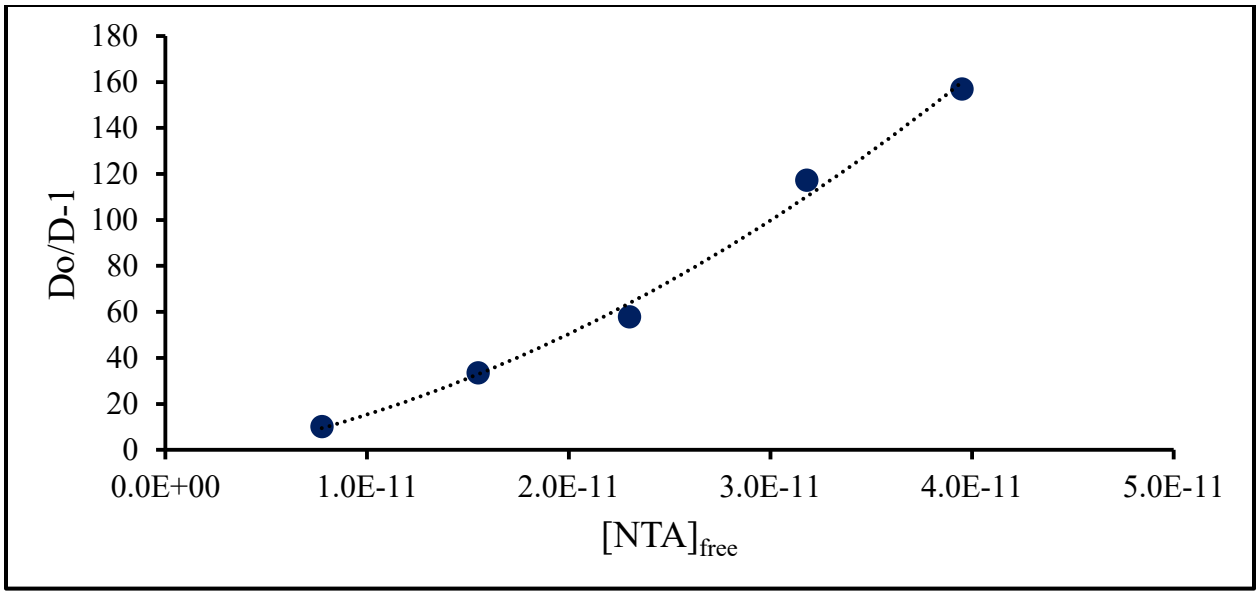

Figure D.73: Fit of Es-NTA T = 15°C data

Table D.74: Es-NTA T = 25° C Raw Data

pcH	D	D error	[NTA] (m)	$[NTA]_{free}$	Do	Do/D-1	Do/D error
2.2	1.7	0.1	9.71E-04	9.91E-12	29.34	16.20	0.06
2.2	0.54	0.03	1.94E-03	1.98E-11	29.34	53.0	0.1
2.2	0.31	0.02	2.88E-03	2.95E-11	29.34	91.5	0.4
2.2	0.17	0.01	3.99E-03	4.07E-11	29.34	175.3	0.9
2.2	0.10	0.01	4.95E-03	5.06E-11	29.34	282	5

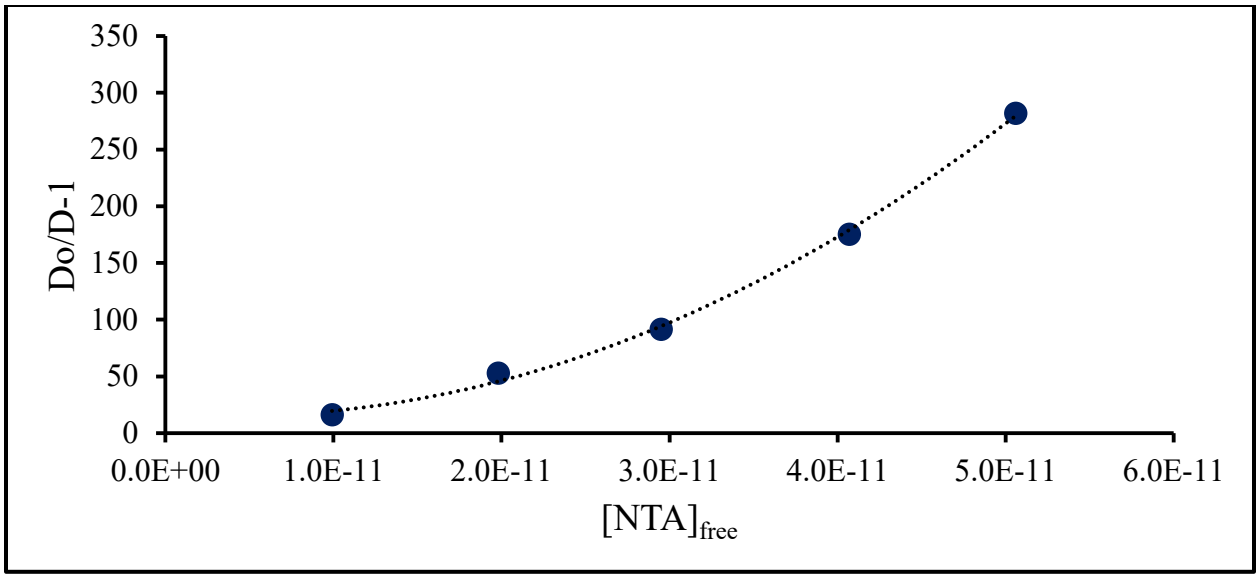

Figure D.74: Fit of Es-NTA T = 25°C data

Table D.75: Es-NTA T = 35° C Raw Data

pcH	D	D error	[NTA] (m)	$[NTA]_{free}$	Do	Do/D-1	Do/D error
2.2	0.982	0.008	9.71E-04	1.24E-11	24.24	23.700	0.002
2.2	0.349	0.006	1.94E-03	2.48E-11	24.24	68.40	0.02
2.2	0.18	0.02	2.88E-03	3.69E-11	24.24	131	2
2.2	0.10	0.01	3.99E-03	5.10E-11	24.24	244	3
2.2	0.072	0.006	4.95E-03	6.33E-11	24.24	337	2

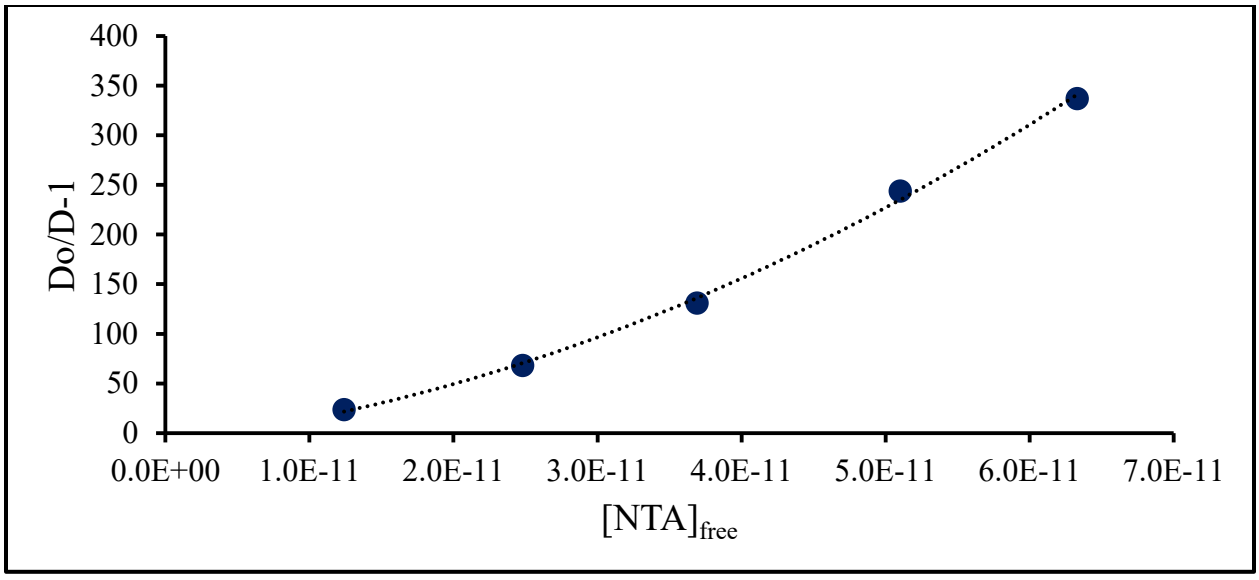

Figure D.75: Fit of Es-NTA T = 35°C data

Table D.76: Es-NTA T = 45° C Raw Data

pcH	D	D error	[NTA] (m)	$[NTA]_{free}$	Do	Do/D-1	Do/D error
2.2	1.00	0.05	9.71E-04	1.52E-11	19.28	18.20	0.05
2.2	0.320	0.007	1.94E-03	3.05E-11	19.28	59.20	0.03
2.2	0.17	0.01	2.88E-03	4.53E-11	19.28	111.1	0.5
2.2	0.10	0.02	3.99E-03	6.26E-11	19.28	198	5
2.2	0.056	0.006	4.95E-03	7.77E-11	19.28	343	4

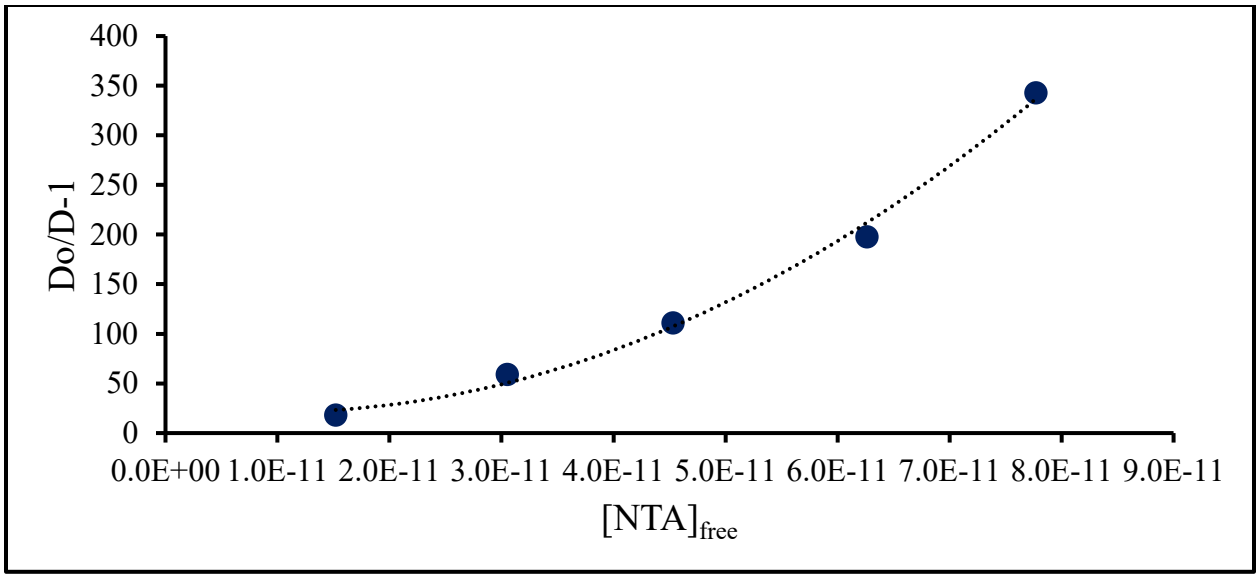

Figure D.76: Fit of Es-NTA T = 45°C data

Table D.77: Es-NTA T = 55° C Raw Data

pcH	D	D error	[NTA] (m)	$[NTA]_{free}$	Do	Do/D-1	Do/D error
2.2	0.44	0.04	9.71E-04	1.84E-11	15.68	34.6	0.3
2.2	0.141	0.007	1.94E-03	3.68E-11	15.68	110.3	0.3
2.2	0.09	0.02	2.88E-03	5.46E-11	15.68	174	7
2.2	0.050	0.005	3.99E-03	7.55E-11	15.68	315	3
2.2	0.039	0.002	4.95E-03	9.38E-11	15.68	398.0	0.8

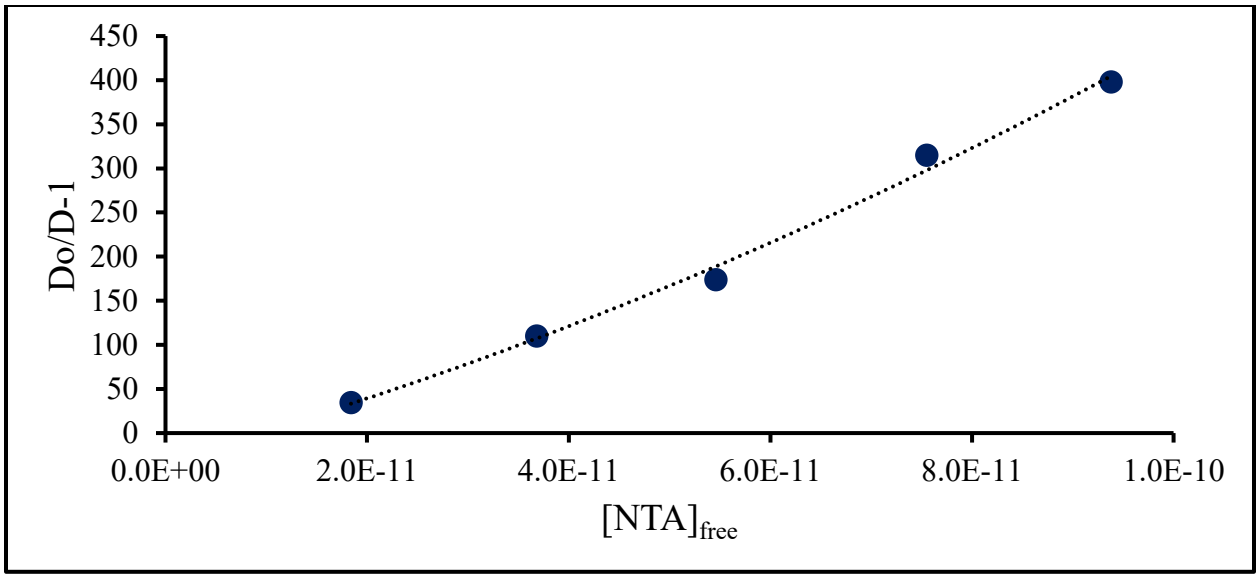

Figure D.77: Fit of Es-NTA T = 55°C data

D.12 Einsteinium-HEDTA

Table D.78: Es-HEDTA T = 15° C Raw Data

pcH	D	D error	[HEDTA] (m)	$[HEDTA]_{free}$	Do	Do/D-1	Do/D error
2.38	27	2	5.07E-04	3.90E-15	1512.3	55.2	0.3
2.38	14.7	0.6	1.00E-03	7.72E-15	1512.3	102.2	0.2
2.38	4.8	0.2	2.96E-03	2.28E-14	1512.3	316.3	0.4
2.38	2.9	0.3	5.03E-03	3.87E-14	1512.3	524	4
2.38	1.98	0.09	7.90E-03	6.08E-14	1512.3	765	2

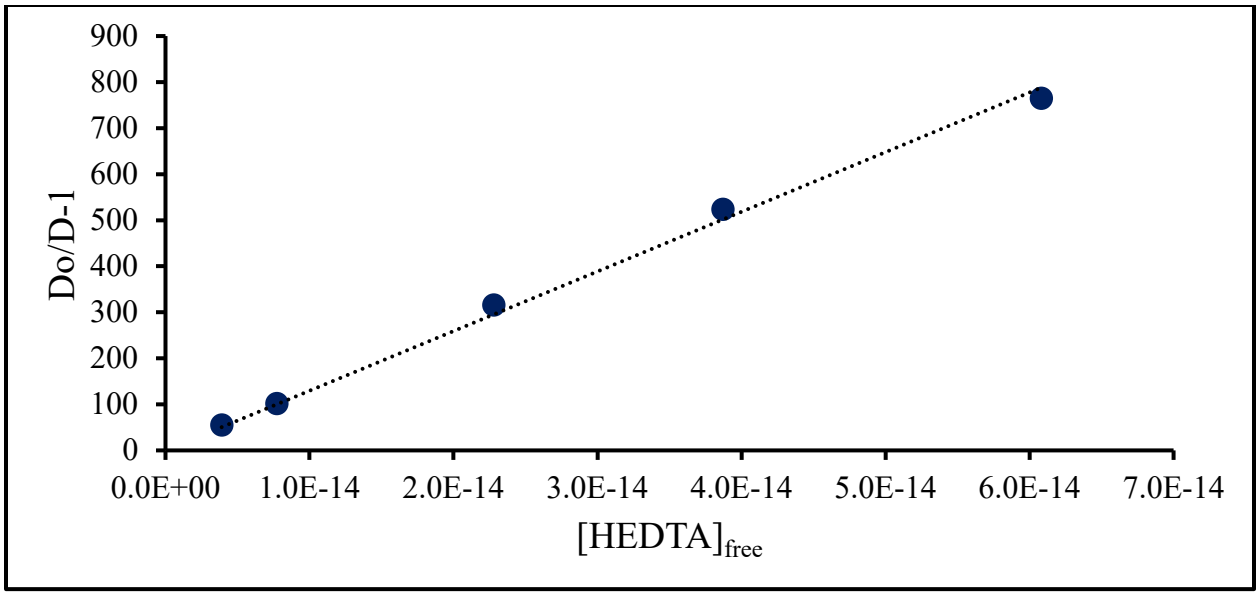

Figure D.78: Fit of Es-HEDTA T = 15°C data

Table D.79: Es-HEDTA T = 25° C Raw Data

pcH	D	D error	[HEDTA] (m)	$[HEDTA]_{free}$	Do	Do/D-1	Do/D error
2.38	11	1	5.07E-04	6.47E-15	1392.5	116	1
2.38	5.9	0.7	1.00E-03	1.28E-14	1392.5	237	4
2.38	2.3	0.2	2.96E-03	3.78E-14	1392.5	605	6
2.38	1.41	0.04	5.03E-03	6.42E-14	1392.5	985.5	0.8
2.38	0.98	0.04	7.90E-03	1.01E-13	1392.5	1416	2

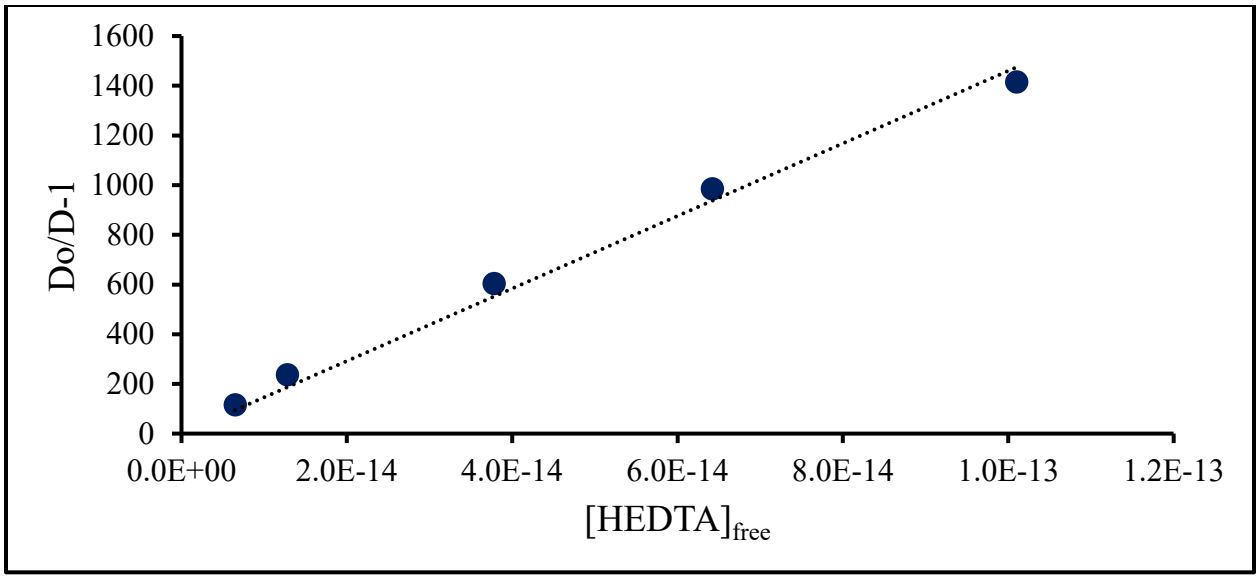

Figure D.79: Fit of Es-HEDTA T = 25°C data

Table D.80: Es-HEDTA T = 35° C Raw Data

pcH	D	D error	[HEDTA] (m)	$[HEDTA]_{free}$	Do	Do/D-1	Do/D error
2.38	8.4	0.5	5.07E-04	1.07E-14	987.59	116.4	0.5
2.38	4.25	0.07	1.00E-03	2.11E-14	987.59	231.30	0.07
2.38	1.49	0.05	2.96E-03	6.22E-14	987.59	660.1	0.8
2.38	0.92	0.03	5.03E-03	1.06E-13	987.59	1068	1
2.38	0.68	0.06	7.90E-03	1.66E-13	987.59	1460	11

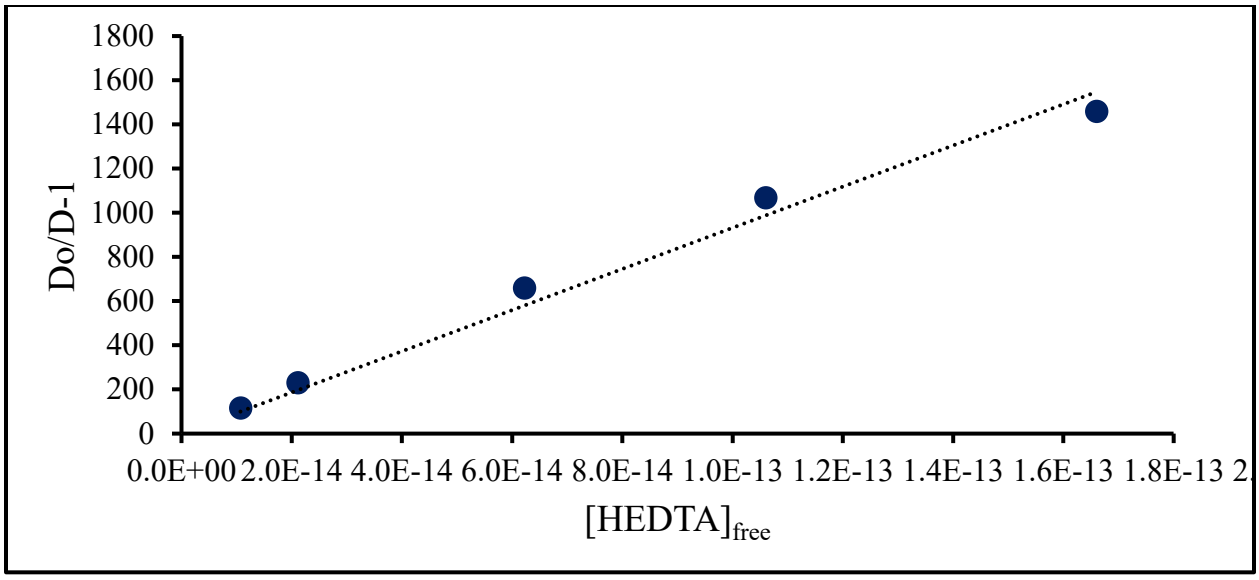

Figure D.80: Fit of Es-HEDTA T = 35°C data

Table D.81: Es-HEDTA T = 45° C Raw Data

pcH	D	D error	[HEDTA] (m)	$[HEDTA]_{free}$	Do	Do/D-1	Do/D error
2.38	8.0	0.6	5.07E-04	1.69E-14	854.97	105.3	0.5
2.38	4.1	0.3	1.00E-03	3.34E-14	854.97	208	1
2.38	1.43	0.05	2.96E-03	9.83E-14	854.97	596.3	0.7
2.38	0.940	0.004	5.03E-03	1.67E-13	854.97	908.20	0.02
2.38	0.65	0.03	7.90E-03	2.63E-13	854.97	1307	3

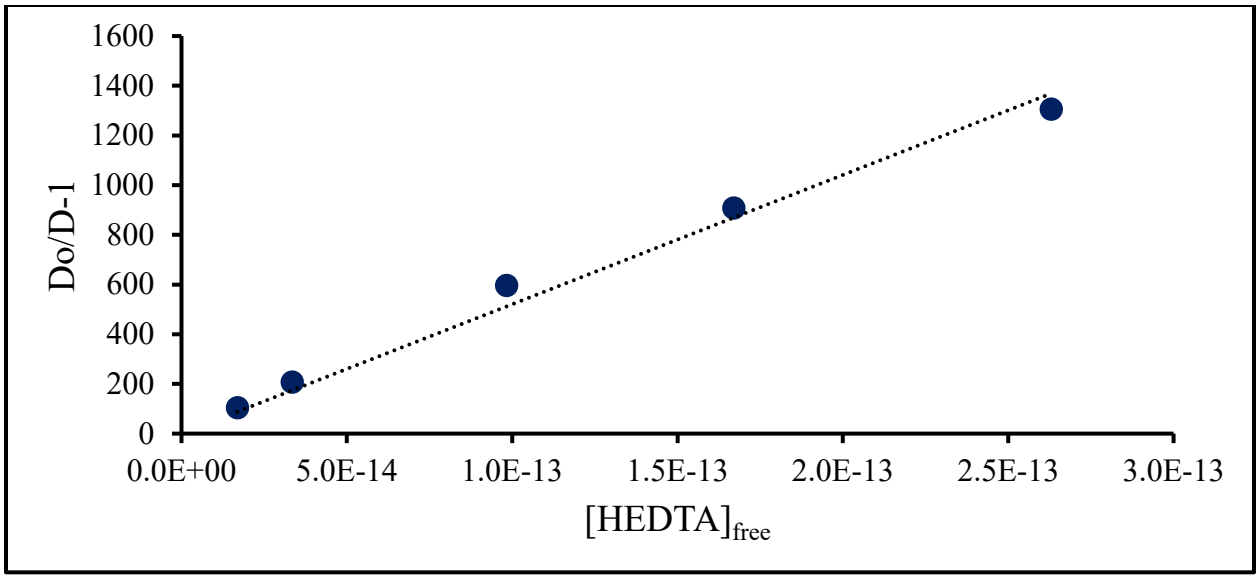

Figure D.81: Fit of Es-HEDTA T = 45°C data

Table D.82: Es-HEDTA T = 55° C Raw Data

pcH	D	D error	[HEDTA] (m)	$[HEDTA]_{free}$	Do	Do/D-1	Do/D error
2.38	5.4	0.5	5.07E-04	2.63E-14	714.18	132	1
2.38	2.7	0.1	1.00E-03	5.21E-14	714.18	263.7	0.7
2.38	0.93	0.04	2.96E-03	1.54E-13	714.18	770	1
2.38	0.60	0.07	5.03E-03	2.61E-13	714.18	1200	14
2.38	0.46	0.04	7.90E-03	4.11E-13	714.18	1540	10

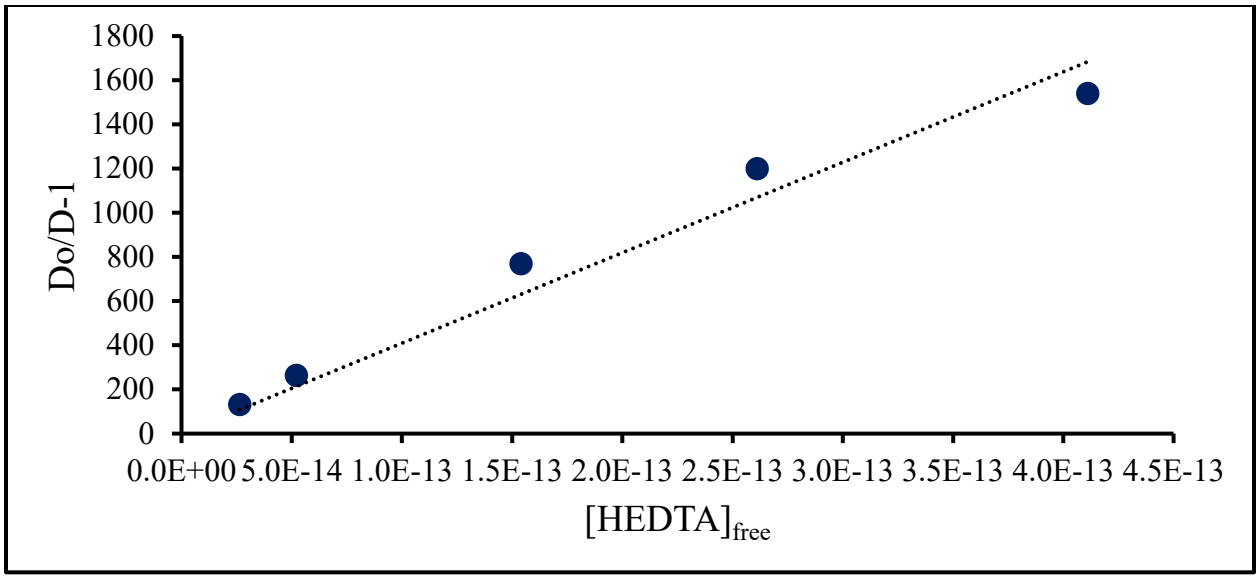

Figure D.82: Fit of Es-HEDTA T = 55°C data

D.13 Einsteinium-CDTA

Table D.83: Es-CDTA T = 15° C Raw Data

pcH	D	D error	[CDTA] (m)	$[CDTA]_{free}$	Do	Do/D-1	Do/D error
2.27	13	1	2.97E-05	5.60E-20	85261	6810	40
2.27	9.0	0.3	4.93E-05	9.31E-20	85261	9466	8
2.27	6.7	0.2	9.83E-05	1.85E-19	85261	12790	10
2.27	4.7	0.3	3.00E-04	5.67E-19	85261	18180	60
2.27	45	5	2.21E-04	4.17E-19	85261	1860	20

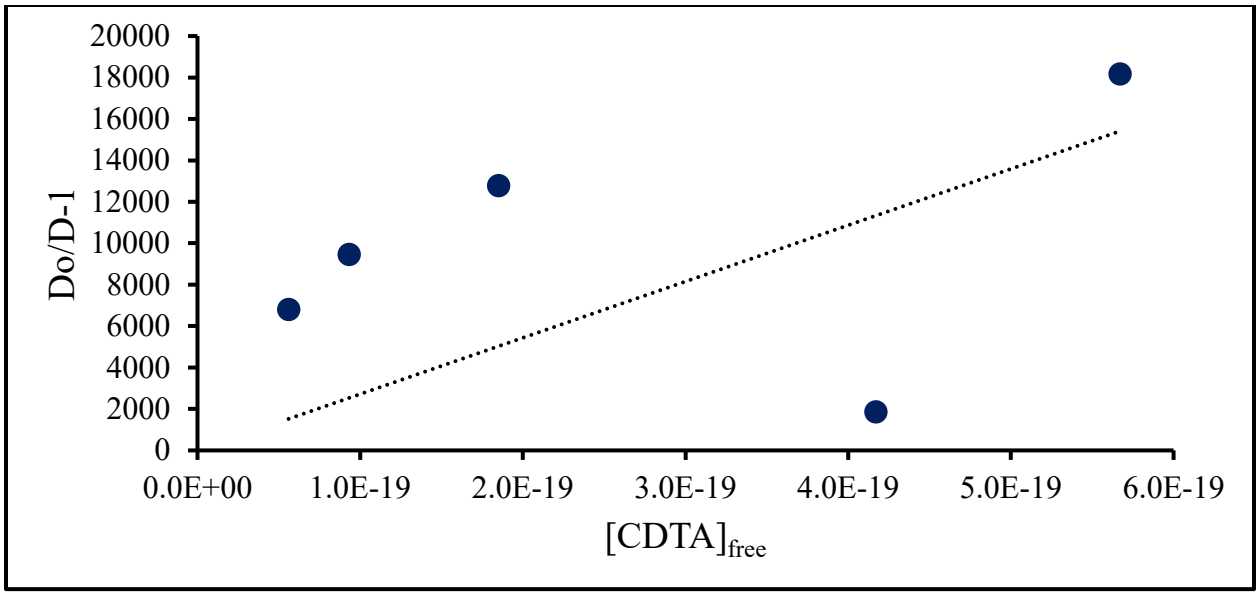

Figure D.83: Fit of Es-CDTA T = 15°C data. The poor fit is probably due to slow kinetics and not reaching equilibrium, so this dataset was discarded.

Table D.84: Es-CDTA T = 25° C Raw Data

pcH	D	D error	[CDTA] (m)	$[CDTA]_{free}$	Do	Do/D-1	Do/D error
2.27	43	4	2.97E-05	1.16E-19	64385	1500	12
2.27	21	5	4.93E-05	1.92E-19	64385	3000	140
2.27	10	1	9.83E-05	3.83E-19	64385	6290	60
2.27	7	3	3.00E-04	1.17E-18	64385	8800	1600
2.27	80	10	2.21E-04	8.62E-19	64385	770	11

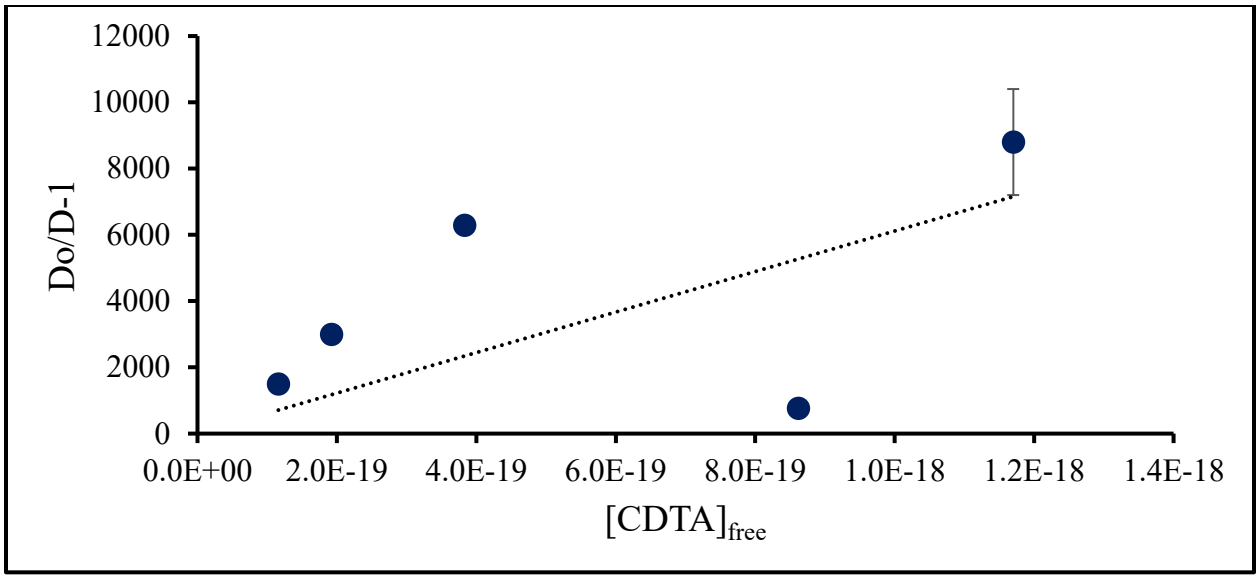

Figure D.84: Fit of Es-CDTA T = 25°C data. The poor fit is probably due to slow kinetics and not reaching equilibrium, so this dataset was discarded.

Table D.85: Es-CDTA T = 35° C Raw Data

pcH	D	D error	[CDTA] (m)	$[CDTA]_{free}$	Do	Do/D-1	Do/D error
2.27	174	40	2.97E-05	2.28E-19	53180	300	10
2.27	69	7	4.93E-05	3.78E-19	53180	769	7
2.27	34	5	9.83E-05	7.54E-19	53180	1560	40
2.27	15	2	3.00E-04	2.30E-18	53180	3440	50
2.27	50	4	2.21E-04	1.70E-18	53180	1053	7

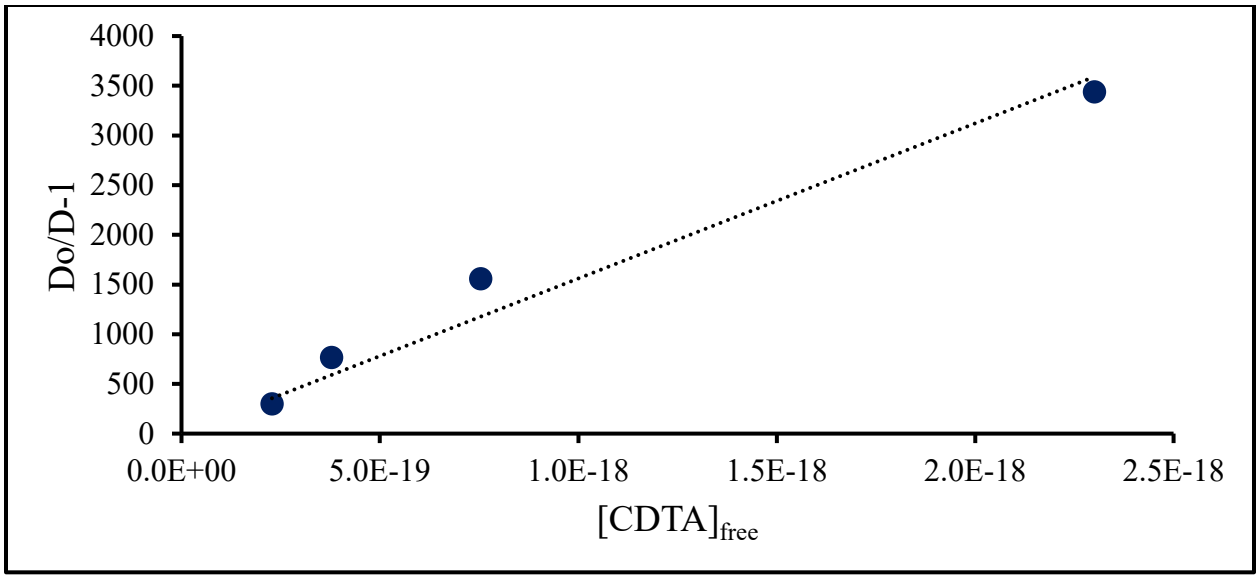

Figure D.85: Fit of Es-CDTA T = 35°C data. Last point omitted for fit.

Table D.86: Es-CDTA T = 45° C Raw Data

pcH	D	D error	[CDTA] (m)	$[CDTA]_{free}$	Do	Do/D-1	Do/D error
2.27	184	8	2.97E-05	4.23E-19	42297	228.5	0.4
2.27	74	6	4.93E-05	7.03E-19	42297	571	4
2.27	41	6	9.83E-05	1.40E-18	42297	1040	24
2.27	15	4	3.00E-04	4.28E-18	42297	2800	233
2.27	46	7	2.21E-04	3.15E-18	42297	930	20

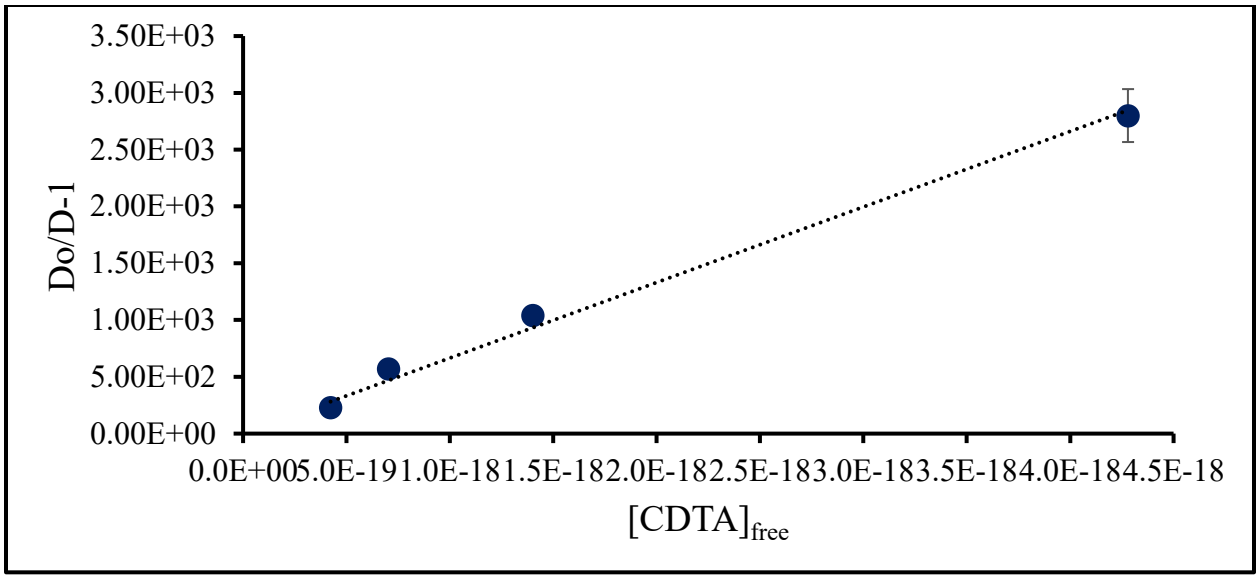

Figure D.86: Fit of Es-CDTA T = 45°C data. Last point omitted for fit.

Table D.87: Es-CDTA T = 55° C Raw Data

pcH	D	D error	[CDTA] (m)	$[CDTA]_{free}$	Do	Do/D-1	Do/D error
2.27	350	90	2.97E-05	7.73E-19	34411	98	6
2.27	90	16	4.93E-05	1.28E-18	34411	380	10
2.27	24	11	9.83E-05	2.56E-18	34411	1400	300
2.27	2.6	0.2	3.00E-04	7.82E-18	34411	13110	50
2.27	30	3	2.21E-04	5.76E-18	34411	1120	10

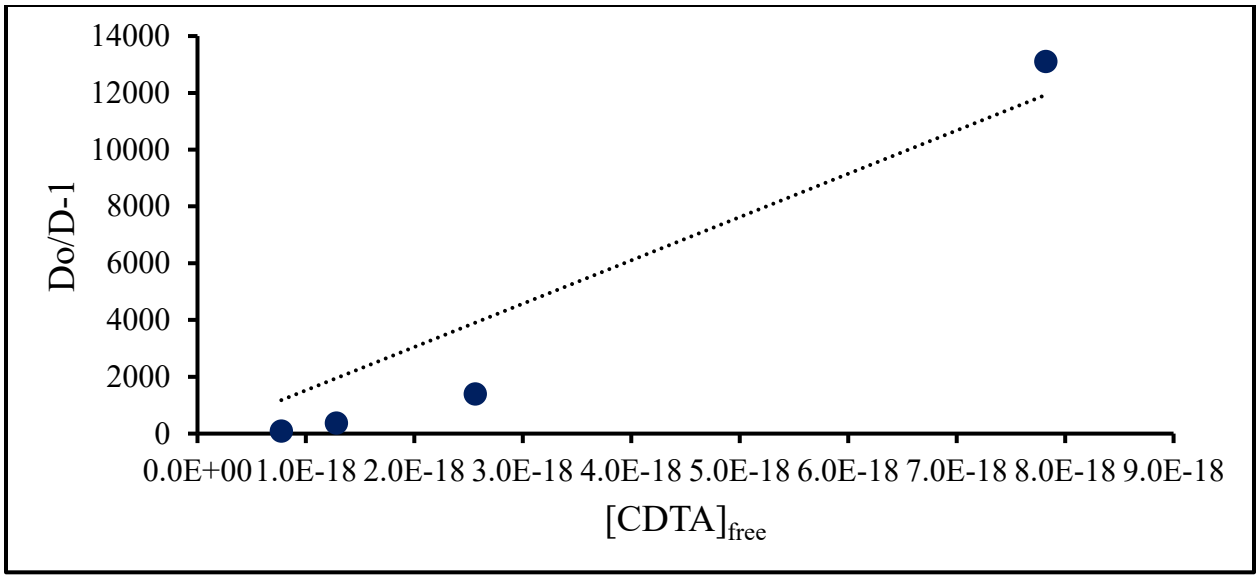

Figure D.87: Fit of Es-CDTA T = 55°C data. Last point omitted for fit.

D.14 Einsteinium-DTPA

Table D.88: Es-DTPA T = 25° C pcH = 2.3

pcH	D	D error	[DTPA] (m)	$[DTPA]_{free}$	Do	Do/D-1	Do/D error
2.29	16.35	0.06	9.82E-05	7.03E-21	104000	6355.80	0.07
2.29	4.98	0.07	2.97E-04	2.13E-20	104000	20862	5
2.29	2.67	0.03	5.18E-04	3.71E-20	104000	38893	3
2.29	1.754	0.007	7.03E-04	5.03E-20	104000	59251	1
2.29	1.25	0.01	1.02E-03	7.28E-20	104000	82951	8

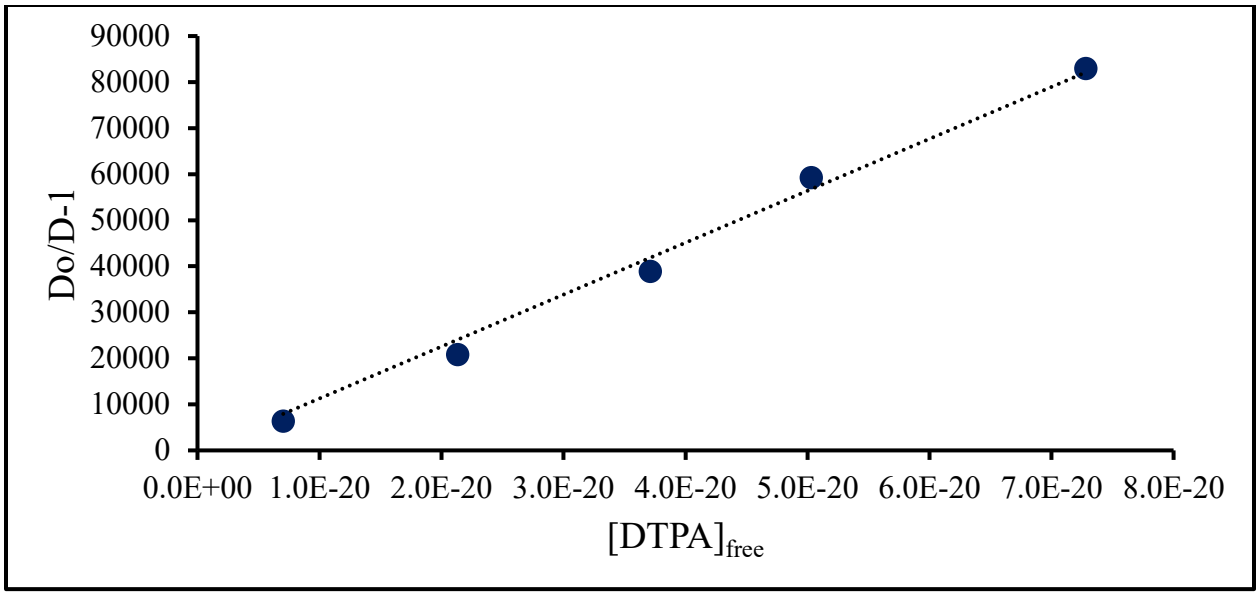

Figure D.88: Fit of Es-DTPA T = 25°C, pcH = 2.3 data

Table D.89: Es-DTPA T = 25° C pcH = 2.1

pcH	D	D error	[DTPA] (m)	$[DTPA]_{free}$	Do	Do/D-1	Do/D error
2.12	24.79	0.09	1.01E-04	1.33E-21	32100	1294.90	0.02
2.12	7.2	0.1	3.02E-04	3.94E-21	32100	4482.7	0.8
2.12	5.26	0.07	4.99E-04	6.51E-21	32100	6110	1
2.12	5.0	0.4	7.40E-04	9.66E-21	32100	6470	50
2.12	2.84	0.01	1.00E-03	1.31E-20	32100	11301.7	0.2

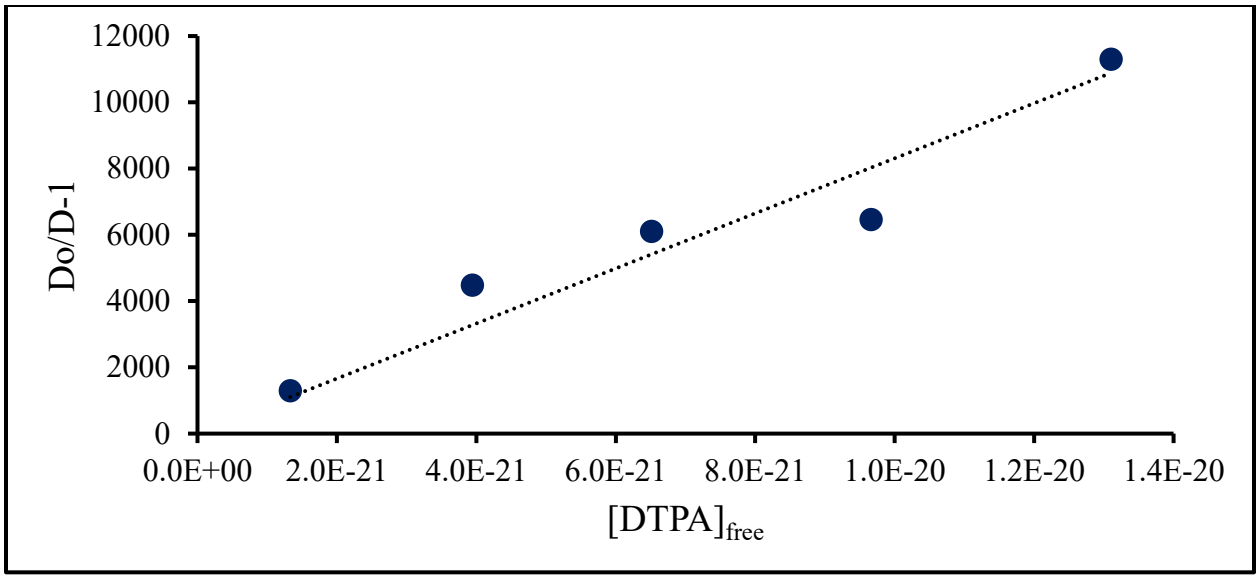

Figure D.89: Fit of Es-DTPA T = 25°C, pcH = 2.1 data

Table D.90: Es-DTPA T = 25° C pcH = 1.9

pcH	D	D error	[DTPA] (m)	$[DTPA]_{free}$	Do	Do/D-1	Do/D error
1.92	62.6	0.4	1.01E-04	1.55E-22	8070	127.900	0.005
1.92	21.00	0.02	3.03E-04	4.67E-22	8070	383.3000	0.0002
1.92	12.43	0.02	5.00E-04	7.69E-22	8070	648.100	0.002
1.92	10.94	0.03	7.06E-04	1.09E-21	8070	736.400	0.006
1.92	6.10	0.05	1.04E-03	1.60E-21	8070	1322.50	0.09

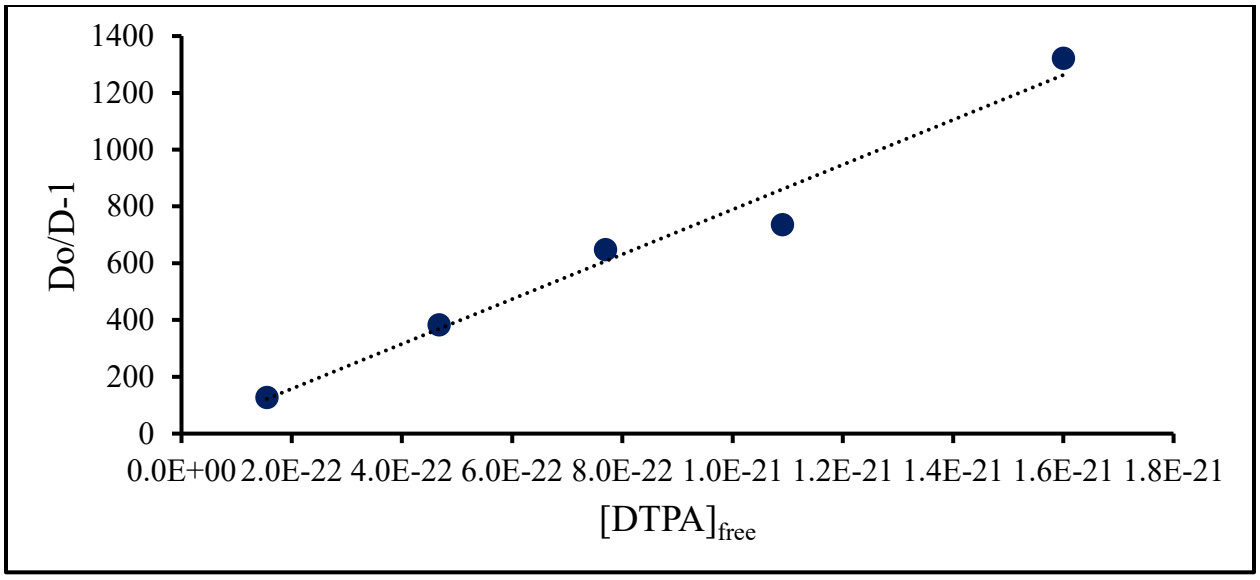

Figure D.90: Fit of Es-DTPA T = 25°C, pcH = 1.9 data

Table D.91: Es-DTPA T = 35° C pcH = 2.3

pcH	D	D error	[DTPA] (m)	$[DTPA]_{free}$	Do	Do/D-1	Do/D error
2.29	10.07	0.02	9.82E-05	1.49E-20	73700	7317.30	0.04
2.29	4.03210	0.00005	2.97E-04	4.51E-20	73700	18282.10	0.00005
2.29	2.182	0.004	5.18E-04	7.86E-20	73700	33791.1	0.1
2.29	1.174	0.008	7.03E-04	1.07E-19	73700	62782	3
2.29	0.84	0.02	1.02E-03	1.54E-19	73700	88120	40

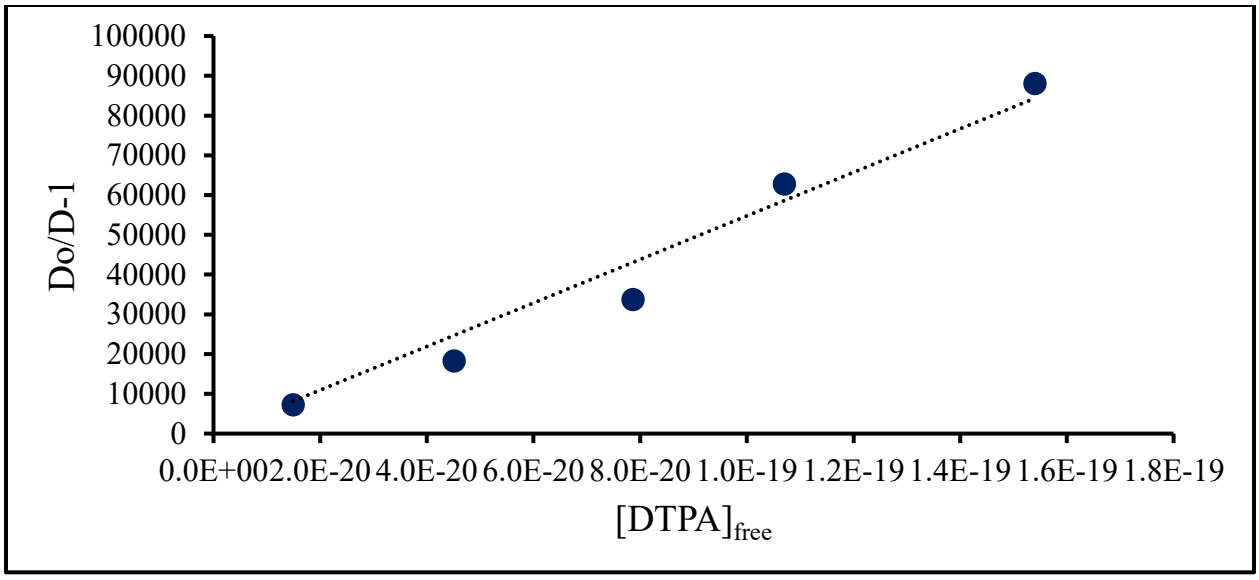

Figure D.91: Fit of Es-STPA T = 35°C, pcH = 2.3 data

Table D.92: Es-DTPA T = 35° C pcH = 2.1

pcH	D	D error	[DTPA] (m)	$[DTPA]_{free}$	Do	Do/D-1	Do/D error
2.12	21.2	0.2	1.01E-04	2.80E-21	22800	1072.80	0.07
2.12	5.9	0.1	3.02E-04	8.34E-21	22800	3832	1
2.12	5.206	0.005	4.99E-04	1.38E-20	22800	4375.200	0.004
2.12	2.83	0.05	7.40E-04	2.04E-20	22800	8062	3
2.12	1.17	0.02	1.00E-03	2.77E-20	22800	19400	6

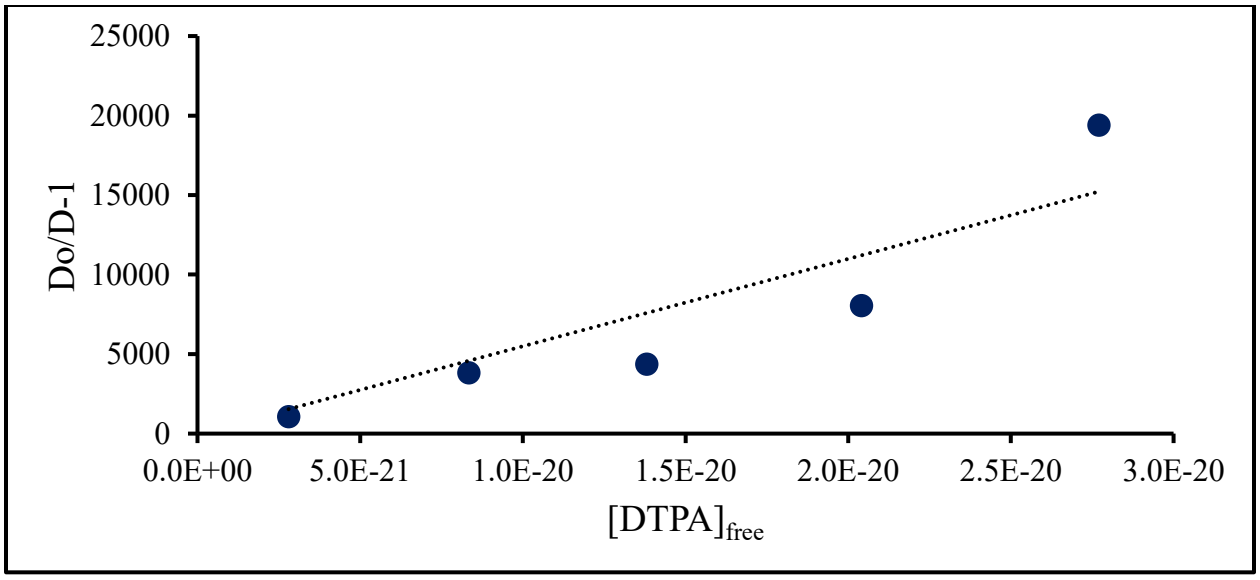

Figure D.92: Fit of Es-DTPA T = 35°C, pcH = 2.1 data

Table D.93: Es-DTPA T = 35° C pcH = 1.9

pcH	D	D error	[DTPA] (m)	$[DTPA]_{free}$	Do	Do/D-1	Do/D error
1.92	56.9	0.9	1.01E-04	3.27E-22	5700	99.60	0.02
1.92	18.82	0.04	3.03E-04	9.85E-22	5700	303.100	0.001
1.92	12.03	0.06	5.00E-04	1.62E-21	5700	474.80	0.01
1.92	10.70	0.07	7.06E-04	2.29E-21	5700	534.10	0.02
1.92	3.94	0.03	1.04E-03	3.37E-21	5700	1451.4	0.1

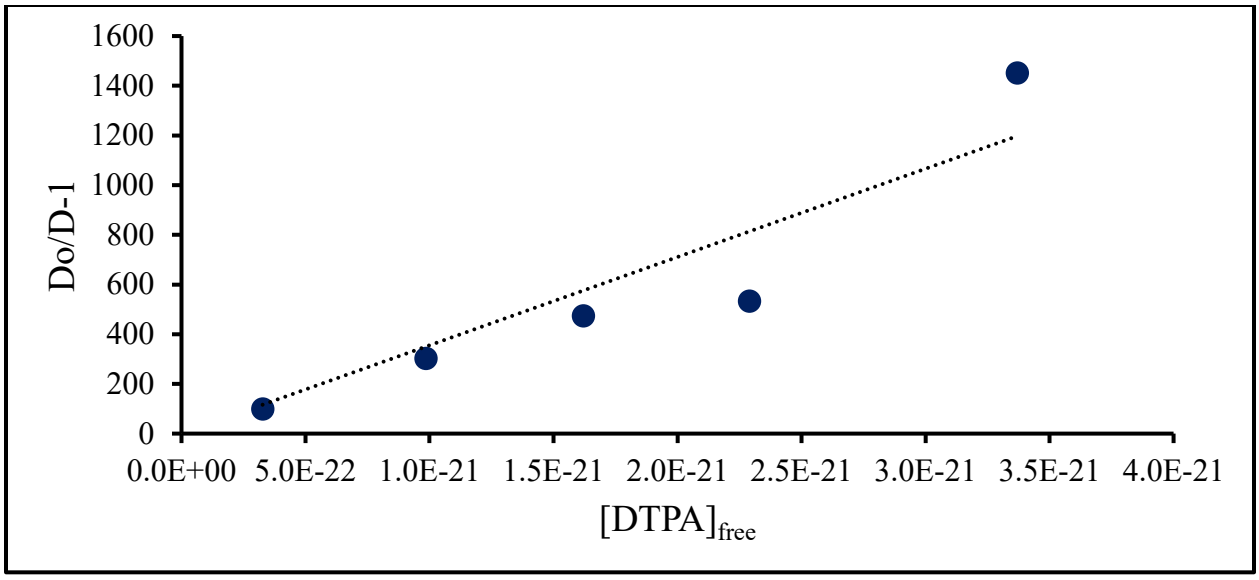

Figure D.93: Fit of Es-DTPA T = 35°C, pcH = 1.9 data

Table D.94: Es-DTPA T = 45° C pcH = 2.3

pcH	D	D error	[DTPA] (m)	$[DTPA]_{free}$	Do	Do/D-1	Do/D error
2.29	5.0	0.1	9.82E-05	2.97E-20	63819	12871	6
2.29	1.54	0.02	2.97E-04	8.98E-20	63819	41340	4
2.29	0.87	0.01	5.18E-04	1.57E-19	63819	73640	17
2.29	0.788	0.006	7.03E-04	2.13E-19	63819	80989	4
2.29	0.57	0.01	1.02E-03	3.08E-19	63819	112880	64

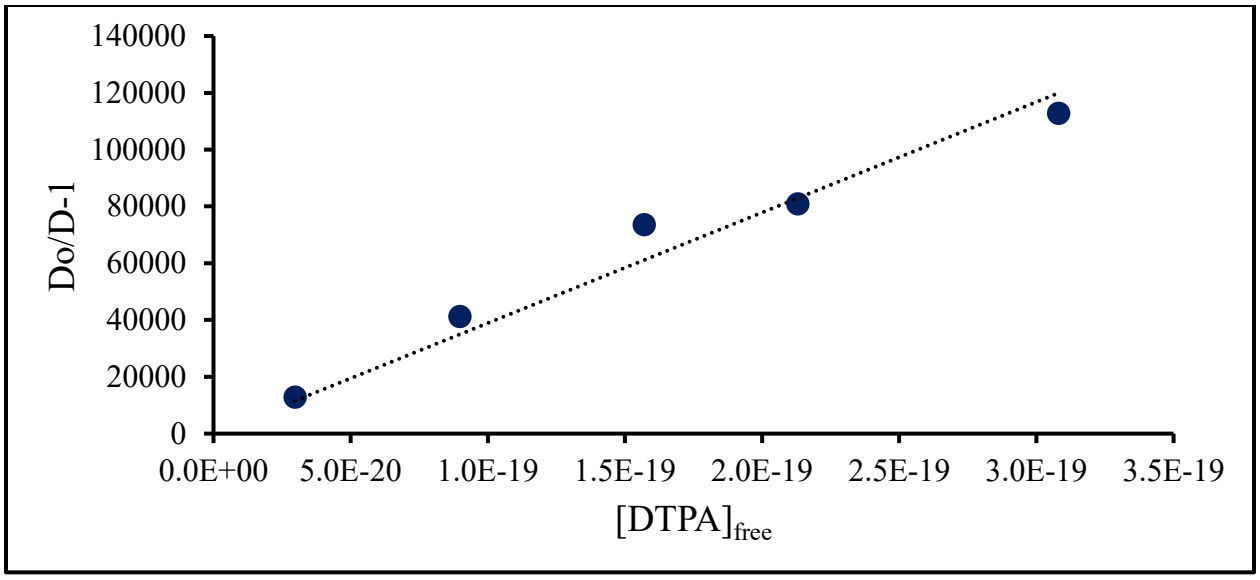

Figure D.94: Fit of Es-DTPA T = 45°C, pcH = 2.3 data

Table D.95: Es-DTPA T = 45° C pcH = 2.1

pcH	D	D error	[DPTA] (m)	$[DPTA]_{free}$	Do	Do/D-1	Do/D error
2.12	8.7	0.1	1.01E-04	5.58E-21	19722	2270.9	0.5
2.12	2.74	0.01	3.02E-04	1.66E-20	19722	7202.7	0.1
2.12	1.86	0.02	4.99E-04	2.74E-20	19722	10575	1
2.12	1.95	0.01	7.40E-04	4.06E-20	19722	10090.5	0.3
2.12	1.145	0.005	1.00E-03	5.50E-20	19722	17227.5	0.4

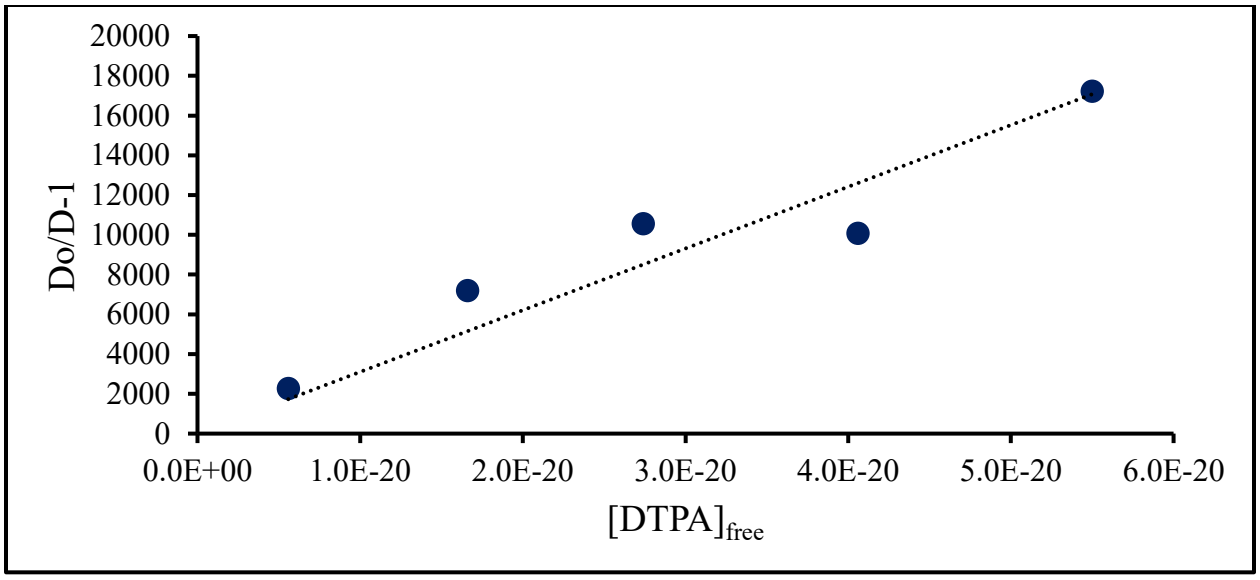

Figure D.95: Fit of Es-DTPA T = 45°C, pcH = 2.1 data

Table D.96: Es-DTPA T = 45° C pcH = 1.9

pcH	D	D error	[DPTA] (m)	$[DPTA]_{free}$	Do	Do/D-1	Do/D error
1.92	22.0	0.4	1.01E-04	6.47E-22	4953.9	223.70	0.07
1.92	7.2	0.1	3.03E-04	1.95E-21	4953.9	684.8	0.1
1.92	3.68	0.06	5.00E-04	3.22E-21	4953.9	1343.5	0.3
1.92	3.74	0.07	7.06E-04	4.55E-21	4953.9	1323.7	0.5
1.92	2.53	0.01	1.04E-03	6.69E-21	4953.9	1954.30	0.06

2

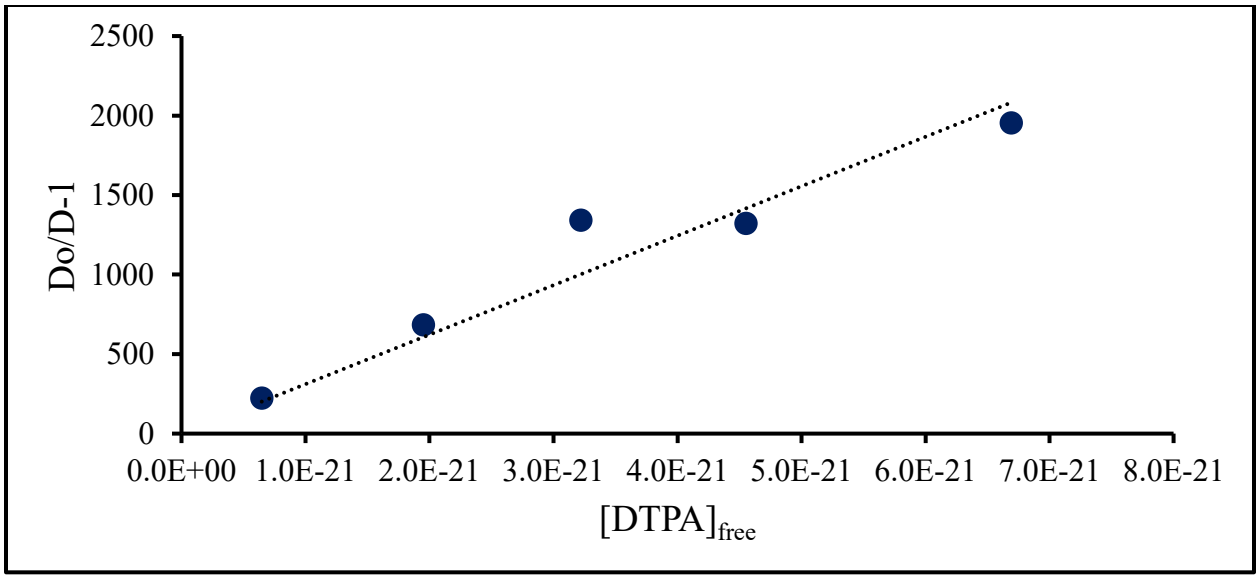

Figure D.96: Fit of Es-DTPA T = 45°C, pcH = 1.9 data